SGW-50056
Revision 0

Resistivity Characterization of 216-C-1, A-Complex, B-Plant, PUREX, S-Complex, T-Plant, and 216-Z-16 Trench Project Sites

Prepared for the U.S. Department of Energy
Assistant Secretary for Environmental Management

Contractor for the
U.S. Department of Energy under Contract DE-AC06-08RL14788

CH2MHILL
Plateau Remediation Company

P.O. Box 1600
Richland, Washington 99352

Approved for Public Release;
Further Dissemination Unlimited

SGW-50056
Revision 0

Resistivity Characterization of 216-C-1, A-Complex, B-Plant, PUREX, S-Complex, T-Plant, and 216-Z-16 Trench Project Sites

Date Published
August 2011

Prepared for the U.S. Department of Energy
Assistant Secretary for Environmental Management

Contractor for the
U.S. Department of Energy under Contract DE-AC06-08RL14788

CH2MHILL
Plateau Remediation Company

P.O. Box 1600
Richland, Washington

LE Bratton 8/4/2011
Release Approval Date

Approved for Public Release;
Further Dissemination Unlimited

TRADEMARK DISCLAIMER

Reference herein to any specific commercial product, process, or service by trade name, trademark, manufacturer, or otherwise, does not necessarily constitute or imply its endorsement, recommendation, or favoring by the United States Government or any agency thereof or its contractors or subcontractors.

This report has been reproduced from the best available copy.

Printed in the United States of America

CONTENTS

SUMMARY 1

APPENDICES

A RPT-2007-046, Rev.1, Resistivity Characterization of 216-C-1, A-Complex, B-Plant, PUREX, S-Complex, T-Plant, and 216-Z-16 Trench Project Sites ..... A-i

METRIC CONVERSION CHART

Into Metric Units			Out of Metric Units		
If you know	*Multiply by*	*To get*	*If you know*	*Multiply by*	*To get*
Length			**Length**		
inches	25.40	millimeters	millimeters	0.0394	inches
inches	2.54	centimeters	centimeters	0.394	inches
feet	0.305	meters	meters	3.281	feet
yards	0.914	meters	meters	1.094	yards
miles (statute)	1.609	kilometers	kilometers	0.621	miles (statute)
Area			**Area**		
sq. inches	6.452	sq. centimeters	sq. centimeters	0.155	sq. inches
sq. feet	0.0929	sq. meters	sq. meters	10.764	sq. feet
sq. yards	0.836	sq. meters	sq. meters	1.196	sq. yards
sq. miles	2.591	sq. kilometers	sq. kilometers	0.386	sq. miles
acres	0.405	hectares	hectares	2.471	acres
Mass (weight)			**Mass (weight)**		
ounces (avoir)	28.349	grams	grams	0.0353	ounces (avoir)
pounds	0.454	kilograms	kilograms	2.205	pounds (avoir)
tons (short)	0.907	ton (metric)	ton (metric)	1.102	tons (short)
Volume			**Volume**		
teaspoons	5	milliliters	milliliters	0.034	ounces (U.S., liquid)
tablespoons	15	milliliters	liters	2.113	pints
ounces (U.S., liquid)	29.573	milliliters	liters	1.057	quarts (U.S., liquid)
cups	0.24	liters	liters	0.264	gallons (U.S., liquid)
pints	0.473	liters	cubic meters	35.315	cubic feet
quarts (U.S., liquid)	0.946	liters	cubic meters	1.308	cubic yards
gallons (U.S., liquid)	3.785	liters			
cubic feet	0.0283	cubic meters			
cubic yards	0.764	cubic meters			
Temperature			**Temperature**		
Fahrenheit	(°F-32)*5/9	Centigrade	Centigrade	(°C*9/5)+32	Fahrenheit
Radioactivity			**Radioactivity**		
picocurie	37	millibecquerel	millibecquerel	0.027	picocurie

SUMMARY

During fiscal year 2007, two-dimensional resistivity surveys were conducted within the Central Plateau along a total of 54 geophysical profiles in both the 200 East and 200 West areas. Of these, four profiles were collected in the vicinity of 216-C-1, nine profiles acquired near waste sites 216-A-7, 216-A-8 and 216-A-19, ten profiles conducted for investigating waste sites 216-B-6, 216-B-10A&B, 216-B-12 and 216-B-55, fifteen profiles were collected south of PUREX in the vicinity of 216-A-10, 216-A-36A and 216-A-45, three profiles collected at 216-S-9, three profiles acquired immediately to the west of 216-S-13, six profiles conducted across 216-T-34 and 216-T-35, four profiles collected in the vicinity of 216-T-3 and 216-T-6, and three profiles acquired for 216-Z-16.

Geophysical profiling using the two-dimensional resistivity method was conducted in order to interrogate the vadose zone subsurface beneath these waste sites using a non-invasive technique to determine whether past waste disposal and/or handling activities have left a measurable electrical signature. The current best model is that nitrate laden waste streams, if allowed to migrate into and through the vadose zone, will produce a low-resistivity anomaly (increased electrical conductivity) due either to increased saturation or to the presence of remnant nitrate. This low-resistivity region would, in turn, define the dominant migration route of the waste streams.

Primary results from this investigation are:

- Data collected around the 216-C-1 were severely impacted by site infrastructure. A shallow zone of low-resistivity (10 m BGS) was observed on 3 of the profiles and located north of 216-C-1. A strong electrically-conductive zone was imaged from 10 m to 50+ m below ground surface (bgs) beneath 216-C-1, though analysis cannot rule this feature being due to interference from the infrastructure..

- The A-Complex site showed near surface conductive features that correlate well with the boundary of the 216-A-19 and -20 waste sites. The conductive feature is limited to the first 15 meters of the subsurface and does not contact the water table.

- Survey lines over the 216-A-8 disposal trench showed a low resistivity anomaly associated with the termination of the inflow pipeline. However, there is evidence of conductive material within the first 10 meters that is characteristic of liquid waste disposal.

- The two survey lines conducted between the 216-A-7 waste site and the 207-A-North and -South ponds were severely impacted by infrastructure. It is unlikely that additional surface survey coverage or processing using three-dimensional inversion would produce additional information in this area due to the infrastructure complexity and the relatively low volume of nitrate disposed of at 216-A-7.

- Survey lines adjacent to the trench 216-B-55 trench indicate a shallow electrically-conductive zone (<12 m bgs) associated with the position of the trench. The character and shape of this conductive zone is not interpreted to be caused by infrastructure and is

likely related to either increased soil moisture or change in soil chemistry due to disposal in the trench.

- Investigations for the 216-B-12 crib showed a conductive feature directly beneath the crib at a depth range of 5 to 40 m below ground surface. The depth and magnitude of the feature suggests the presence of increased soil moisture or nitrate-salt concentration.

- The two west-to-east surveys conducted within the B-Plant are severely impacted by infrastructure and cannot currently be used to provide information regarding subsurface waste streams. Two south-to-north profiles collected across the 216-B-10A&B waste sites were also unable to discern waste related subsurface features due to the extreme interference in the vicinity of the B-Plant.

- Resistivity profiling south of the PUREX site indicates a broad zone of low-resistivity beneath the 216-A-36 A/B waste site. Good lateral definition of this feature is provided by the cross-lines (trench perpendicular surveys). The contractor estimated the subsurface feature to be in contact with groundwater, though using results from the BC-Cribs surveys, the base of this feature is likely in the 55-65 m depth range with the geophysical modeling smearing the water table effect with that of the subsurface anomaly.

- Near surface electrically conductive features are visible near the 216-A-10 waste area, but there is insufficient data to determine the possible cause of the anomalies. Maximum depth of these features is approximately 15 m bgs.

- A relatively shallow zone of low-to-intermediate resistivity (more electrically conductive) is modeled beneath the 216-A-45 trench. Maximum depth of this feature is approximately 10 m bgs and the lateral dimensions are consistent with the trench location.

- PUREX related surveys conducted within the fenced area were severely impacted by infrastructure with resulting model results indicating a broad (profile length) zone of extremely low-resistivity starting at 10 m depth and extending to the base of the model. Results are consistent with previous surveys in this area and are due to the existing infrastructure short-circuiting the resistivity data.

- A conductive feature on the eastern edge of the 216-S-13 survey area increases with depth and is in close proximity to the 216-S-13 disposal site. The shape and magnitude of the response is not necessarily indicative of infrastructure and could be due to the increased soil moisture or salt concentration from the liquid waste disposal site to the east.

- The 216-S-9 characterization area was negatively impacted by pipeline interference, which resulted in strong, low-resistivity anomalies that dominate the three profiles collected. The northwest-southwest profile that crossed 216-S-9, however, did image a shallow zone (<10 m bgs) of decreased resistivity associated with the waste site. This zone is modeled to increase in depth at the southeast end of the 216-S-9 to about 25-to-30 m bgs where it merges with a broad zone of very low resistivity.

- Results for the 216-T-34 and 216-T-35 surveys showed a significant electrical interference due to the presence of the railway lines and subsurface pipes that is manifested as large zones (>30 m in width) of extreme low-resistivity. Despite these interference effects, a zone of intermediate resistivity likely related to past disposal can be discerned in the 15-30 m depth range beneath the southwestern third of 216-T-34.

- Resistivity surveys across 216-T-35 did image zones of low-resistivity in the very near surface (<15 m bgs) that are likely due to increased soil moisture or nitrate-salt content related to past disposal in this trench. A broad zone of low-resistivity is modeled on the trench central and eastern profile that has a characteristic shape similar to that observed at other waste disposal sites. Depth to top is in the 25 to 30 m depth range and the bulk of the anomaly is located above the water table. It is not known whether this anomaly is related to disposal at either 216-T-34 or 216-T-35, or some combination of both.

- Results for surveys conducted across the 216-T-6 cribs, as well as the 216-T-3 reverse well indicate an approximate 20-to-25 m wide zone of lower resistivity extending from near the base of the eastern most crib to a depth of 35 m bgs. A similar decrease in resistivity is observed in the vicinity of the perforated interval of the 216-T-3 reverse well, suggesting a waste stream provenance for the low-resistivity anomaly. It is unclear whether a broader west-to-east decrease in resistivity at an average depth of 45 m bgs is related discharge into the 216-T-6 cribs or 216-T-3 reverse well.

- Model results for three west-to-east profiles collected across 216-Z-16 shows a zone of decreased resistivity in the 16-to-30 m depth range beneath the western half of the trench. A broader zone of low-resistivity modeled at 25-to-40 m in depth is probably related to the tank-farm infrastructure located south of the profiles (the anomaly top is deeper and strength decreases towards the north).

APPENDIX A

RPT-2007-046, REV.1, RESISTIVITY CHARACTERIZATION OF 216-C-1, A-COMPLEX, B-PLANT, PUREX, S-COMPLEX, T-PLANT, AND 216-Z-16 TRENCH PROJECT SITES

This page intentionally left blank.

RPT-2007-046, Rev. 1

Final Report

RESISTIVITY CHARACTERIZATION OF 216-C-1, A-COMPLEX, B-PLANT, PUREX, S-COMPLEX, T-PLANT, AND 216-Z-16 TRENCH PROJECT SITES

M. Levitt
D. Glaser, M.Sc.
G. O'Brien
M. McNeill
B. Cubbage
D. Rucker, Ph.D.

hydroGEOPHYSICS, Inc.

2302 North Forbes Boulevard, Tucson, Arizona 85745 USA

Date Published
March 2008

Prepared for Fluor Hanford, Inc.

and
Battelle Memorial Institute, Pacific Northwest Division (Battelle)
Contract: PNNL RFP NO. 51569

EXECUTIVE SUMMARY

hydroGEOPHYSICS, Inc. and Pacific Northwest National Laboratory were contracted by Fluor Hanford, Inc. to conduct a geophysical investigation of several locations at the Hanford Site in Richland, Washington. Sites within the 200 East area selected for this investigation included four resistivity lines at 216-C-1, nine resistivity lines at A-Complex, ten resistivity lines at B-Plant, and seven resistivity lines at PUREX. Sites within the 200 West area selected for this investigation included six resistivity lines at S-Complex, ten resistivity lines at T-Plant, and three resistivity lines at 216-Z-16 Trench. A geophysical investigation of these areas is part of a broader characterization of the Central Plateau waste sites, which are suspected to have contributed to subsurface contamination. The objective of the investigation was to map the near-surface conditions using a non-invasive geophysical technique, electrical resistivity, to investigate the lateral and vertical extent of possible contaminant waste plumes. The results of the surveys showed the following information:

- The 216-C-1 site was one of the most heavily infrastructure-dominated project sites. Despite the severe infrastructure, the data revealed a few interesting resistivity anomalies where the displayed values appeared too conductive to represent saturated soil, yet the character did not resemble a typical infrastructure response.

- The A-Complex site showed near-surface conductive features that correlate well with the boundary of the 216-A-19 and -20 waste sites. The conductive feature is limited to the first 15 meters of the subsurface and does not contact the water table.

- Survey lines over the 216-A-8 disposal trench showed a low resistivity anomaly associated with the termination of the inflow pipeline. However, there is evidence of conductive material within the first 10 meters that is characteristic of liquid waste disposal.

- The two survey lines conducted between the 216-A-7 waste site and the 207-A-North and -South ponds were greatly impacted by infrastructure. It is unlikely that additional surface survey coverage or processing using three-dimensional inversion would produce additional information in this area due to the infrastructure complexity.

- The two survey lines adjacent to the trench 216-B-55 trench provided acceptable data that shows little evidence of a change in soil moisture or chemistry associated with the past liquid waste disposal.

- The 216-B-12 crib showed a conductive feature directly over the crib within the first 5 to 40 meters. The depth and magnitude of the feature suggests the presence of increased soil moisture or salt concentration. However, the survey line completed directly over the crib shows a heavy distortion of the conductive feature, which is most likely caused by subsurface infrastructure within the crib.

- The most significant conductive feature at the PUREX site is located beneath the 216-A-36 A/B waste site. The resistivity low extends beyond 75 meters and is likely to

be in contact with groundwater. Two small near-surface conductive features are visible near the 216-A-10 waste area, but there is insufficient data to determine the possible cause of the anomalies.

- Two-dimensional inversion sections show some conductive features over the 216-A-45 waste area within the first 10 meters of the ground surface. Enhancement of the resistivity results could be accomplished by completing a three-dimensional inversion model with additional data.

- A conductive feature on the eastern edge of the 216-S-13 survey area increases with depth and is in close proximity to the 216-S-13 disposal site. The shape and magnitude of the response is not necessarily indicative of infrastructure and could be due to the increased soil moisture or salt concentration from the liquid waste disposal site to the east.

- The 216-S-9 characterization area was greatly hampered by pipeline disturbances. However, besides the pipeline induced anomalies and the water table, there is little evidence of increased soil moisture or a change in soil and water chemistry as supported by the high resistivity values shown in the near-surface.

- Results for the 216-T-34 and -35 areas showed a significant distortion due to the railway lines and subsurface pipes. Despite the distortions, there was a noticeable increase in conductivity near the 216-T-35 trench that is likely caused by an increase in moisture content or salt concentration relative to the surrounding background material. Additional lines and three-dimensional inversion may help resolve these anomalies.

- In general, the 216-Z-16 shows a slightly reduced resistivity relative to background values. However, the values are much higher than seen at other sites that received liquid waste indicating minimal adverse impact of past practices to the soil.

Recommendations for the future work include:

- Complete a survey design that includes a reconnaissance electromagnetic induction and magnetic gradiometry survey to locate subsurface infrastructure. Surface resistivity lines should avoid these areas as much as possible.

- In areas that do contain substantial infrastructure, resistivity data can still be useful if acquired using a borehole-based electrical resistivity tomography survey. Electrical resistivity tomography data are acquired between two vertical sets of electrodes placed in parallel boreholes. The electrodes would be placed far below the infrastructure allowing imaging of increased soil moisture or salt concentration.

- Well-to-well data have proved to be invaluable to plume mapping for other projects within the Hanford Site. It is recommended that well-to-well measurements be acquired on future deployments where sufficient well distributions are available. The disadvantage of the well-to-well data is that depth information is lost. Therefore, it is

recommended that as many deep electrodes be placed within and around a target waste area as possible and be distributed at a low spatial density.

- Resistivity is a three-dimensional volumetric property, which can be greatly influenced by subsurface features near survey lines in addition to directly beneath the survey lines. The interpretation of the data sets is likely to improve with a more suited three-dimensional inversion processing technique. However, to perform three-dimensional inversion, suitable survey design (i.e., line location, spacing, geometry) is required.

TABLE OF CONTENTS

1.0 INTRODUCTION 1-1
1.1 SITE LOCATION 1-1
1.2 OBJECTIVE OF INVESTIGATION 1-2
1.3 SCOPE OF WORK 1-2

2.0 BACKGROUND 2-1
2.1 216-C-1 STUDY AREA DISPOSAL SUMMARY 2-1
2.2 A-COMPLEX STUDY AREA DISPOSAL SUMMARY 2-2
2.3 B-PLANT STUDY AREA DISPOSAL SUMMARY 2-7
2.4 PUREX STUDY AREA DISPOSAL SUMMARY 2-7
2.5 S-COMPLEX STUDY AREA DISPOSAL SUMMARY 2-8
2.6 T-PLANT STUDY AREA DISPOSAL SUMMARY 2-19
2.7 216-Z-16 TRENCH STUDY AREA DISPOSAL SUMMARY 2-24

3.0 GEOPHYSICAL THEORY 3-1
3.1 HIGH RESOLUTION RESISTIVITY (HRR) 3-1
3.2 TARGET DISCRIMINATION WITH APPARENT RESISTIVITY 3-4

4.0 METHODOLOGY 4-1
4.1 SURVEY AREA AND LOGISTICS 4-1
4.1.1 Resistivity Line location and Acquisition 4-1
4.1.1.1 216-C-1 4-2
4.1.1.2 A-Complex 4-3
4.1.1.3 B-Plant 4-4
4.1.1.4 PUREX Plant 4-6
4.1.1.5 S-Complex 4-9
4.1.1.6 T-Plant 4-10
4.1.1.7 216-Z-16 Trench 4-12
4.2 EQUIPMENT 4-13
4.2.1 Electrical Resistivity 4-13
4.2.2 Global Positioning System 4-14
4.3 CONTACT RESISTANCE TESTING 4-14
4.4 DATA PROCESSING & PLOTTING 4-15
4.4.1 Management of Field Data 4-15
4.4.2 Data Reduction: Filtering, Editing, Quality Assurance / Quality Control 4-16
4.4.3 2D Resistivity Inversion 4-20
4.4.4 2D Plotting 4-26
4.4.5 3D Visualization 4-29

5.0 RESULTS & INTERPRETATION 5-1
5.1 200 EAST PROJECT SITES 5-4
5.1.1 216-C-1 5-4
5.1.1.1 2D Inversion Results 5-4
5.1.1.2 3D Rendering of 2D Inversion Results 5-10

5.1.2 A-Complex 5-15
5.1.2.1 2D Inversion Results 5-15
5.1.2.2 3D Rendering of 2D Inversion Results 5-23
5.1.3 B-Plant 5-28
5.1.3.1 2D Inversion Results 5-28
5.1.3.2 3D Rendering of 2D Inversion Results 5-37
5.1.4 PUREX Plant 5-42
5.1.4.1 2D Inversion Results 5-42
5.1.4.2 3D Rendering of 2D Inversion Results 5-53
5.2 200 WEST 5-58
5.2.1 S-Complex 5-58
5.2.1.1 2D Inversion Results 5-58
5.2.1.2 3D Rendering of 2D Inversion Results 5-65
5.2.2 T-Plant 5-75
5.2.2.1 2D Inversion Results 5-75
5.2.2.2 3D Rendering of 2D Inversion Results 5-86
5.2.3 216-Z-16 Trench 5-96
5.2.3.1 2D Inversion Results 5-96
5.2.3.2 3D Rendering of 2D Inversion Results 5-100

6.0 CONCLUSIONS 6-1

7.0 LESSONS LEARNED & RECOMMENDATIONS 7-1
7.1 SURVEY DESIGN 7-1
7.2 DATA ACQUISITION 7-2
7.3 DATA PROCESSING AND MODELING 7-2

8.0 REFERENCES 8-1

APPENDICES

A. SUPPLEMENTAL TWO-DIMENSIONAL INVERSION RESULTS ..... A-i

LIST OF FIGURES

Figure 1-1. General Site Map Showing Location of Resistivity Surveys at the 200 West and 200 East Areas. 1-1
Figure 2-1. Waste Summary for the 216-C-1 Study Area Showing Groundwater Nitrate Contours (mg/L) and Total Liquid Disposal (mGal). 2-3
Figure 2-2. Waste Summary for the 216-C-1 Study Area Showing Groundwater Nitrate Contours (mg/L) and Major Anion Disposal (kg). 2-4
Figure 2-3. Waste Summary for A-Complex Study Area Showing Groundwater Nitrate Contours and Total Liquid Disposal. 2-5
Figure 2-4. Waste Summary for the A-Complex Study Area Showing Groundwater Nitrate Contours and Major Anion Disposal. 2-6
Figure 2-5. Waste Summary for B-Plant Southeast Study Area Showing Groundwater Nitrate Contours and Total Liquid Disposal. 2-9
Figure 2-6. Waste Summary for B-Plant Northwest Study Area Showing Groundwater Nitrate Contours and Total Liquid Disposal. 2-10
Figure 2-7. Waste Summary for the B-Plant Southeast Study Area Showing Groundwater Nitrate Contours and Major Anion Disposal. 2-11
Figure 2-8. Waste Summary for the B-Plant Northwest Study Area Showing Groundwater Nitrate Contours and Major Anion Disposal. 2-12
Figure 2-9. Waste Summary for PUREX Study Area Showing Groundwater Nitrate Contours and Total Liquid Disposal. 2-13
Figure 2-10. Waste Summary for the PUREX Study Area Showing Groundwater Nitrate Contours and Major Anion Disposal. 2-14
Figure 2-11. Waste Summary for S-Complex Southern Study Area Showing Groundwater Nitrate Contours and Total Liquid Disposal. 2-15
Figure 2-12. Waste Summary for S-Complex Northern Study Area Showing Groundwater Nitrate Contours and Total Liquid Disposal. 2-16
Figure 2-13. Waste Summary for the S-Complex Southern Study Area Showing Groundwater Nitrate Contours and Major Anion Disposal. 2-17
Figure 2-14. Waste Summary for the S-Complex Northern Study Area Showing Groundwater Nitrate Contours and Major Anion Disposal. 2-18
Figure 2-15 Waste Summary for the T-Complex Northern Study Area Showing Groundwater Nitrate Contours and Major Anion Disposal. 2-20
Figure 2-16. Waste Summary for the T-Complex Southern Study Area Showing Groundwater Nitrate Contours and Major Anion Disposal. 2-21
Figure 2-17. Waste Summary for the T-Complex Northern Study Area Showing Groundwater Nitrate Contours and Major Anion Disposal. 2-22

Figure 2-18. Waste Summary for the T-Complex Southern Study Area Showing Groundwater Nitrate Contours and Major Anion Disposal. 2-23
Figure 2-19. Waste Summary for 216-Z-16 Trench Study Area Showing Groundwater Nitrate Contours and Total Liquid Disposal. 2-25
Figure 2-20. Waste Summary for the 216-Z-16 Trench Study Area Showing Groundwater Nitrate Contours and Major Anion Disposal. 2-26
Figure 3-1: Setup of the Resistivity 4-Pole Array and Pseudo-Section Plotting Methodology. 3-3
Figure 3-2. Apparent Resistivity Pseudo-Section Comparisons for the Schlumberger, Pole-Dipole, Dipole-Dipole, and Pole-Pole Array Types for a Discrete Conductive Target in a Resistive Homogeneous Background. 3-4
Figure 3-3. A) Vertical Slices through Apparent Resistivity Data for Schlumberger, Dipole-Dipole, and Pole-Pole at 65 m (beside target) and 81 m (within target); B) Schematic of Linear and Nonlinear Pseudo-Section Plotting. 3-5
Figure 3-4. Contours of Resistivity for the Different Interpretation Algorithms Including Linear Pseudo-Section, Nonlinear Pseudo-Section, Robust Inversion (L_1-Normalization), and Smooth Inversion (L_2-Normalization). 3-7
Figure 3-5. Vertical Slices for Comparison of Interpretation Algorithms Including Pseudo-Section Apparent Resistivity and Inverted True Resistivity for a Discrete Conductive Target at A) 10 m BGS, B) 20 m BGS, and C) 30 m BGS. 3-7
Figure 4-1. Resistivity Line Locations for the 216-C-1 Survey. 4-3
Figure 4-2. Resistivity Line Locations for the A-Complex Survey. 4-5
Figure 4-3. Resistivity Line Locations for the B-Plant Survey. 4-6
Figure 4-4. Resistivity Line Locations for the PUREX Survey. 4-8
Figure 4-5. Resistivity Line Locations for the S-Complex Survey. 4-10
Figure 4-6. Resistivity Line Locations for the T-Plant Survey. 4-11
Figure 4-7. Resistivity Line Locations for the 216-Z-16 Trench Survey. 4-12
Figure 4-8. Example of Noisy Data Removal using Repeat Error and Electrical Current. 4-16
Figure 4-9. Example of Data Scatter (Plotted as Linear Pseudo-Section), Before and After Noisy Data Rejection. 4-17
Figure 4-10. Example of Spike Rejection of Transfer Resistance Data for Transmitter Electrode 237. 4-18
Figure 4-11. Initial Setting used for Inversion Stages 1 and 2. 4-22
Figure 4-12. Forward Modeling Selections used for Inversion Stages 1 and 2. 4-23
Figure 4-13. Resistivity Inversion Settings used for Inversion Stages 1 and 2. 4-25

Figure 4-14. Example of Data Removal Filter at a Maximum Limit of 5% of Total Data Removed. In this case, the data removed are in the 20% misfit histogram bin (> = 15%). 4-26
Figure 4-15. Initial Setting used for Inversion Stage 3. 4-27
Figure 4-16. Example of Inversion Error due to missing data for Line 200EPX06. 4-28
Figure 4-17. Example of Contour plot showing removal of inversion error for Line 200EPX06. 4-28
Figure 4-18. Forward Modeling Selections used for Inversion Stage 3. 4-29
Figure 4-19. Resistivity Inversion Settings used for Inversion Stage 3. 4-30
Figure 5-1. Comparison of color scales used within this report to "Hanford Site" color scale used on previous reports. 5-2
Figure 5-2. Histogram of apparent resistivity data for the 216-C-1 project site. 5-6
Figure 5-3. Inversion results for 216-C-1 Line 200EC101 5-7
Figure 5-4. Inversion Results for 216-C-1 Line 200EC102. 5-8
Figure 5-5. Inversion Results for 216-C-1 Line 200EC103. 5-9
Figure 5-6. Inversion Results for 216-C-1 Line 200EC104. 5-10
Figure 5-7. Results from the 3D Visualization at a Depth of 15 m BGS. 5-11
Figure 5-8. Results from the 3D Visualization at a Depth of 30 m BGS. 5-12
Figure 5-9. Results from the 3D Visualization at a Depth of 45 m BGS. 5-13
Figure 5-10. Results from the 3D Visualization at a Depth of 60 m BGS. 5-14
Figure 5-11. Results from the 3D Visualization at a Depth of 75 m BGS. 5-15
Figure 5-12. Histogram of apparent resistivity data for the A-complex project site. 5-16
Figure 5-13. Inversion Results for A-Complex Line 200EAC01. 5-18
Figure 5-14. Inversion Results for A-Complex Line 200EAC02. 5-19
Figure 5-15. Inversion Results for A-Complex Line 200EAC03. 5-20
Figure 5-16. Inversion Results for A-Complex Line 200EAC04. 5-20
Figure 5-17. Inversion Results for A-Complex Line 200EAC05. 5-21
Figure 5-18. Inversion Results for A-Complex Line 200EAC06. 5-21
Figure 5-19. Inversion Results for A-Complex Line 200EAC07. 5-22
Figure 5-20. Inversion Results for A-Complex Line 200EAC08. 5-22
Figure 5-21. Inversion Results for A-Complex Line 200EAC09. 5-23
Figure 5-22. Results from the 3D Visualization at a Depth of 15 m BGS. 5-24
Figure 5-23. Results from the 3D Visualization at a Depth of 30 m BGS. 5-25
Figure 5-24. Results from the 3D Visualization at a Depth of 45 m BGS. 5-26
Figure 5-25. Results from the 3D Visualization at a Depth of 60 m BGS. 5-27
Figure 5-26. Results from the 3D Visualization at a Depth of 75 m BGS. 5-28
Figure 5-27. Histogram of apparent resistivity data for the B-Plant project site. 5-30

Figure 5-28. Inversion Results for B-Plant Line 200EBP01. 5-31
Figure 5-29. Inversion Results for B-Plant Line 200EBP03. 5-31
Figure 5-30. Inversion Results for B-Plant Line 200EBP04. 5-32
Figure 5-31. Inversion Results for B-Plant Line 200EBP05. 5-33
Figure 5-32. Inversion Results for B-Plant Line 200EBP06. 5-33
Figure 5-33. Inversion Results for B-Plant Line 200EBP07. 5-34
Figure 5-34. Inversion Results for B-Plant Line 200EBP08. 5-35
Figure 5-35. Inversion Results for B-Plant Line 200EBP09. 5-36
Figure 5-36. Inversion Results for B-Plant Line 200EBP10. 5-37
Figure 5-37. Results from the 3D Visualization for B-Plant at a Depth of 15 m BGS. 5-38
Figure 5-38. Results from the 3D Visualization for B-Plant at a Depth of 30 m BGS. 5-39
Figure 5-39. Results from the 3D Visualization for B-Plant at a Depth of 45 m BGS. 5-40
Figure 5-40. Results from the 3D Visualization for B-Plant at a Depth of 60 m BGS. 5-41
Figure 5-41. Results from the 3D Visualization for B-Plant at a Depth of 75 m BGS. 5-42
Figure 5-42. Histogram of apparent resistivity data for the Purex project site. 5-44
Figure 5-43. Inversion Results for PUREX Line 200EPX02 Old Line 1 and 5. 5-45
Figure 5-44. Inversion Results for PUREX Line 200EPX03 Old Line 7. 5-45
Figure 5-45. Inversion Results for PUREX Line 200EPX04 Old Line 8. 5-46
Figure 5-46. Inversion Results for PUREX Line 200EPX06 Old Line 6. 5-46
Figure 5-47. Inversion Results for PUREX Line 200EPX08 Old Line 4. 5-47
Figure 5-48. Inversion Results for PUREX Line 200EPX09. 5-48
Figure 5-49. Inversion Results for PUREX Line 200EPX10. 5-49
Figure 5-50. Inversion Results for PUREX Line 200EPX11. 5-50
Figure 5-51. Inversion Results for PUREX Line 200EPX12. 5-51
Figure 5-52. Inversion Results for PUREX Line 200EPX13. 5-52
Figure 5-53. Inversion Results for PUREX Line 200EPX14. 5-52
Figure 5-54. Inversion Results for PUREX Line 200EPX15. 5-53
Figure 5-55. Results from the 3D Visualization for PUREX at a Depth of 15 m BGS. 5-54
Figure 5-56. Results from the 3D Visualization for PUREX at a Depth of 30 m BGS. 5-55
Figure 5-57. Results from the 3D Visualization for PUREX at a Depth of 45 m BGS. 5-56

Figure 5-58. Results from the 3D Visualization for PUREX at a Depth of 60 m BGS. 5-57
Figure 5-59. Results from the 3D Visualization for PUREX at a Depth of 75 m BGS. 5-58
Figure 5-60. Histogram of apparent resistivity data for the Purex project site. 5-60
Figure 5-61. Inversion Results for S-Complex Line 200WSC01. 5-61
Figure 5-62. Inversion Results for S-Complex Line 200WSC02. 5-62
Figure 5-63. Inversion Results for S-Complex Line 200WSC03. 5-62
Figure 5-64. Inversion Results for S-Complex Line 200WSC04. 5-63
Figure 5-65. Inversion Results for S-Complex Line 200WSC05. 5-64
Figure 5-66. Inversion Results for S-Complex Line 200WSC06. 5-65
Figure 5-67. Results from the 3D Visualization for S-Complex A at a Depth of 15 m BGS. 5-66
Figure 5-68. Results from the 3D Visualization for S-Complex A at a Depth of 30 m BGS. 5-67
Figure 5-69. Results from the 3D Visualization for S-Complex A at a Depth of 45 m BGS. 5-68
Figure 5-70. Results from the 3D Visualization for S-Complex A at a Depth of 60 m BGS. 5-69
Figure 5-71. Results from the 3D Visualization for S-Complex A at a Depth of 75 m BGS. 5-70
Figure 5-72. Results from the 3D Visualization for S-Complex B at a Depth of 15 m BGS. 5-71
Figure 5-73. Results from the 3D Visualization for S-Complex B at a Depth of 30 m BGS. 5-72
Figure 5-74. Results from the 3D Visualization for S-Complex B at a Depth of 45 m BGS. 5-73
Figure 5-75. Results from the 3D Visualization for S-Complex B at a Depth of 60 m BGS. 5-74
Figure 5-76. Results from the 3D Visualization for S-Complex B at a Depth of 75 m BGS. 5-75
Figure 5-77. Histogram of apparent resistivity data for the T-Plant project site. 5-77
Figure 5-78. Inversion Results for T-Plant Line 200WTP01. 5-78
Figure 5-79. Inversion Results for T-Plant Line 200WTP02. 5-79
Figure 5-80. Inversion Results for T-Plant Line 200WTP03. 5-80
Figure 5-81. Inversion Results for T-Plant Line 200WTP04. 5-81
Figure 5-82. Inversion Results for T-Plant Line 200WTP05. 5-82
Figure 5-83. Inversion Results for T-Plant Line 200WTP06. 5-82
Figure 5-84. Inversion Results for T-Plant Line 200WTP07. 5-83

Figure 5-85. Inversion Results for T-Plant Line 200WTP08. 5-84
Figure 5-86. Inversion Results for T-Plant Line 200WTP09. 5-85
Figure 5-87. Inversion Results for T-Plant Line 200WTP10. 5-86
Figure 5-88. Results from the 3D Visualization for T-Plant A at a Depth of 15 m BGS. 5-87
Figure 5-89. Results from the 3D Visualization for T-Plant A at a Depth of 30 m BGS. 5-88
Figure 5-90. Results from the 3D Visualization for T-Plant A at a Depth of 45 m BGS. 5-89
Figure 5-91. Results from the 3D Visualization for T-Plant A at a Depth of 60 m BGS. 5-90
Figure 5-92. Results from the 3D Visualization for T-Plant A at a Depth of 75 m BGS. 5-91
Figure 5-93. Results from the 3D Visualization for T-Plant B at a Depth of 15 m BGS. 5-92
Figure 5-94. Results from the 3D Visualization for T-Plant B at a Depth of 30 m BGS. 5-93
Figure 5-95. Results from the 3D Visualization for T-Plant B at a Depth of 45 m BGS. 5-94
Figure 5-96. Results from the 3D Visualization for T-Plant B at a Depth of 60 m BGS. 5-95
Figure 5-97. Results from the 3D Visualization for T-Plant B at a Depth of 75 m BGS. 5-96
Figure 5-98. Histogram of apparent resistivity data for the 216-Z-16 project site. 5-97
Figure 5-99. Inversion Results for 216-Z-16 Trench Line 200WZT01 5-98
Figure 5-100. Inversion Results for 216-Z-16 Trench Line 200WZT02 5-99
Figure 5-101. Inversion results for 216-Z-16 Trench Line 200WZT03. 5-99
Figure 5-102. Results from the 3D Visualization at a Depth of 15 m BGS. 5-100
Figure 5-103. Results from the 3D Visualization at a Depth of 30 m BGS. 5-101
Figure 5-104. Results from the 3D Visualization at a Depth of 45 m BGS. 5-102
Figure 5-105. Results from the 3D Visualization at a Depth of 60 m BGS. 5-103
Figure 5-106. Results from the 3D Visualization at a Depth of 75 m BGS. 5-104

LIST OF TABLES

Table 4-1. Listing of Old and New Resistivity Line Names. 4-7
Table 4-2. Calibration 4-13
Table 4-3. Comparison of contact resistance values for each project site. 4-15

Table 4-4. Specific Line Information for HRR Data Collected within the 200 East Area. 4-19
Table 4-5. Specific Line Information for HRR Data Collected within the 200 West Area. 4-20
Table 5-1. Final Inversion Statistics for the 216-C-1 Waste Site. 5-5
Table 5-2. Final Inversion Statistics for A-Complex. 5-16
Table 5-3. Final Inversion Statistics for B-Plant. 5-29
Table 5-4. Final Inversion Statistics for PUREX Plant. 5-43
Table 5-5. Final Inversion Statistics for S-Complex. 5-59
Table 5-6. Final Inversion Statistics for T-Plant. 5-76
Table 5-7. Final Inversion Statistics for the 216-Z-16 Trench Waste Site. 5-97

LIST OF TERMS

Electrical Conductivity: The ability of a material to transmit or conduct an electric current; reciprocal of resistivity.

Infrastructure: A collective grouping of any subsurface or surface man made or artificial mechanical structures or devices that are likely to be adverse to resistivity data quality. Infrastructure may include, surface and subsurface structures, foundations, concrete pads with rebar, railway lines, pipes, utilities, fences, disposal cribs, wells, disposal trenches or any other linear metallic and conductive items.

Inversion: Inversion, or inverse modeling, attempts to reconstruct subsurface features from a given set of geophysical measurements, and to do so in a manner that the model response fits the observations according to some measure of error.

Resistance: The opposition of a material to current passing through it; received voltage normalized by transmitted current.

Resistivity: A material property that is measured as its resistance to current per unit length for a uniform cross-section; reciprocal of conductivity.

Tomography: A method of producing a three-dimensional image of a volumetric object (plume) by the observation and recording of the differences in the effects on the passage of waves of energy impinging on that object.

LIST OF ABBREVIATIONS AND ACRONYMS

2D	two-dimensional
3D	three-dimensional
ATV	all-terrain vehicle
BGS	belowground surface
.DAT	data file
DC	direct current
DIC	depth of investigation characteristics
DOE	U.S. Department of Energy
ERT	electrical resistivity tomography
GIS	Geographical Information System
GPS	Global Positioning System
HAZWOPER	Hazardous Waste Operations and Emergency Response
HGET	Hanford General Employee Training

HGI	hydroGEOPHYSICS, Inc.
HRR™	High Resolution Resistivity
I.D.	identification (number)
IP	induced polarization
L_2	measure of data misfit normalized to the number of data points
OSHA	Occupational Safety and Health Administration
PFP	Plutonium Finishing Plant
PNNL	Pacific Northwest National Laboratory
PPE	personal protection equipment
PUREX	Plutonium-Uranium Extraction (Plant)
QA	quality assurance
QC	quality control
RFP	Request for Proposal
RMS	root-mean-square
RTK	Real-Time Kinematic
USGS	U.S. Geological Survey
.STG	Sting™ file format
SOW	Scope of Work
STS	surface-to-surface
UPR	unplanned release
WTW	well-to-well
WIDS	waste information database system

Units

cm	centimeter
kg	kilograms
km	kilometers
m	meter
MGal	million gallons
mg/L	milligrams per liter
ohm-m	Ohm-meters

™ High Resolution Resistivity (HRR) is a trademark of hydroGEOPHYSICS, Inc., Tucson, Arizona.
™ Sting is a trademark of Advanced Geosciences, Inc. in the United States, other countries, or both.

1.0 INTRODUCTION

1.1 SITE LOCATION

The Hanford Site is located in the south-central portion of Washington State in the Columbia River Valley near Richland, Washington. The areas of interest are located within both the 200 East and 200 West areas of the Hanford Site. Sites within the 200 East area selected for this investigation are A-Complex (216-A-7, 216-A-8, and 216-A-19), Plutonium-Uranium Extraction (PUREX) Plant (216-A-10, 216-A-36A & -B and 216-A-45), B-Plant (216-B-6, 216-B-10A & -B, 216-B-12 and 216-B-55), and 216-C-1. Sites within the 200 West area included in this investigation are S-Complex (216-S-9 and 216-S-13), (216-Z-16), and T-Plant (216-T-6, 216-T-34, 216-T-35). Figure 1-1 shows the locations of the electrical resistivity surveys for these areas. The two areas include waste sites comprised of unlined disposal trenches, ponds, and disposal cribs, which were used for the planned disposal of liquid waste derived from uranium and plutonium processing.

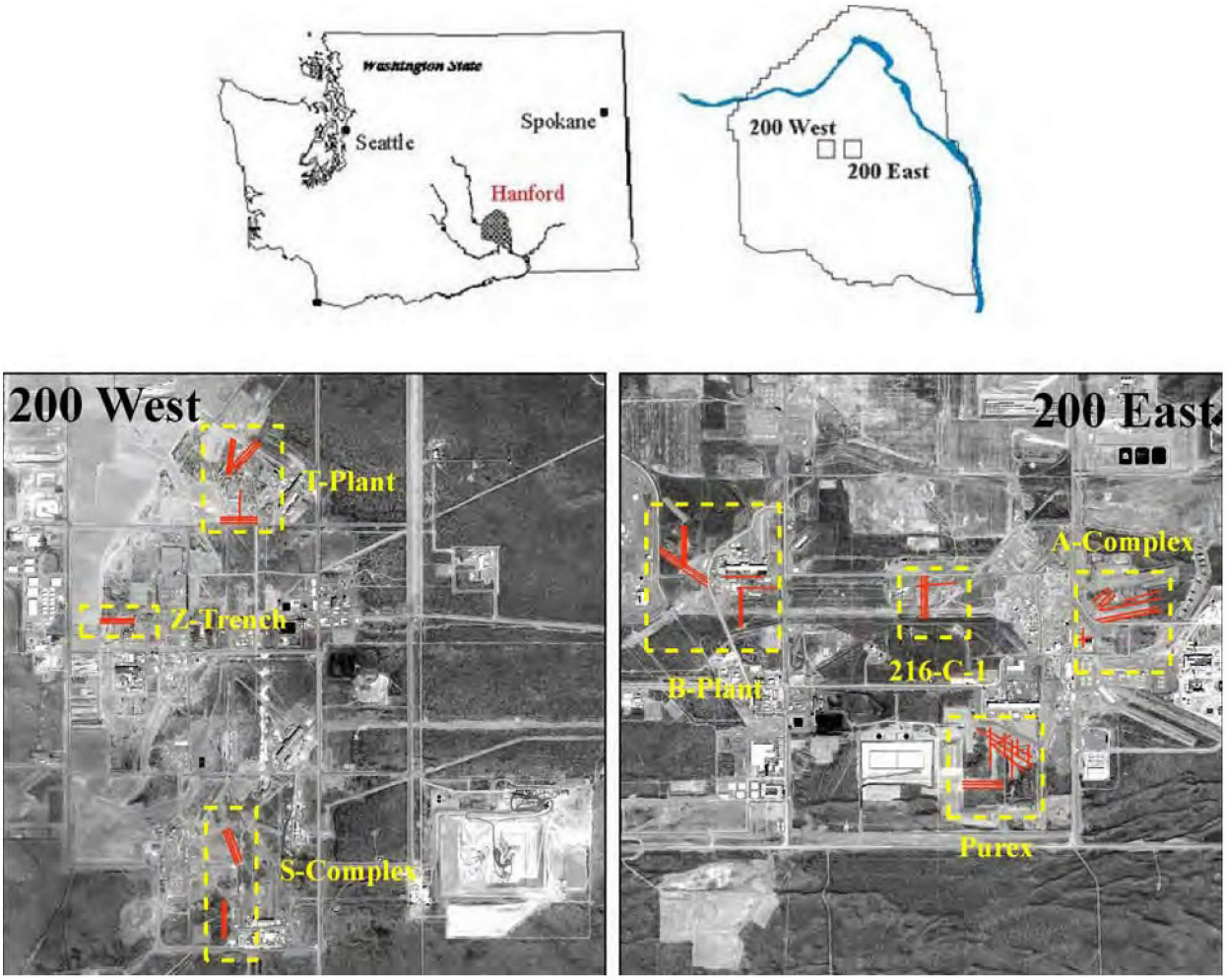

Figure 1-1. General Site Map Showing Location of Resistivity Surveys at the 200 West and 200 East Areas.

1.2 OBJECTIVE OF INVESTIGATION

The principal objective of the investigation was to characterize subsurface electrical properties within the selected waste sites using the electrical resistivity method. The electrical resistivity method is a geophysical technique that aims to discriminate differences in the material property electrical resistivity, which describes a resistance of electrical current flow. The geophysical characterization focused on the evaluation of subsurface areas that possess anomalously low electrical resistivity that could be ascribed to past waste disposal practices.

1.3 SCOPE OF WORK

The Scope of Work (SOW) was performed under contract to Battelle Memorial Institute, Pacific Northwest Division (Battelle) for work requested within Pacific Northwest National Laboratory (PNNL) Request for Proposal (RFP) Number 51569. PNNL and Fluor Hanford, Inc. specified the selected methodology and survey layout including line location, spacing, orientation, and survey coverage within the contract. PNNL and Fluor Hanford, Inc. selected the method of data processing (i.e., two-dimensional [2D] inversion), plotting (i.e., 2D cross-section contour maps), and three-dimensional (3D) visualization of 2D inversion data.

hydroGEOPHYSICS, Inc. (HGI) developed a survey design to address the specifics of the SOW, including selection of equipment, inversion software, and electrode spacing. The electrode spacing was selected by HGI in response to the target depth of investigation specified within the RFP. Inversion software was selected based on successful performance criteria and ability to match hardware and software platforms. Equipment was selected based on prior use, as well as the ability to meet both the geophysical and site safety requirements.

2.0 BACKGROUND

All Hanford processing areas produced radioactive liquid waste, which was disposed to the soil adjacent to the facility generating the waste (Battelle Press 2003). The primary method for introducing the liquid waste to the soil was through French drains, cribs, trenches, reverse wells, and ponds. Disposal methods were chosen based on disposal standards of the time, type of radionuclide, and the specific concentration of materials in the waste product.

Cribs were constructed of concrete walls and loosely spaced timber floors several meters belowground level. The underground chambers created cavities approximately 10s of cubic meters in size where liquid waste was introduced and allowed to percolate into the underlying soil (Battelle Press 2003). "The central plateau of Hanford was considered ideal for waste disposal because it was underlain by 200 feet of nearly dry sediment that acted like a sponge to physically retain contaminates" (Gephart 2003).

The electrical resistivity surveys discussed in this report are divided into seven study areas that are within 200 East and 200 West. The 200 East study areas include 216-C-1, A-Complex, B-Plant, and PUREX, and the 200 West study areas include S-Complex, T-Plant, and 216-Z-16 Trench. Data derived from the *Hanford Soil Inventory Model* (PNNL-15367) was used to generate a series of waste disposal illustrations for the seven study areas. Figures 2-1 through 2-20 show the resistivity survey lines, site infrastructure, and groundwater nitrate concentrations plotted with respect to either total volume of waste disposed or anion distribution.

2.1 216-C-1 STUDY AREA DISPOSAL SUMMARY

The 216-C-1 study area is dominated by subsurface infrastructure (blue lines on Figures 2-1 and 2-2) as well as surface structures that include aboveground piping, concrete pads, small buildings, and mounded dirt with concrete. The abundant subsurface infrastructure will adversely affect the electrical resistivity data because it provides a preferential current pathway, which results in distorted resistivity values. Figure 2-1 shows several liquid disposal sites within the study area reporting less than 1 mGal and two larger disposal volumes less than 10 mGal located at the 216-C-1 waste information database system (WIDS) site and the 216-C-9 WIDS site just north of the study area.

In addition to the changes in saturation of the subsurface, electrical resistivity is sensitive to the concentration of electrolytes. The electrolytes are inorganic constituents that have free ions capable of carrying an electrical charge (e.g., nitrate or sulfate compounds). Figure 2-2 shows the distribution of major anions disposed within the 216-C-1 study area, of which the most significant anion disposal is the 216-C-1 WIDS site. Assuming a homogeneous subsurface geology, the increase in anions should decrease the electrical resistivity of the soil.

Because of the high volumes of disposal around the site, nitrate and other analytes have reached the water table (approximately 80 m belowground surface [BGS]) at several locations. Figures 2-1 and 2-2 show contour lines representing the distribution of nitrate from groundwater monitoring wells recorded during the period of July 2003 through January 2004. The contours of the nitrate concentration were developed with an inverse distance interpolation scheme. There are only three wells with reported nitrate data that define the nitrate contour distribution within

the study area as presented in Figures 2-1 and 2-2. Monitoring well 299-E24-8 is located just southwest of the 216-C-1 WIDS site and shows a 15 mg/L nitrate concentration. The distribution increases towards the northeast (92 mg/L – 299-E27-4) and to a lesser degree towards the southeast (26 mg/L – 299-E24-5).

2.2 A-COMPLEX STUDY AREA DISPOSAL SUMMARY

By contrast, the A-Complex study area has few subsurface infrastructure components (blue lines on Figures 2-3 and 2-4), but the southern portion does contain paved roads and a large retention basin (207-A-North and South). In general, the subsurface and aboveground infrastructure increases to the west towards AX farm and to the southwest towards AP farm. Figure 2-3 shows four liquid disposal sites near the survey lines (shown in red) reporting less 1 mGal and two larger disposal volumes between 11 to 100 mGal located at the 216-A-8 trench and the 216-A-24 trench. Several other liquid releases are located within and surrounding AX farm and are all less than 1 mGal.

Figure 2-4 shows the distribution of major anions disposed within the A-Complex study area of which the most significant disposal anion was sulfate over the 216-A-8 and 216-A-24 trenches.

Both Figures 2-3 and 2-4 contain contour lines representing nitrate concentrations from reporting wells in 2003 and 2004. There are only three wells with reported nitrate data that define the nitrate contour distribution within the study area presented in Figures 2-3 and 2-4. For the study area, the nitrate distribution increases towards the southwest controlled by data from monitoring well 299-E25-2 (90 mg/L) and towards the north controlled by monitoring well 299-E26-5 (88 mg/L). The lowest nitrate concentration occurs over the 216-A-8 trench with contours representing less than 10 mg/L.

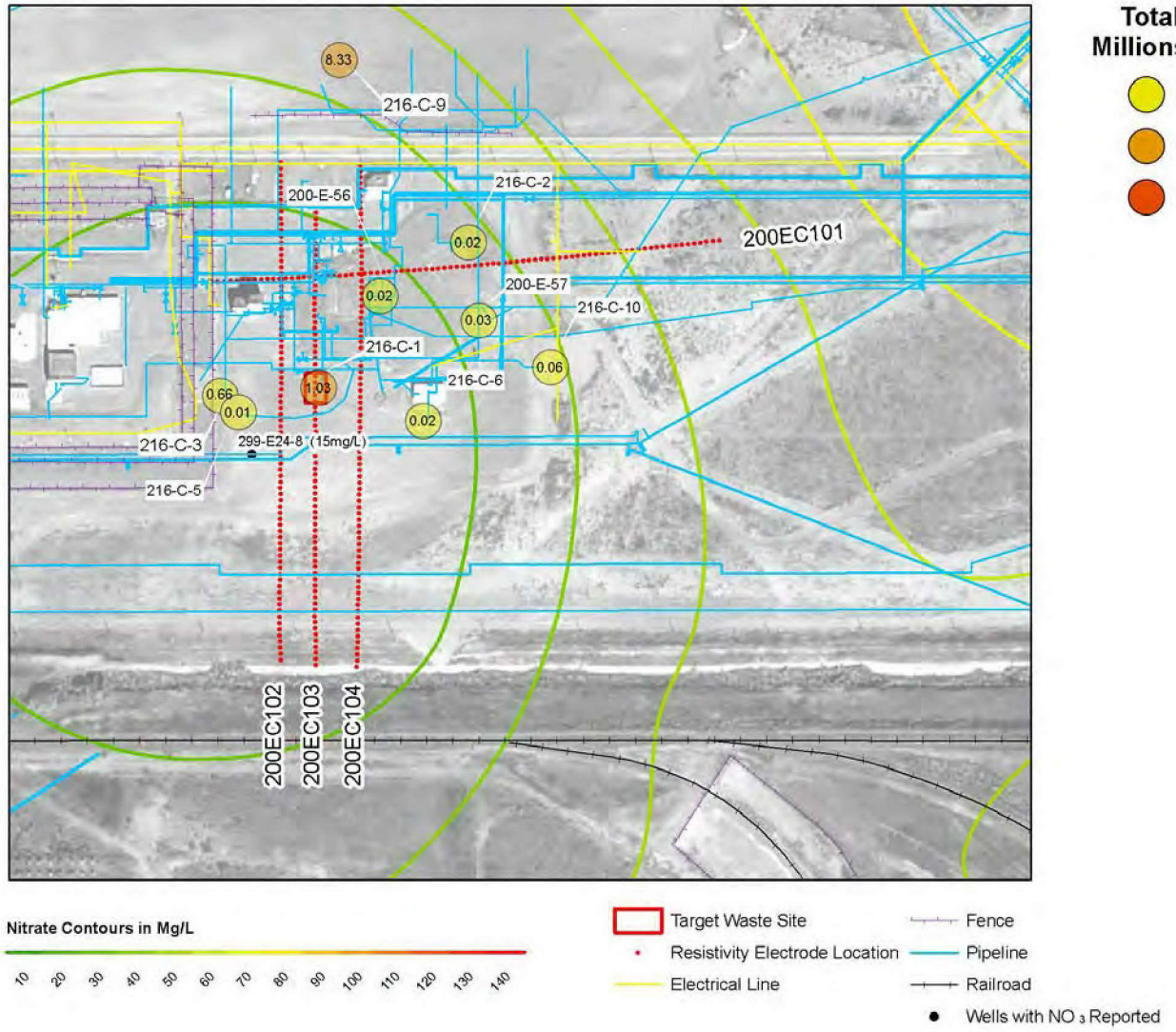

Figure 2-1. Waste Summary for the 216-C-1 Study Area Showing Groundwater Nitrate Contours (mg/L) and Total Liquid Disposal (mGal).

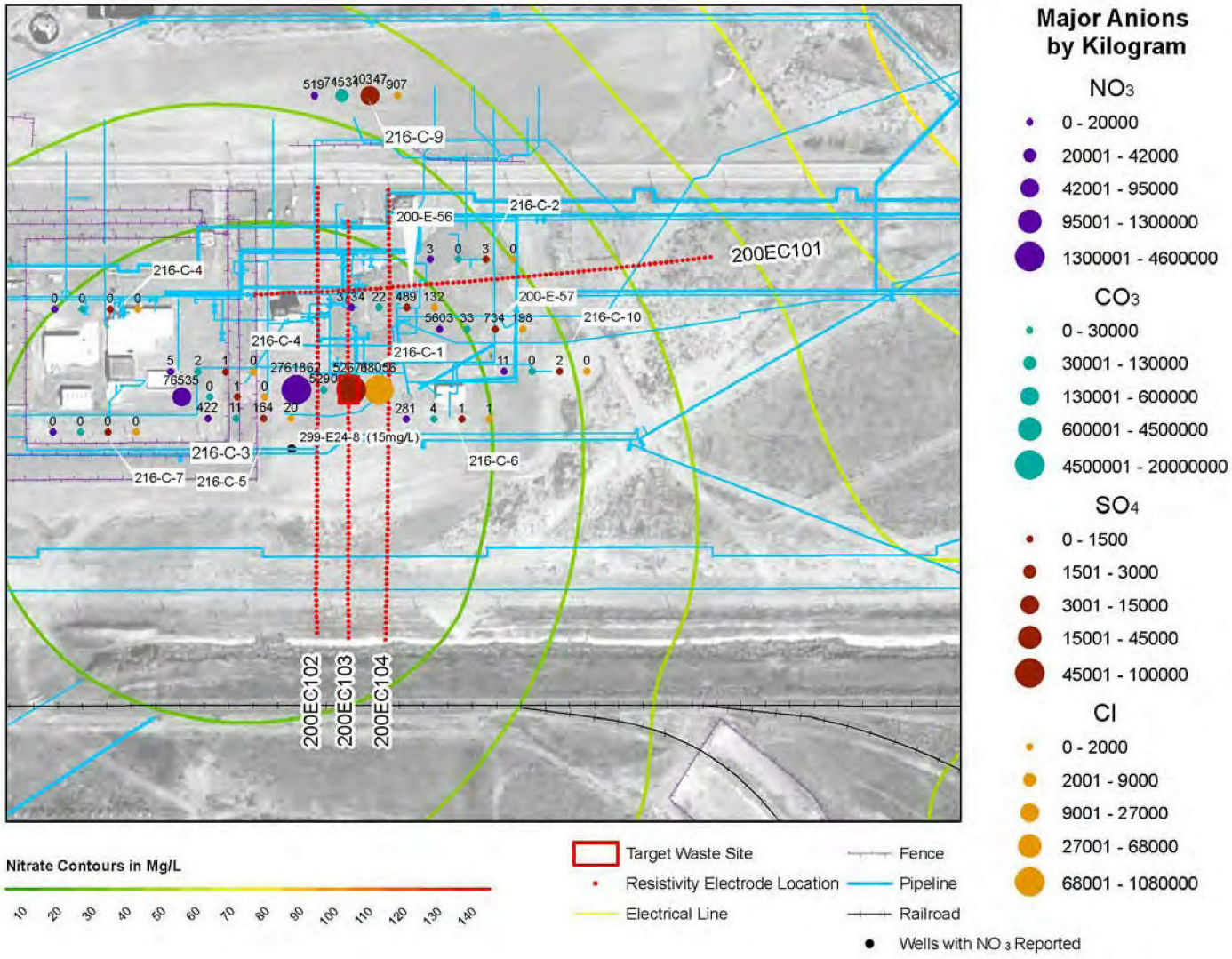

Figure 2-2. Waste Summary for the 216-C-1 Study Area Showing Groundwater Nitrate Contours (mg/L) and Major Anion Disposal (kg).

www.hgiworld.com
2302 NORTH FORBES BLVD., TUCSON, ARIZONA 85745
tel: 520.647.3315 fax: 520.647.3428

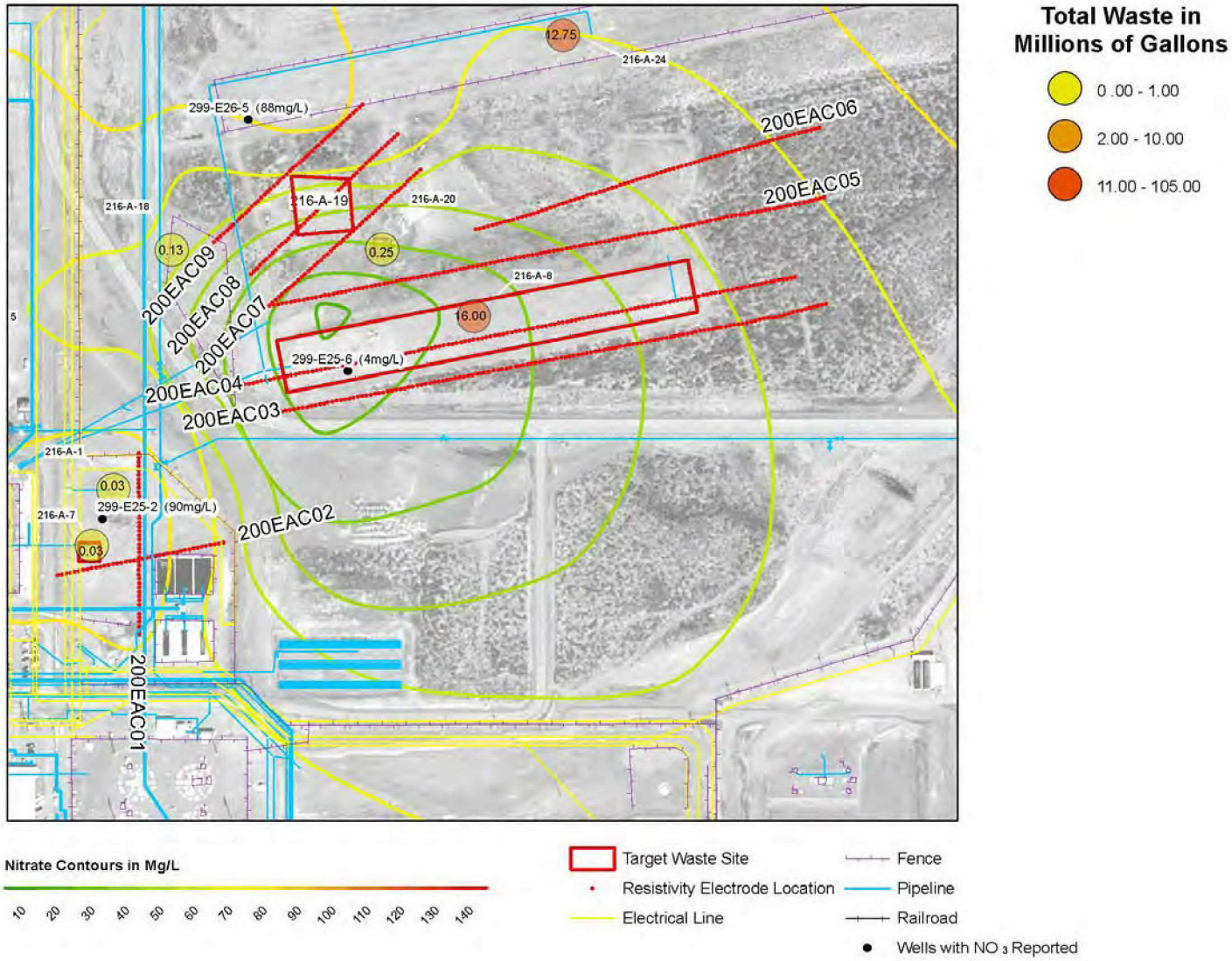

Figure 2-3. Waste Summary for A-Complex Study Area Showing Groundwater Nitrate Contours and Total Liquid Disposal.

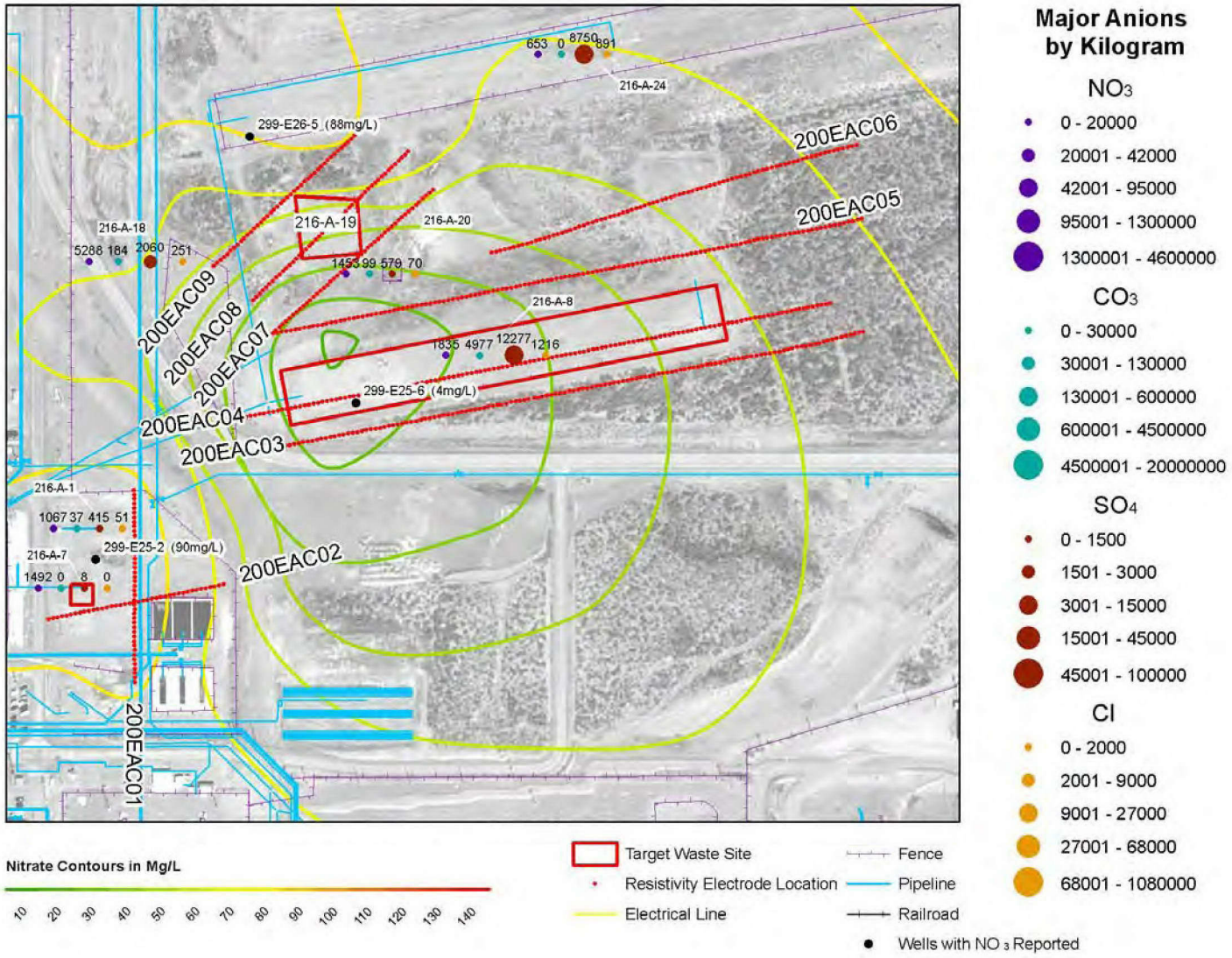

Figure 2-4. Waste Summary for the A-Complex Study Area Showing Groundwater Nitrate Contours and Major Anion Disposal.

www.hgiworld.com
2302 NORTH FORBES BLVD., TUCSON, ARIZONA 85745
tel: 520.647.3315 fax: 520.647.3428

2.3 B-PLANT STUDY AREA DISPOSAL SUMMARY

The B-Plant study area represents an industrial complex that is dominated by aboveground structures, paved roads, compacted and grouted soil area, and concrete slabs. In addition, the area contains an abundance of subsurface infrastructure components that include utilities, disposal cribs, and trenches (blue lines on Figures 2-5 through 2-8). The majority of the infrastructure is located within and surrounding B-Plant with extensions to the south and west.

Figure 2-6 shows two large liquid disposal sites near the survey lines (shown in red) reporting between 10 and 100 mGal. The sites are located at the 216-B-55 trench and the 216-B-12 WIDS site. Several other liquid release are located within and surrounding B-Plant facility and are all less than 1 mGal.

Figures 2-7 and 2-8 show the distribution of major anions disposed within the B-Plant study area of which the most significant disposal anion was nitrate over at the 216-B-12 WIDS site, which exceeded 1,300,000 kg. Another nitrate high exists just south of B-Plant at the 216-B-6 WIDS site showing over 95,000 kg. The 216-B-55 trench shows an increase in sulfate (over 3,000 kg) and carbonate (over 30,000 kg). Several other smaller disposal areas exist within the B-Plant industrial complex.

Figures 2-5 through 2-8 contain contour lines representing nitrate concentrations from reporting wells in 2003 and 2004. The information presented herein is extrapolated from nearby monitoring wells as no monitoring wells reporting nitrate concentrations exist within the study area boundaries shown in Figures 2-5 through 2-8. Therefore, the contour lines for this study area are poorly defined and caution should be used when relating nitrate concentrations to other geophysical data. However, nitrate concentrations appear to increase from 30 to 40 mg/L in the southeast to over 100 mg/L in the northwest.

2.4 PUREX STUDY AREA DISPOSAL SUMMARY

The northern PUREX study area represents another industrial complex that is dominated by aboveground structures, paved roads, compacted and grouted soil areas, and concrete slabs. In addition, the northern area contains an abundance of subsurface infrastructure components that include utilities, disposal cribs, and trenches (blue lines on Figures 2-9 and 2-10). In general, the majority of the infrastructure is located within and surrounding the PUREX Plant which is north of the geophysical survey lines. Some scattered subsurface utilities extend south from PUREX and cross several of the resistivity survey lines.

Figure 2-9 shows several large volume liquid disposal sites south of PUREX that range in size from 2 mGal to 1000 mGal. The largest two disposal volumes are located at the 216-A-5 WIDS site (over 100 mGal) and over the 216-A-10 WIDS site (over 100 mGal). The 216-A-45, 216-A-21, and 216-A-36B WIDS sites also receiving between 10 and 100 mGal. Several other smaller liquid waste disposal sites occur within the project site.

Figure 2-10 shows the distribution of major anions disposed within the PUREX study area of which the most significant disposal anion was nitrate, sulfate, and chlorine. Nitrate exceeding 95,000 kg was disposed at the 216-A-2, 216-A5, 216-A10, 216-A-21, 216-A-36B and the 216-A-45 WIDS sites. The two largest chlorine disposal areas are over the 216-A-10 and 216-A-5 sites both exceeding 68,000 kg.

Figures 2-9 and 2-10 contain contour lines representing nitrate concentrations from reporting wells in 2003 and 2004. Only one monitoring well reporting nitrate concentrations exists within the study area boundaries shown in Figures 2-9 and 2-10. Therefore, the contour lines for this study area are poorly defined and caution should be used when relating nitrate concentrations to other geophysical data. Well 299-E17-1 is located just south of the 216-A-10 WIDS site and shows a nitrate concentration of 122 mg/L. This high concentration value forms a "hot spot" within the nitrate contour distribution centered just south of the PUREX Plant.

2.5 S-COMPLEX STUDY AREA DISPOSAL SUMMARY

The S-Complex study area is located between the S, SX and SY Tank Farms and the 202S Facility. In contrast to many of the other study areas, there is little surface infrastructure other than fences, roads and disturbed soil areas. However, there is an abundance of subsurface infrastructure (likely utilities and transfer lines) that connect the tank farms to the west to the 202S Facility to the east. Several known infrastructure lines (blue) cross the resistivity survey lines (red) as seen in Figures 2-11 through 2-14.

Figures 2-11 and 2-12 show several large volume liquid disposal sites within the study area that range in size from 2 mGal to 1000 mGal. The three largest disposal volumes are located at the 216-S-1 and -2 (10 to 100 mGal), the 216-S-7 (100 to 1000 mGal), and the 216-S-9 WIDS site (10 to 100 mGal). Two smaller liquid disposal areas for volumes between 2 and 10 mGal exist at 216-S-8 and 216-S-13. Several other smaller liquid waste disposal sites occur within the project site mostly centered on the SX Tank Farm.

Figures 2-13 and 2-14 show the distribution of major anions disposed within the S-Complex study area of which the most significant disposal area is the 216-S-8 WIDS site located just east of SX farm and the 216-S-7 WIDS site located between the two groupings of resistivity survey lines. The 216-S-8 site contains elevated nitrate (over 1,300,000 kg), sulfate (over 15,000 kg), and chlorine (over 27,000 kg). The 216-S-7 contains high nitrate levels with a reported disposal greater than 95,000 kg. Several other smaller disposal volumes exist within the project area.

Figures 2-11 through 2-14 contain contour lines representing nitrate concentrations from reporting wells in 2003 and 2004. The information presented herein is extrapolated from nearby monitoring wells as no monitoring wells reporting nitrate concentrations exist within the study area boundaries shown in Figures 2-11 through 2-14. Therefore, the contour lines for this study area are poorly defined and caution should be used when relating nitrate concentrations to other geophysical data. However, nitrate concentrations appear to increase from 20 mg/L over SX farm (west) to over 100 mg/L towards the south.

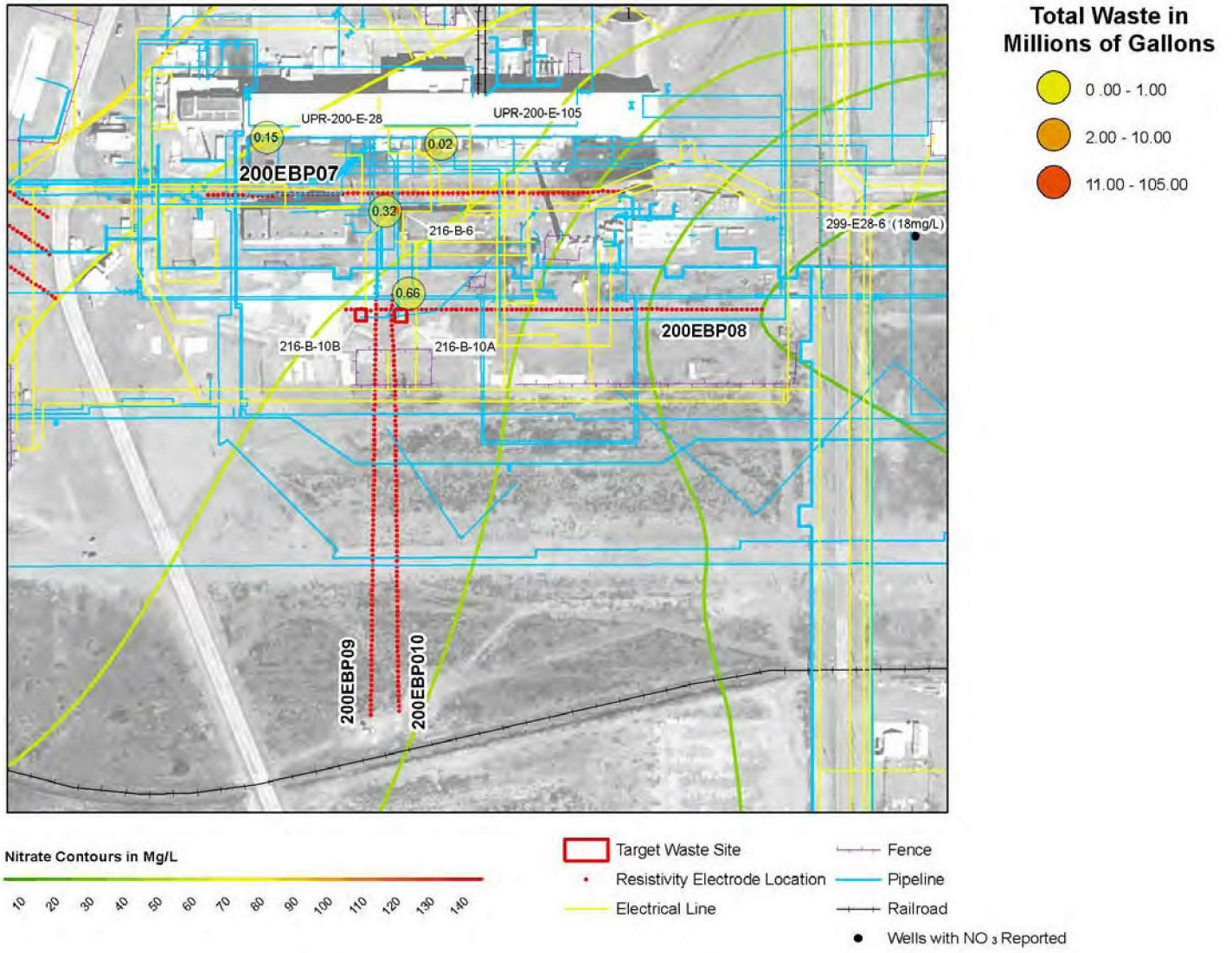

Figure 2-5. Waste Summary for B-Plant Southeast Study Area Showing Groundwater Nitrate Contours and Total Liquid Disposal.

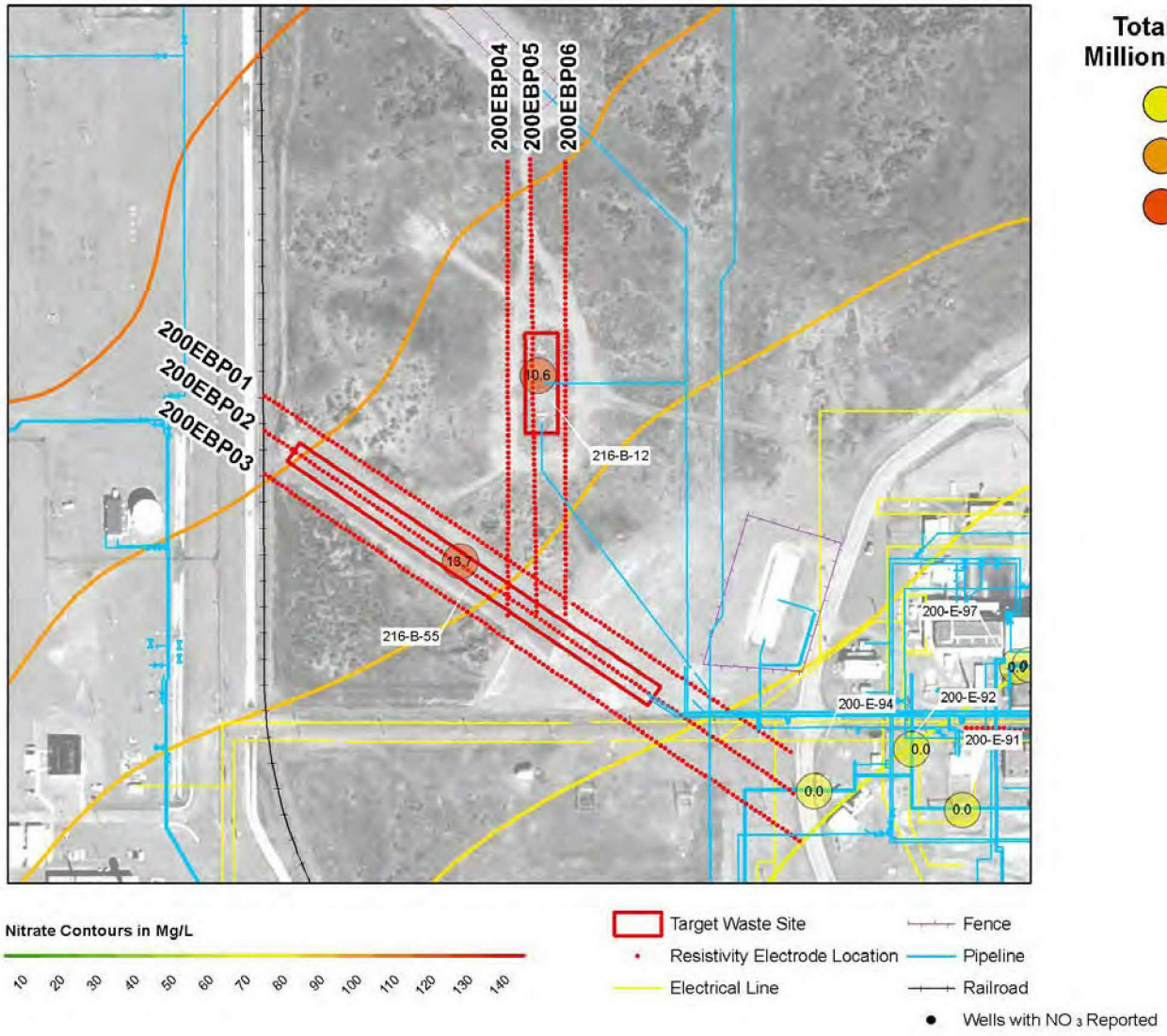

Figure 2-6. Waste Summary for B-Plant Northwest Study Area Showing Groundwater Nitrate Contours and Total Liquid Disposal.

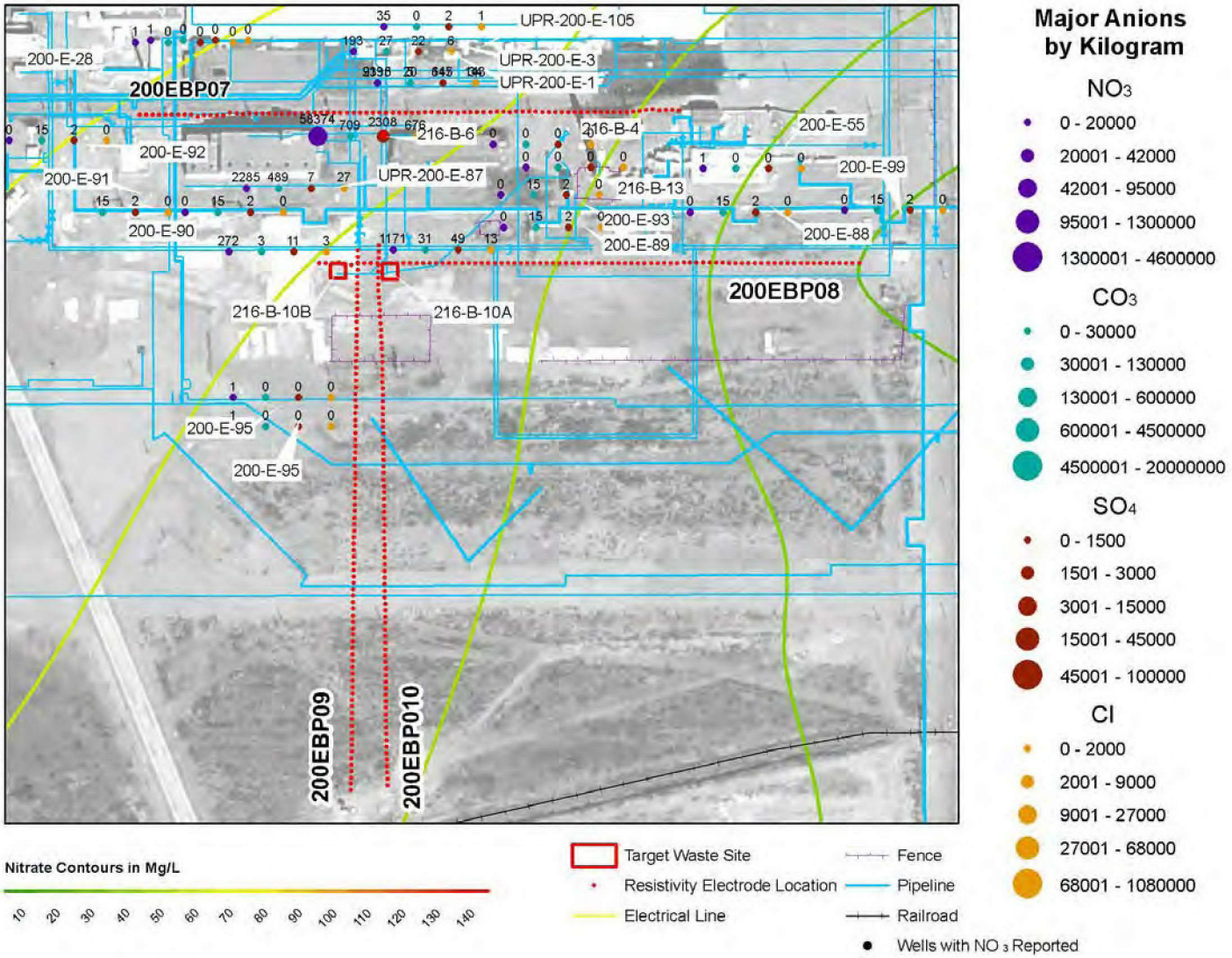

Figure 2-7. Waste Summary for the B-Plant Southeast Study Area Showing Groundwater Nitrate Contours and Major Anion Disposal.

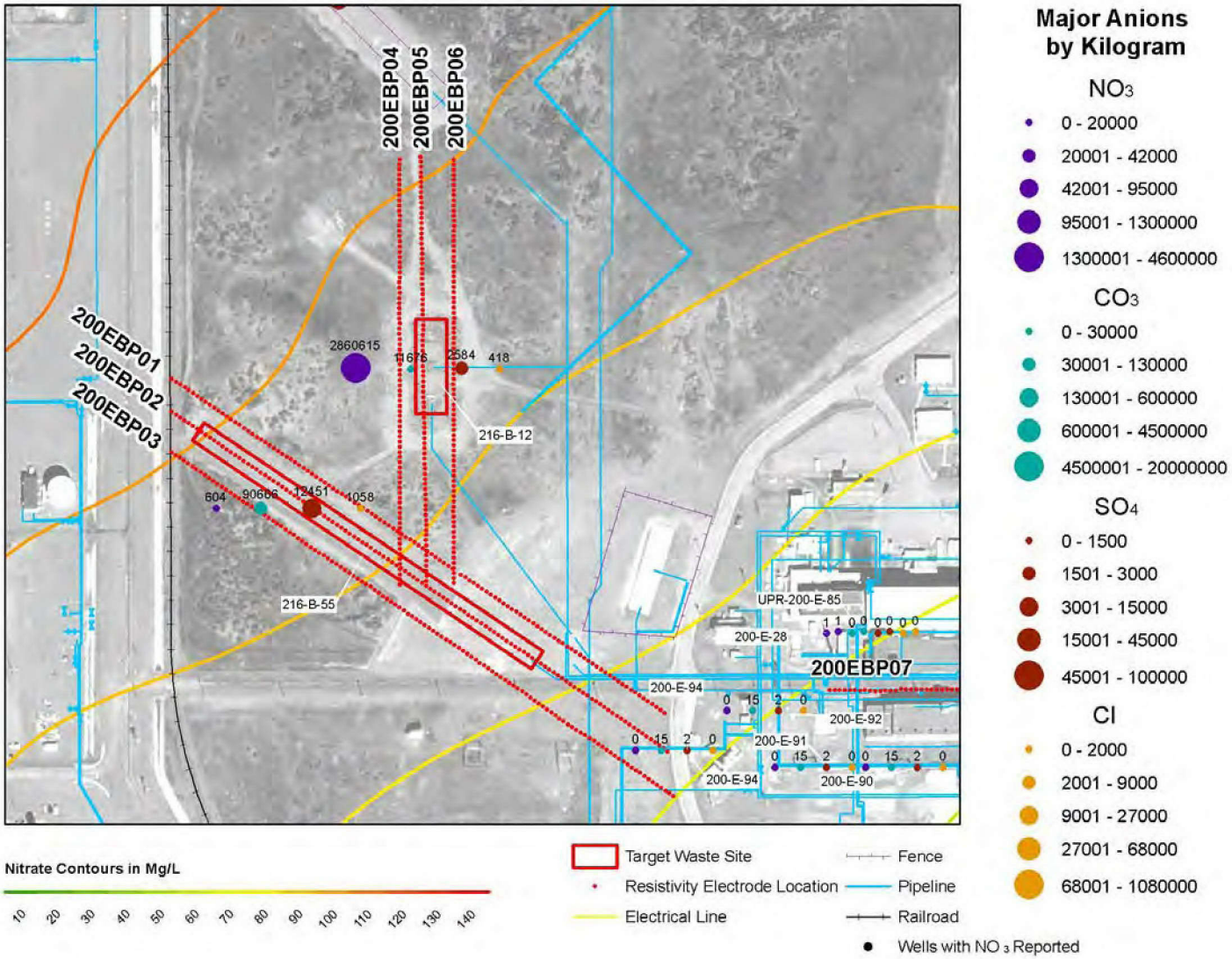

Figure 2-8. Waste Summary for the B-Plant Northwest Study Area Showing Groundwater Nitrate Contours and Major Anion Disposal.

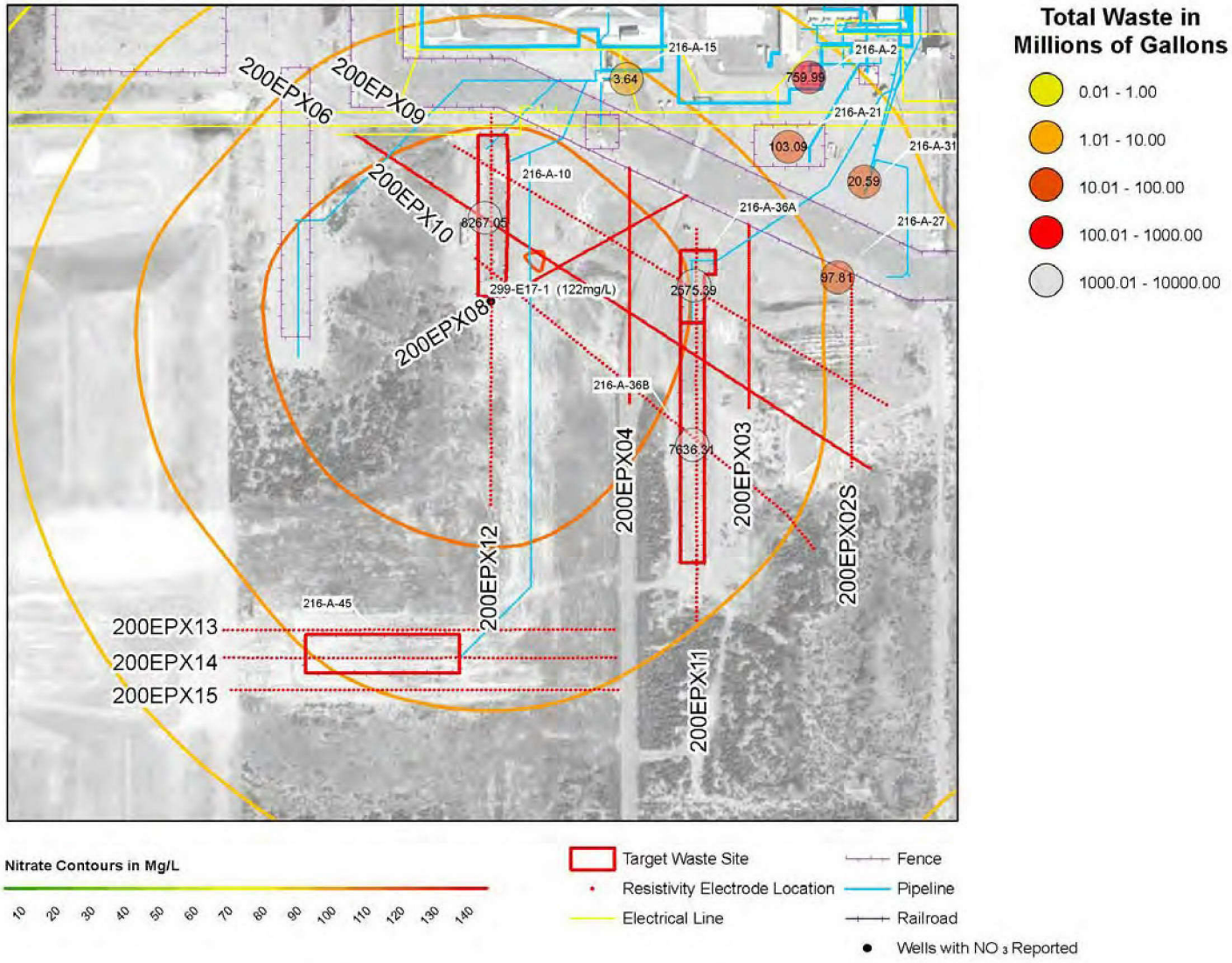

Figure 2-9. Waste Summary for PUREX Study Area Showing Groundwater Nitrate Contours and Total Liquid Disposal.

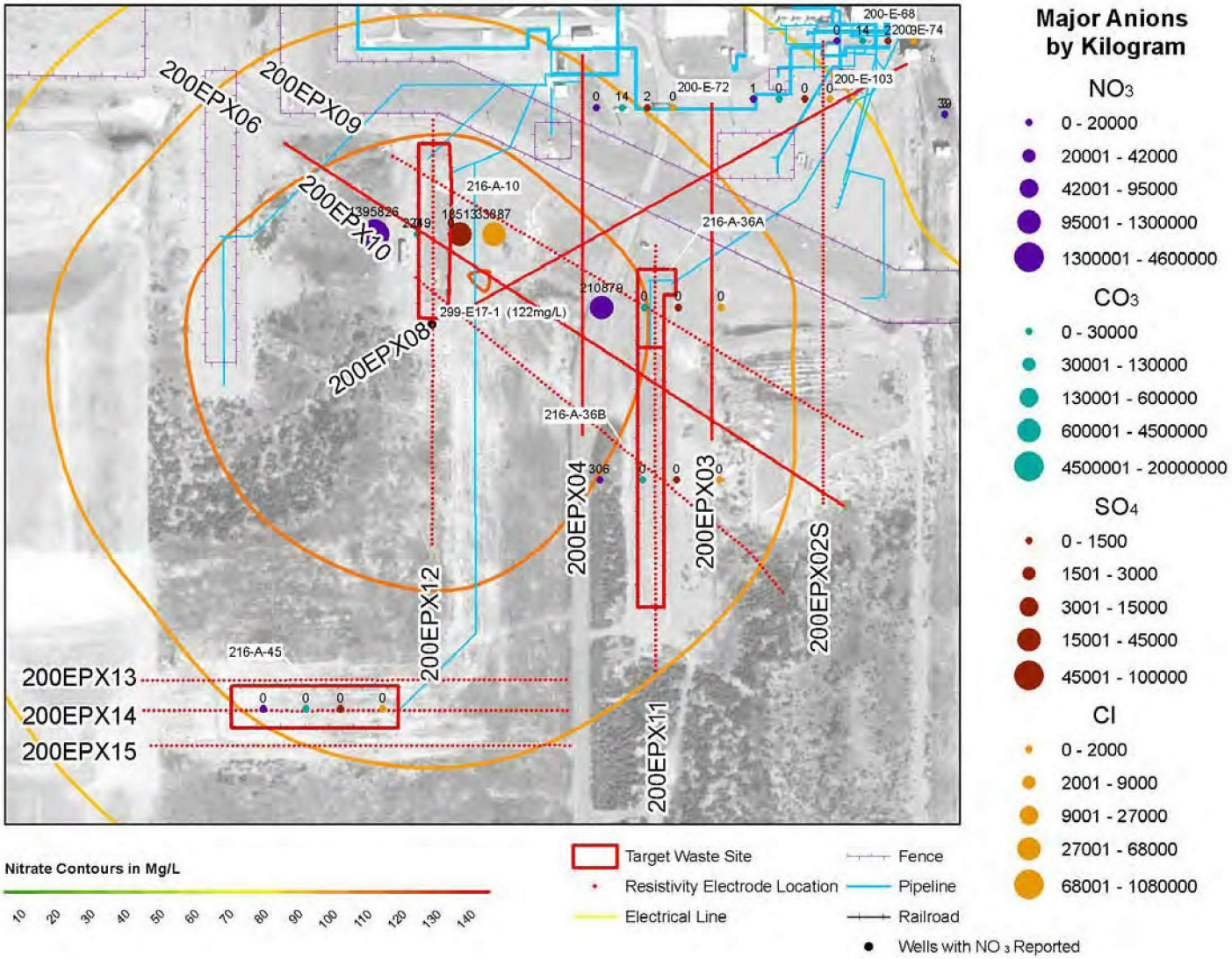

Figure 2-10. Waste Summary for the PUREX Study Area Showing Groundwater Nitrate Contours and Major Anion Disposal.

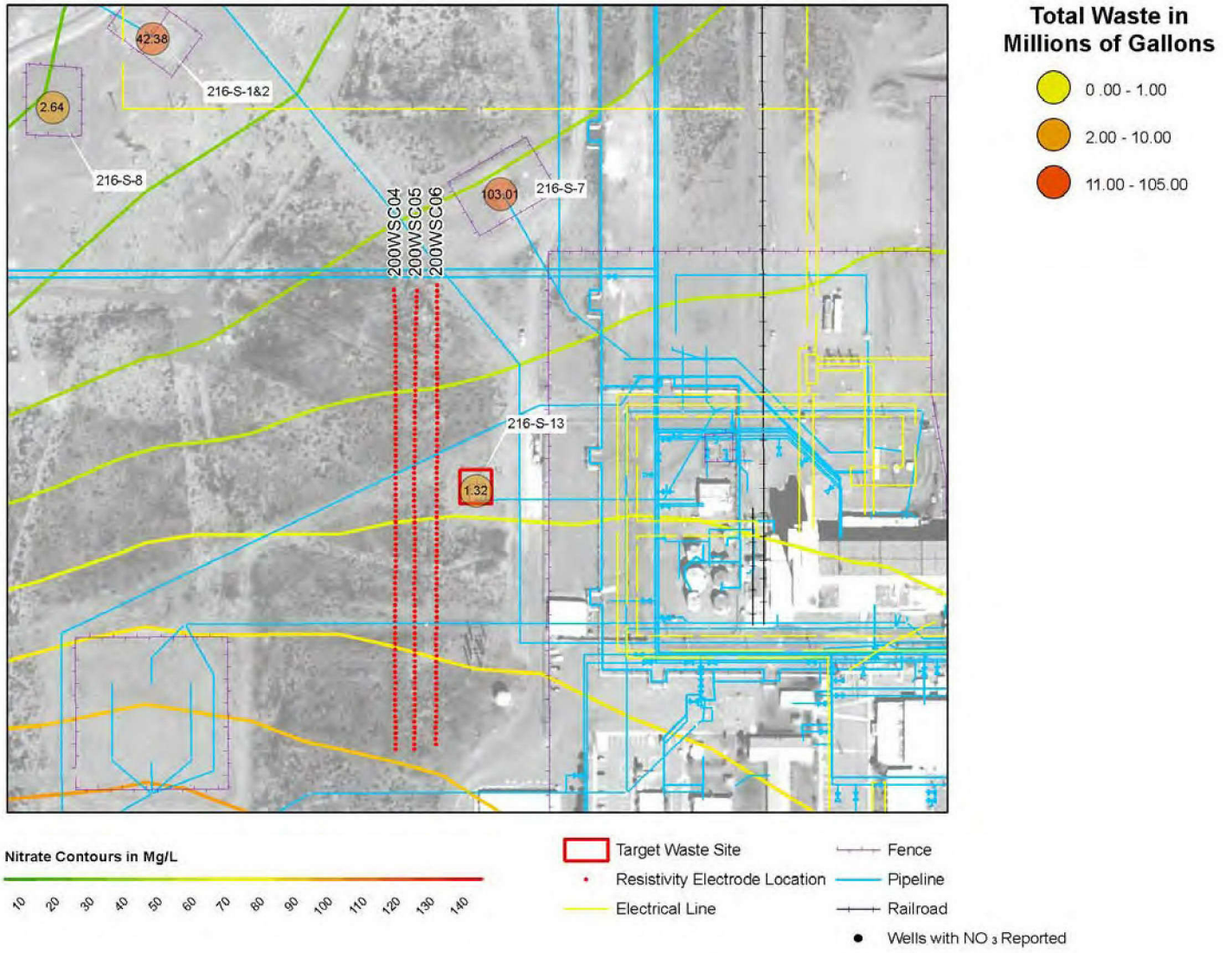

Figure 2-11. Waste Summary for S-Complex Southern Study Area Showing Groundwater Nitrate Contours and Total Liquid Disposal.

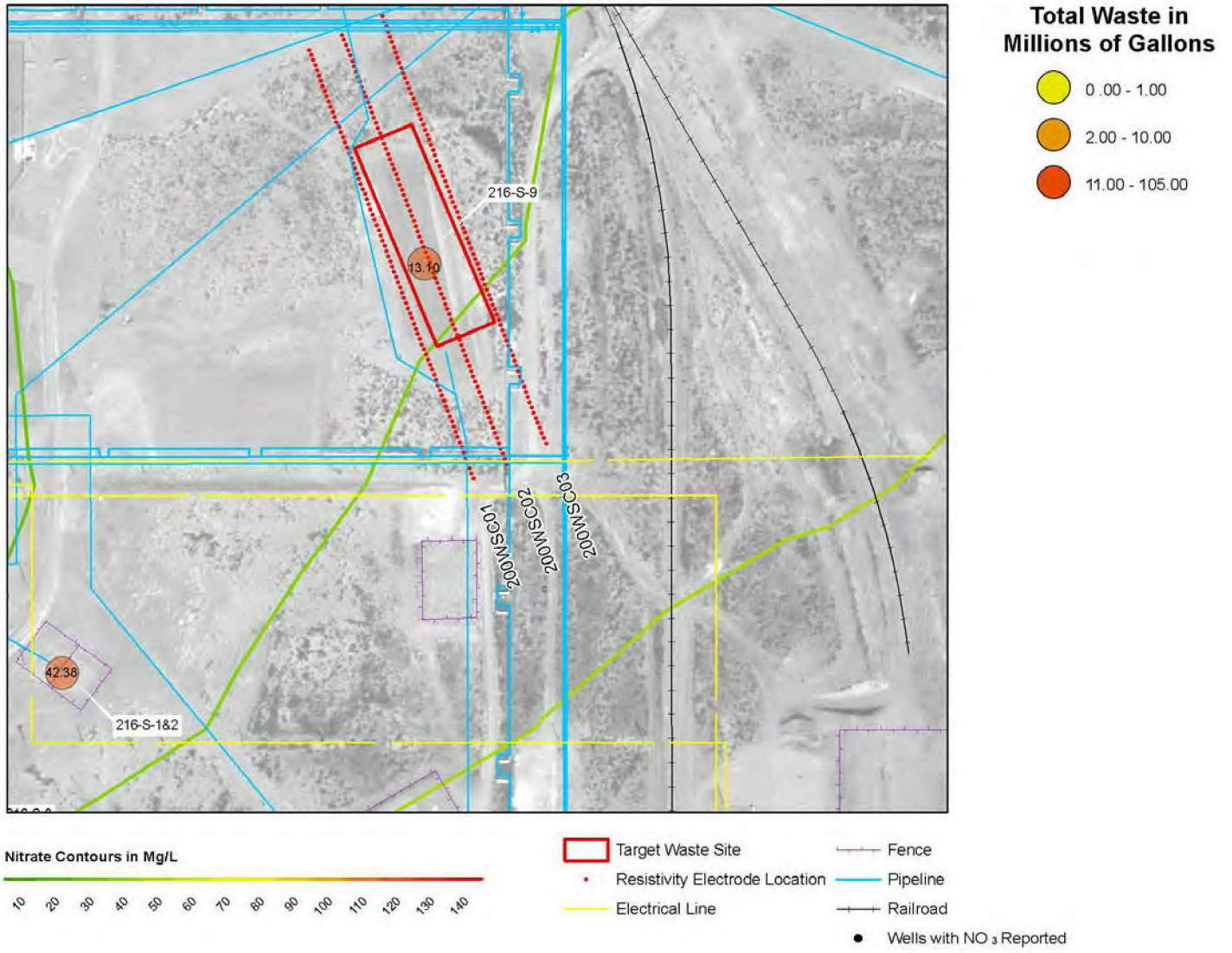

Figure 2-12. Waste Summary for S-Complex Northern Study Area Showing Groundwater Nitrate Contours and Total Liquid Disposal.

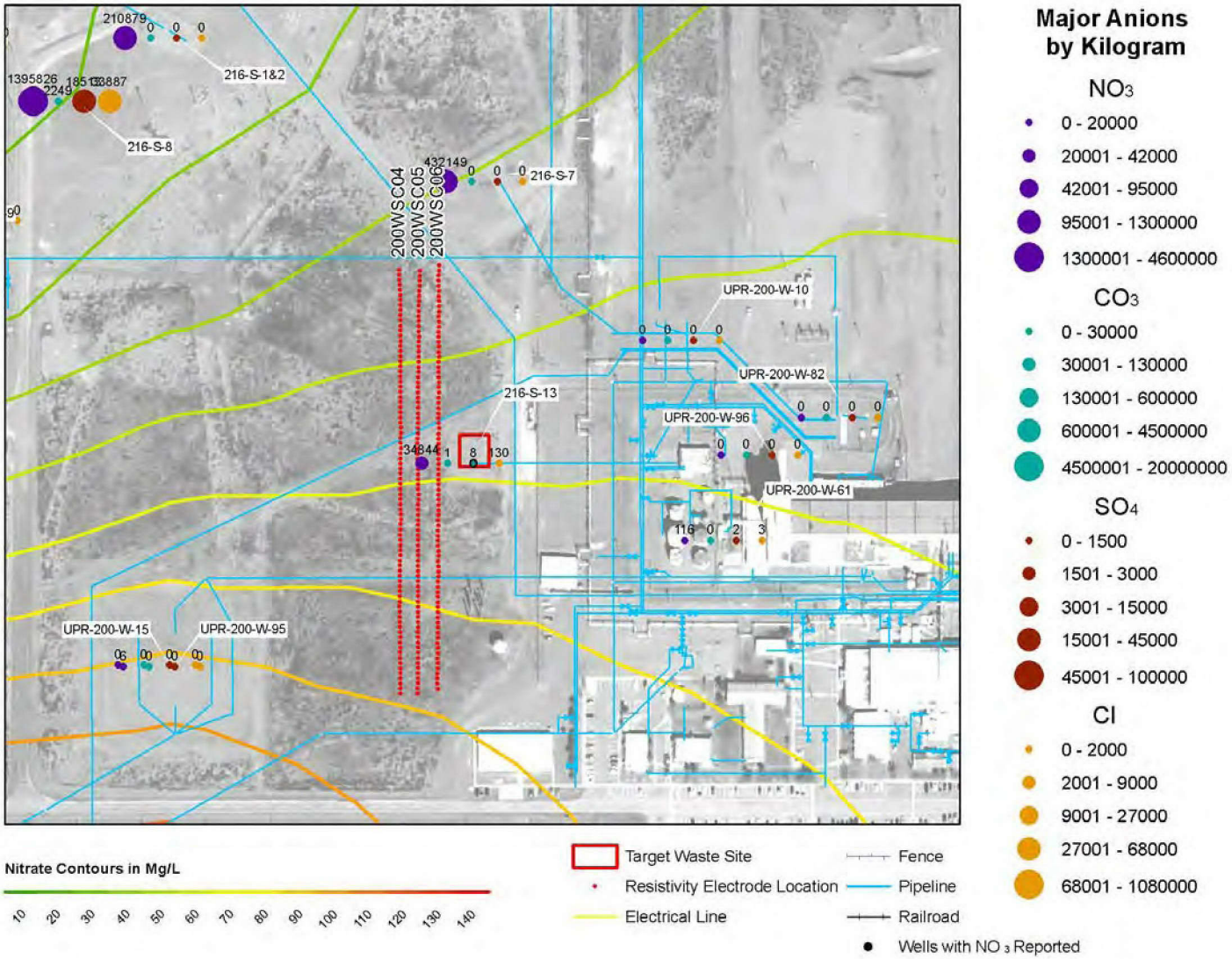

Figure 2-13. Waste Summary for the S-Complex Southern Study Area Showing Groundwater Nitrate Contours and Major Anion Disposal.

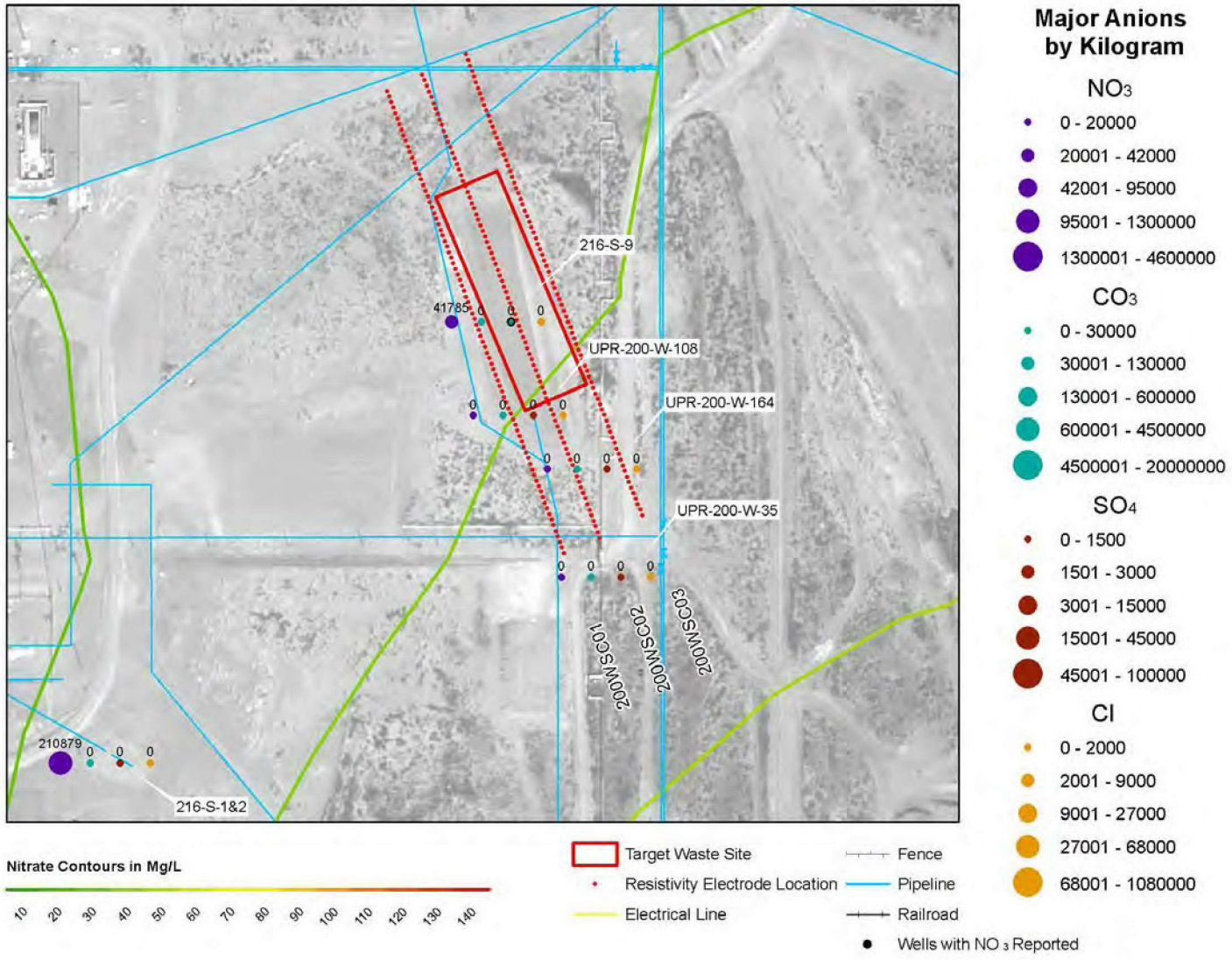

Figure 2-14. Waste Summary for the S-Complex Northern Study Area Showing Groundwater Nitrate Contours and Major Anion Disposal.

2.6 T-PLANT STUDY AREA DISPOSAL SUMMARY

The T-Plant study area is located west of T-Plant and east of T farm. The resistivity survey lines are grouped into two areas: northern and southern. The northern has only two subsurface utilities that appear to connect T-Plant to the T-16-34 and 35 disposal trenches. The land surface of the disposal trenches is raised by additional fill material and includes several steel fence posts and markers. A railway junction area with two railway lines is located just north of the 216-T-35 trench and crosses three of the survey lines. The railway lines are well grounded through a series of steel straps that connect the steel rails to the ground. The railway lines are therefore a preferential current pathway and adversely impact the resistivity data in much the same way as subsurface infrastructure does.

Subsurface infrastructure and another two railway lines towards the west side of the survey lines dominate the southern T-Plant study area. In addition to the subsurface infrastructure, cathodic protection anodes, paved roads, cave-in areas, subsurface metal structures (possibly tanks), steel risers, concrete and steel valve boxes, and fence lines complicate the area. The spacing of the infrastructure is so dense that it is impossible to predict the current flow path from the resistivity transmitter. Therefore, all data within this region should be viewed with caution.

Figures 2-15 and 2-16 shows three large volume liquid disposal sites within the study area that represent between 2 and 10 mGal. The two nearest to the resistivity lines are located at the 216-T-3 and 216-T-12 WIDS sites. Several other smaller liquid waste disposal sites are located within the project site, but most are associated with T farm.

Figures 2-17 and 2-18 shows the distribution of major anions disposed within the S-Complex study area of which the most significant disposal area is the 216-T-15, 16, and 17 WIDS sites (northeast of T Farm) and the 216-T-3 site towards the south. The two areas show elevated levels of nitrate (over 1,300,000 kg) and sulfate (over 15,000 kg).

Figures 2-15 through 2-18 contain contour lines representing nitrate concentrations from reporting wells in 2003 and 2004. Two monitoring wells reporting nitrate concentrations exist within the study area boundaries shown in Figures 2-15 through 2-18. Therefore, the contour lines for this study area are poorly defined and caution should be used when relating nitrate concentrations to other geophysical data. Both monitoring wells show high levels of nitrate in the groundwater. Well 299-W11-7 located at the 216-T-3 WIDS site shows 107 mg/L and well 299-W10-8, located north of T farm, shows 132 mg/L. The resulting contour distribution shows the two “hot spot” areas and a gradual decrease in nitrate concentrations towards the north.

SGW-50056 REV 0

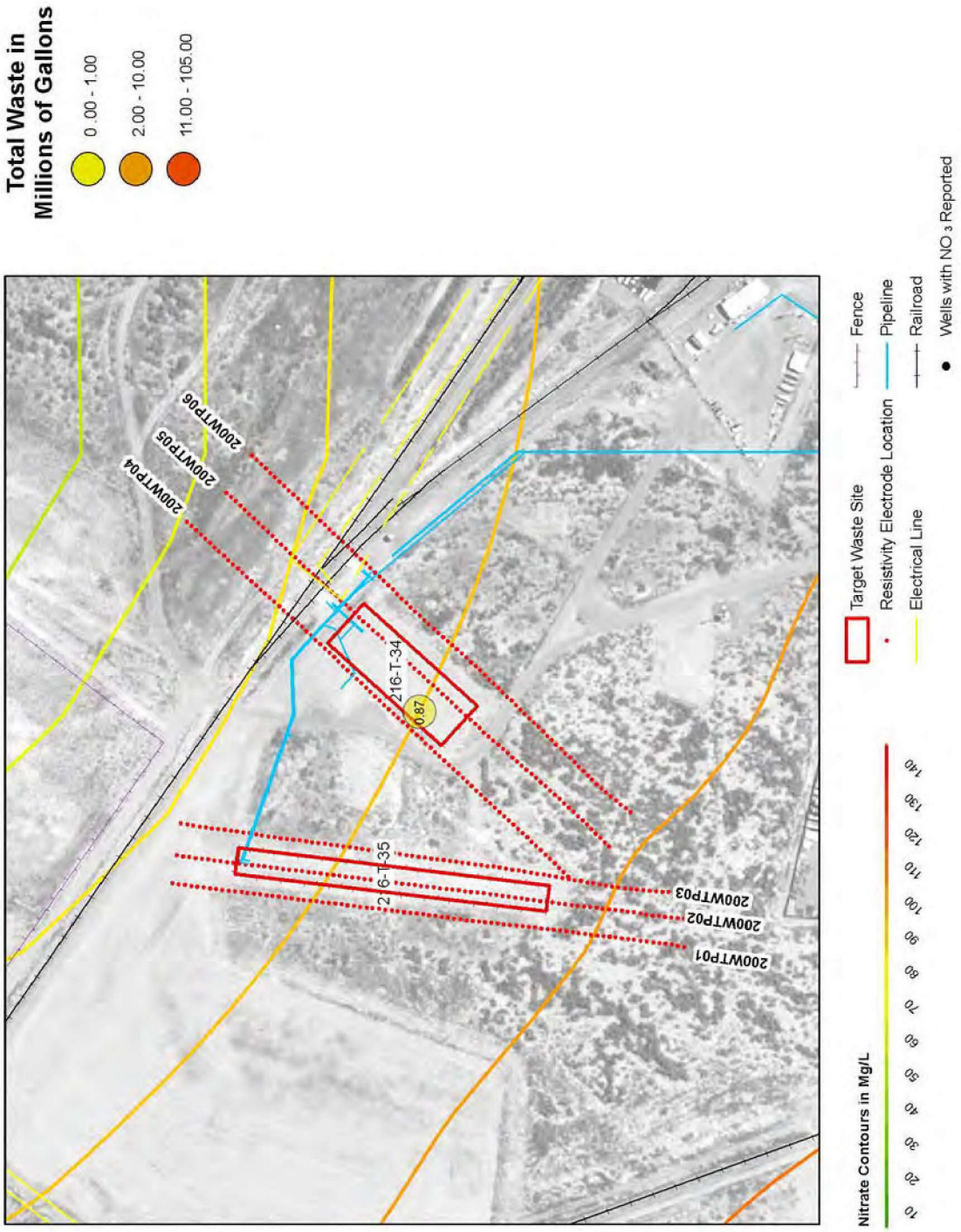

Figure 2-15 Waste Summary for the T-Complex Northern Study Area Showing Groundwater Nitrate Contours and Major Anion Disposal.

A-37

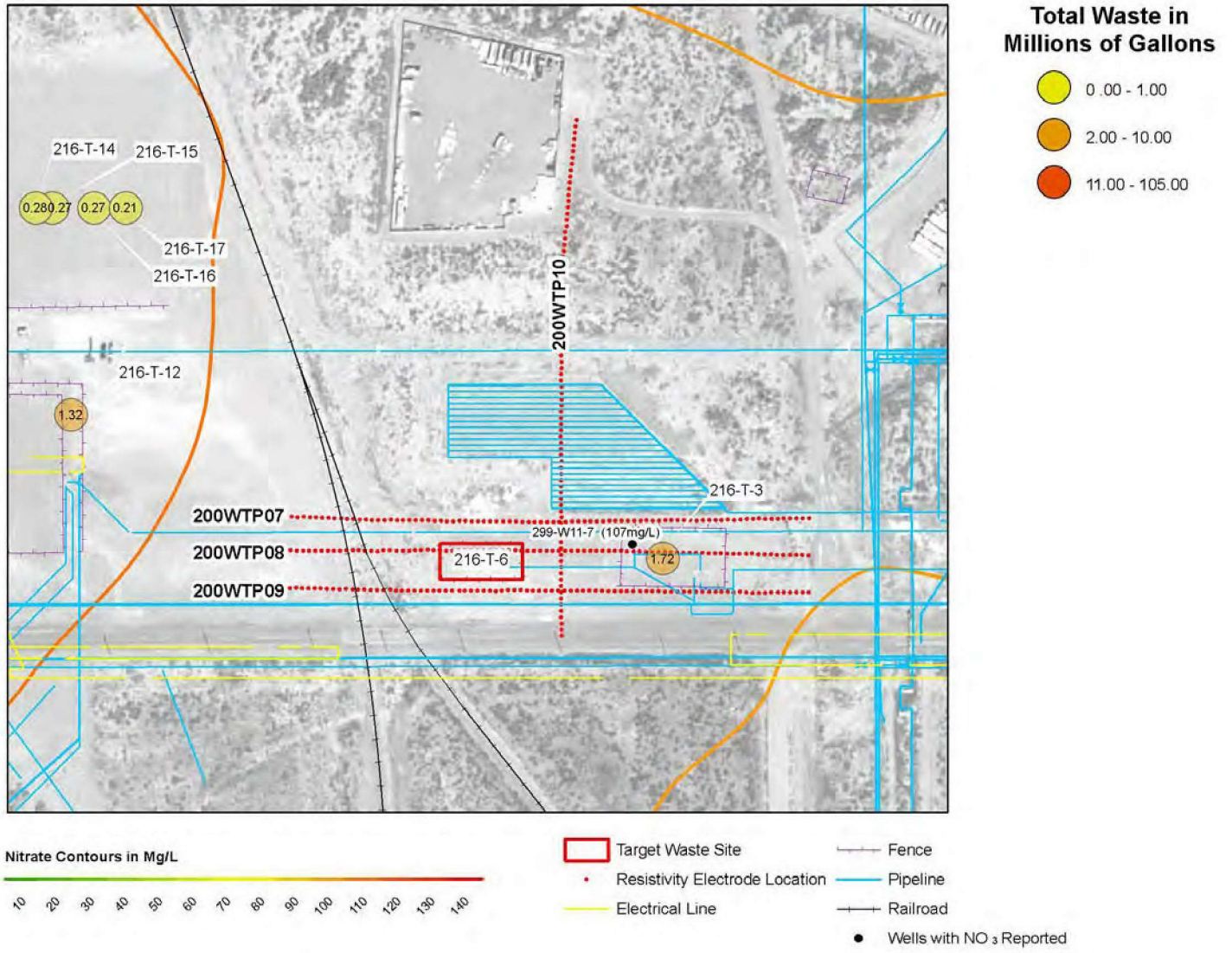

Figure 2-16. Waste Summary for the T-Complex Southern Study Area Showing Groundwater Nitrate Contours and Major Anion Disposal.

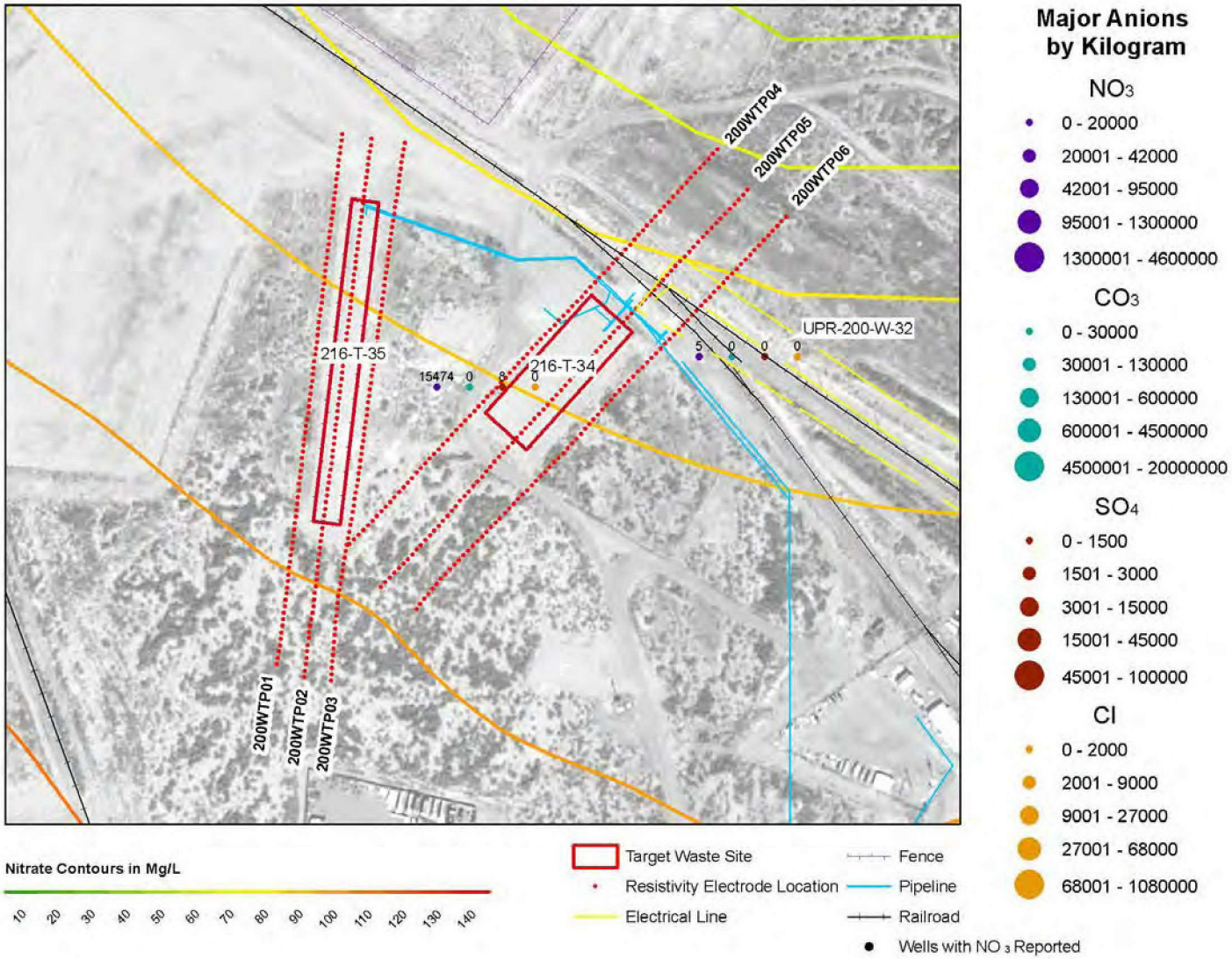

Figure 2-17. Waste Summary for the T-Complex Northern Study Area Showing Groundwater Nitrate Contours and Major Anion Disposal.

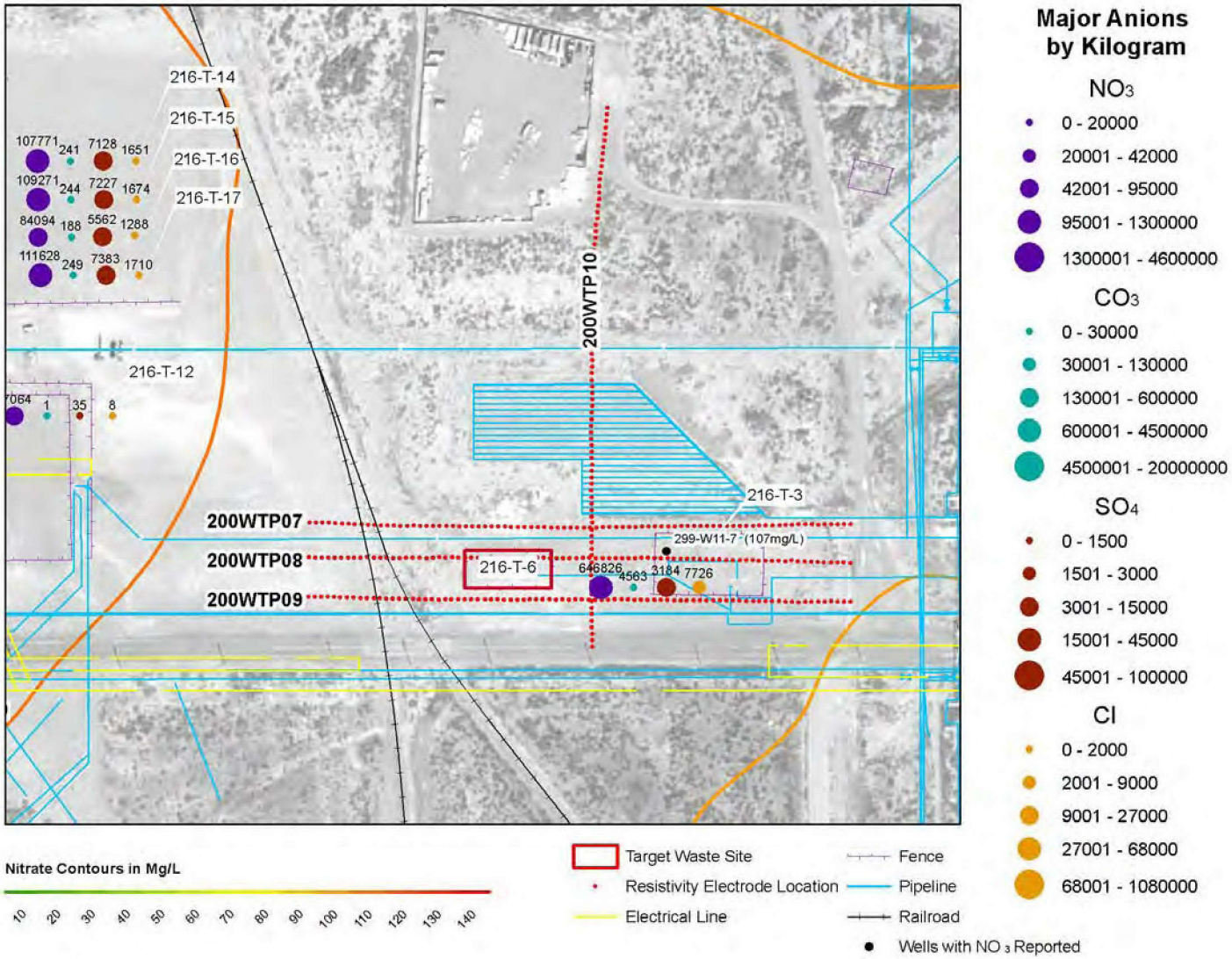

Figure 2-18. Waste Summary for the T-Complex Southern Study Area Showing Groundwater Nitrate Contours and Major Anion Disposal.

2.7 216-Z-16 TRENCH STUDY AREA DISPOSAL SUMMARY

The 216-Z-16 Trench study area is located directly north of the Plutonium Finishing Plant (PFP). Despite its proximity to the industrial complex to the south, the area has few subsurface utilities that are listed on the available Hanford maps. However, onsite inspection of the area revealed an abundance of infrastructure within and surrounding the 216-Z-16 WIDS site. Infrastructure includes cathodic protection anodes, paved roads, subsurface metal structures (possibly tanks), steel risers, concrete and steel valve boxes, and fence lines. The surface of the disposal area is raised by additional fill material and includes several steel fence posts and markers. A railway line runs along the western side of the project area.

Figure 2-19 shows a large volume liquid disposal centered at the 216-Z-16 WIDS site that is between 2 and 10 mGal. There are three other large volume liquid disposal areas to the southeast of the resistivity survey lines (shown in red) that range between 2 and 100 mGal of liquid waste. A few other smaller volume sites (less than 1 mGal) exist within the project area.

Figure 2-20 shows the distribution of major anions disposed within the 216-Z-16 Trench study area of which the most significant disposal area is the 216-Z-16 and 216-Z-7 WIDS sites and the 216-T-21 to 25 disposal trenches. The 216-Z-16 shows a high chlorine disposal exceeding 68,000 kg, and elevated levels of nitrate and sulfate over the 216-Z-7 WIDS site and 216-T-21 through 25 trenches.

Figures 2-19 and 2-20 contain contour lines representing nitrate concentrations from reporting wells in 2003 and 2004. Three monitoring wells reporting nitrate concentrations exist within the study area boundaries shown in Figures 2-19 and 2-20. Two of which are located in close proximity to each other, just northeast of PFP. The two monitoring wells west of PFP, 299-W15-1 and 299-W15-7 show over 100 mg/L of nitrate in the groundwater. By contrast, monitoring well 299-W15-2 located at the far northwestern edge of the study area shows 10 mg/L. The contour distribution shows a sharp gradient extending from the high in the southeast to the low in the northwest.

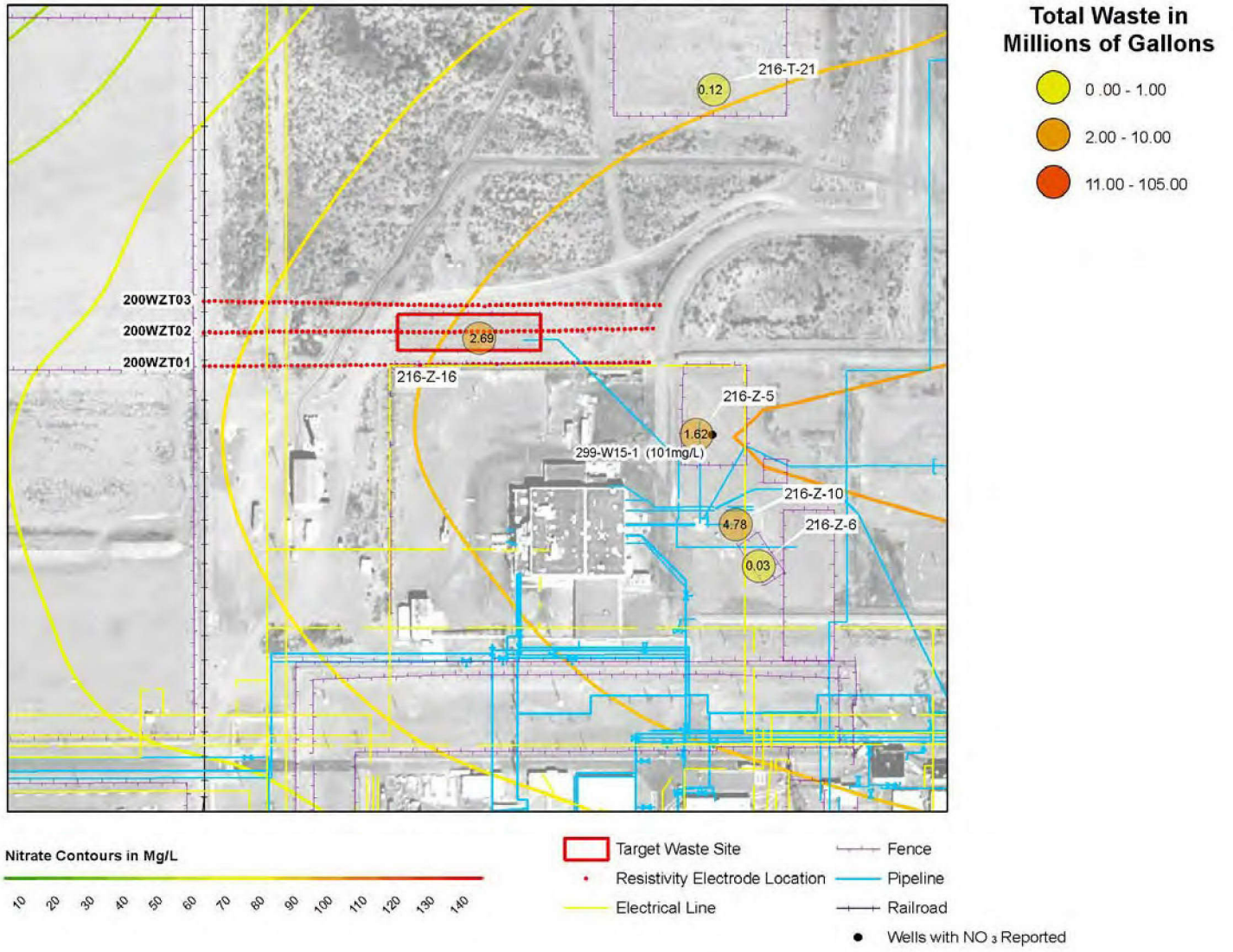

Figure 2-19. Waste Summary for 216-Z-16 Trench Study Area Showing Groundwater Nitrate Contours and Total Liquid Disposal.

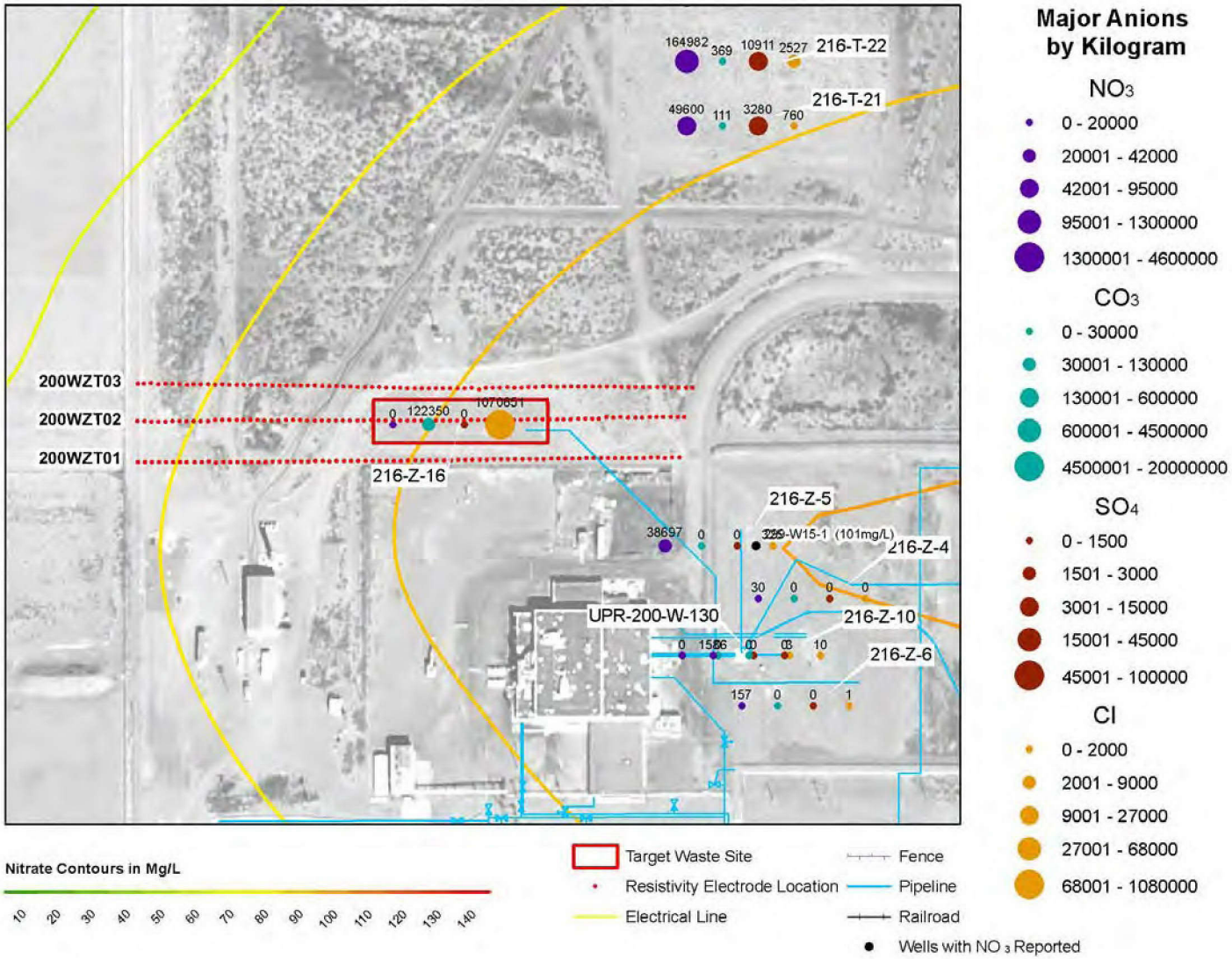

Figure 2-20. Waste Summary for the 216-Z-16 Trench Study Area Showing Groundwater Nitrate Contours and Major Anion Disposal.

www.hgiworld.com
2302 NORTH FORBES BLVD., TUCSON, ARIZONA 85745
tel: 520.647.3315 fax: 520.647.3428

3.0 GEOPHYSICAL THEORY

3.1 HIGH RESOLUTION RESISTIVITY (HRR™)

Resistivity (ρ_a) is a volumetric property that describes the resistance of electrical current flow within a medium. Induced direct electrical current is propagated into rock formations or unconsolidated detritus and minerals by electrolytic means. Electronic conduction only occurs in metallic-luster sulfide minerals, where free electrons are available. Rocks and non-metallic minerals have extremely high resistivities (i.e., low conductivities) and direct current (DC) transmission through this material is difficult. On the other hand, porous media that retain moisture can carry a current through ions by way of electrolytic conduction. Electrolytic conduction relies on the dissociated ionic species within a pore space. Here, the conduction varies with the mobility, concentration, and degree of dissociation. Electrolytic conduction is relatively slow with respect to electronic conduction due to mass transfer rate limiting processes and is strongly influenced by the structure of the medium.

Estimating resistivity is not a direct process. When current (I) is applied and voltage (V) measured, Ohms Law is assumed and resistance is measured. Resistivity and resistance are then related through a geometric factor over which the measurement is made. The simplest example is a solid cylinder with a cross-sectional area of A and length, L:

$$\rho = R\frac{A}{L} \qquad (1)$$

In such cases where the actual volume involved in the measurement is known, the result is called the "true" resistivity and is considered a physical property of that material. However, field measurements involve an unknown volume of earth. Consequently, resistivity calculations are based on the hypothetical response for the given electrode geometry over a homogeneous, isotropic half-space. This results in what is termed as "apparent" resistivity; however, it is more accurately referred to as a "half-space" resistivity.

Field data are generally acquired using a selected electrode array. A four-electrode array employs electric current injected into the earth through one pair of electrodes (transmitting dipole) and the resultant voltage potential is measured by another pair (receiving dipole). The ratio of the transmitted current and observed potential is called the transfer resistance. Some commonly deployed electrode configurations are dipole-dipole, Wenner, and Schlumberger arrays. The proper selection of an array depends upon onsite conditions and the information desired. Figure 3-1(A), adapted from Telford et al. (1990), shows a schematic of the dipole-dipole configuration, where C1 and C2 are connected to the current source (i.e., transmitting

™ High Resolution Resistivity (HRR) is a trademark of hydroGEOPHYSICS, Inc., Tucson, Arizona.

electrodes), and P1 and P2 are connected to the voltmeter (i.e., receiving electrodes). For the four-electrode array, the geometric factor, K is:

$$K = 2\pi \frac{1}{\left(\frac{1}{r_1} - \frac{1}{r_2}\right) - \left(\frac{1}{r_3} - \frac{1}{r_4}\right)}, \tag{2}$$

where r_1 through r_4 are defined in Figure 3-1(A). Equations (1) and (2) are used to estimate an apparent resistivity, which assumes that each measurement of transfer resistance was a result of point electrodes on the surface of a homogeneous, isotropic, and half-space:

$$\rho_a = 2\pi \frac{V}{I} K \tag{3}$$

where subscript "a" in ρ_a denotes the *apparent* resistivity. The apparent resistivity is not necessarily the true resistivity of the formation, but a simplified resistivity that provides a beginning point for subsurface evaluation. Other assumptions used in Equation 3 are isotropy (i.e., no directional dependence of resistivity), no displacement currents (using a DC or low frequency current application), and that resistivity is constant throughout such that Laplace's equation can be assumed. Since the degree of heterogeneity is not known beforehand, a true resistivity is not calculated from Equation 3. To obtain a true resistivity, electrical resistivity tomography (ERT) is required, which generates a model of true resistivity using an iterative inverse methodology given the measurements of apparent resistivity, electrode arrangement, and other boundary conditions. Discussions of ERT and the methods by which the true resistivity is calculated can be found in several sources, including Loke and Barker (1996), LaBrecque et al. (1996), and Oldenburg and Li (1999).

An alternative to the four-electrode array is the two-electrode pole-pole array. The pole-pole array is a modification of the four pole arrays where, one electrode from each of the current and potential pairs is fixed effectively at infinity, while the other current and potential electrodes act as "rover" electrodes within the survey transect. Practically, the infinite electrodes are spaced approximately 5 to 10 times the distance of the furthest separation of the rover electrodes, which can be up to 300 m apart for a near-surface geophysical survey. The pole-pole array provides higher data density, increased signal to noise ratio, and requires less transmitted energy. Roy and Apparao (1971) discuss the superiority of the pole-pole method when conducting shallow surveys. Additionally, in some very conductive environments where potential gradients are low, one may be forced to use the pole-pole array to measure a signal above the noise level of the data acquisition instrument.

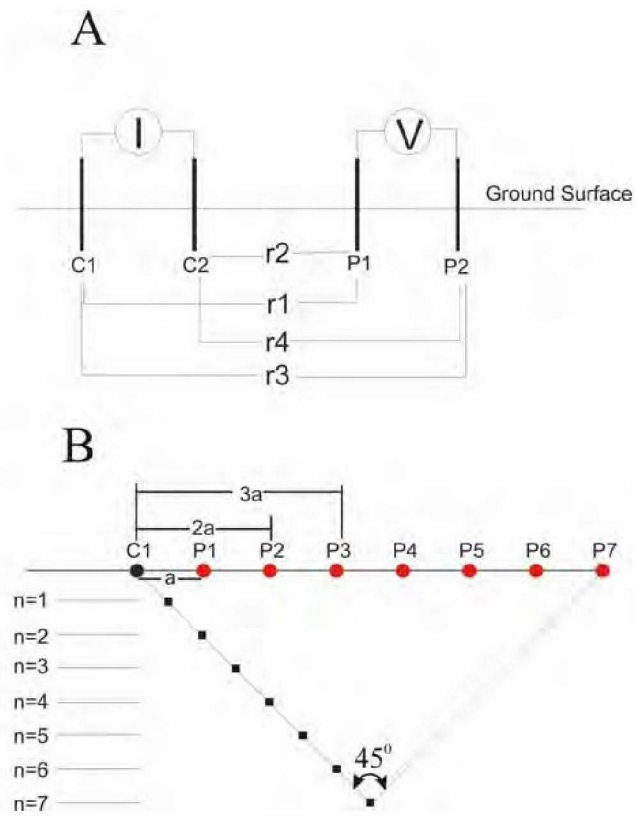

Figure 3-1 Setup of the Resistivity 4-Pole Array and Pseudo-Section Plotting Methodology.

The calculation of apparent resistivity is simplified in the pole-pole array:

$$\rho_a = 2\pi \frac{V}{I}(n * a) \tag{4}$$

where a is the basic electrode spacing and n is the integer multiplier as the current and potential electrodes incrementally separate. Figure 3-1(B) demonstrates a linear transect of electrodes on the surface with the a-spacing being the separation between each electrode and the n spacing increasing as the potential electrode moves away from the current electrode. For a complete survey, each electrode has one turn at transmission, while potential measurements are acquired at all other electrodes in the array. Automated resistivity meters, such as the SuperSting™ R8 portable memory earth resistivity meter (Advanced Geosciences, Inc. [AGI], Austin, Texas), has the ability to conduct multi-channel sweeps of potential measurements to significantly decrease measurement time.

™ SuperSting is a trademark of Advanced Geosciences, Inc. in the United States, other countries, or both.

3.2 TARGET DISCRIMINATION WITH APPARENT RESISTIVITY

The linear transect arrangement of electrodes produces a 2D data set of apparent resistivity as a function of x and z, where z is the dimension into the earth and x is along the surface. Although apparent resistivity is a function of the volume over which the measurement is made, its location is typically plotted as a point for ease of representation. The location of the point is a function of n and is loosely related to the depth of investigation. Hallof (1957) demonstrated that the intersection of two 45^0 lines extending downward from each of the current and voltage potential electrodes would produce a suitable pseudo-section for interpretation. Others have used similar techniques to plot, for example, the depth to the maximum sensitivity in the electrode separation, (see Roy and Apparao 1971). Using the Hallof approach, the pole-pole array has data plotted at a pseudo-depth of:

$$-z_{pseudo} = 0.5na\,, \tag{5}$$

which is a linear plotting method.

Figure 3-2 is an apparent resistivity demonstration of several array types, including the pole-pole array with a resistive half-space earth (400 ohm-m) and a graded conductive target (20 ohm-m). The target dimensions are 21x10 m, and the top of the target is located at 10 m BGS. The target was modeled with a forward resistivity model in AGI EarthImager™ 2D inversion and modeling software using the basic algorithm of Dey and Morrison (1979). Many electrical resistivity modeling codes use some elements of this algorithm, including RES2DINV (Loke and Barker 1996) and DCIP2D (Li and Oldenburg 1994).

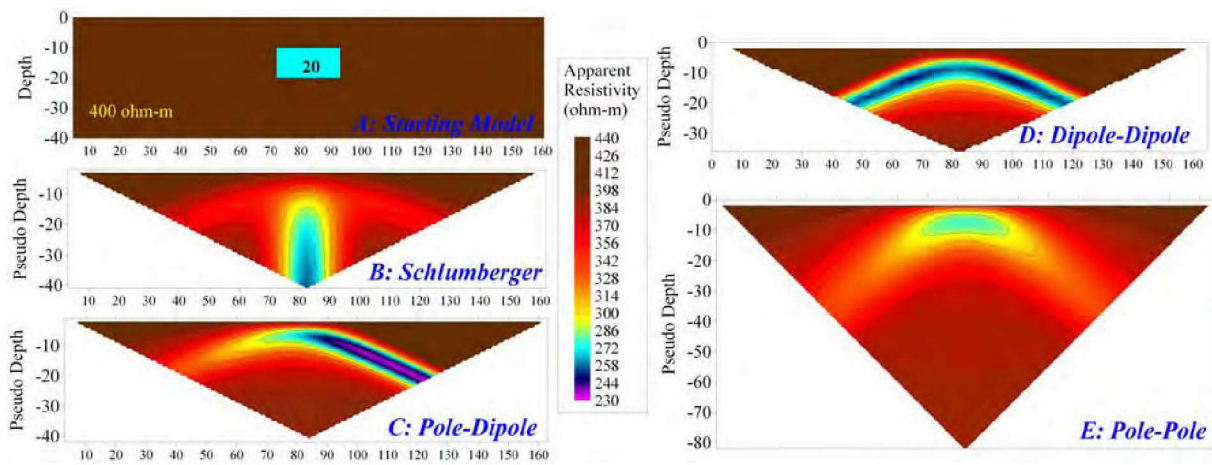

Figure 3-2. Apparent Resistivity Pseudo-Section Comparisons for the Schlumberger, Pole-Dipole, Dipole-Dipole, and Pole-Pole Array Types for a Discrete Conductive Target in a Resistive Homogeneous Background.

™ EarthImager is a trademark of Advanced Geosciences, Inc. in the United States, other countries, or both.

Qualitatively, the pole-pole apparent resistivity pseudo-section in Figure 3-2 resembles the starting target more closely than the other arrays. The dipole-dipole and pole-dipole show extremely conductive "pant leg" effects, where the target's edge has been smeared diagonally downward. Since the apparent resistivity, plotting routine contains information based on a volume-averaged measurement; artifacts such as pant legs can be expected. The apparent resistivity plot of the Schlumberger array shows a straight vertical smearing as if it were an intrusive conductive dike. On the other hand, the pole-pole array measures the electrical potential gradient relative to a fixed pole at infinity. In the earth, the infinite pole should essentially not interact with the electrical field and is modeled near the boundary condition of $V|_{\infty} = 0$. The result is a measurement of the actual potential as opposed to the gradient in potential measured for closely spaced dipoles, and a less pronounced pantleg smearing effect.

Another view of the apparent resistivity data can be seen in Figure 3-3, where vertical slices of data have been extracted at 81 m (center of the domain) and at 65 m. Figure 3-3(A) shows these slices as a function of the pseudo-depth for all but the pole-dipole array. In general, the pole-pole and dipole-dipole array show a decrease in resistivity at 81 m (solid lines) that is loosely coincident with the target depth, while the Schlumberger array does not resemble the character of the target at all. Off-center at 65 m (dashed lines), where the actual resistivity is a resistive homogeneous body, the pseudo-section of the pole-pole shows less of an effect than the dipole-dipole. The Schlumberger array resembles the actual background better at the 65 m slice.

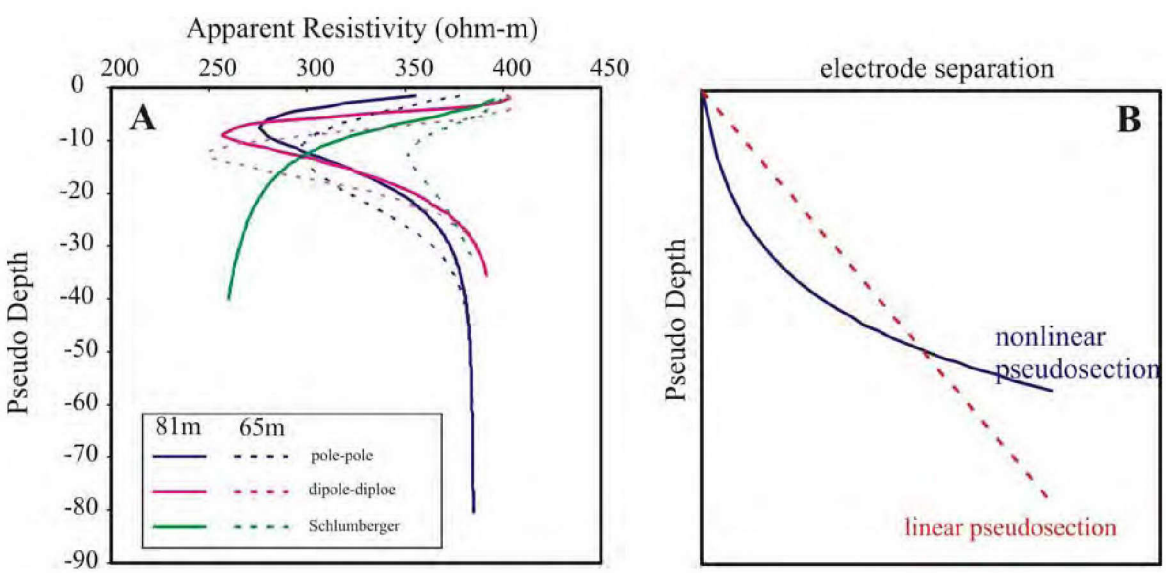

Figure 3-3. A) Vertical Slices through Apparent Resistivity Data for Schlumberger, Dipole-Dipole, and Pole-Pole at 65 m (beside target) and 81 m (within target); B) Schematic of Linear and Nonlinear Pseudo-Section Plotting.

The depth of investigation stems from a need to relate a measurement made at the surface to some particular depth in order that survey parameters can be optimized for target identification (Barker 1989). Before tomographic inversion was common practice among geophysicists to estimate the true resistivity from measured apparent resistivity, apparent resistivity

pseudo-sections were used primarily for interpretation of subsurface electrical anomalies. Field practitioners became quite efficient at locating the depth to specific targets, such as ore bodies. The presentation of the pseudo-section is important in these regards. Additionally, the pole-pole array, above all others, provides the weakest edge effects, thereby facilitating the direct interpretation of these data more reliably (Robain et al. 1999).

The traditional linear pseudo-section of Hallof (1957) has limitations with respect to a physical meaning of the earth. Therefore, many researchers have taken a closer examination of the plotting method to allow for a more reasonable geological interpretation. The most widely accepted depth of investigation studies are those presented by Roy and Apparao (1971), Roy (1972), and Koefoed (1972), who defined a depth of investigation characteristics (DIC) model for determining the depth of a measurement. The DIC was determined by finding the depth at which a thin horizontal layer within a homogeneous background makes the maximum contribution to the total measured signal at the surface. The results were consistent in that the depth of investigation is a nearly logarithmic function of electrode spacing, regardless of how the depth of investigation is defined. This suggests a modification of the linear pseudo-section (Edwards 1977 and Fink 1980). Figure 3-3(B) shows an example of a nonlinear pseudo-section, based on a logarithmically-based depth interpretation based on the electrode separation.

To facilitate the nonlinear depth plotting of apparent resistivity data, a function of the logarithm of the n-spacing value can be used. The coefficients of the function is usually determined by using collocated borehole data or based on standardized values developed over years of experience. The consequences of a nonlinear pseudo-section is shown in Figure 3-3(B), where the resistivity values near the surface are pushed deeper relative to the linear pseudo-section and the deeper resistivity is pulled up relative to the linear pseudo-section. At one point, the two plotting strategies have the same depth location for a given electrode separation.

Typically, after data collection, the apparent resistivity data are run through an inversion routine to estimate the true resistivity values that give rise to the measured resistivity. These models are based on either finite element or finite difference. In any case, the inversion method is nonlinear and requires an iterative solver. During the iterations, distributions of true resistivities are estimated and the forward model calculates the voltage at the surface coincident with electrode locations. The differences between measured and modeled voltages are compared, and resistivities in regions showing large discrepancies are changed. The inversion model runs until the measured and modeled data are satisfactorily compared. In this way, the objective of the inversion is to minimize the difference between the modeled and measured resistivity, usually in a least squares sense. The objective function can be defined in many different ways, such as using the L_1-normalization (robust inversion) or L_2-normalization (smooth inversion) (Dahlin and Zhou 2004). Compared to the damped least squares method with no normalization and L_1-normalization, the L_2-normalization is optimal at resolving smoother boundaries typical for conductive plumes and most hydrologic boundaries (deGroot-Hedlin and Constable 1990 and 2004, and Loke et al. 2003).

For the simple target problem identified in Figure 3-2, the measured apparent resistivity data were inverted using AGI EarthImager 2D. Both robust and smooth models were evaluated with the results of the inversion shown in Figure 3-4. The final goodness-of-fit statistic, as measured

by the root-mean-square (RMS) error, was 0.91 and 0.67 for the robust and smooth inversion results, respectively. For comparison, the linear and nonlinear pseudo-section data are plotted to the left of the inversion results. All of the contoured resistivity and apparent resistivity data show a target in the general location of the actual target location. Additionally, all methods appear to smear the information laterally or vertically, referring to a smooth condition where boundaries may not be as well defined. For the apparent resistivity plots, pantleg effects smear the lateral boundaries of the interpreted target. For the inverted resistivity plots, the vertical information below the target is smeared.

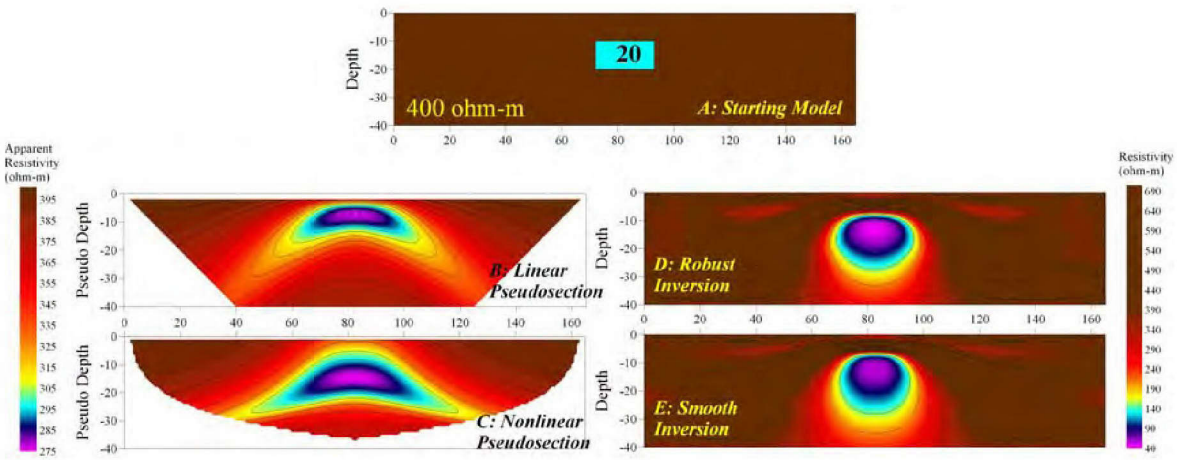

Figure 3-4. Contours of Resistivity for the Different Interpretation Algorithms Including Linear Pseudo-Section, Nonlinear Pseudo-Section, Robust Inversion (L_1-Normalization), and Smooth Inversion (L_2-Normalization).

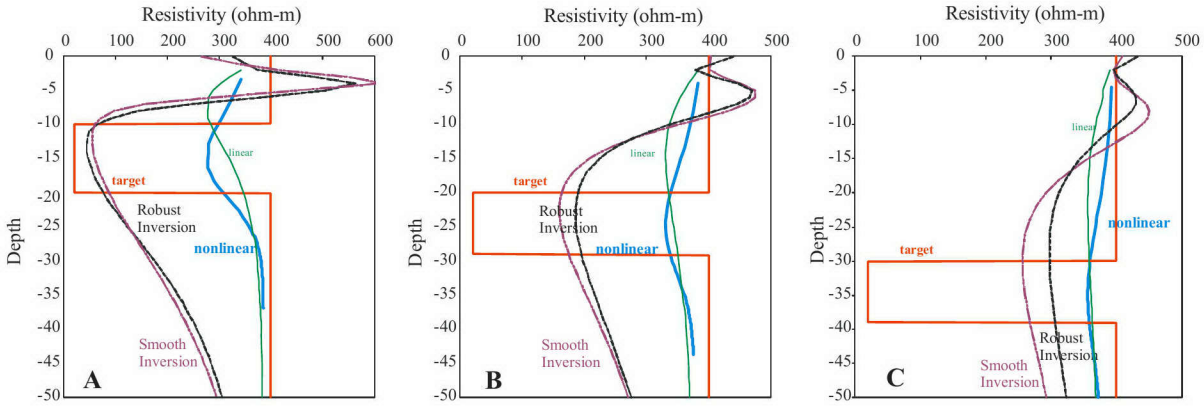

Figure 3-5. Vertical Slices for Comparison of Interpretation Algorithms Including Pseudo-Section Apparent Resistivity and Inverted True Resistivity for a Discrete Conductive Target at A) 10 m BGS, B) 20 m BGS, and C) 30 m BGS.

To demonstrate the vertical smearing effects more concretely, Figure 3-5 includes vertical resistivity slices at 81 m along the transect for both sets of inversions and for all three target models examined. In all three models, the minimum resistivity value is closer to the surface for the inversion results than the nonlinear pseudo-section; however, not as close as the linear pseudo-section. Another major observation is that the gradient of resistivity is more asymmetrical for the inversion, where the change in resistivity to define the target is high close to the surface and low at-depth. With these simplified models, it appears that the apparent resistivity may prove to be a useful tool for preliminary interpretation of simple discrete subsurface targets prior to inversion. Furthermore, if external information exists such as borehole information, the pseudo-depth can be converted to a depth that is closer to the target horizon.

4.0 METHODOLOGY

4.1 SURVEY AREA AND LOGISTICS

Approximately 12 km of data acquisition were completed in total, with approximately 7.7 km acquired within the 200 East area and approximately 4.4 km acquired within the 200 West area. The electrical resistivity surveys for the 200 East area were completed from October through December 2007. The selected HRR locations within the 200 East area include 216-C-1, A-Complex, B-Plant, and PUREX Plant. The electrical resistivity surveys for the 200 West area were completed during the months of November and December 2007. The selected HRR locations within the 200 West area include S-Complex, T-Plant, and 216-Z-16 Trench.

4.1.1 Resistivity Line location and Acquisition

Figures 4-1 through 4-4 show survey coverage for each site located within the 200 East area. While Figures 4-5 through 4-7 show survey coverage for each site located within the 200 West area. Locations are shown overlain on aerial photographs, displaying the resistivity line (red) proximity to prominent infrastructure and other features at each site.

Due to the increasing number of resistivity surveys required onsite, a more detailed naming convention has been developed. Previous reports have simply referred to individual resistivity lines as "Line XX" where XX represents the numerical progression of the lines acquired at each site. As presented in the following sections the new naming convention establishes whether a survey location is in the 200 East area or the 200 West area in the first four digits. The next two digits describe the nearest site (i.e., T-Plant is represented as "TP"). The last two digits represent the numeric line number. For example, line number 5 at T-Plant is referred to as "200WTP05."

The endpoints of each resistivity line were positioned in agreement with the statement of work as requested in PNNL RFP NO. 51569. A Leica GPS1200, Real-Time Kinematic (RTK) Global Positioning System (GPS) unit (Leica Geosystems AG, St. Gallen, Switzerland), was used to lay out line location markers every 100 m, with the intermediate electrode locations determined using a surveyor's tape measure. A station spacing of 3 m was implemented for each line in accordance with the resolution and depth of investigation target specified within the RFP. Upon completion of the data acquisition phase at each site, the Leica GPS1200 was again used to acquire the coordinates of all electrode locations with an accuracy of ± 0.03 m.

Data acquisition for each line was completed by implementing the following steps:

1. Survey design – determine total line length, electrode spacing, orientation, and particular features to be crossed.
2. Line location – locate line endpoints and orient line using reference maps and survey grade RTK GPS.
3. Line layout – measure and locate inter-electrode spacing using fiberglass surveyor's tape, in meters.
4. Electrode location – locates and digitally stores each electrode location using RTK GPS.

5. Remote electrode layout – determine orientation and placement of remote electrodes. Build remote electrode nest and string 16 gauge shielded wire to the electrode locations.
6. Create resistivity data acquisition command files for the AGI SuperSting R8.
7. Data acquisition – acquire data using an AGI SuperSting R8 resistivity meter in the pole-pole array configuration.
8. Log field procedures on standardized field data acquisition forms. These notes include survey date, time, crew leader, crew members, site location, line number, command file identification (I.D.), and data file I.D.
9. Download data and perform in-field data quality control (QC) protocols to ensure suitable data for each survey line.
10. Transmit data to the data archival server in Tucson, Arizona.
11. Perform office based data processing procedures (see Section 4.3 for a detailed explanation).
12. QC and edit, when required, GPS line and electrode location data.
13. Post RTK GPS data onto aerial/satellite photo based site maps.
14. Plot and QC resistivity data using HGI's logarithmic HRR pseudo-sectional format in order to inspect data quality prior to 2D inversion.
15. Perform data editing and filtering procedures for 2D inversion preparation (see Section 4.3.2 for detailed explanation).
16. Invert data using AGI EarthImager 2D inversion software.
17. Create 2D cross-section plots of inverted resistivity data.
18. Integrate 2D inversion data to form 3D interpolated visualization models, where applicable.

All HGI onsite personnel completed the following training prior to commencing field work:

1. Occupational Safety and Health Administration (OSHA), Hazardous Waste Operations and Emergency Response (HAZWOPER) standard (29 CFR 1910.120)
2. Hanford General Employee Training (HGET)
3. Hanford specific lock-out/tag-out training
4. Radiological worker II training
5. All-terrain vehicle (ATV) safety operation training.

Personal protective equipment (PPE) included steel-toed boots, personal dosimeters, safety glasses, hardhat, hearing protection, and work gloves. Additionally, upon project completion, personnel and equipment were surveyed for radiological contamination by a radiological technician where necessary.

4.1.1.1 216-C-1

The 216-C-1 resistivity data were acquired from December 4 to December 5, 2007 and consisted of four pole-pole resistivity lines varying in length from 228 to 249 m based on survey design or site limiting infrastructure. Figure 4-1 displays the location of these lines relative to the surface infrastructure as seen from an aerial photograph. Line 200EC101 was collected in an approximate east west direction, while Lines 200EC102, 200EC103, and 200EC104 were acquired trending north south. The red lines represent the resistivity line locations. The location

of line 200EC101 was modified from the RFP location after inspection of lines 200EC02 through 04 showed a preferential location north of the original location. In addition, the original location placed the line over significant infrastructure that would have greatly reduced data quality. The intersection of lines 200EC101 and 200EC104 is located to the northwest of waste site 200-E-56, while the center of 200EC101 is south of 216-C-2. Significant metallic infrastructure and utilities were noted across the site. A more detailed description of site infrastructure and disposal volumes can be viewed in Section 2.0.

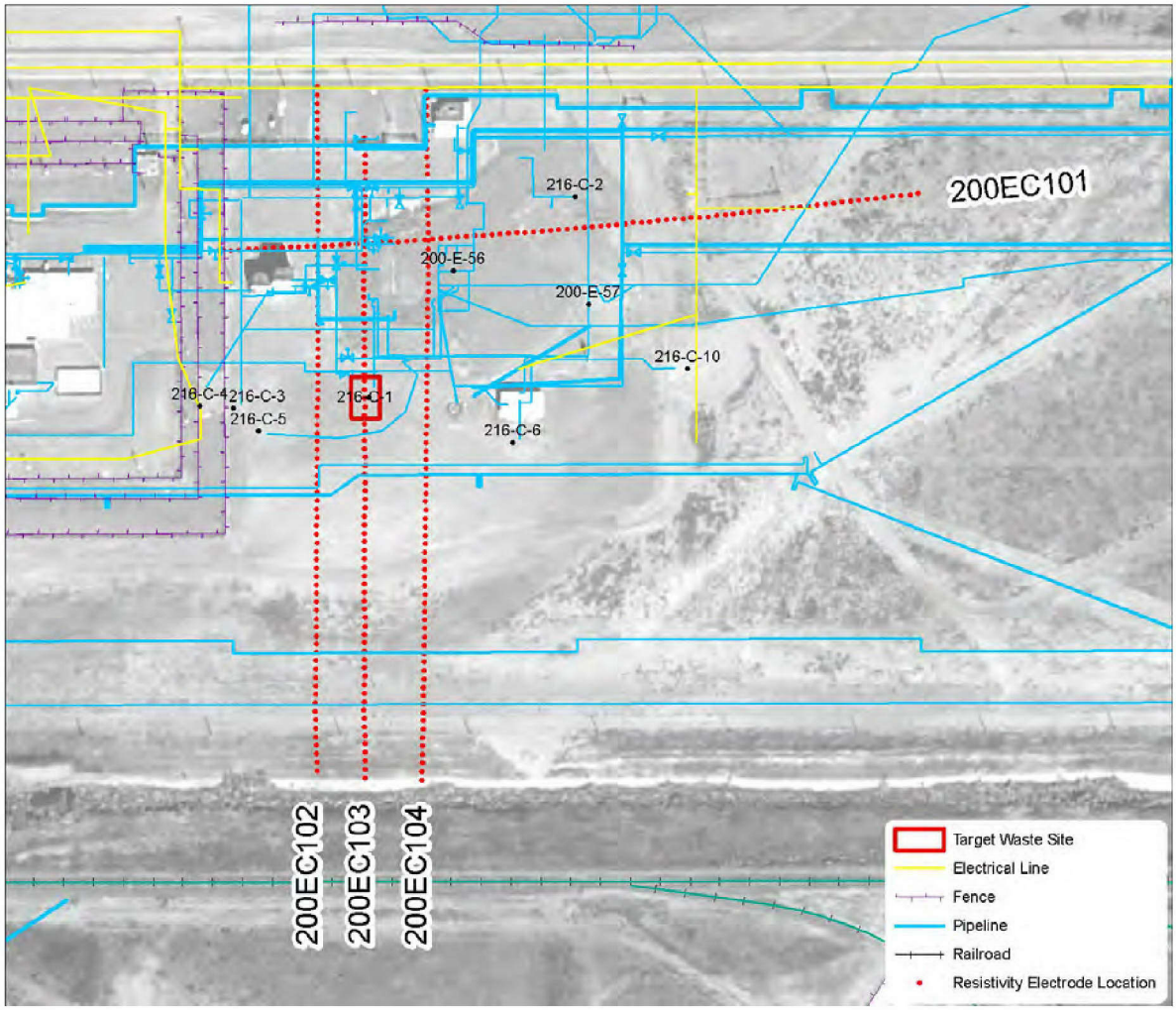

Figure 4-1. Resistivity Line Locations for the 216-C-1 Survey.

4.1.1.2 A-Complex

Figure 4-2 shows the locations of the nine-resistivity lines with respect to infrastructure within the A-Complex. A total of nine pole-pole resistivity lines were acquired, which varied in length from 117 to 393 m. The lines for the A-Complex survey are numbered 200EAC01 through 200EAC09. The red lines represent the resistivity line locations. The A-Complex resistivity

data were acquired from October 18 to October 24, 2007 and consisted of nine pole-pole resistivity lines. Line 200EAC01 trends north to south and is located adjacent and to the east of 216-A-7, and 216-A-1. Line 200EAC01 crosses a pipeline in the south, and parallels a pipeline for the complete length of the line. Line 200EAC02 bisects 200EAC01, and trends approximately east to west, south of 216-A-7 and 216-A-1. The location of lines 200EAC01 and 200EAC02 were designed to investigate the 216-A-7 waste site, however, an error in location maps resulted in the lines being located approximately 25 meters east of the original location.

Lines 200EAC03 and 200EAC04 also approximate an east west trend and are located south of 216-A-8 with 200EAC04 transecting the southernmost edge of the 216-A-8 Crib. At the same strike as lines 200EAC03 and 200EAC04, line 200EAC05 is located north of, and parallel to, 216-A-8. The beginning of the line transects crib 216-A-34 and near the east end, the line crosses an extension of crib 216-A-8. Line 200EAC06 was completed north of line 200EAC05 and was centered over the extension of 216-A-8. Lines 200EAC07, 200EAC08, and 200EAC09 were completed trending northeast to southwest, between 216-A-18 and 216-A-20. A more detailed description of site infrastructure and disposal volumes can be viewed in Section 2.0.

4.1.1.3 B-Plant

Ten pole-pole resistivity lines were acquired within the vicinity of B-Plant, which varied in length from 249 to 357 m. Data acquisition occurred from December 6 to December 13, 2007. The locations of the resistivity lines are presented in Figure 4-3 with respect to local infrastructure. The lines for the B-Plant survey are numbered 200EBP01 through 200EBP10. The red lines represent the resistivity line locations.

Lines 200EBP01, 200EBP02, and 200EBP03 were acquired on a trend of southeast to northwest in a parallel configuration. The three lines were acquired with 200EBP02 centered over the 216-B-55 waste site. Acquisition of data associated with line 200EBP02 was subject to unknown interference that prevented the acquisition of acceptable data. Several attempts to acquire this data set were made resulting in unreasonable, invalid data. Onsite inspection of the soil properties over much of the line showed a well-cemented and compacted artificial material that may have contained conductive clays from previous drilling in the area. The area also contained several steel risers emanating from the ground that may be connected to subsurface infrastructure. Subsurface geologic conditions and/or infrastructure were not conducive to acquiring data at this location. A more detailed description of site infrastructure and disposal volumes can be viewed in Section 2.0.

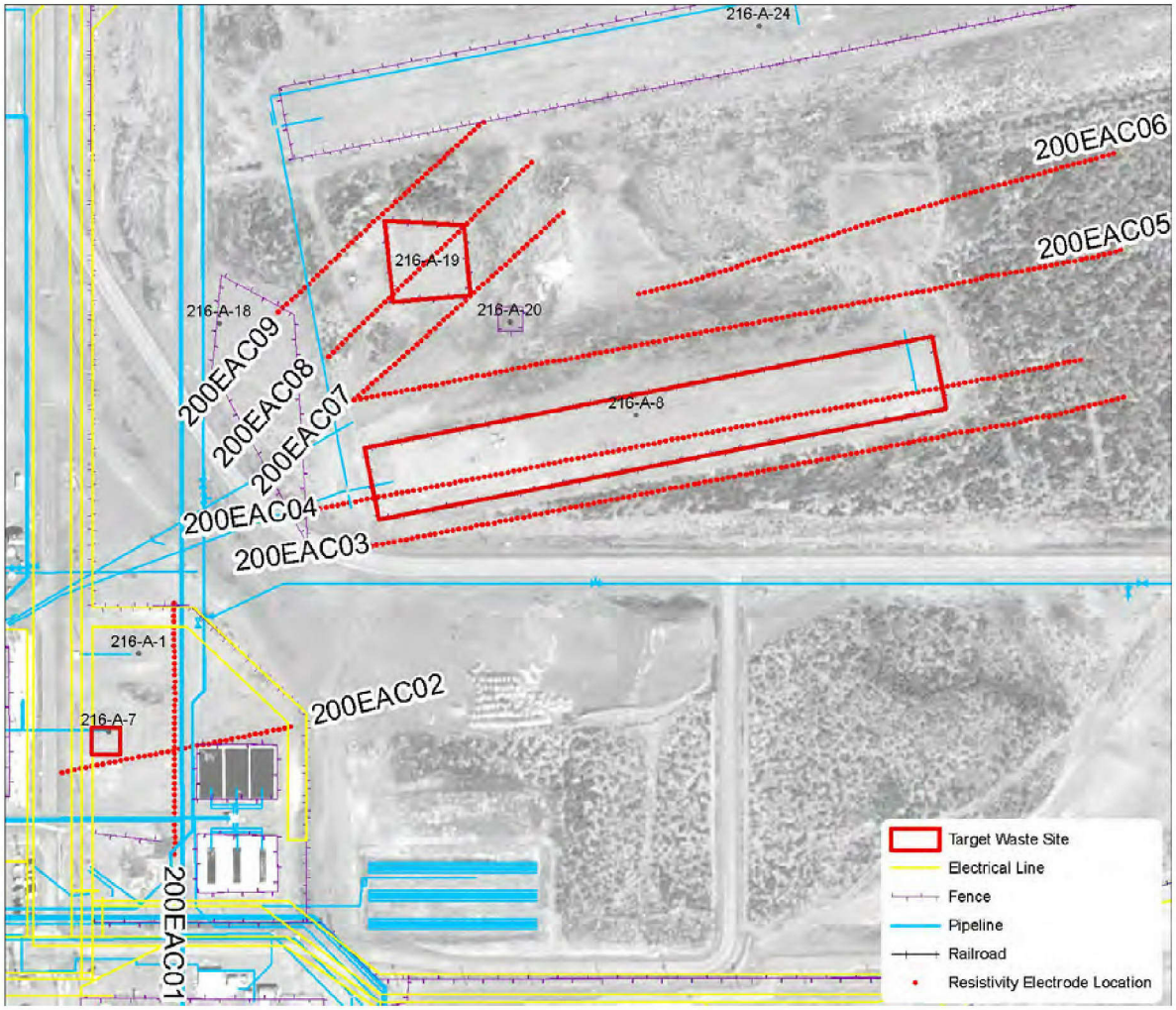

Figure 4-2. Resistivity Line Locations for the A-Complex Survey.

Lines 200EBP04, 200EBP05, and 200EBP06 were acquired on a trend of south to north in a parallel configuration, directly north of the 216-B-55 waste site. Line 200EBP05 was centered directly over the 216-B-12 waste site. Line 200EBP07 was acquired east to west directly south of the B-Plant access road, in an area heavily dominated by infrastructure.

Lines 200EBP08, 200EBP09, and 200EBP10 were acquired on the southeast portion of the site. Line 200EBP08 was acquired trending west to east, while lines 200EBP09 and 200EBP10 trend north to south. The intersection of the three lines occurs adjacent to the 216-B10 A and B waste sites. The entire extent of line 200EBP08 is heavily dominated by infrastructure. However, lines 200EBP09 and 200EBP10 only cross into the infrastructure rich environment on the northern ends. A pipeline intersects 200EBP09 and 200EBP10 near the southern end of the lines. A more detailed description of site infrastructure and disposal volumes can be viewed in Section 2.0.

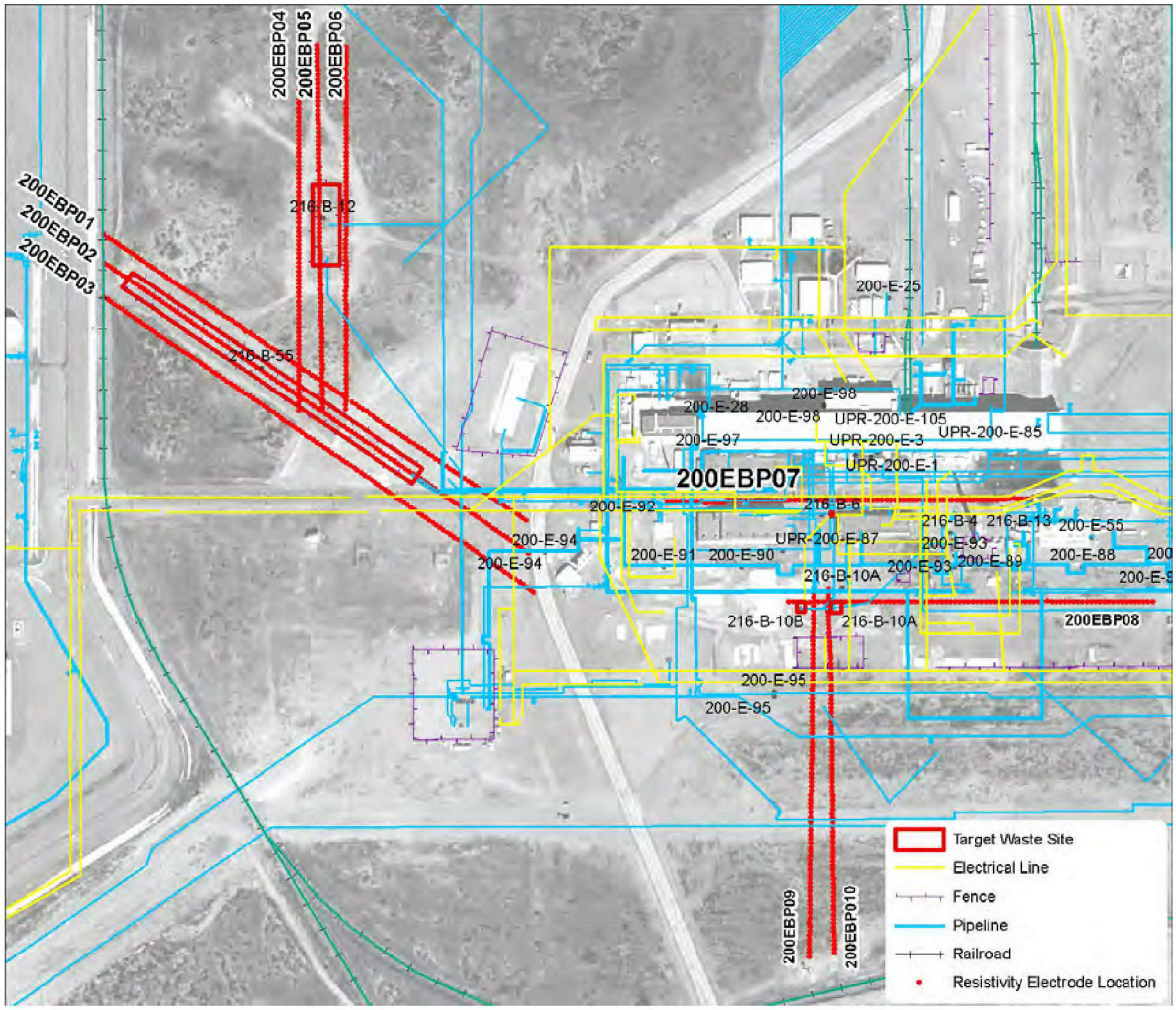

Figure 4-3. Resistivity Line Locations for the B-Plant Survey.

4.1.1.4 PUREX Plant

Seven pole-pole resistivity lines were acquired within the vicinity of PUREX Plant, which varied in length from 249 to 321 m. Data acquisition occurred from November 8 to November 12, 2007. The locations of the resistivity lines are presented in Figure 4-4 with respect to local infrastructure. The lines for the PUREX survey are numbered 200EPX09 through 200EPX15.

HGI has completed previous HRR surveys at the PUREX site resulting in resistivity lines 200EPX01 through 200EPX08. (Note: a change in naming convention has transpired since this report was published; a conversion table is listed in Table 4-1 below relating the current naming convention to the previous convention.) Portions of the previously surveyed lines have been selected for inclusion and interpretation for this report, using the northwest to southeast trending chain-link fence line in the northeast portion of the site as the cutoff boundary. These

lines are indicated in the site map and include portions of 200EPX02, 200EPX03, 200EPX04, and 200EPX08. It also includes the entirety of 200EPX06.

Table 4-1. Listing of Old and New Resistivity Line Names.

Previous Line Name	New Line Name
Line 1	200EPX02 North
Line 2	200EPX07
Line 3	200EPX05
Line 4	200EPX08
Line 5	200EPX02 South
Line 6	200EPX06
Line 7	200EPX03
Line 8	200EPX04
Line 9	200EPX01

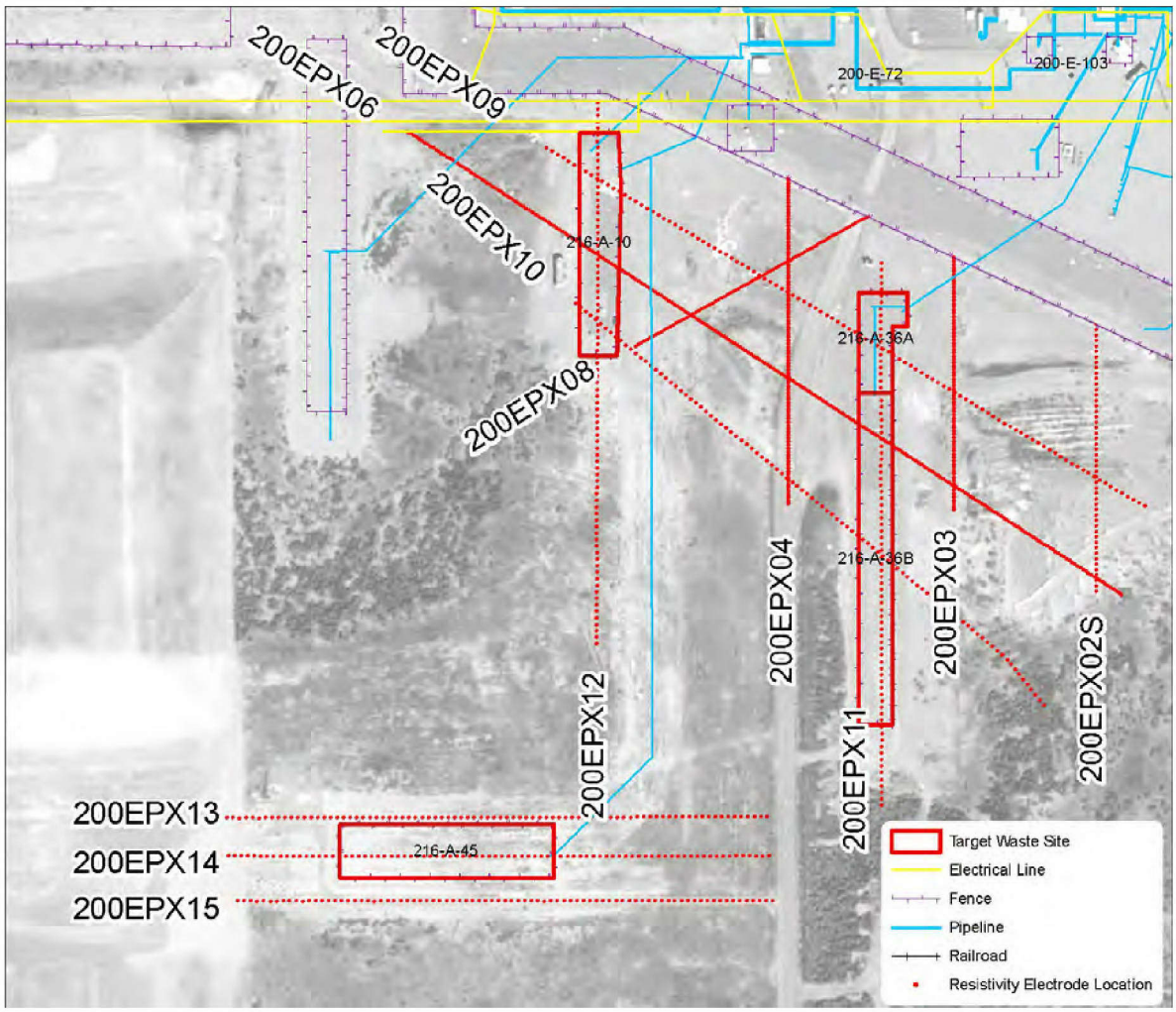

Figure 4-4. Resistivity Line Locations for the PUREX Survey.

Lines 200EPX09 and 200EPX10 were acquired on a trend of northwest to southeast in a near parallel configuration. The two lines flank line 200EPX06 from the previous survey. Both lines extend through two different waste sites from east to west. These sites are 216-A-36 A/B and 216-A-10, respectively. Additionally, both lines are bisected by a paved roadway. Lines 200EPX11 and 200EPX12 were both completed from north to south starting at the previously described chain-link fence. Lines 200EPX11 and 200EPX12 were centered over the 216-A-36 A/B and 216-A-10 waste sites, respectively.

Lines 200EPX13, 200EPX14, and 200EPX15 were acquired on a trend of west to east in a parallel configuration. The lines initiate on the side of a large raised gravel area, and terminate prior to intersecting the paved roadway. Lines 200EPX13 and 200EPX14 cross a known pipeline just east of the 216-A-45 waste area. Line 200EPX14 was centered directly over the 216-A-45 waste site. Line 200EPX15 parallels the gravel access road south of the 216-A-45

waste site. A more detailed description of site infrastructure and disposal volumes can be viewed in Section 2.0.

4.1.1.5 S-Complex

Six 249-meter long, pole-pole resistivity lines were acquired within the vicinity of S-Complex, in the 200 West area. Data acquisition occurred from November 5 to November 6, 2007. The locations of the resistivity lines are presented in Figure 4-5 with respect to local infrastructure. The lines for the S-Complex survey are numbered 200WSC01 through 200WSC06.

Lines 200WSC01, 200WSC02, and 200WSC03 were acquired on a trend of northwest to southeast in a parallel configuration. The lines extend through the Unplanned Release (UPR)-200-W-108 and UPR-200-W-164 waste areas. Line 200WSC02 is centered over the UPR-200-W-108 area. All three lines cross multiple above and belowground pipelines, providing for a difficult environment for resistivity data acquisition.

Lines 200WSC04, 200WSC05, and 200WSC06 were acquired on a trend of north to south in a parallel configuration. The lines cross at least two pipelines and were acquired approximately 20 m south of an additional pipeline. The lines are located east of the 216-S-13 waste site. A more detailed description of site infrastructure and disposal volumes can be viewed in Section 2.0.

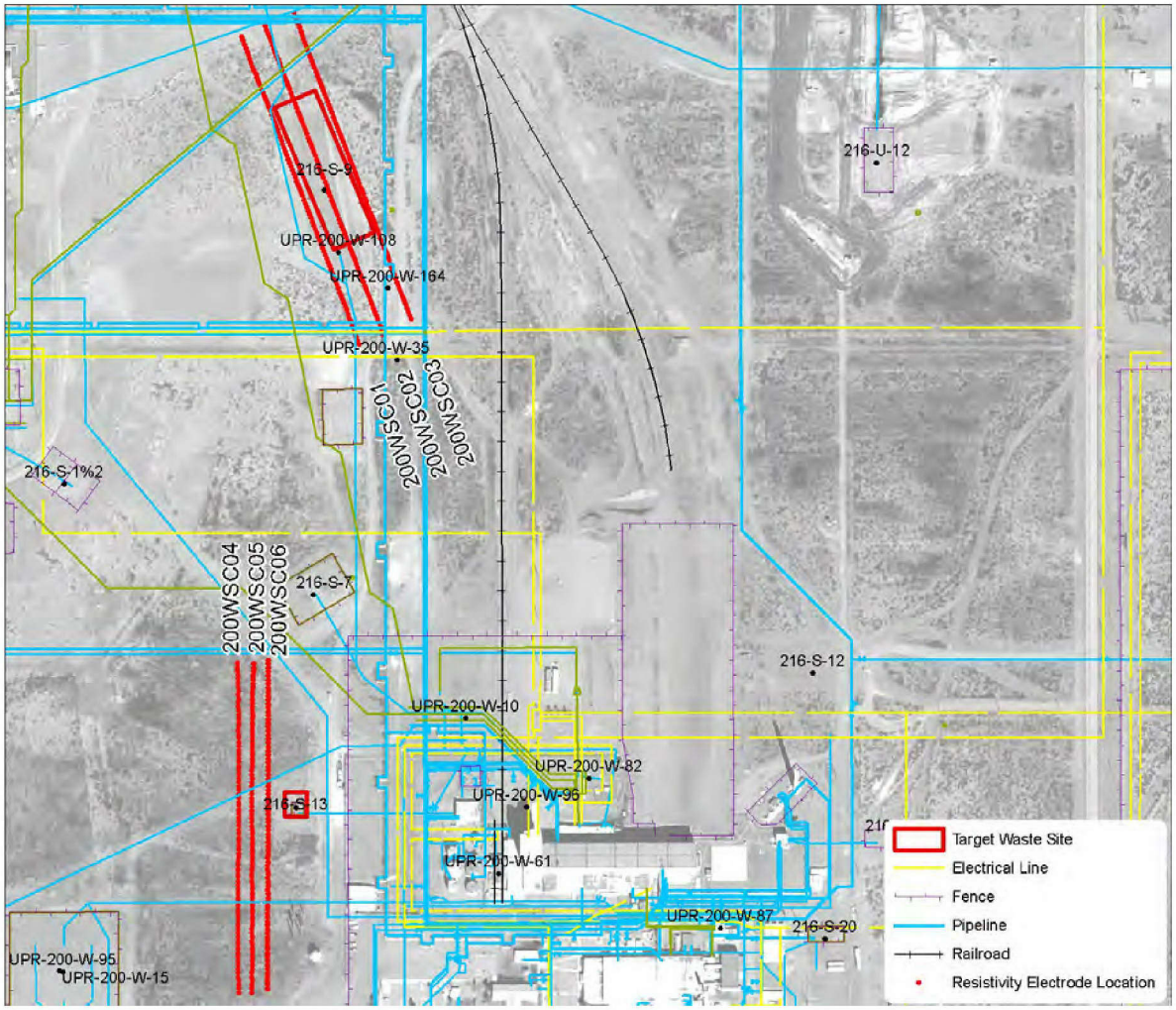

Figure 4-5. Resistivity Line Locations for the S-Complex Survey.

4.1.1.6 T-Plant

Ten 249-meter long, pole-pole resistivity lines were acquired within the vicinity of T-Plant, in the 200 West area. Data acquisition occurred from December 6 to December 16, 2007. The locations of the resistivity lines are presented in Figure 4-6 with respect to local infrastructure. The lines for the T-Plant survey are numbered 200WTP01 through 200WTP10.

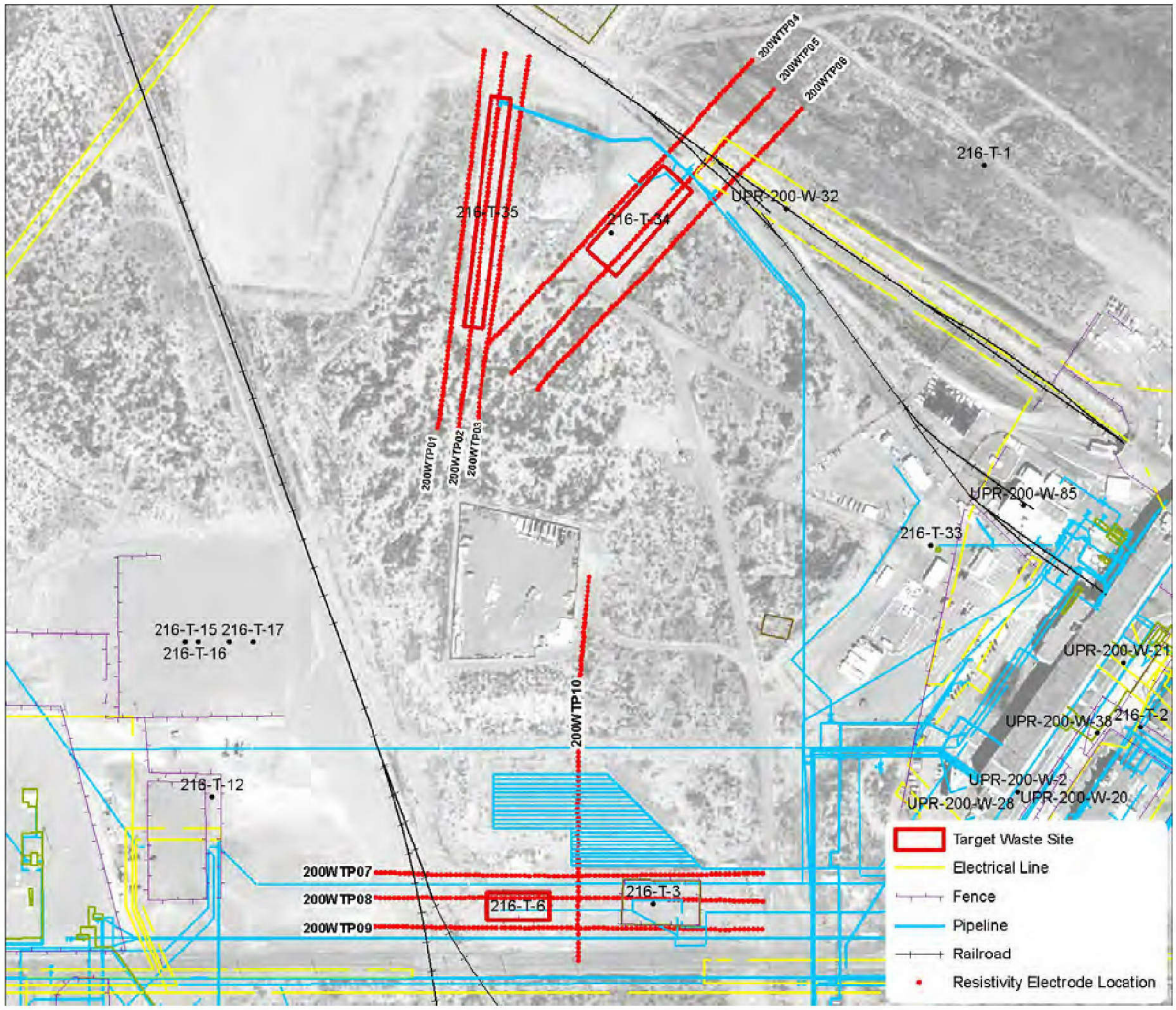

Figure 4-6. Resistivity Line Locations for the T-Plant Survey.

Lines 200WTP01, 200WTP02, and 200WTP03 were acquired on a trend of approximately north to south in a parallel configuration. The three lines were acquired with 200WTP02 centered over the 216-T-34 waste site. A pipeline is known to cross both 200WTP02 and 200WTP03 near the northern end of the line. A dirt road is also present at the northern end of the line. The southern end of the line appeared to be native vegetation.

Lines 200WTP04, 200WTP05, and 200WTP06 were acquired on a trend of northeast to southwest in a parallel configuration. Line 200WTP05 was centered directly over the 216-T-35 waste site. All three lines crossed at least two gravel access roads, a pipeline, and a railroad.

Lines 200WTP07, 200WTP08, and 200WTP9 were acquired on the southern portion of the site. All three lines were acquired west to east, with 200WTP08 centered over the 216-T-3 waste site. The resistivity lines were collected adjacent and parallel to known pipelines. The entire extent of lines 200WTP08 and 200WTP09 are heavily dominated by infrastructure. The southern end of

line 200WTP10 bisects lines 200WTP07, 200WTP08, and 200WTP9. Line 200WTP10 trends north to south and much of the center of line 200WTP10 crosses a sanitary leach field. A more detailed description of site infrastructure and disposal volumes can be viewed in Section 2.0.

4.1.1.7 216-Z-16 Trench

The 216-Z-16 Trench resistivity data were acquired on December 14 and consisted of three pole-pole resistivity lines varying in length from 228 to 234 m. Figure 4-7 displays the location of these lines relative to the surface infrastructure as seen from an aerial photograph. All three lines were acquired in an approximate east-west direction, with Line 200WZT02 centered over the 216-Z-16 trench site. All three lines start at the railroad tracks, cross two known electrical lines and one gravel access road. The lines terminate prior to crossing a second access road. Line 200WZT01 parallels an east west trending gravel access road and a known electrical line. A more detailed description of site infrastructure and disposal volumes can be viewed in Section 2.0.

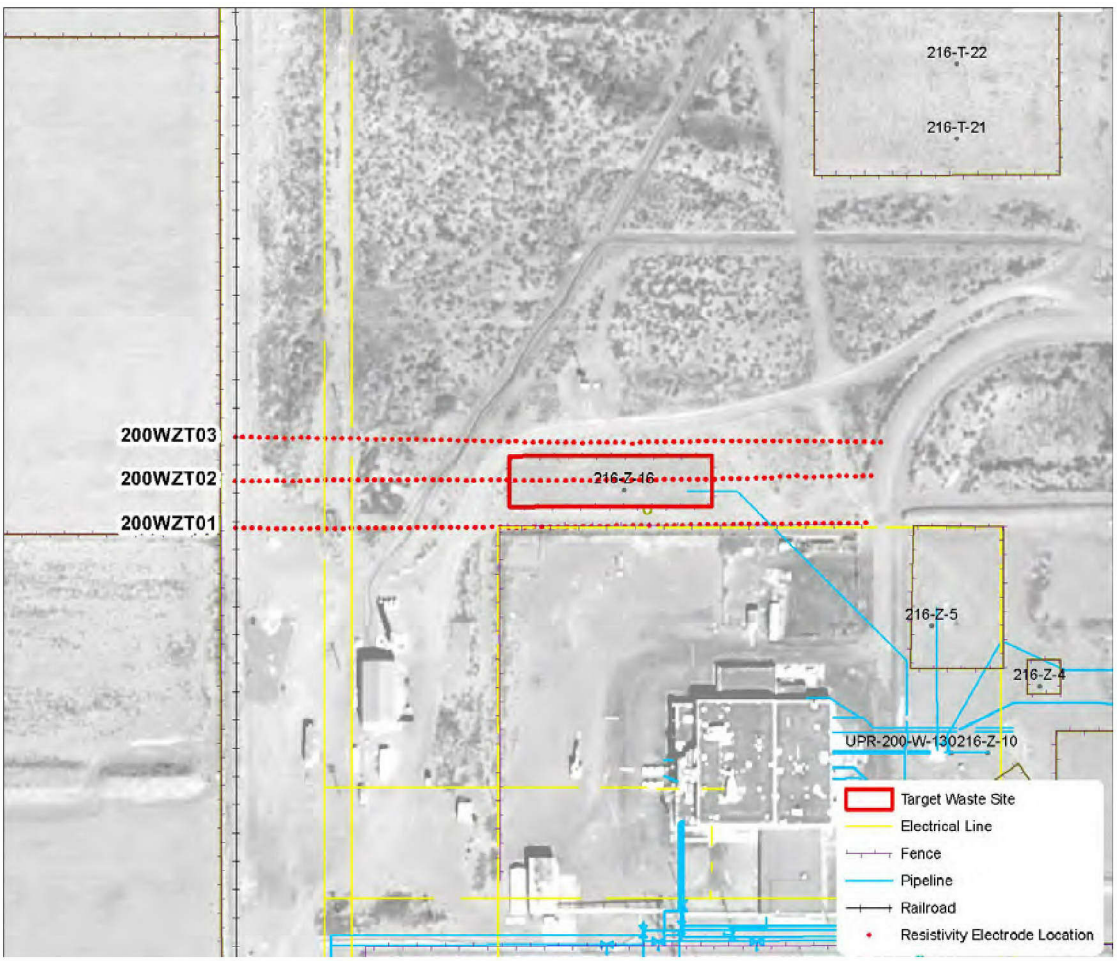

Figure 4-7. Resistivity Line Locations for the 216-Z-16 Trench Survey.

4.2 EQUIPMENT

4.2.1 Electrical Resistivity

Resistivity data were acquired using an AGI SuperSting R8 resistivity instrument using the pole-pole array configuration. The unit is a DC-powered, battery operated, low voltage, low amperage, automatic, eight-channel resistivity system. This system employs specialized cables that can be attached in series to stainless steel electrodes that are in direct contact with the ground. Each electrode acts as either a low-amperage current transmitter or as a potential measuring receiver as the survey progresses.

For each resistivity data collection, the serial number of the AGI SuperSting R8 instrument was recorded. Instrument calibration is maintained and tracked to ensure superior data quality. Table 4-2 shows a listing of instrument serial number and calibration check.

Table 4-2. Calibration.

Line I.D.	Serial Number	Calibrated		Line I.D.	Serial Number	Calibrated
200EAC01	SS0207151	Yes*		200EPX11	SS0207151	Yes*
200EAC02	SS0207151	Yes*		200EPX12	SS0207151	Yes*
200EAC03	SS0207151	Yes*		200EPX13	SS0207151	Yes*
200EAC04	SS0207151	Yes*		200EPX14	SS0207151	Yes*
200EAC05	SS0207151	Yes*		200EPX15	SS0207151	Yes*
200EAC06	SS0207151	Yes*		200WSC01	SS0207151	Yes*
200EAC07	SS0207151	Yes*		200WSC02	SS0207151	Yes*
200EAC08	SS0207151	Yes*		200WSC03	SS0207151	Yes*
200EAC09	SS0207151	Yes*		200WSC04	SS0207151	Yes*
200EBP01	SS0207151	Yes*		200WSC05	SS0207151	Yes*
200EBP02	SS0207151	Yes*		200WSC06	SS0207151	Yes*
200EBP03	SS0207151	Yes*		200WTP01	SS0207151	Yes*
200EBP04	SS0207151	Yes*		200WTP02	SS0501289	Yes*
200EBP05	SS0501289	Yes*		200WTP03	SS0207151	Yes*
200EBP06	SS0207151	Yes*		200WTP04	SS0207151	Yes*
200EBP07	SS0501289	Yes*		200WTP05	SS0207151	Yes*
200EBP08	SS0501289	Yes*		200WTP06	SS0207151	Yes*
200EBP09	SS0501289	Yes*		200WTP07	SS0501289	Yes*
200EBP10	SS0501289	Yes*		200WTP08	SS0501289	Yes*
200EC101	SS0207151	Yes*		200WTP09	SS0501289	Yes*

Table 4-2. Calibration.

Line I.D.	Serial Number	Calibrated	Line I.D.	Serial Number	Calibrated
200EC102	SS0207151	Yes*	200WTP10	SS0501289	Yes*
200EC103	SS0207151	Yes*	200WZT01	SS0501289	Yes*
200EC104	SS0207151	Yes*	200WZT02	SS0501289	Yes*
200EPX09	SS0207151	Yes*	200WZT03	SS0501289	Yes*
200EPX10	SS0207151	Yes*			

*A copy of the calibration record for this instrument is maintained by HGI and is available upon request.
I.D. = identification

The AGI SuperSting R8 has the capability of automatically switching between electrodes without having to physically move the electrode connections after initial set-up. Automatic switching, or multiplexing decreases physical labor, reduces human transcription and tracking errors, enhances operator control of array and data acquisition logistics, and increases the rate and density of data acquired. The AGI SuperSting R8 was programmed to operate a survey line spread of smart electrode take-outs that are line specific variable as well as variable electrode spacing. The survey lines, where necessary, were moved forward incrementally by removing an 12 to 84-electrode segment (depending on the line geometry and cable type) from the trailing end of the survey line spread and placing it at the front of the spread between measurement runs. The movement of cable segments from the back of the line to the front is referred as a roll-along survey.

4.2.2 Global Positioning System

The location of the endpoints of each HRR line were initially established using a Leica GPS1200 RTK GPS unit (Leica Geosystems AG, St. Gallen, Switzerland). Wooden lath stakes were placed in the ground as survey orientation guides at regular intervals along the HRR line. After HRR data acquisition, the same GPS was used for horizontal and vertical control at each electrode location. The Leica GPS1200 unit has ± 0.03 m spherical accuracy. The elevation data were additionally quality checked against topographic contours on U.S. Geological Survey (USGS) 7.5-minute quadrangle maps. Once GPS data were collected they were downloaded and validated using the manufacturer software (i.e., Leica Geo Office).

4.3 CONTACT RESISTANCE TESTING

A contact resistance test was completed prior to the data collection of each survey line. The data was analyzed in order to optimize suspect electrode stations that presented unusually high contact resistance. Optimization of the electrode station may have included applying additional water to increase electrical conductivity between electrode and earth, checking the wire connection between survey cable and electrode, or physically moving the electrode to a more

suitable location. Table 4.3 contains a comparison of contact resistance readings for all electrodes within each project site. The target was to have contact resistances between electrodes less than 2 KOhm, however, in some locations, this was not possible. It was more important to monitor the change in contact resistance between each subsequent electrode and to try to ensure a change of less than 5 percent. Where this was not possible, the electrode number was flagged for possible removal during data filtering.

Table 4-3. Comparison of contact resistance values for each project site.

	Contact Resistance in KOhms		
	Median	**Maximum**	**Minimum**
A Complex	1.95	19.86	0.74
B Plant	0.93	4.80	0.36
216-C-1	0.83	2.15	0.35
Purex	1.39	8.39	0.57
S Complex	2.04	50.76	0.46
T Plant	0.85	2.69	0.23
Z Trench	0.86	2.03	0.49

4.4 DATA PROCESSING & PLOTTING

4.4.1 Management of Field Data

The geophysical data for the resistivity survey, including measured voltage, current, measurement error, and electrode position are recorded digitally with the AGI SuperSting R8 resistivity meter. Each line is recorded with a separate file name. Following field data collection, the raw resistivity and GPS data files are transmitted to the HGI server located in Tucson, Arizona. Data quality is inspected and checked for consistency with respect to adjacent line results, and then are saved to designated folders on the server. The server is backed up nightly and back-up tapes are stored at an offsite location on a weekly and monthly basis.

Survey configuration, location, time and date, field manager, equipment used, environmental conditions, proximal infrastructure and other useful information are recorded during data acquisition on standard HGI resistivity field forms. These forms are submitted with the raw

resistivity and GPS data and are subsequently saved to the HGI- Tucson server. The information is then archived within a Microsoft Access™ database.

4.4.2 Data Reduction: Filtering, Editing, Quality Assurance / Quality Control

Raw resistivity data are imported and parsed using the HGI Pro (v 3.4.2) Software. This software provides a simple means for quality checking and preliminary assessment by using a Microsoft Excel® template, which charts specific data parameters.

After parsing, the raw data are evaluated for measurement noise. Those data that appear to be extremely noisy and fall outside the normal range of accepted conditions are removed. Examples of conditions that would cause data to be removed include negative or very low voltages, high-calculated apparent resistivity, extremely low current, and high repeat measurement error. Figure 4-8 shows an example of data that would be targeted for removal. To ensure that the original data are retained and error removal can be repeated, the edited data are saved to an appropriately designated folder with a descriptive file name.

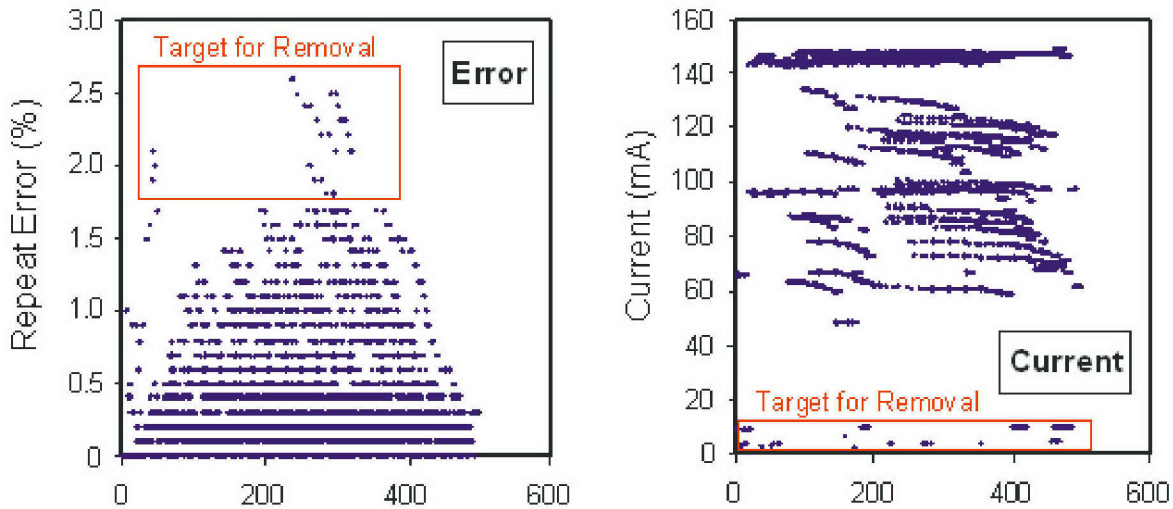

Figure 4-8. Example of Noisy Data Removal using Repeat Error and Electrical Current.

An example of the effect of data removal based on noise is shown in Figure 4-9. The top plot of Figure 4-9 shows the distribution of all measurements (all raw data), plotted as a linear pseudo-section. The bottom plot of Figure 4-9 shows the distribution of data after removal of noisy data. In this example, of the 3902 data records in the raw data file, 120 were removed for failing the HGI data quality standards criteria.

After rejection of noisy data, the remaining data are evaluated for physical impossibilities based on potential field theory. This step requires that the transfer resistance (V/I) for each transmitter

™ Microsoft Access is trademark of Microsoft Corporation in the United States and/or other countries.
® Microsoft Excel is a registered trademark of Microsoft Corporation in the United States and/or other countries.

electrode be plotted with all of the receiver electrodes. The plot should show a smoothly varying function as the separation of the transmitter and receiver electrode increases. Large spikes in the function are physical impossibilities in natural media, and those data are removed from the data set. Figure 4-10 demonstrates an example of a data spike that would be targeted for removal. In this example, the transmitter electrode is number 237, and has the spatial coordinates of 566354.53 and 133619.49. The processing of data for spike rejection also includes plotting each receiver electrode individually with its associated transmitter electrode set.

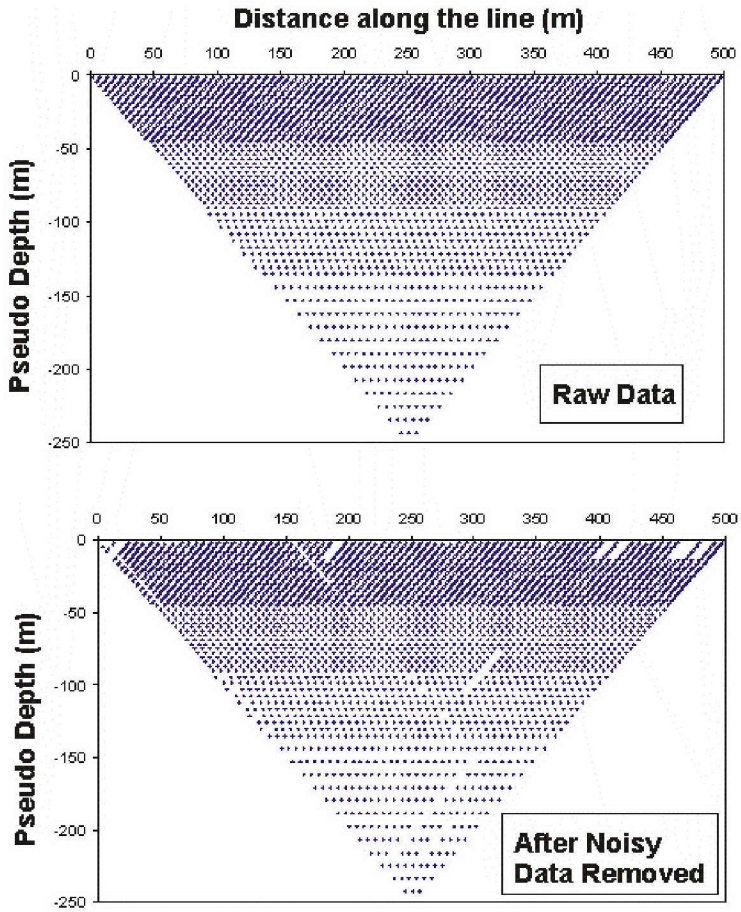

Figure 4-9. Example of Data Scatter (Plotted as Linear Pseudo-Section), Before and After Noisy Data Rejection.

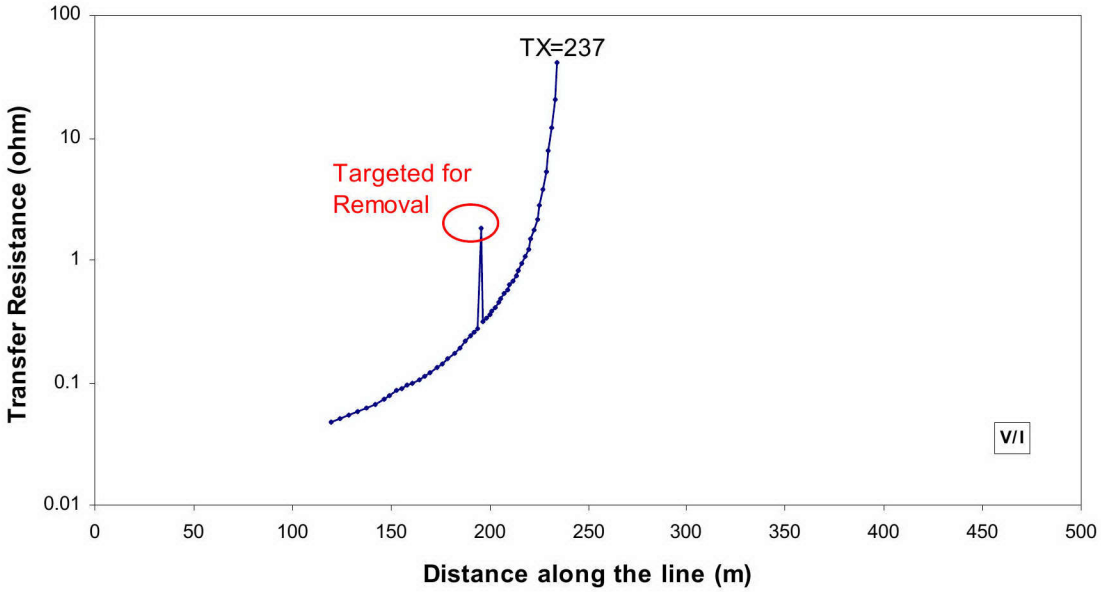

Figure 4-10. Example of Spike Rejection of Transfer Resistance Data for Transmitter Electrode 237.

After eliminating all data that are considered low quality, the data are plotted as HRR color-contoured cross-sections using Surfer® software package Version 8.02. The HRR routine places the measured apparent resistivity value at a depth BGS that best represents its location. The plot is only used as a quality check of data and data coverage, while also providing an initial approximation to the depth of the target.

Table 4-4 lists specific line information and data editing statistics for the sites located within the 200 East area, and Table 4-5 lists the same information for the sites located within the 200 West area. The tables identify the number of lines completed per site, line I.D., data acquisition date, total line length, total number of raw points acquired, and the remaining number of raw points after editing.

® Surfer is a registered trademark of Golden Software, Inc., Golden, Colorado.

Table 4-4. Specific Line Information for HRR Data Collected within the 200 East Area.

Site	Line I.D.	Acquisition Date	Line Length (meters)	Total Raw Points	Points After Editing
216-C-1	200EC101	12/5/07	249	1369	1369
	200EC102	12/4/07	246	1312	1197
	200EC103	12/4/07	228	1159	1135
	200EC104	12/4/07	246	1271	1271
A-Complex	200EAC01	10/18/07	129	883	618
	200EAC02	10/18/07	117	780	730
	200EAC03	10/19/07	393	2421	1955
	200EAC04	10/22/07	393	2582	2073
	200EAC05	10/23/07	393	2500	2130
	200EAC06	10/23/07	249	1364	1174
	200EAC07	10/24/07	141	1128	1128
	200EAC08	10/24/07	141	1128	1106
	200EAC09	10/24/07	141	1037	1035
B-Plant	200EBP01	12/7/07	345	2010	1688
	200EBP02	12/10/07	351	2219	1405
	200EBP03	12/8/07	357	2180	1832
	200EBP04	12/6/07	249	1352	1226
	200EBP05	12/6/07	249	1364	1262
	200EBP06	12/7/07	249	1364	1163
	200EBP07	12/13/07	249	1364	1240
	200EBP08	12/12/07	249	1364	1294
	200EBP09	12/12/07	249	1418	1166
	200EBP10	12/12/07	249	1363	1134
PUREX	200EPX09	11/9/07	321	1843	1540
	200EPX10	11/9/07	285	1455	1176
	200EPX11	11/9/07	249	1323	1138
	200EPX12	11/12/07	249	1364	1123
	200EPX13	11/8/07	249	1323	1138
	200EPX14	11/8/07	249	1272	1093
	200EPX15	11/8/07	249	1307	1126

I.D. = identification.

Table 4-5. Specific Line Information for HRR Data Collected within the 200 West Area.

Site	Line I.D.	Acquisition Date	Line Length (meters)	Total Raw Points	Points After Editing
S-Complex	200WSC01	11/6/07	249	1364	1225
	200WSC02	11/6/07	249	1316	1218
	200WSC03	11/6/07	249	1364	1263
	200WSC04	11/5/07	249	1362	1043
	200WSC05	11/5/07	249	1278	989
	200WSC06	11/5/07	249	1363	1007
T-Plant	200WTP01	12/6/07	249	1268	1115
	200WTP02	12/6/07	249	2709	2313
	200WTP03	12/7/07	249	1406	1371
	200WTP04	12/7/07	249	1357	1319
	200WTP05	12/10/07	249	1364	1350
	200WTP06	12/10/07	249	1338	1195
	200WTP07	12/14/07	249	1345	1246
	200WTP08	12/16/07	249	1356	1272
	200WTP09	12/14/07	249	1268	1229
	200WTP10	12/16/07	249	1312	1151
216-Z-16 Trench	200WZT01	12/14/07	228	1191	1141
	200WZT02	12/14/07	231	1209	1128
	200WZT03	12/14/07	234	1241	1147

I.D. = identification.

4.4.3 2D Resistivity Inversion

AGI EarthImager 2D software is used for inversion process. An input file is created from the edited resistivity data (discussed in Section 4.3.2) and inversion parameters are chosen to maximize the likelihood of convergence. It is important to note that up to this point, no resistivity data values have been manipulated or changed, such as smoothing routines or box filters.

The inversion process follows a set of stages that utilize constant inversion parameters to maintain consistency between each model. Inversion parameter choices include the smoothing constraint, the starting model, the inversion routine (robust or smooth), and various routine halting criteria that automatically determine when an inversion is complete.

In the cases that the inversion models do not converge to the first criteria set, the edited data file are re-evaluated and additional data may be removed through editing. Convergence is judged whether the model correctly estimated the subsurface properties, whereby the modeled voltage is equivalent to the measured voltage. A difference of 5 percent or less between modeled and measured data is considered acceptable. If, after 20 iterations within AGI EarthImager 2D the difference is greater than 5 percent, those data that are identified are evaluated for removal. Another important metric is the L_2 factor, which determines the ratio of the modeled cells that are changed relative to beginning conditions.

To standardize and streamline the inversion process for each line of resistivity data acquired (53 total lines), a system of "stages" was created and applied to the inversion process. This system consists of consecutive steps that are triggered based on a "pass" or "fail" of the initial run. A run is defined as a set of 20 iterations. To pass a run the data must meet set stop criteria, in this case an RMS value less than or equal to 5 and an L_2 value less than or equal to 1, in 20 or less iterations. This signifies the completion of "Stage 1." If the data do not converge at completion of Stage 1, the operator will complete "Stage 2" steps. During Stage 2, a filter is applied to remove problem data. If upon completion of Stage 2, convergence is still not achieved, "Stage 3" steps will be initiated. A detailed explanation of each inversion stage is discussed below. All inversions, regardless in which stage convergence may or may not occur, are ultimately reviewed and approved by an HGI senior inversion specialist in a final pass review.

Inversion Routine – Stage 1

Stage 1 involves taking the edited resistivity data in Sting™ file format (.STG), reading the file into AGI EarthImager 2D, and running the inversion routine with a set of standardized base settings. Screen captures showing the base settings are presented in Figures 4-11 through 4-13. If data converge, based on an RMS of < = 5 and L_2 < = 1, the model is considered successful and assigned a "passing" score. If they do not converge, the models are considered unsuccessful and assigned a "failing" score. Models that "fail" are sent for additional filtering and modeling under Stage 2.

™ Sting is a trademark of Advanced Geosciences, Inc. in the United States, other countries, or both.

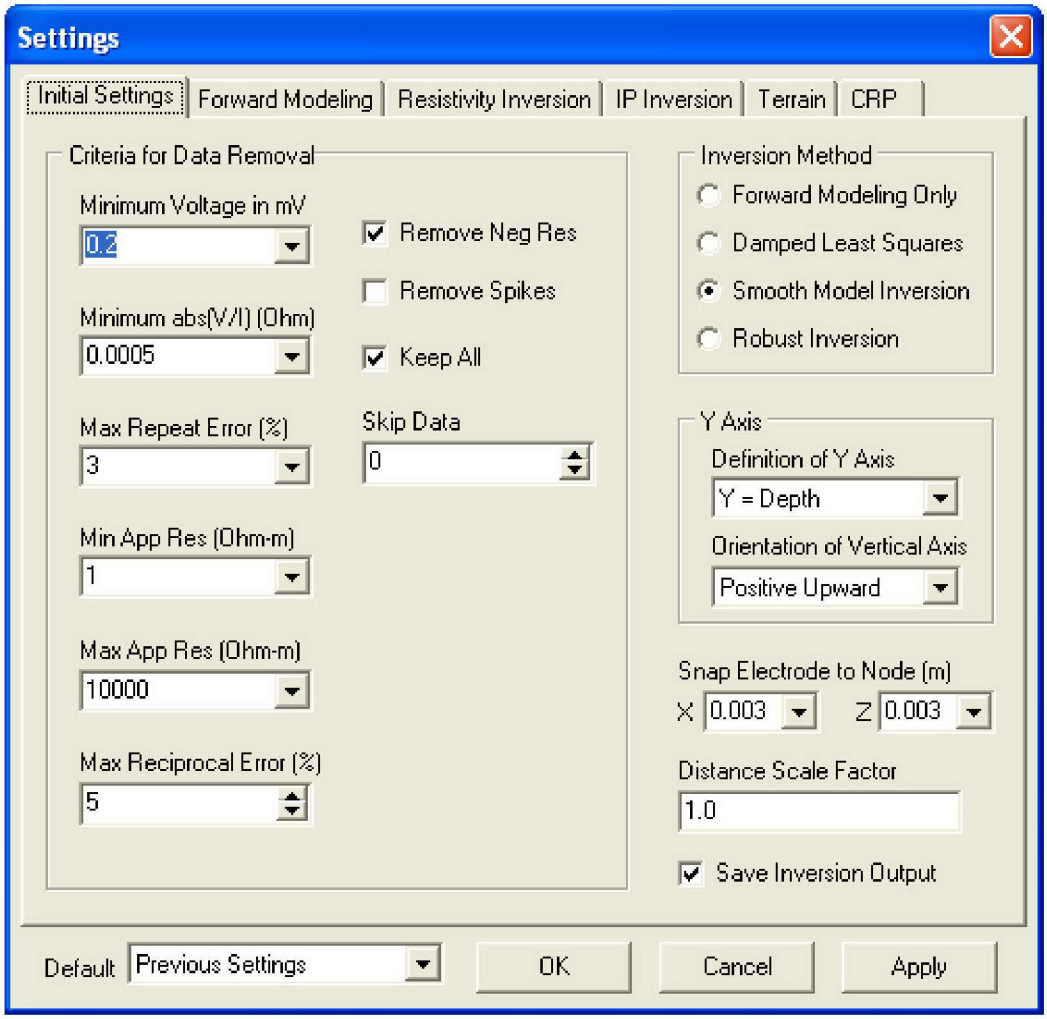

Figure 4-11. Initial Setting used for Inversion Stages 1 and 2.

Inversion Routine – Stage 2

During Stage 2, a filter is applied to the Stage 1 failed inversion model using the internal AGI EarthImager 2D data misfit histogram and data removal tool. The standard removal criteria used is "all data greater than 15 percent data misfit are removed" (with a ± 5 percent window threshold to account for nonflexible range bins in AGI EarthImager). Data are then run through the inversion routine using the same inversion parameters as in Stage 1. If the data converge within 20 iterations, based on an RMS of < = 5 or L_2 < = 1, the models are considered successful and "pass." If they do not converge, the models are considered unsuccessful and "fail." Models that "fail" are sent for additional filtering and modeling under Stage 3.

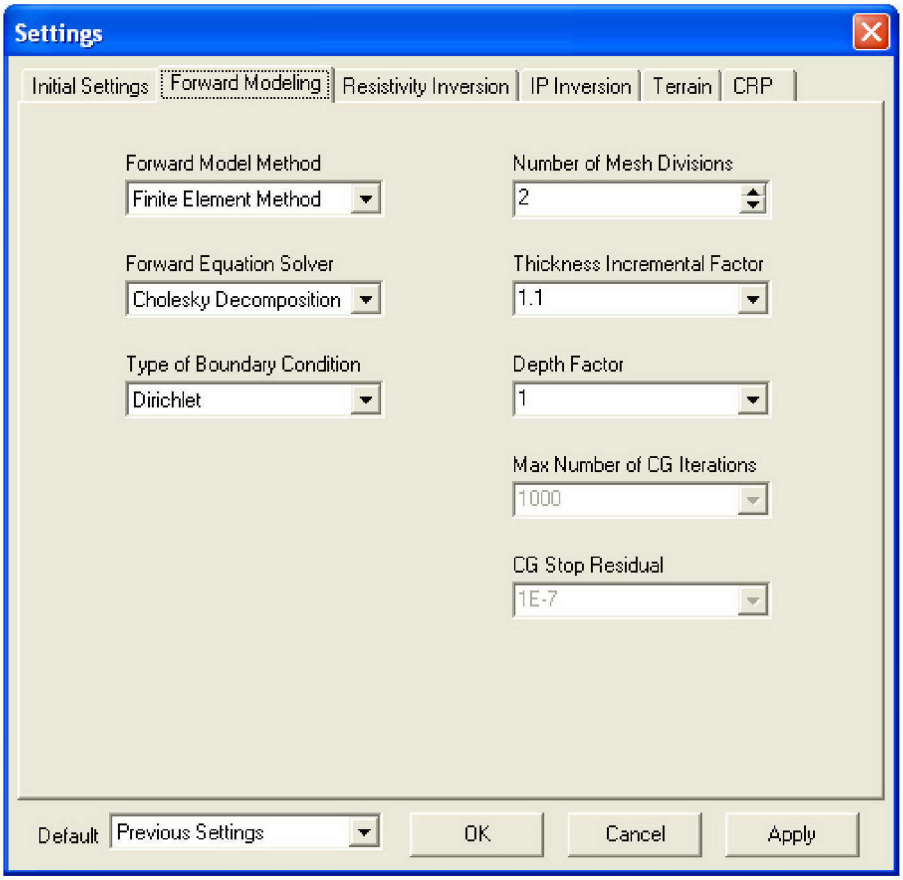

Figure 4-12. Forward Modeling Selections used for Inversion Stages 1 and 2.

Inversion Routine – Stage 3

If the data set does not converge after Stages 1 and 2, the data are forwarded to an HGI senior inversion specialist and an in-depth analysis is completed. The data are scrutinized for deviations in data that do not conform to the inversion parameters used during previous attempts. Based on professional experience, the specialist may change particular settings that might affect successful convergence of recorded versus modeled data. The specific Stage 3 recommendations performed for the inversion lines presented in this report are as follows:

First Run: Run original edited AGI™ .STG file using a new set of base parameters. These parameters are presented in Figures 4-15 through 4-17.

First Misfit Data Removal Filter: Remove all data > = 15 percent misfit in the histogram filter window (with a ± 5 percent window threshold to account for nonflexible range bins in

™ AGI is a trademark of Advanced Geosciences, Inc. in the United States, other countries, or both.

AGI EarthImager). If this first filter will remove more than 30 percent of the total data points, reduce the misfit criteria to a lower histogram bin, which removes < 30 percent of the total data.

Additional Misfit Data Removal Filters: Choose the data removal histogram bin which is >= 15 percent model misfit (with a ± 5 percent window threshold to account for nonflexible range bins in AGI EarthImager) and removes no more than 5 percent of total data points (Figure 4-14). Continue these smaller step filters until the model converges. Stop any models where > 30 percent of the total data points will be removed.

Using the Stage 3 recommendations, all 2D inversions that did not pass Stages 1 or 2 attempts converged successfully.

All passing Stage 1 and 2 inversions are also reviewed by an inversion specialist to ensure that batch processing does not result in running a model beyond reasonable limits.. If this is the case, an earlier iteration may be selected for plotting and presentation. If an earlier iteration is selected for a Stage 1 or 2 inversion, the results are then labeled as a Stage 3 iteration, indicating that special analysis has been applied.

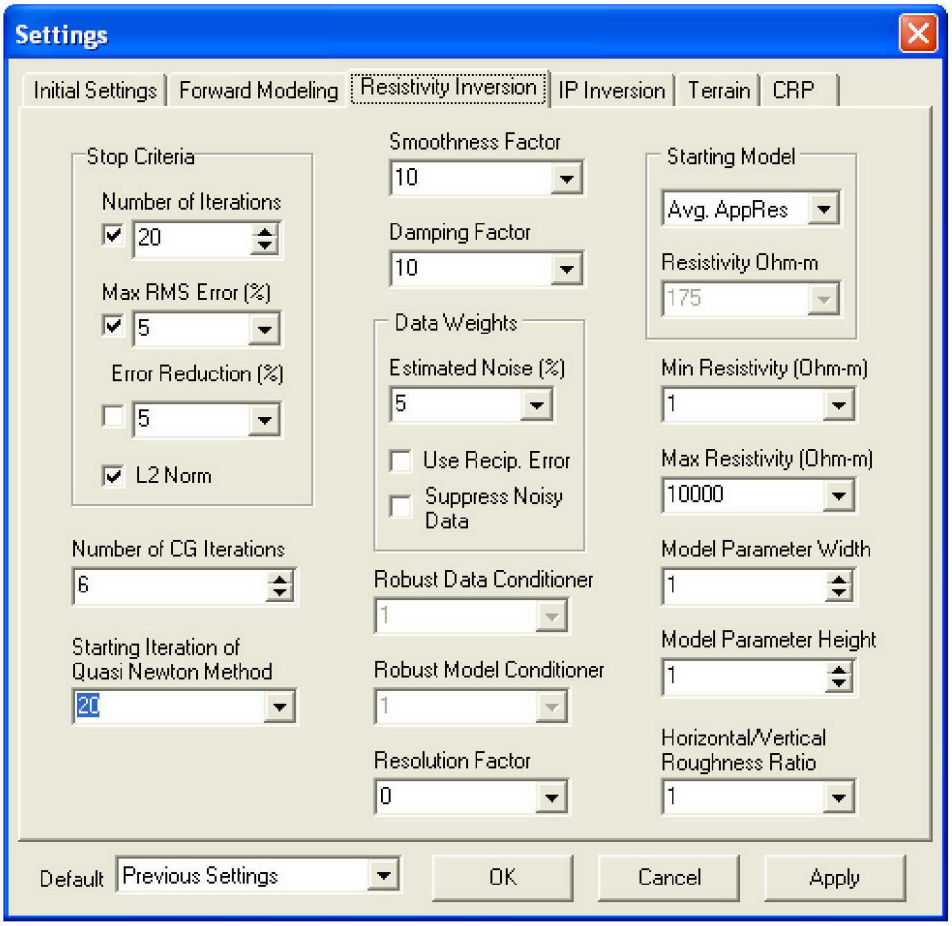

Figure 4-13. Resistivity Inversion Settings used for Inversion Stages 1 and 2.

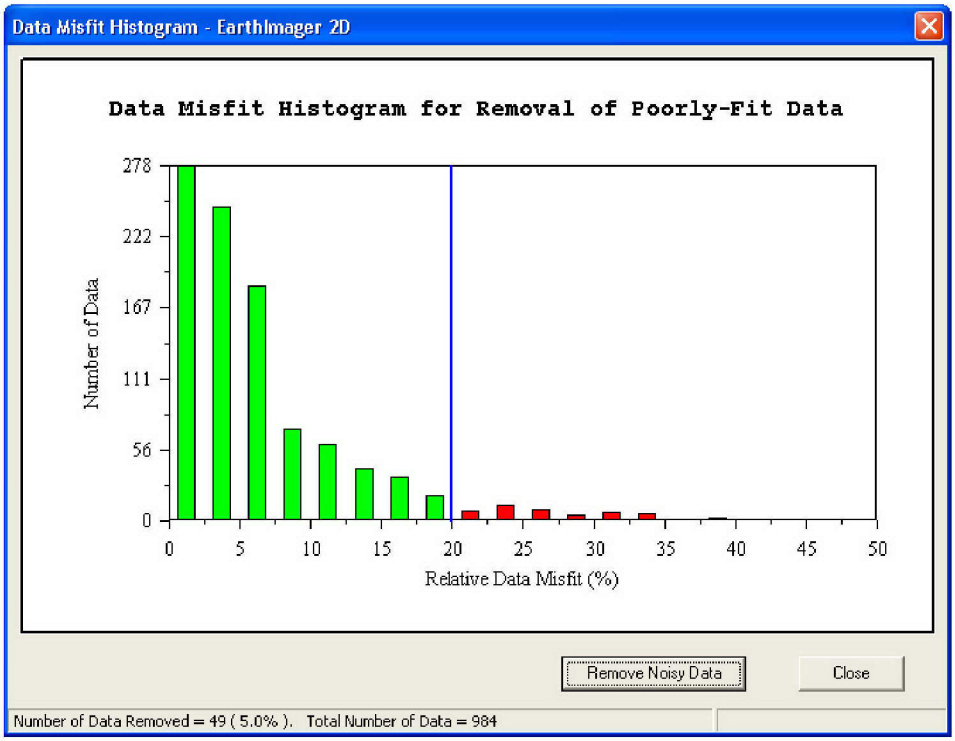

Figure 4-14. Example of Data Removal Filter at a Maximum Limit of 5% of Total Data Removed. In this case, the data removed are in the 20% misfit histogram bin (> = 15%).

4.4.4 2D Plotting

The inverted data are output from AGI EarthImager 2D into an XYZ data file (.DAT) and are then gridded in Surfer using the Kriging algorithm with an x and y grid spacing of 0.5 m. The grid files are then contoured using Surfer, a site-wide standardized color file is applied, and a blanking file is used to correct for absent data. Geographical Information System (GIS) information such as roadways, pipelines and other infrastructure, resistivity line intersections and other relevant line features are posted above the resistivity section to assist in data analysis. Qualified in-house inversion specialists subject each profile to a final review.

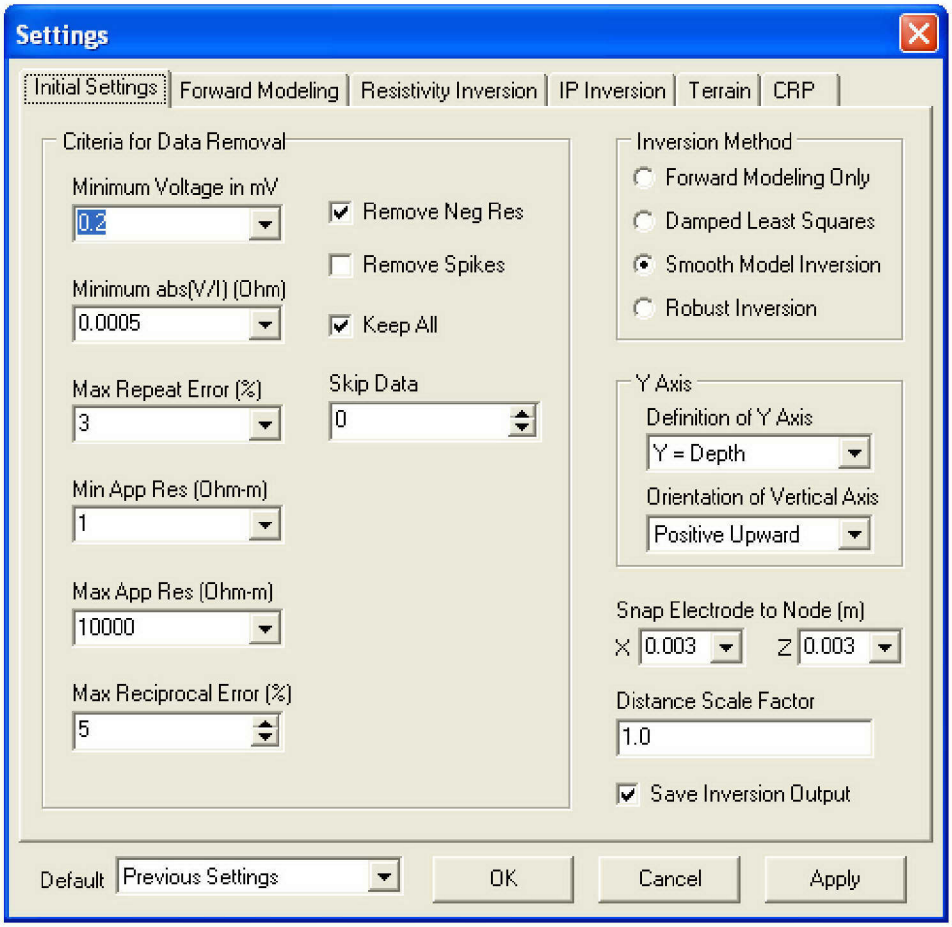

Figure 4-15. Initial Setting used for Inversion Stage 3.

Inversion Errors

Appendix A contains exported screen captures from the EarthImager 2D inversion software. The images are segmented into three sections; the top showing raw data, the middle showing the forward model solution and the bottom showing the inversion model. An example of the 2D inversion screen captures can be viewed in Figure 4-16. The screen captures are considered while completing quality control in preparation of the 2D contour images presented in the results section of this report (Section 5). Noisy electrodes are removed prior to inversion modeling to improve modeling results. However, the inversion software automatically populates any missing model cells with interpreted raw data before completing a forward solution. For areas near missing electrodes, the interpreted raw data calculated by EarthImager 2D is not generally a smooth or realistic approximation. An example of this can be viewed in Figure 4-16 where the red circle highlights an area of removed data that has been interpolated incorrectly by the inversion software. In order to minimize this problem, these areas of interpreted data are

removed prior to final gridding and contouring to show a smoother and more continuous interpretation across the areas of missing. Figure 4-17 shows the same resistivity profile as Figure 4-16 but the area of missing data has been smoothed correctly.

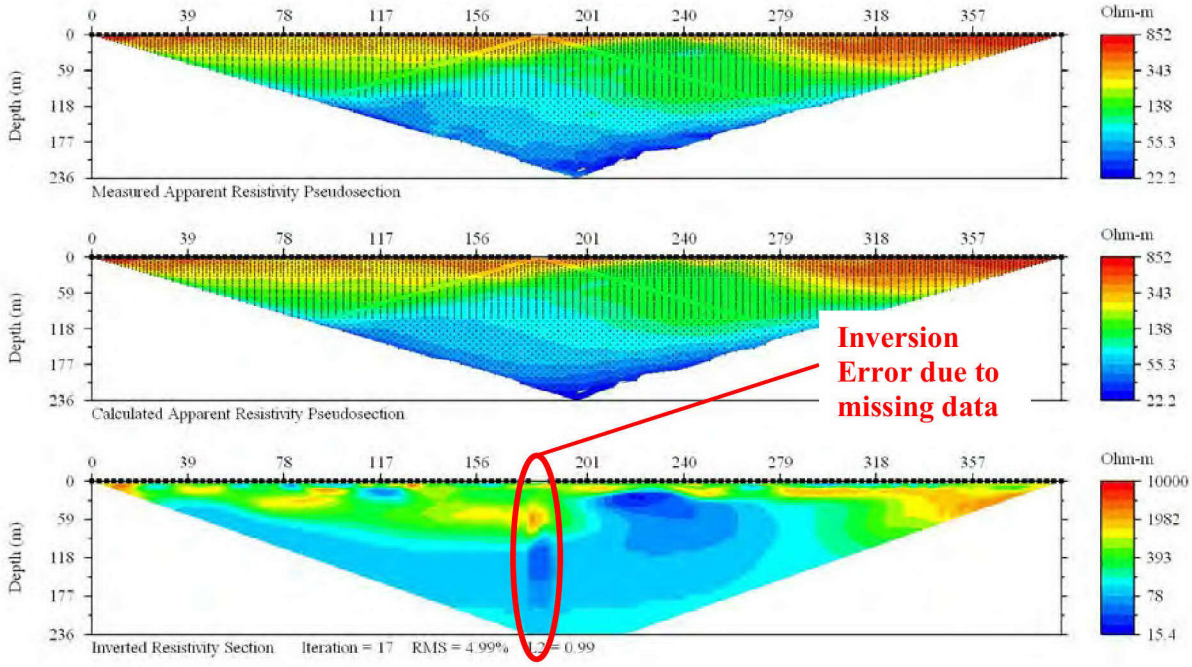

Figure 4-16. Example of Inversion Error due to missing data for Line 200EPX06.

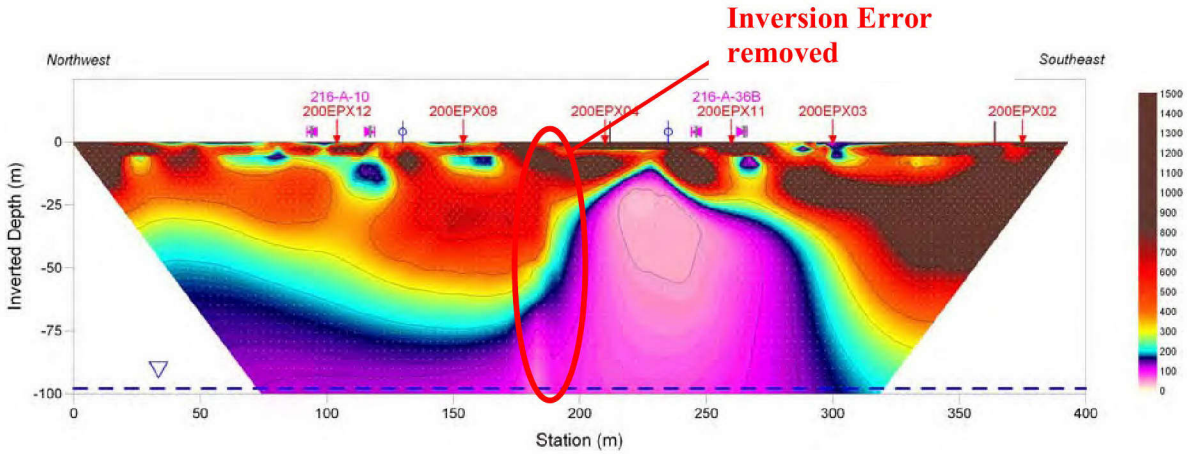

Figure 4-17. Example of Contour plot showing removal of inversion error for Line 200EPX06.

4.4.5 3D Visualization

Once the 2D inversion results are finalized and approved, the inversions are grouped into subsets to produce 3D interpretations using RockWorks™ 2007 (Version 6.3) 3D visualization software. The 2D data are grouped based on proximity and geometry, and then RockWorks2007 software is used to produce a 3D model, or rendering, based on the 2D data. RockWorks2007 software uses modeling algorithms to create a continuous model of the 2D data based on user input spatial boundaries and XYZ data. The solid model is then filtered to display data of a specific value in order to pull out features and targets of interest. Horizontal resistivity slices are also created to display data at different depths BGS. The 3D interpretations are geo-referenced and plotted along with an aerial image of the site. Site infrastructure, such as pipes and waste sites, are inserted into the 3D space to assist in interpretation.

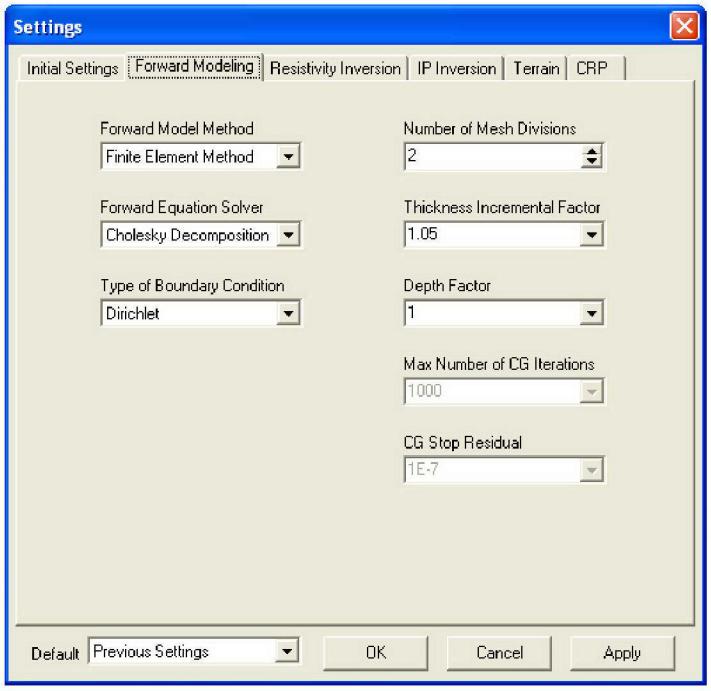

Figure 4-18. Forward Modeling Selections used for Inversion Stage 3.

™ RockWorks is a trademark of RockWare, Inc. in the United States, other countries, or both.

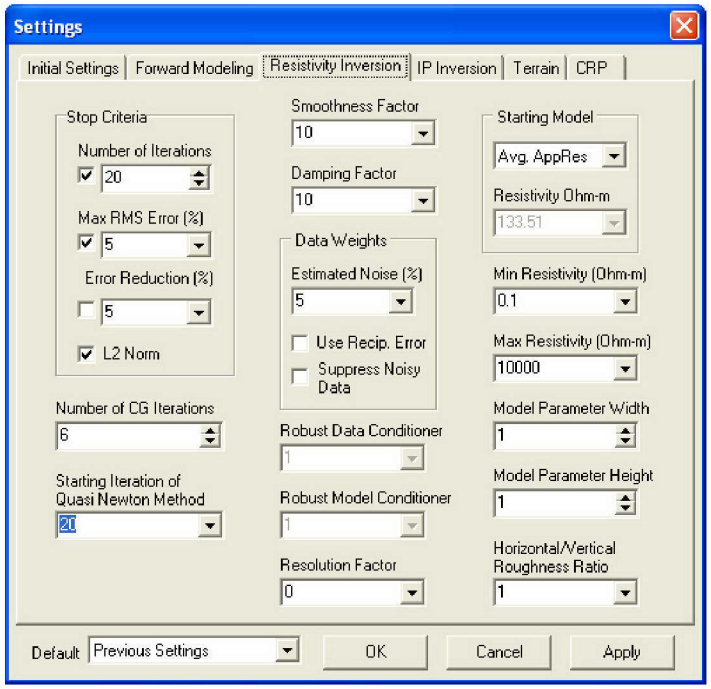

Figure 4-19. Resistivity Inversion Settings used for Inversion Stage 3.

5.0 RESULTS & INTERPRETATION

The following section describes the results for 2D inversion and 3D visualization of apparent resistivity data. AGI EarthImager 2D was selected as the primary numerical modeling software used to perform the 2D inversion of each line. In addition, several survey lines were also inverted using RES2DINV Version 3.55 (Geotomo, Ltd.) software as part of a quality control comparison. Specific model parameters are discussed in detail within Section 4.3. Appendix A includes a set of output images from AGI EarthImager 2D showing the measured pseudo-section, modeled pseudo-section, and inverted results for each survey line. To satisfy quality assurance needs, resistivity inversion parameters and methodology were implemented as uniformly as possible. Unfortunately, the complexity of the project sites and the lack of variation in modeling parameters created some undesirable artifacts in the 2D section. Most notably is the "ringing" in the near-surface data that is noticeable on many of the result plots.

The resistivity data for this project was inverted using a 2D inversion code in accordance with the project contract and provided SOW. However, several characterization sites presented complex subsurface features that represent 3D targets, which cannot be adequately defined or imaged using 2D inversion techniques. Where this occurs it is likely that nearby or off-line targets may present preferential current pathways that result in a resistivity anomaly indicative of modeling or interference effects and not changes in subsurface soil properties. These modeling or interference anomalies are typically of higher magnitude than increased soil moisture due to waste disposal and therefore complicate interpretation. This is especially true where multiple modeling or interference anomalies are located in close proximity and are merged or smeared by the contouring process.

Interpreting Color Scales:

Two-dimensional cross-sections were generated from the completed 2D inversion data using a site specific color scale that was developed through a statistical analysis of the apparent resistivity values for each of the seven project sites in the 200E and 200W areas. A histogram based on data from all survey lines within each project site was used to generate a color gradient that is sensitive to the resistivity range of each particular site. For example, the S Complex site has a concentration of data in the range of 100-200 Ohm-m and very little data greater than 450 Ohm-m. Therefore, the color scale must have a greater variety of hues in the 100-200 ohm-m range while it is acceptable to assign a single color to all values greater than 450 ohm-m where little change occurs. Similarities in the S Complex and 216-C-1 data sets allowed for a shared color scale, while all other sites have unique scales. The T Plant and B Plant sites each had several lines that were dominated by infrastructure which are not diagnostic of the target waste disposal volume. Therefore, these lines were excluded from the histogram analysis.

Past resistivity projects used a standard color scale that was uniformly applied to all sites that allowed comparison of resistivity magnitudes between the individual sites. This color file

became known as the "Hanford Site Standard" color scale. However, it should be noted that the standard Hanford Site resistivity color scale was originally developed for one particular field site that is likely not to contain the identical geology, soil chemistry, and subsurface infrastructure as several other sites that it has been used for. Fluor Hanford scientists asked HGI to prepare color scales that were tailored to the resistivity range of each site. For reference, Figure 5-1 provides a comparison of color scales used within this report to the "Hanford Site Standard" color scale used on previous reports. The histograms used to generate each color scale are presented in Section 5.1.1.

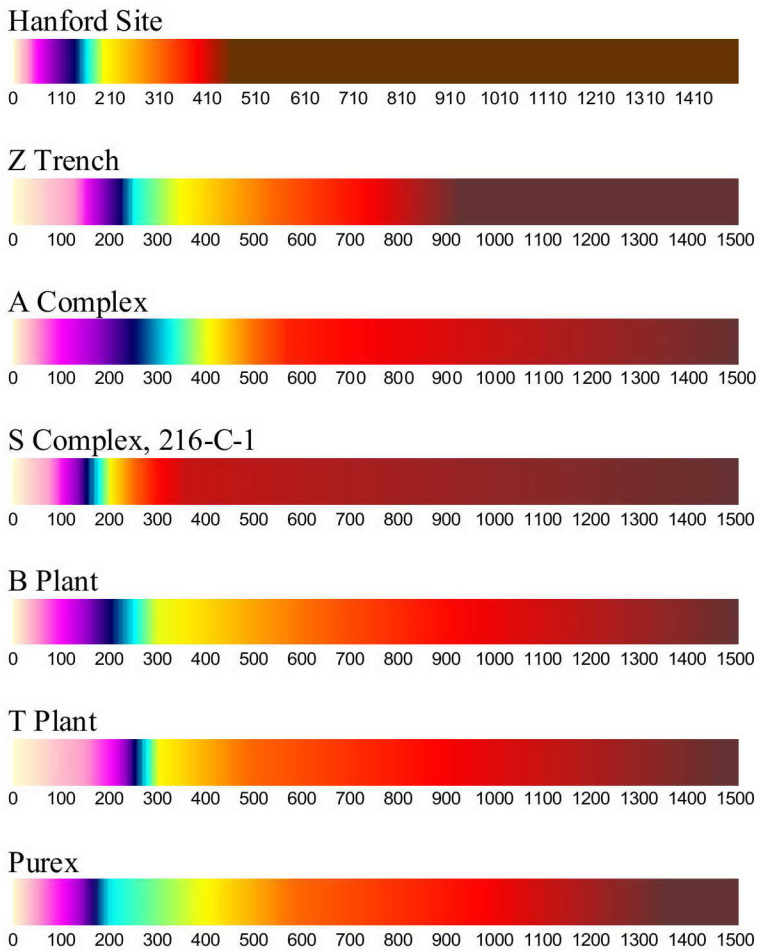

Figure 5-1. Comparison of color scales used within this report to "Hanford Site" color scale used on previous reports.

Two-Dimensional Inversion Plot Interpretation:

The 2D inversion contour plots are presented with a variety of information that is designed to assist the reader with interpretation. Each plot contains the following:

- Line Notes - a series of line and feature notes that are posted at the known location along each line. Line and feature notes may include locations of infrastructure, locations of waste disposal sites and locations of crossing resistivity profiles.

- Inversion Parameters – shows the 2D inversion RMS value for the selected iteration used for the contour plot and the associated inversion convergence curve highlighting the selected iteration.

- Interpretation Features – highlights conductive anomalies that are associated with the following interpretations

    - Yellow - Conductive anomaly magnitude or character is indicative of infrastructure and-or correlates to known infrastructure location (unlikely to be increased soil moisture or salts).

    - Green - Conductive anomaly magnitude or character may be indicative of either infrastructure or an increase in soil moister or salt and may correlate to known location of infrastructure and-or known waste disposal area. (possibly a combination of infrastructure and increase in soil moisture or salts).

    - Blue - Conductive anomaly magnitude or character is not indicative of infrastructure and-or does not correlate to known infrastructure location (possible increased soil moisture or salts).

- Color Scale – shows the resistivity color gradient and the associated resistivity values used to generate the color contour plot.

- Data Points – white dots are used to show locations where data are present, the reader is cautioned to be suspicious of areas that show conductive anomalies near areas of low data density. Data may have been removed as part of the filtering process based on high error.

Three-Dimensional Visualization:

A 3D visualization model using the output from the 2D inversion model was constructed for each project site using RockWorks2007 software. The software was used to generate an interpolated volumetric resistivity distribution. The complexity of many of the sites makes it challenging to visualize in a 3D isometric and volumetric view. Therefore, "depth slices" from the 3D volumetric distribution were extracted and shown in plan view. In this manner, it is more efficient to show the relative site infrastructure in association with resistivity changes. Depth

slices, at-depths 15, 30, 45, 60, and 75 m BGS, were selected and are presented for the applicable sites. This representation of the data lends itself to more accurate correlations of the data with infrastructure. The "Hanford Site Standard" resistivity color scale was used on all 3D depth slices.

The 3D visualization was generated by application of a 3D numerical interpolator to 2D acquired and 2D inverted data. The resulting 3D visualization is therefore not a true 3D visualization but rather a 3D interpolation of 2D data. For the purposes of this report, any mention of 3D visualization represents interpolated 2D data.

Survey Position and Elevation Control:

Elevations and coordinates along the lines were collected using a survey grade Global Positioning System. The elevations were incorporated and used to generate the HRR quality control plots. Elevations were not used as part of the 2D inversion because all but the 216-C-1 site contained minimal topographic change relative to the length of the line.. The limited topographic changes would be of minimal value in relation to complexity of the abundant infrastructure (at almost all project sites) interference. The 216-C-1 site contained significant topographic change along profile 200EC103 due to a above ground concrete vault that was covered with soil. This model was completed with and without topographic elevations in order to assess the impact. The 2D inversion software had great difficulty resolving the concrete vault and produced poor convergence and minimally useful results regardless of topographic elevation. This is considered a worst case example and illustrates why topography was not used for the 2D and 2D inversion models.

Contact Resistance Values:

A contact resistance test was completed prior to the data collection of each survey line. The data was analyzed in order to optimize suspect electrode stations that presented unusually high contact resistance. A more detailed discussion can be viewed in section 4.3.

5.1 200 EAST PROJECT SITES

5.1.1 216-C-1

5.1.1.1 2D Inversion Results

The 2D inversion results for resistivity surveys performed at the 216-C-1 site are displayed in Figures 5-3 through 5-11 below. Figures 5-3 through 5-6 display the results in a cross-sectional format, while Figures 5-7 through 5-11 display the results of a 3D visualization of the same data

set. Presenting plan view "depth slices" from the 3D visualization provides a tool for correlating resistivity responses to infrastructure, changes in soil moisture, or changes in soil chemistry.

Four resistivity lines were acquired at the 216-C-1 project site; 200EC101 (Figure 5-3), 200EC102 (Figure 5-4), 200EC103 (Figure 5-5), and 200EC104 (Figure 5-6). The resistivity data were processed according to Section 4.3 using a 2D inversion algorithm (AGI EarthImager 2D). Table 5-1 shows the inversion statistics for goodness of fit in each line at the 216-C-1 waste site. An explanation of the table parameters is discussed in detail within Section 4.3.3.

Table 5-1. Final Inversion Statistics for the 216-C-1 Waste Site.

Line #	Stage	Trial	Iterations	RMS	L_2
200EC101	3	1	3	10.52	4.42
200EC102	3	2	6	13.86	7.68
200EC103	3	2	6	10.48	4.39
200EC104	3	3	3	38.37	58.89

RMS = root-mean-square.

A site specific color scale was developed through a statistical analysis of the apparent resistivity values for all data collected within the 216-C-1 site. A histogram, shown in Figure 5-2, was used to generate a color gradient that is sensitive to the resistivity range.

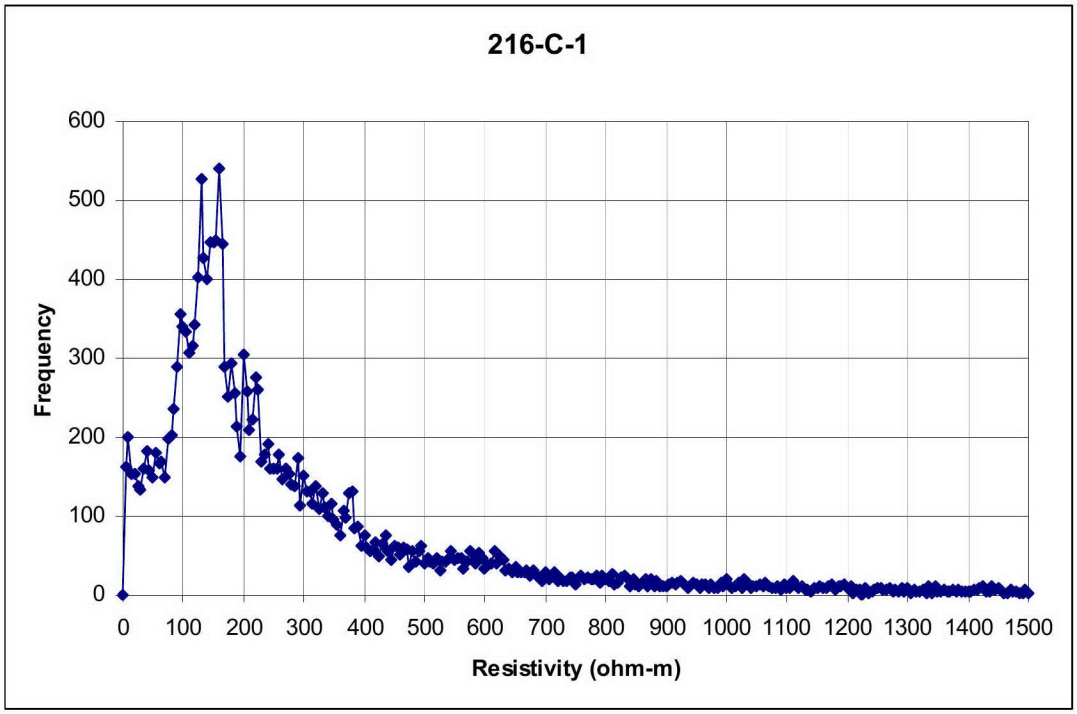

Figure 5-2. Histogram of apparent resistivity data for the 216-C-1 project site.

Interference from subsurface infrastructure dominates much of the near-surface data at the 216-C-1 site. All four lines cross multiple known subsurface pipelines resulting in the large conductive anomalies noticeable throughout the sections. Overall, there is a decrease in resistivity with depth on each of the three profiles, suggesting an increase in moisture content with depth. Depth to groundwater in the area has been recorded at approximately 88 m BGS. The conductive feature at-depth appears to correlate with the depth to groundwater.

Nine pipelines cross survey line 200EC101. The section shows a moderately conductive feature at approximately 160 m along the line that correlates with an electric distribution line. Electric lines do not typically create interference effects unless the lines are grounded or in electrically conductive conduit. The feature is considerably deeper than one would expect for a pipeline but the depth may be an inversion modeling problem that is exacerbated by the smearing/merging of the anomaly with the conductive feature at-depth (water table). Two more highly conductive anomalies can be seen on the western half of line 200EC101, near the surface from approximately 0 to 15 m BGS near several utilities. A very small resistive area separates the two features however, modeling sensitivity is low relative to the size of the resistive discontinuity and it is possible that there is only one conductive feature. This section of the line is directly adjacent to and north of the 200-E-56 waste site. The resistivity magnitudes (40 to 100 Ohm-m) seem too conductive to represent saturated soil alone. However, the extent of the conductive anomaly seems too large to be the result of infrastructure alone. It is possible that a combination of infrastructure and increased soil moisture is responsible for the anomaly. The complexity of subsurface infrastructure makes it is difficult to correlate the features along line 200EC101 with

the results of the three resistivity lines that cross. Line 200EC102 shows a conductive anomaly at a depth of approximately 20 m BGS where it crosses line 200EC101. There is only a slight agreement because the conductive anomaly on line 200EC102 is considerably more conductive and remains conductive to the full depth of the section. There is a resistivity low relative to background which does not resemble a typical infrastructure interference (compare to the feature at station 160 m), and the feature is visible on the three intersecting survey lines. This may suggest a combination of increased soil moisture and infrastructure. It is also likely that 2D inversion is not suitable for the complexity of the subsurface.

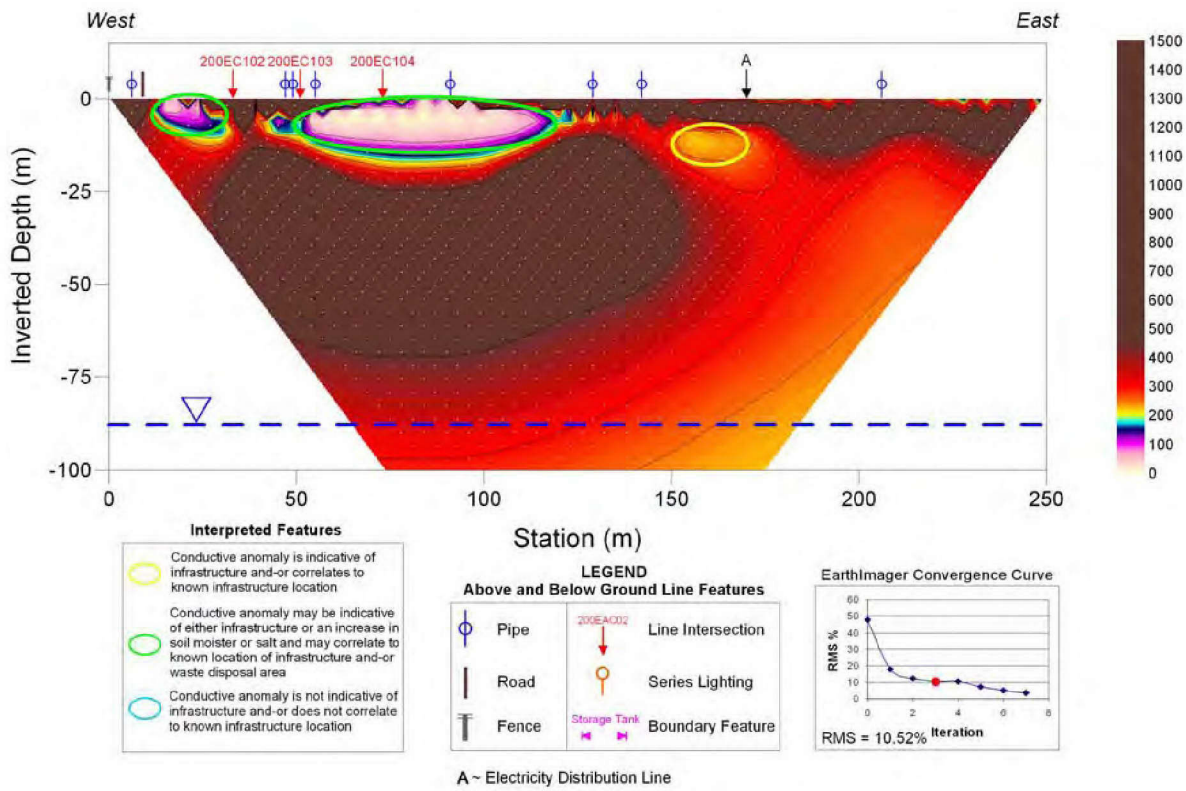

Figure 5-3. Inversion results for 216-C-1 Line 200EC101.

Lines 200EC102, 200EC103, and 200EC104 all display vague correlations with pipeline features and a relative increase in conductivity with depth. Near-surface features are heavily dominated by infrastructure making accurate correlations with non-infrastructure related features difficult in the 2D sections. It is also interesting to note that the deeper sections for the three north-south lines are significantly more conductive than the east-west cross line.

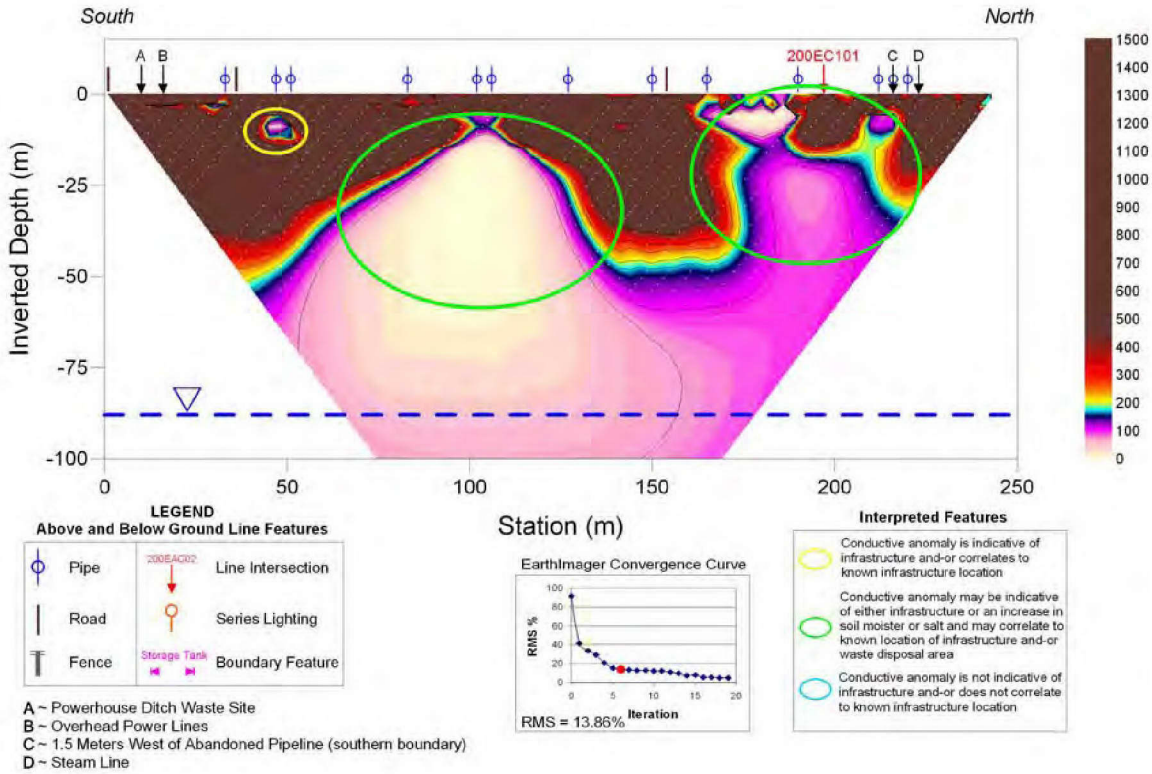

Figure 5-4. Inversion Results for 216-C-1 Line 200EC102.

Line 200EC102 has 13 pipelines that cross the section and a several above ground infrastructure objects. A significant quantity of data was removed due to high data error and noise resulting from infrastructure. A small infrastructure related conductive anomaly is located at approximately 45 meters along the survey line. There are two more highly conductive features centered near station 100 and 175 m and a resistivity high centered near station 150 m. This combination is an inversion artifact that is likely to be caused by 2D inversion being unable to accurately represent a 3D target. It is therefore not possible to correlate the anomaly to a specific cause with 2D inversion alone.

Lines 200EC103 and 200EC104 have 16 pipelines that cross the two sections and several above ground infrastructure objects. A significant quantity of data was removed due to high data error and noise resulting from infrastructure. Both show an infrastructure related conductive anomaly located at approximately 45 meters along the survey line that correlates with line 200EC102. A large highly conductive anomaly is located from station 140 to 210 meters that correlates well with a similar feature shown on line 200EC101. The abundance of infrastructure and the likely inversion errors due to a 3D subsurface complexity, makes it impossible to determine if the anomaly is related to infrastructure or the combination of infrastructure and increased soil

moisture. There is a large highly conductive anomaly centered on station 100 meters that is distorted due to the proximity of the conductive water table at depth. The feature correlates with a similar magnitude anomaly on all three north-south lines.

It should be noted that while there are features as a result of infrastructure like pipelines not all of the pipelines have associated features. This is likely a result of the proximity of the individual pipes to the individual electrodes, along with the physical properties and uses of the pipelines. Physical properties include overall pipeline dimensions, material, contents, depth relative to the electrodes, and lastly whether the pipeline is positioned above, on, or below the ground.

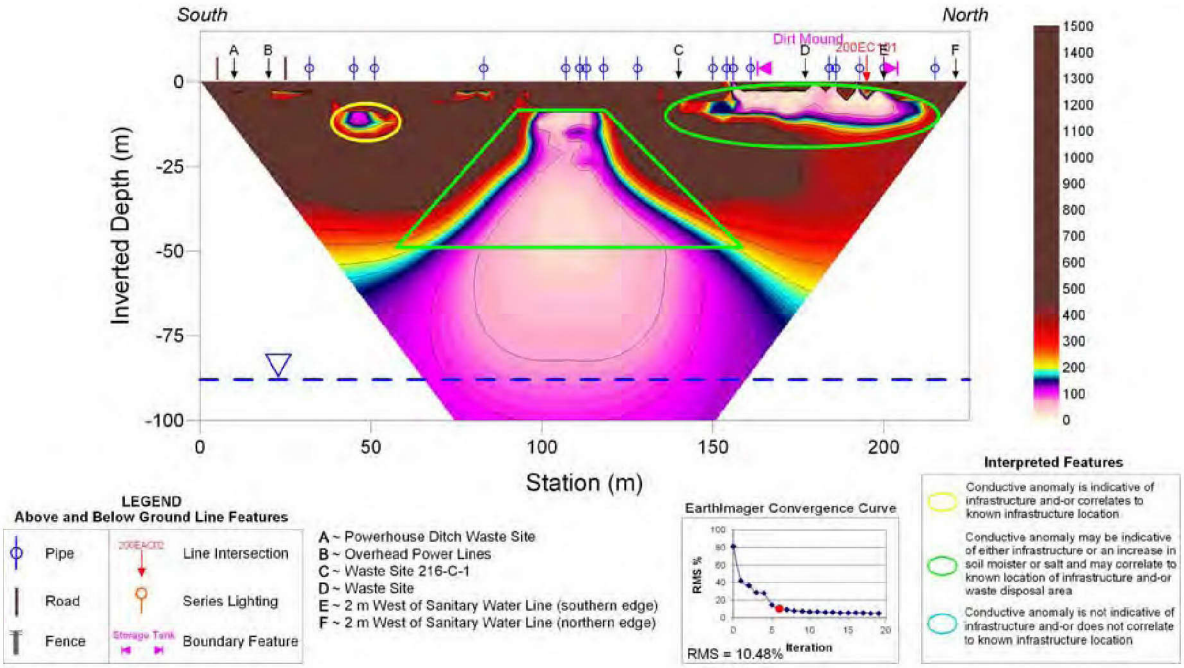

Figure 5-5. Inversion Results for 216-C-1 Line 200EC103.

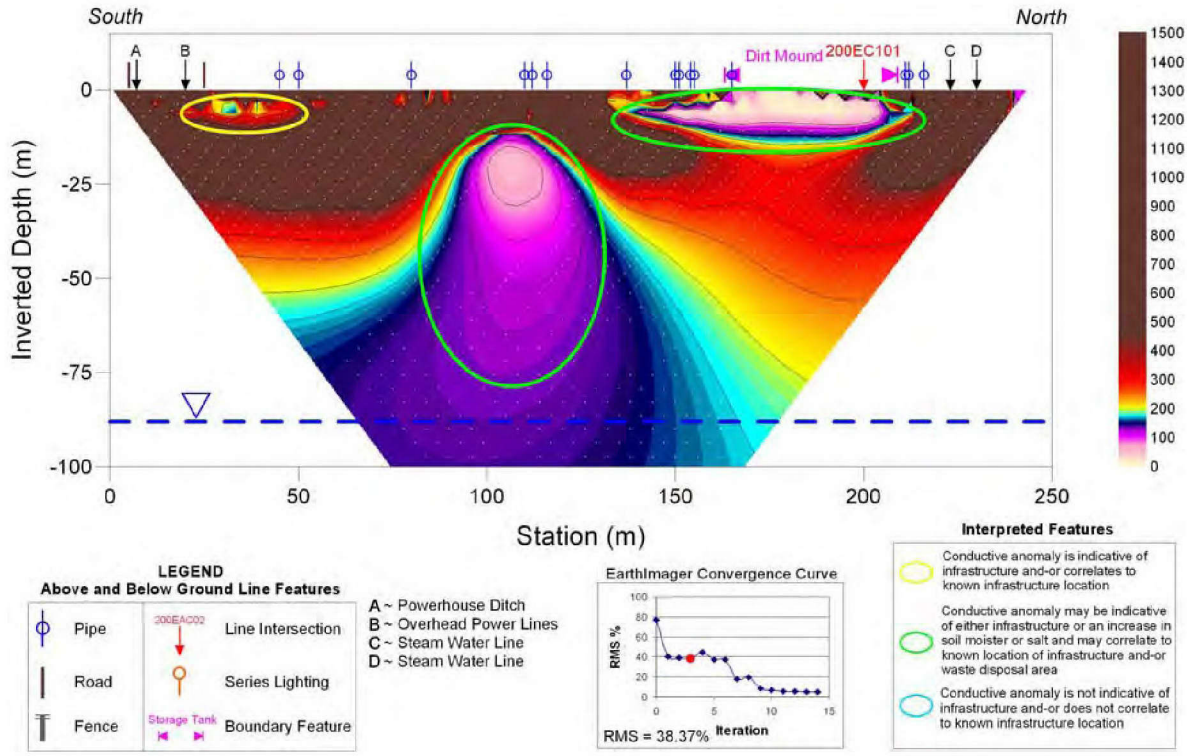

Figure 5-6. Inversion Results for 216-C-1 Line 200EC104.

5.1.1.2 3D Rendering of 2D Inversion Results

Figures 5-7 through 5-11 show the plan view resistivity distribution at-depths increasing in 15-meter increments, from 15 m to 75 m. Note the predictable decreasing resistivity with depth. The infrastructure mentioned in the above 2D section can be seen as resistivity lows throughout the depth slices. The feature, as in the 2D image, increases laterally with depth. However, the extrapolated geometries of the associated resistivity lows vary. Eventually, with depth, the sections display a regional decrease in resistivity, associated with the increased moisture content at-depth (Figure 7-11) most likely associated with the water table.

Resistivity data should only be adversely impacted by electrically conductive infrastructure that will provide a preferential current pathway. This is evident by the fact that many of the conductive features correlate with infrastructure but not all. Separating resistivity anomalies associated with disposal volumes from the significant quantity of subsurface infrastructure at this project site was not possible. Therefore, no conductive features associated with increased soil moisture or salts are discernable from the pipeline disturbances within this data.

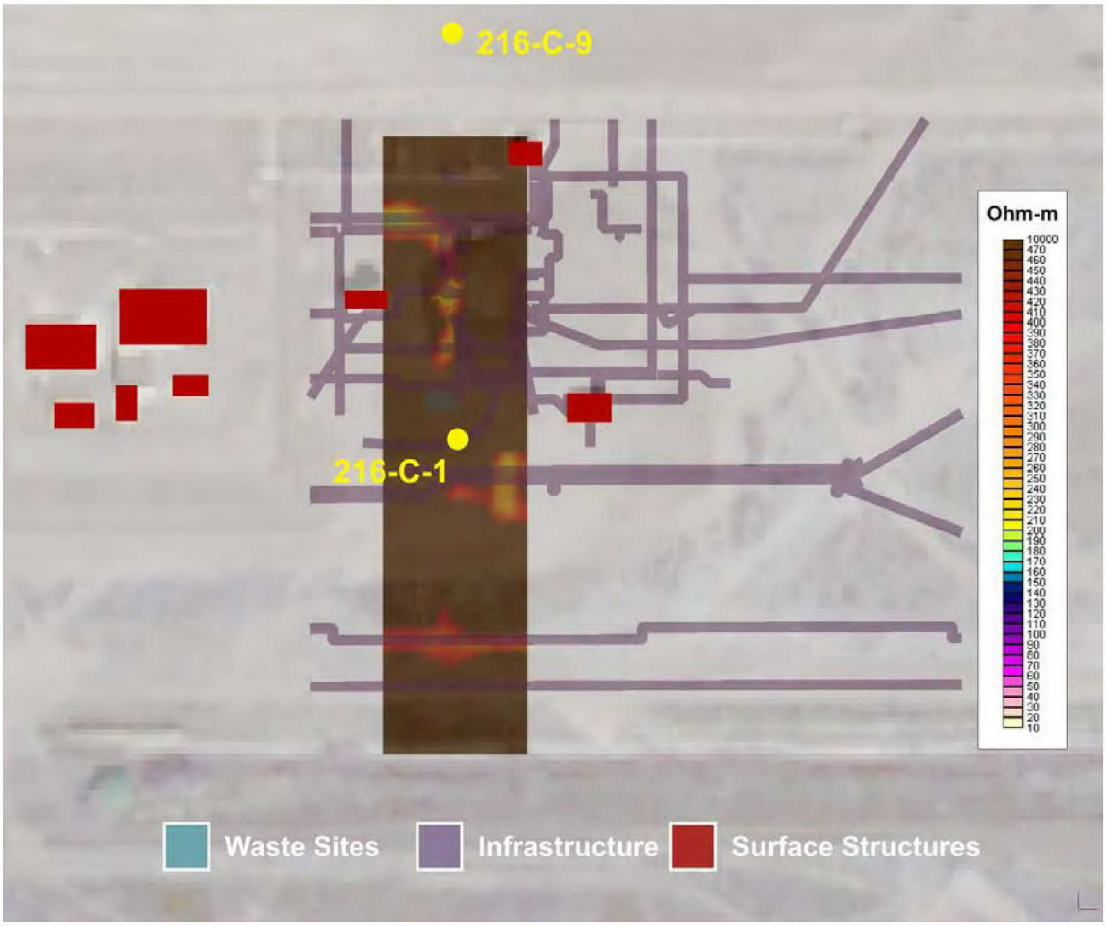

Figure 5-7. Results from the 3D Visualization at a Depth of 15 m BGS.

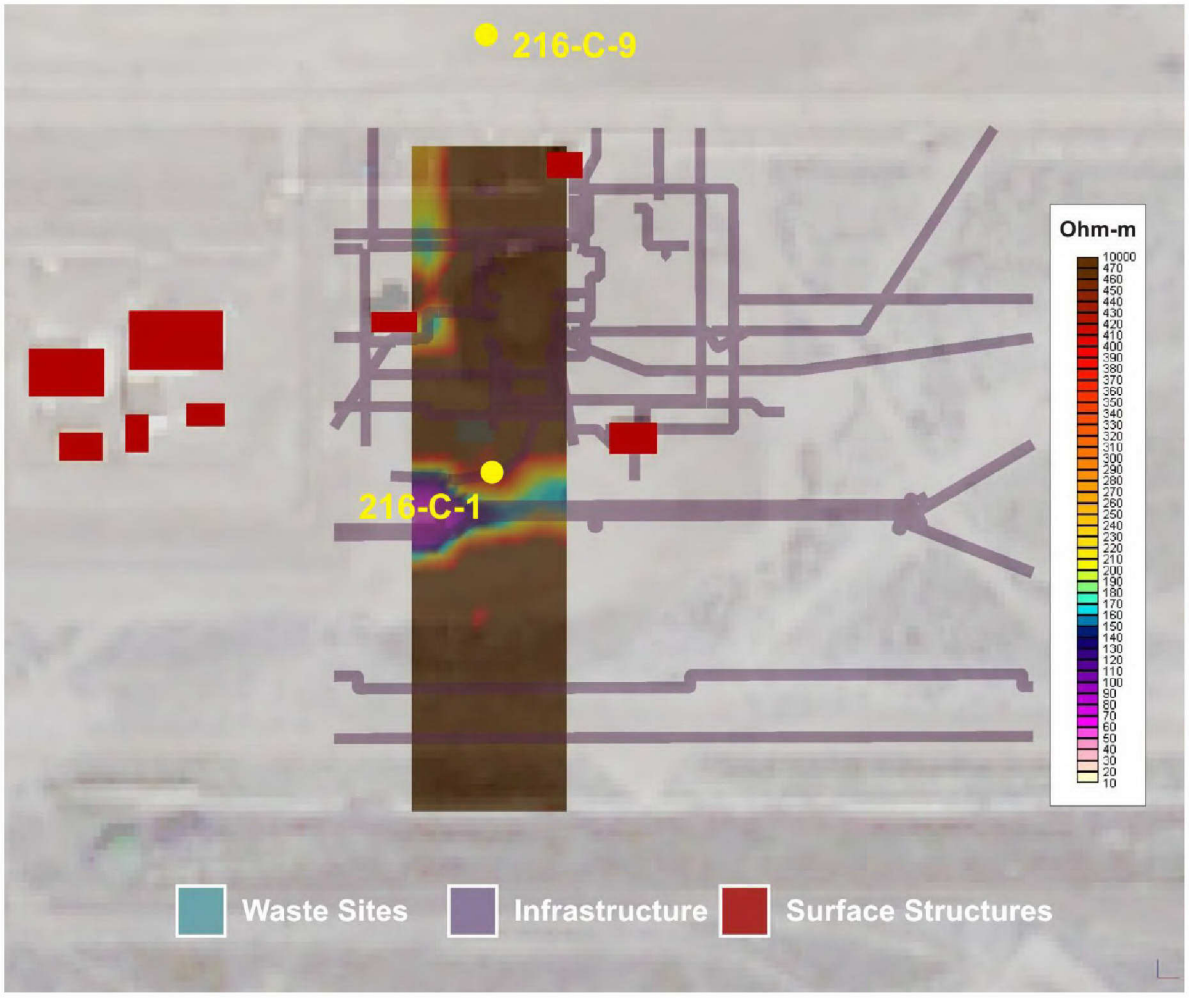

Figure 5-8. Results from the 3D Visualization at a Depth of 30 m BGS.

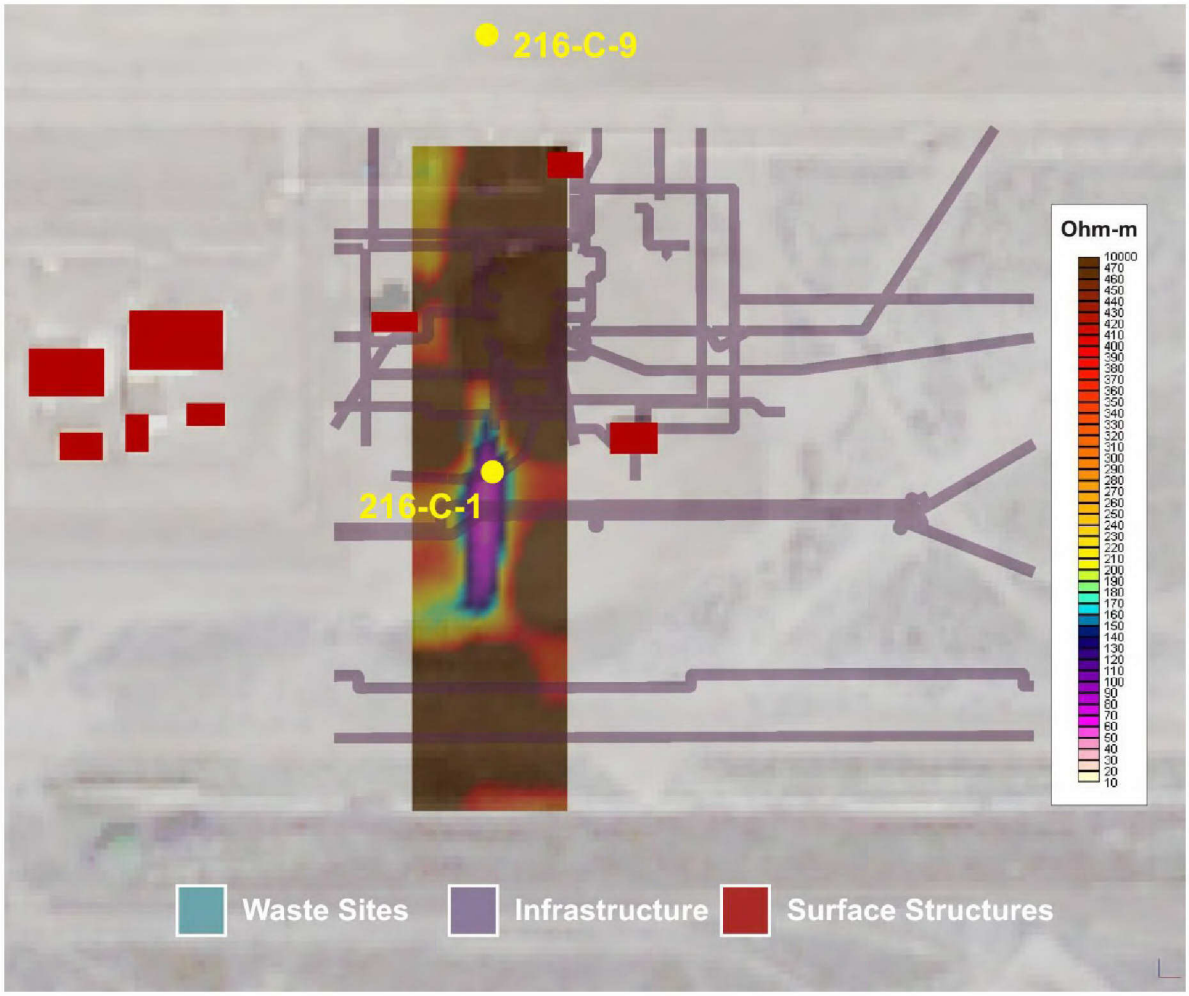

Figure 5-9. Results from the 3D Visualization at a Depth of 45 m BGS.

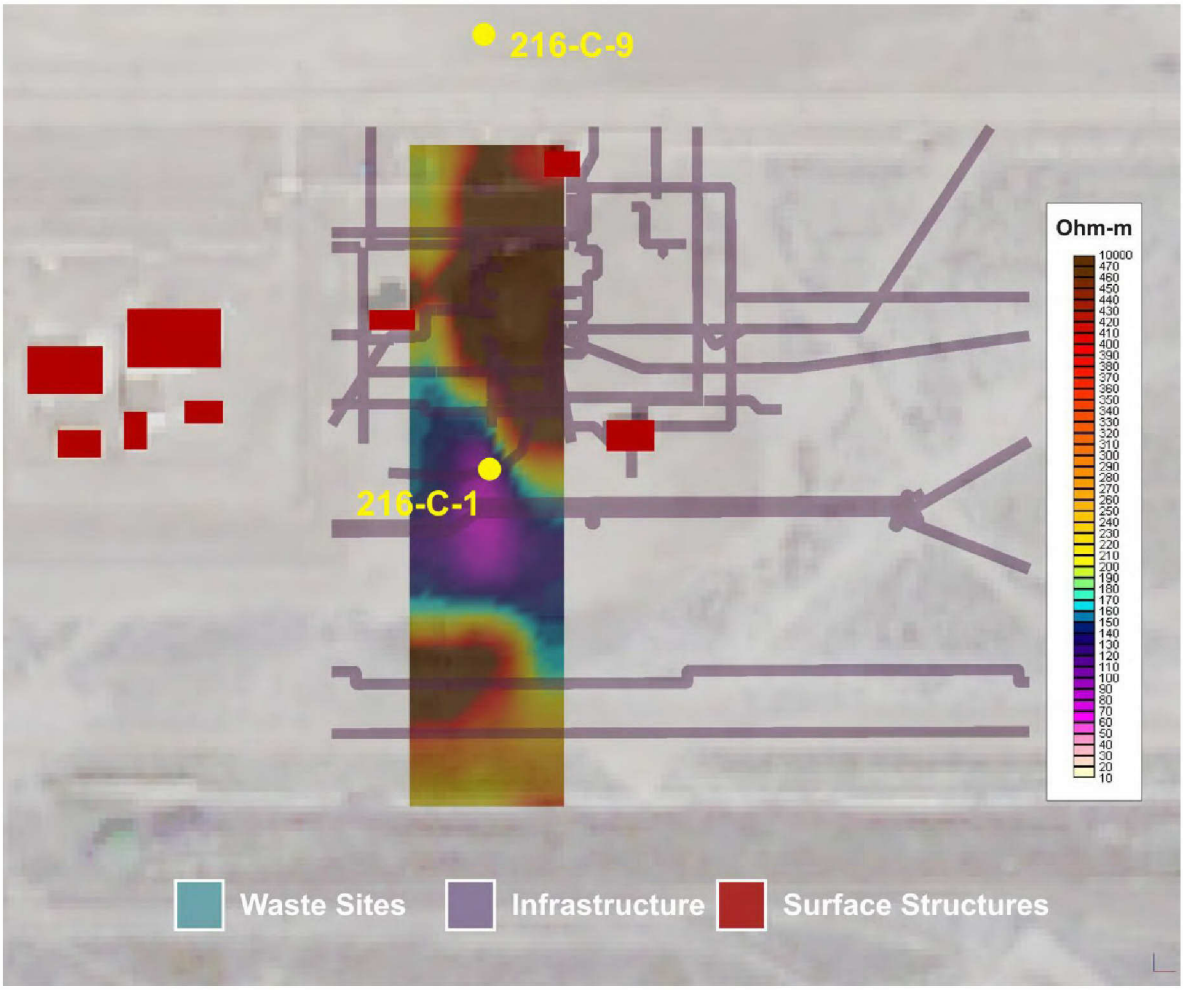

Figure 5-10. Results from the 3D Visualization at a Depth of 60 m BGS.

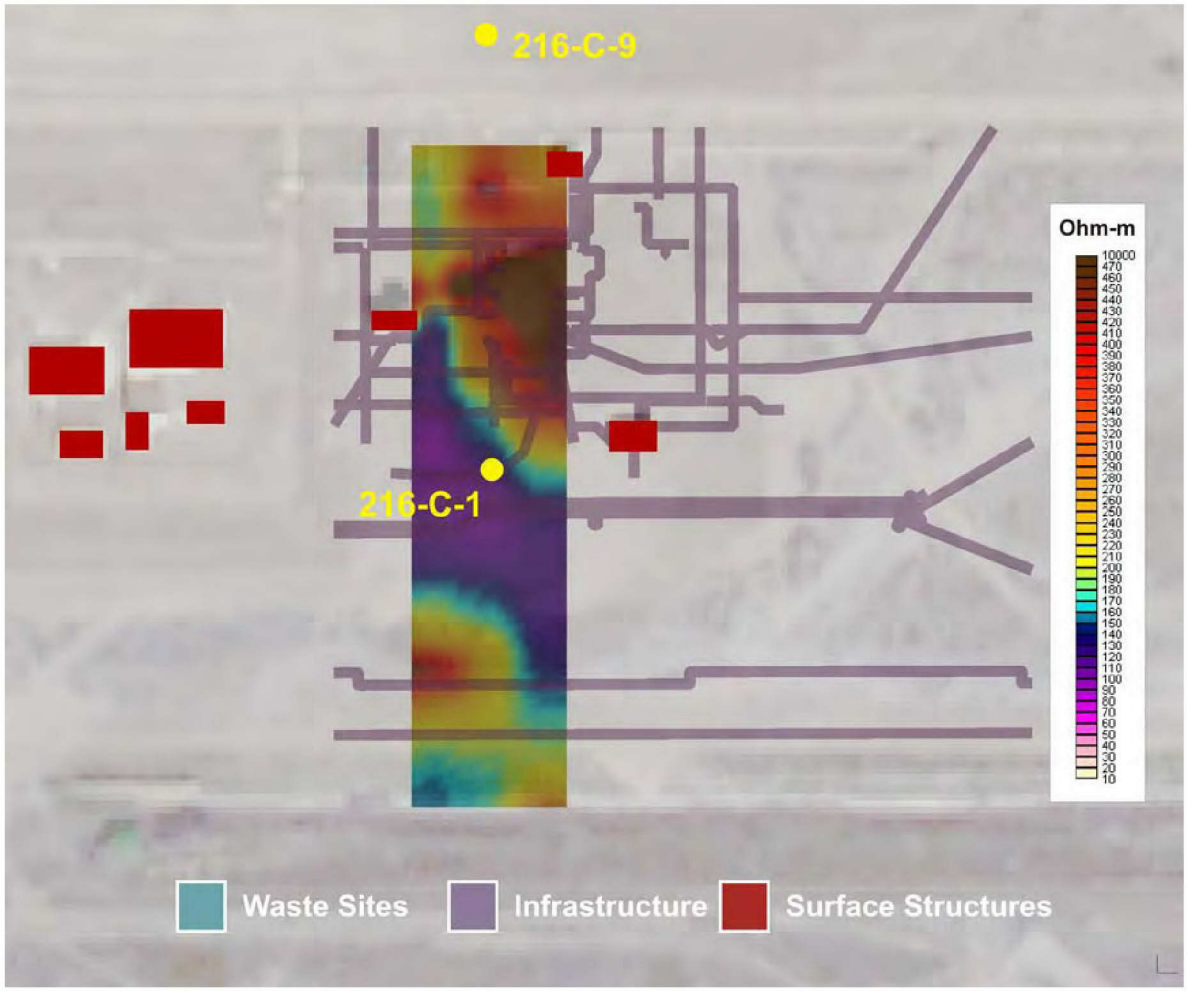

Figure 5-11. Results from the 3D Visualization at a Depth of 75 m BGS.

5.1.2 A-Complex

5.1.2.1 2D Inversion Results

The 2D inversion results of the resistivity survey performed at A-Complex can be viewed in Figures 5-13 through 5-26 below. Figures 5-13 through 5-21 display the results in a cross-sectional format, while Figures 5-22 through 5-26 display the results of a 3D visualization of the same data set.

Nine resistivity lines were acquired at A-Complex; 200EAC01 (Figure 5-13), 200EAC02 (Figure 5-14), 200EAC03 (Figure 5-15), 200EAC04 (Figure 5-16), 200EAC05 (Figure 5-17), 200EAC06 (Figure 5-18), 200EAC07 (Figure 5-19), 200EAC08 (Figure 5-20), and 200EAC09 (Figure 5-21). The resistivity data was processed according to Section 4.3 using a 2D inversion algorithm (AGI EarthImager 2D). Table 5-2 shows the inversion statistics for goodness of fit in

each line at A-Complex. An explanation of the table parameters is discussed in detail within Section 4.3.3.

Table 5-2. Final Inversion Statistics for A-Complex.

Line #	Stage	Trial	Iterations	RMS	L_2
200EAC01	2	2	3	7.41	2.19
200EAC02	3	4	3	6.73	1.81
200EAC03	3	1	3	5.55	1.23
200EAC04	3	1	3	5.68	1.29
200EAC05	1	1	3	4.36	0.76
200EAC06	1	1	2	3.05	0.37
200EAC07	1	1	2	4.66	0.87
200EAC08	1	1	2	4.80	0.92
200EAC09	1	1	2	3.60	0.52

RMS = root-mean-square.

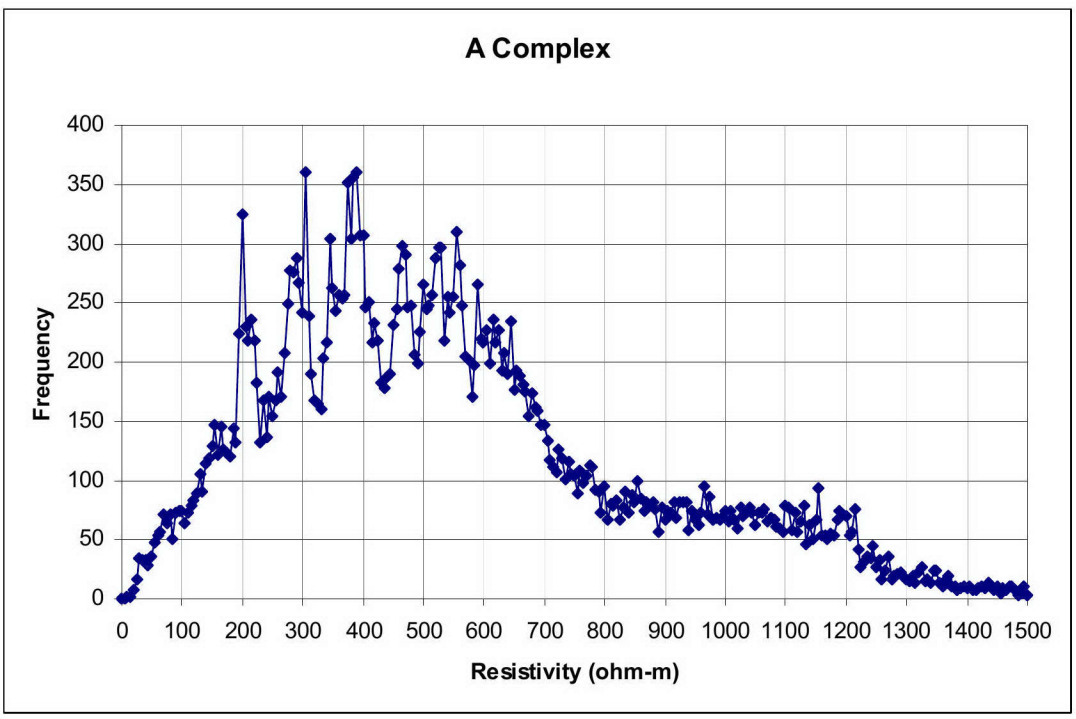

Figure 5-12. Histogram of apparent resistivity data for the A-complex project site.

A site specific color scale was developed through a statistical analysis of the apparent resistivity values for all data collected within the A-Complex site. A histogram, shown in Figure 5-12, was used to generate a color gradient that is sensitive to the resistivity range.

Interference from subsurface infrastructure dominates much of the near-surface data at A-Complex. Overall, there is a decrease in resistivity with depth on each of the ten profiles as the sections approach the expected water table at 83 m depth. Survey lines 200EAC01, 200EAC02, 200EAC07, 200EAC08 and 200EAC09 were not long enough to produce an investigation depth suitable for imaging the water table. The remaining five survey lines have suitable line length and maximum electrode spacing to adequately image to a depth greater than the water table. However, very few of the longer survey lines show a correlation between low resistivity values and the approximate depth of groundwater. The best examples of this occur on lines 200EAC05 and 200EAC06 where there is a gradient that trends to a lower resistivity near the water table. The limited correlation is likely a result of interference due to near surface infrastructure and the inability of the inversion algorithm to resolve the complexity. Preferential current channeling interference due to electrically conductive infrastructure are disruptive to inversion modeling for larger transmitter receiver pairs which produce deeper sections of the 2D models. In addition, there may be small-scale geological controls, or variations in subsurface geological conditions, contributing to the inconsistent resistivity values at-depth.

Lines 200EAC01 and 200EAC02 (Figures 5-13 and 5-14) are located in a separate grouping from the remaining seven survey lines and were acquired in a near orthogonal configuration to characterize the 216-A-7 waste area. The location of lines 200EAC01 and 200EAC02 were designed to investigate the 216-A-7 waste site, however, an error in location maps resulted in the lines being located approximately 25 meters east of the original location. The line locations are close enough to provide some information pertaining to the 216-A-7 waste site. The area around 216-A-7 shows a high groundwater nitrate concentration of 90 mg/L (from well 299-E25-2) and less than a million gallons of liquid waste disposal (see Section 2.0 for more details). Each line crosses a few pipelines, which causes a great deal of interference. An added complexity is that both lines show a general resistivity low at-depth (water table) that merges with the high conductivity pipeline features. This is particularly evident over the first half of line 200EAC01 and the center of line 200EAC02. In addition, a resistivity low between station 75 and 110 m, within the near-surface of line 200EAC01 appears to correlate with the location of the 216-A-7 waste site locate approximately 25 meters to the west. The conductive feature does not correlate with known infrastructure and the magnitude (approximately 150 to 200 Ohm-m) is more resistive than would be expected of infrastructure. The character of response appears distorted as if interference from an unknown infrastructure is present. It is not possible to determine if the conductive anomaly is caused by increased soil moisture or conductive infrastructure. Line 200EAC02 runs just south of the 216-A-7 waste site, which is centered near station 25 meters. There is a small near surface (>10 meters) conductive feature between station 15 and 30 meters that correlates spatially with the location of the 216-A-7 waste site. The conductive feature does not correlate with known infrastructure but the magnitude (approximately 150 to 200 Ohm-m) and character are similar to other infrastructure features within the 200E area. It is also possible that the small size and moderate conductivity indicates this is the southern edge of an increased soil moisture zone associated with the 216-A-7 waste site. The resistivity magnitude a location

is similar to that of the conductive anomaly between station 75 and 110 m along line 200EAC01 and may represent one feature. Interpretation of subsurface soil moisture content and chemistry is greatly hindered by the infrastructure artifacts of both lines and additional data is needed to determine the exact cause of the conductive anomaly.

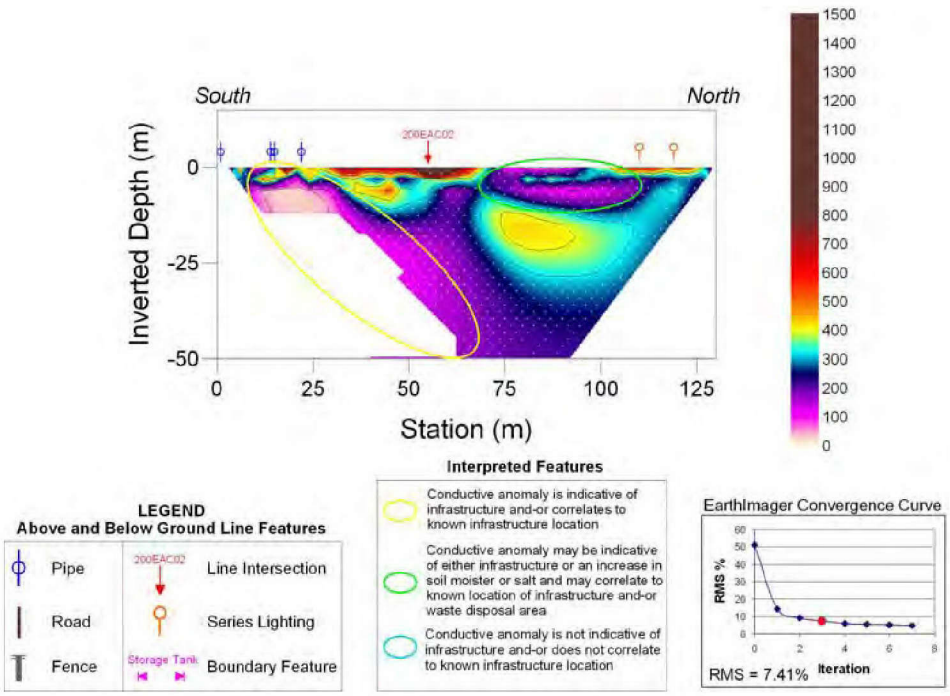

Figure 5-13. Inversion Results for A-Complex Line 200EAC01.

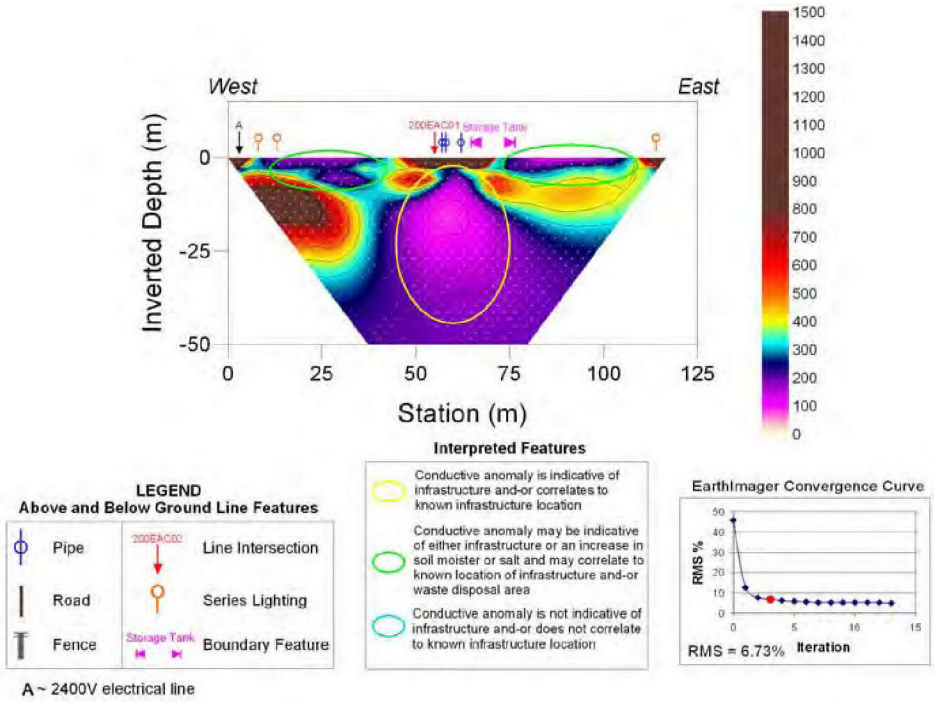

Figure 5-14. Inversion Results for A-Complex Line 200EAC02.

Lines 200EAC03, 200EAC04, 200EAC05, and 200EAC06 were completed to characterize the 216-A-8 waste site that received between 10 and 100 mGal of liquid waste (see Section 2.0 for more details). The first near surface (>15 m BGS) shows a moderately conductive anomaly (150 to 350 ohm-m) relative to background (> 500 ohm-m). This is most evident in 200EAC05 and 200EAC06 and less evident on 200EAC03. There is no indication of infrastructure so the moderately conductive feature may be associated with the 216-A-8 disposal volume or metallic debris. An combination magnetic and electromagnetic survey over the disposal trench would help discriminate.

Lines 200EAC03, 200EAC04, and 200EAC05 also display a conductive region between stations 50 to 100 m. This is most prominent in 200EAC04 where the conductive body is centered at a depth of approximately 45 m. There is a known utility at station 5 m that parallels the line in close proximity until approximately station 35 m. Although the conductive feature does not look diagnostic of a pipeline feature, from experience with 2D inversion software, it is likely a combination of infrastructure and edge effects from 2D inversion. When a pipeline exists at the very edge of a measured section (first few or last few electrodes), these 2D inversion codes will fit an extremely difficult 2D model using essentially 1D measured data. The lateral sensitivity is much higher in this part of the model and the depth information if very weak. Also, if only one

side of the pant leg artifact is present (clipped), the anomaly will shift away from the missing section laterally as is the case with this feature.

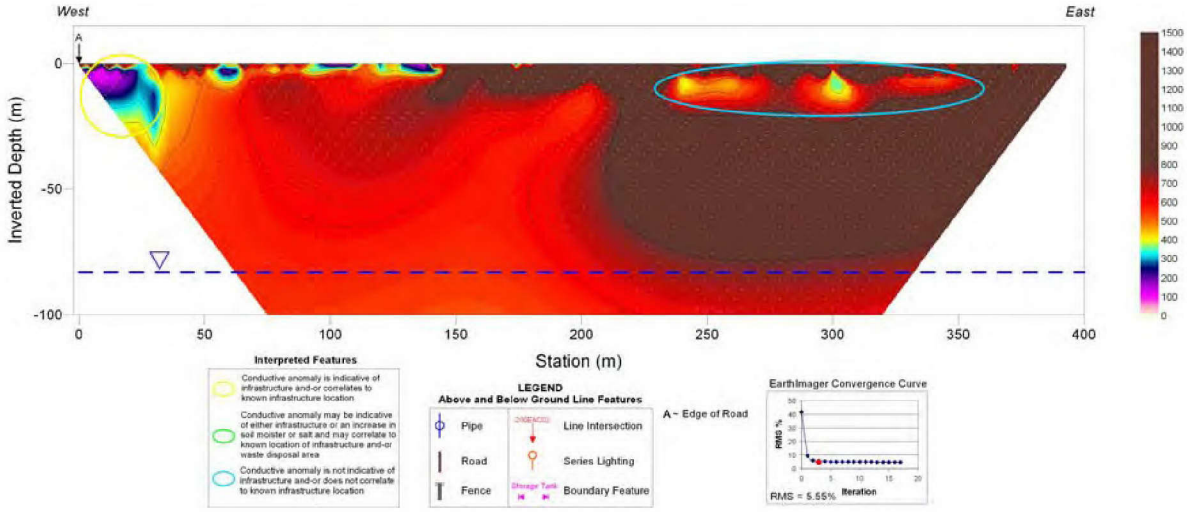

Figure 5-15. Inversion Results for A-Complex Line 200EAC03.

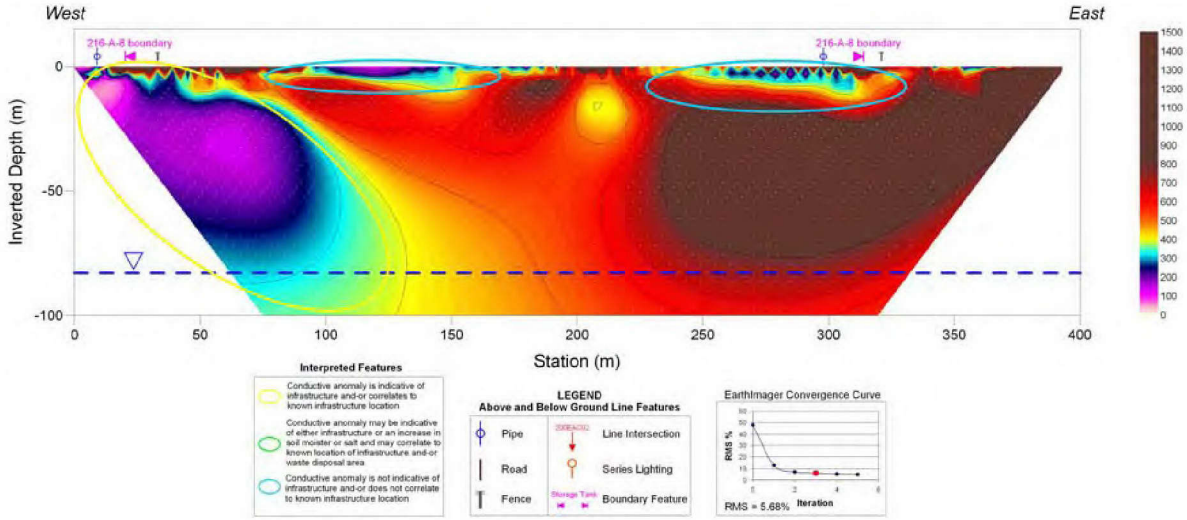

Figure 5-16. Inversion Results for A-Complex Line 200EAC04.

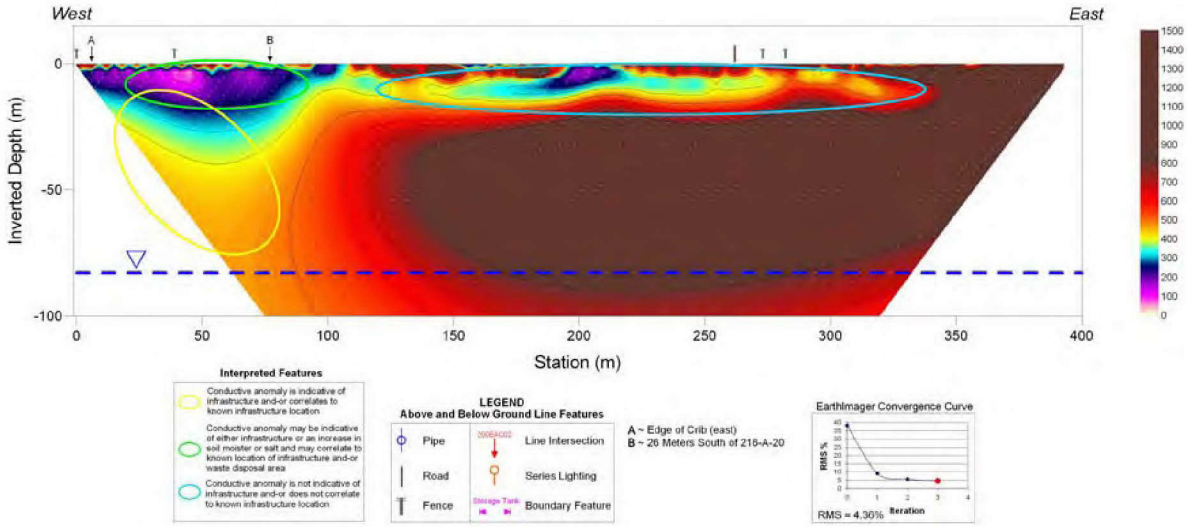

Figure 5-17. Inversion Results for A-Complex Line 200EAC05.

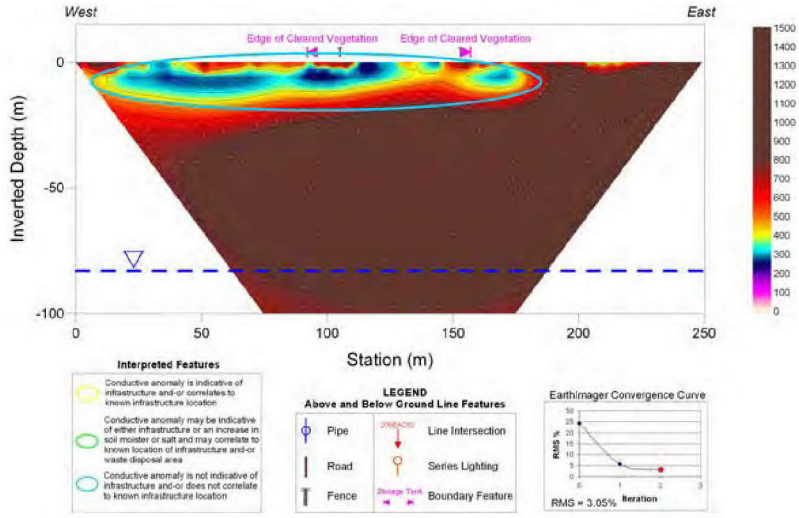

Figure 5-18. Inversion Results for A-Complex Line 200EAC06.

Lines 200EAC07 and 200EAC08 display a prominent conductive body within the first 10 m of the surface that is centered on the 216-A-19 WIDS site. Due to the length of these lines, the investigation depth is limited to approximately 50 m on the sections, such that minimal influence from the groundwater at-depth can be seen in the sections. There appears to be little influence due to infrastructure so the resistivity low is suspect and may be the result of increased soil moisture or a change in soil chemistry. The near-surface conductive body seen in the previous two lines is considerably smaller in the results of Line 200EAC09 and may indicate the northwestern boundary of the conductive anomaly. The survey line is influenced by a pipeline at the southwestern end, and displays minimal additional variation.

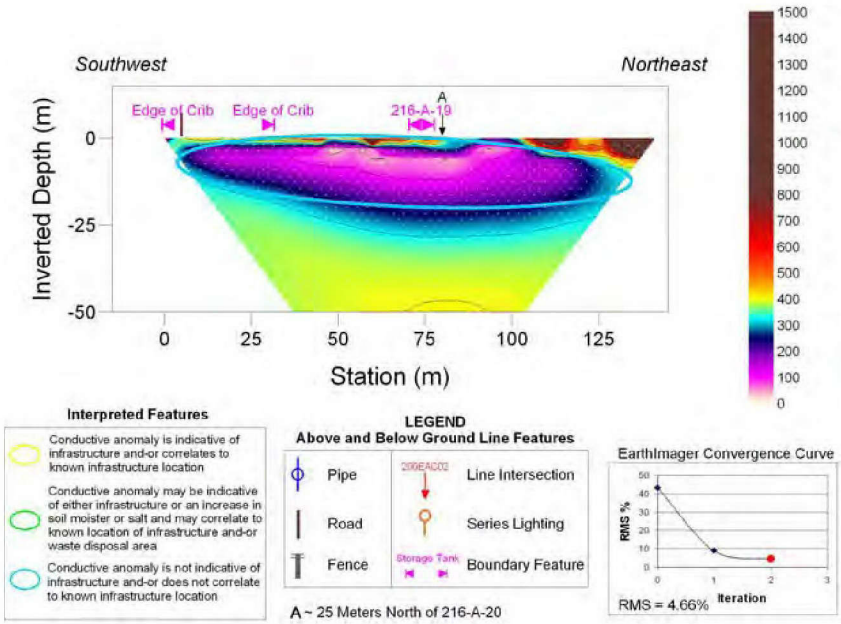

Figure 5-19. Inversion Results for A-Complex Line 200EAC07.

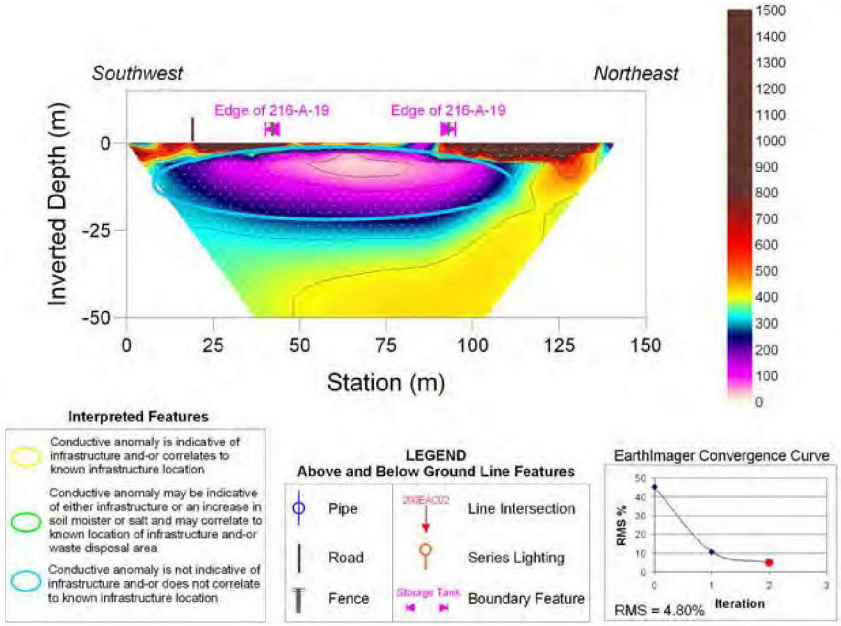

Figure 5-20. Inversion Results for A-Complex Line 200EAC08.

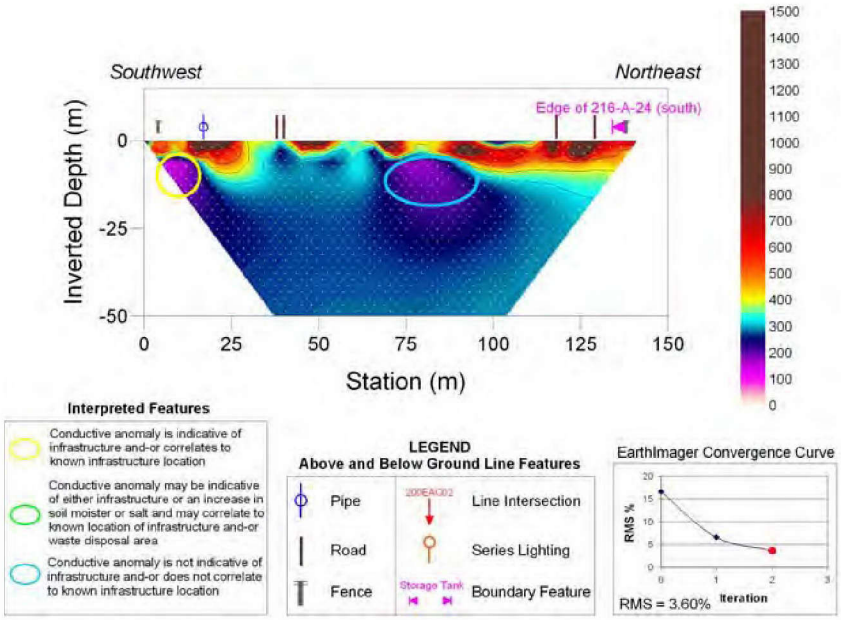

Figure 5-21. Inversion Results for A-Complex Line 200EAC09.

5.1.2.2 3D Rendering of 2D Inversion Results

Figures 5-22 through 5-26 show the plan view resistivity distribution at-depths increasing in 15-meter increments, from 15 to 75 m, respectively. Because of the varying depths of investigation, the 3D visualization of A-Complex does not show results for the southwestern area of investigation deeper than 45 m.

The resistivity distribution centered near the 216-A-7 waste site (Lines 200EAC01 and 200EAC02) located in the southwestern area of investigation display background values near the surface with a conductive anomaly near the center of the investigation area. The shape and character of the conductive response and its proximity suggest it may be a result of the conductive local infrastructure (shown as purple lines) and not necessarily an increase in soil moisture at-depth.

The resistivity distribution centered over the 216-A-8, 216-A-19 and -20 waste sites (lines 200EAC03 through 200EAC09) shows a near-surface conductive body within the first 15 m over the 216-A-19 and -20 waste sites and a small feature to the west of the 216-A-8 trench that correlates with infrastructure. The shape of the conductive body at 216-A-19 and -20 correlates well with the known extents of the waste site boundary. The conductive body is likely the result of increased salts or moisture from historical liquid waste disposal practices.

The deeper images show a significant decrease in the conductive feature located over the 216-A-19 and -20 waste sites. The lower extent of this conductive target appears to be limited to the first 30 to 45 m. The depth slice at 30 m BGS shows a small conductive feature over the western side of the 216-A-8 area, near the approximate termination of the trench pipeline. As

described above, this is likely a response due to the infrastructure where 2D inversion is ill-suited for reconstructing this type of complexity. Inversion of these data in 3D with the addition of a few well-placed lines would greatly enhance the utility of the resistivity method at this site.

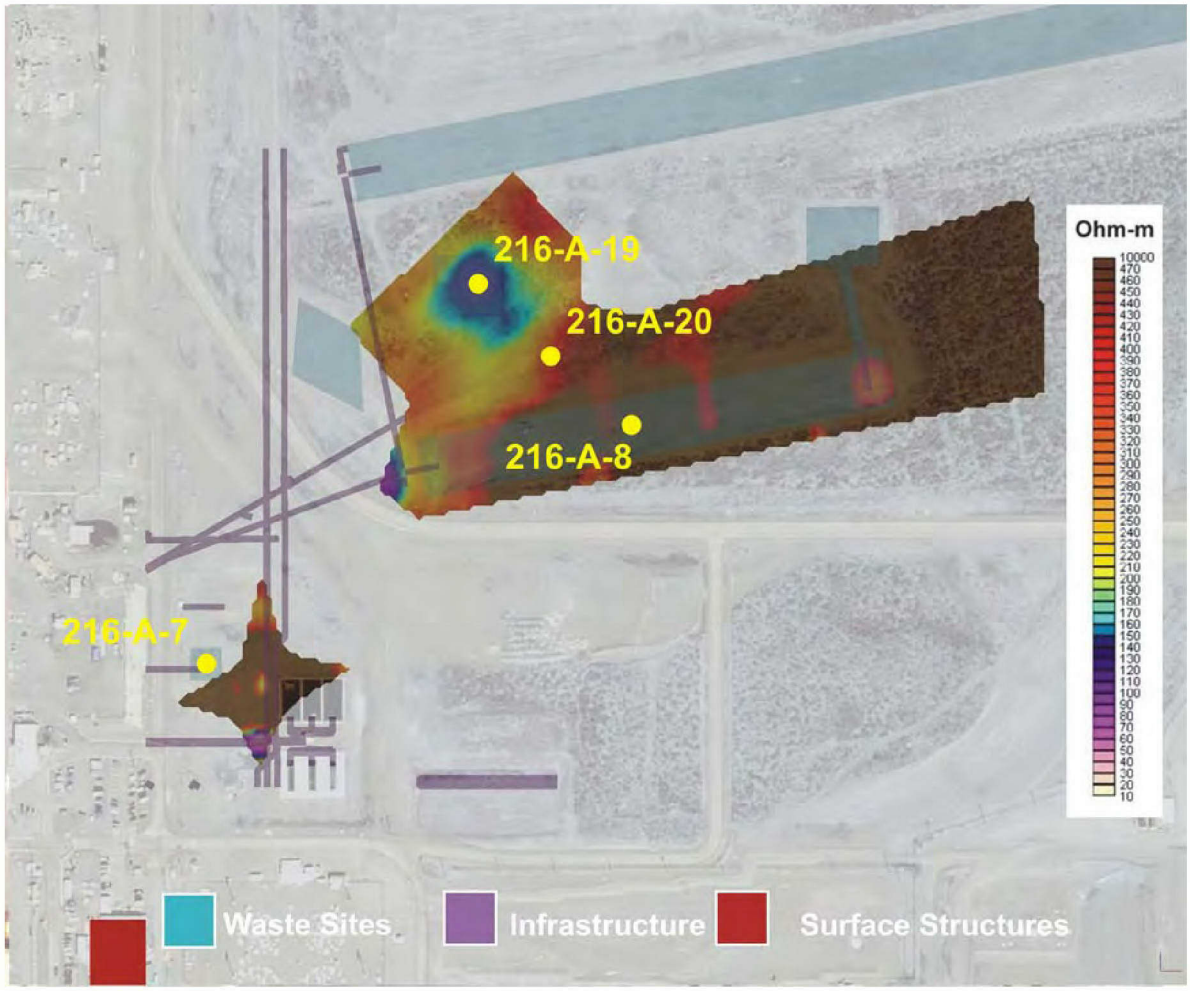

Figure 5-22. Results from the 3D Visualization at a Depth of 15 m BGS.

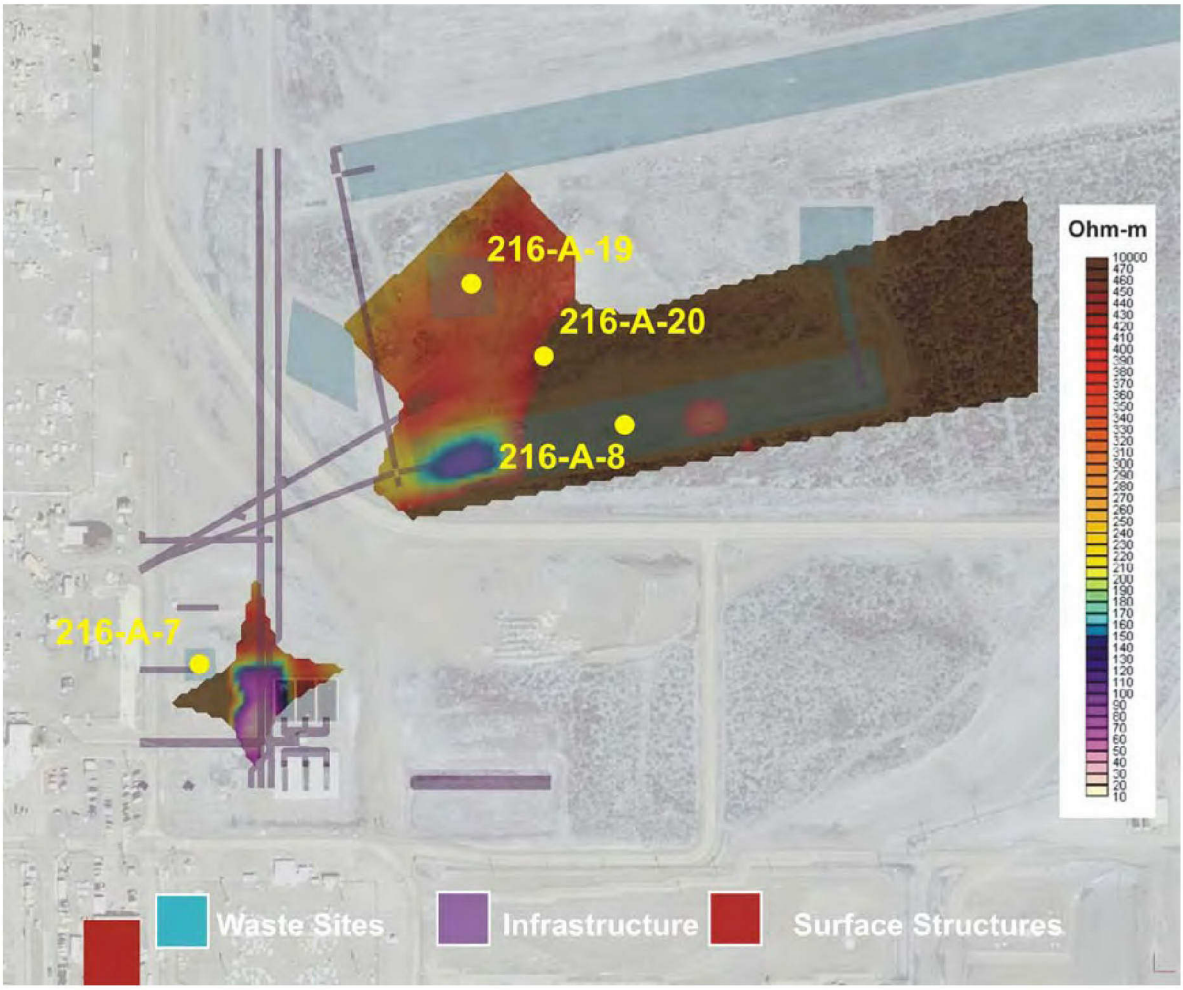

Figure 5-23. Results from the 3D Visualization at a Depth of 30 m BGS.

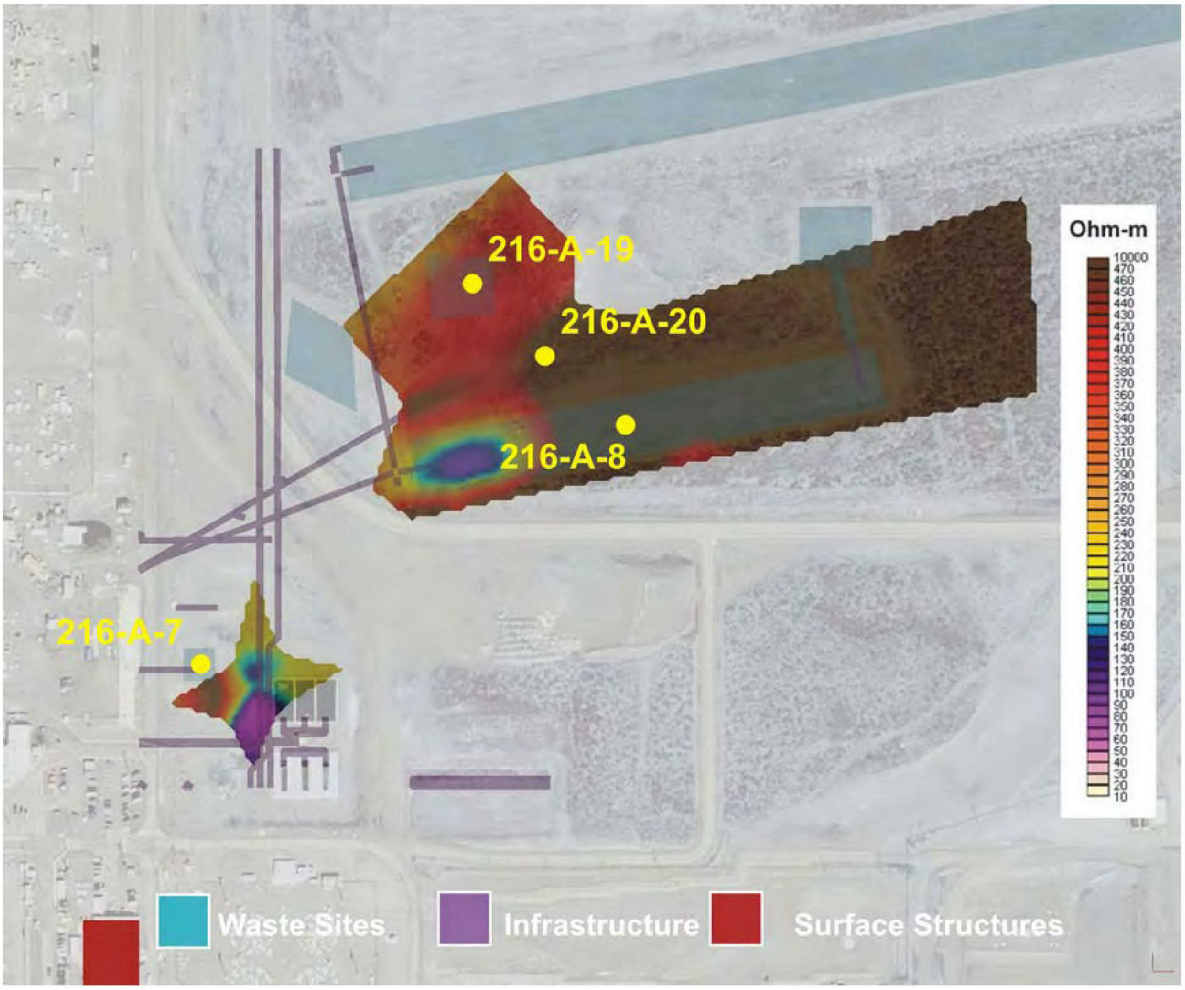

Figure 5-24. Results from the 3D Visualization at a Depth of 45 m BGS.

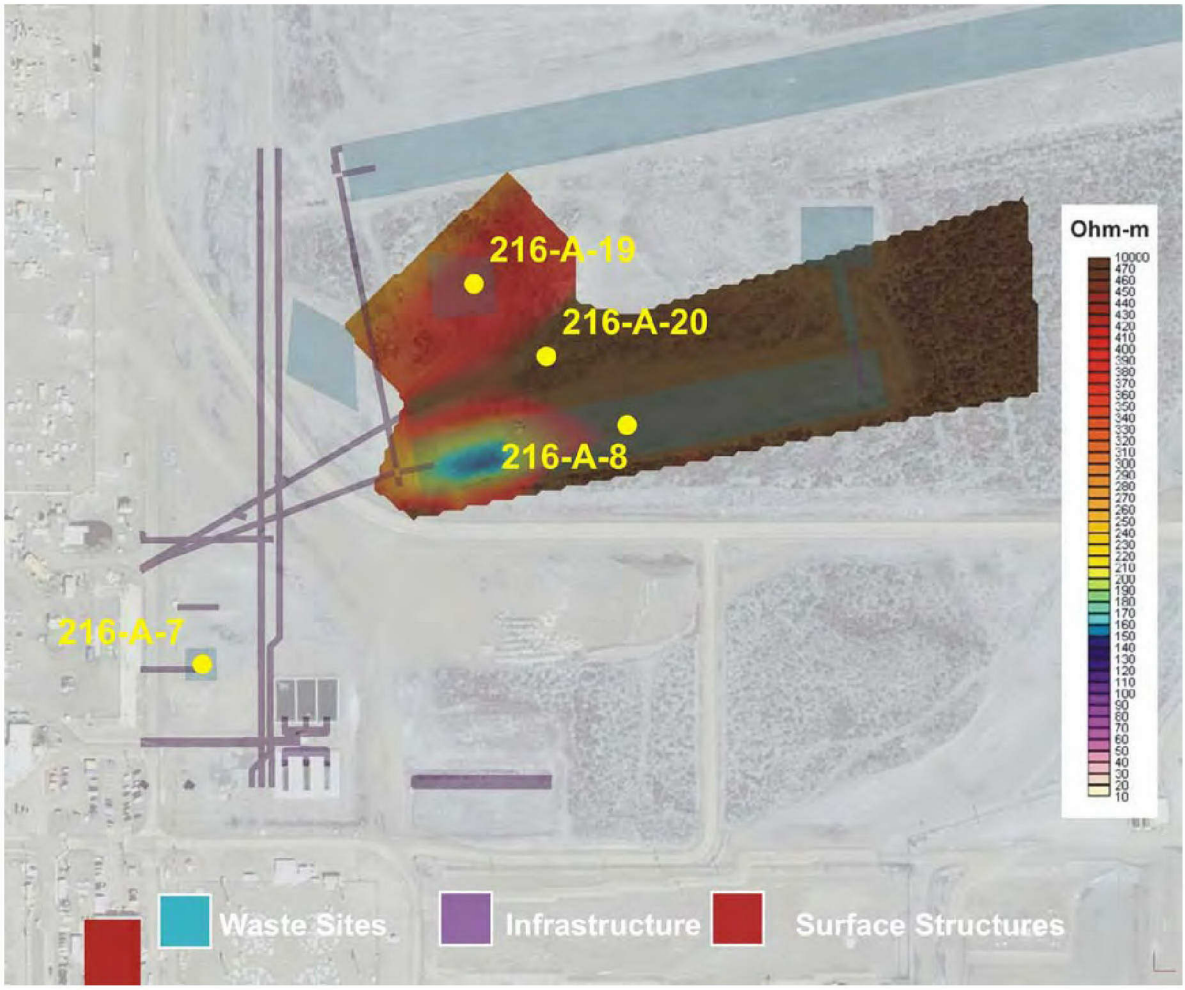

Figure 5-25. Results from the 3D Visualization at a Depth of 60 m BGS.

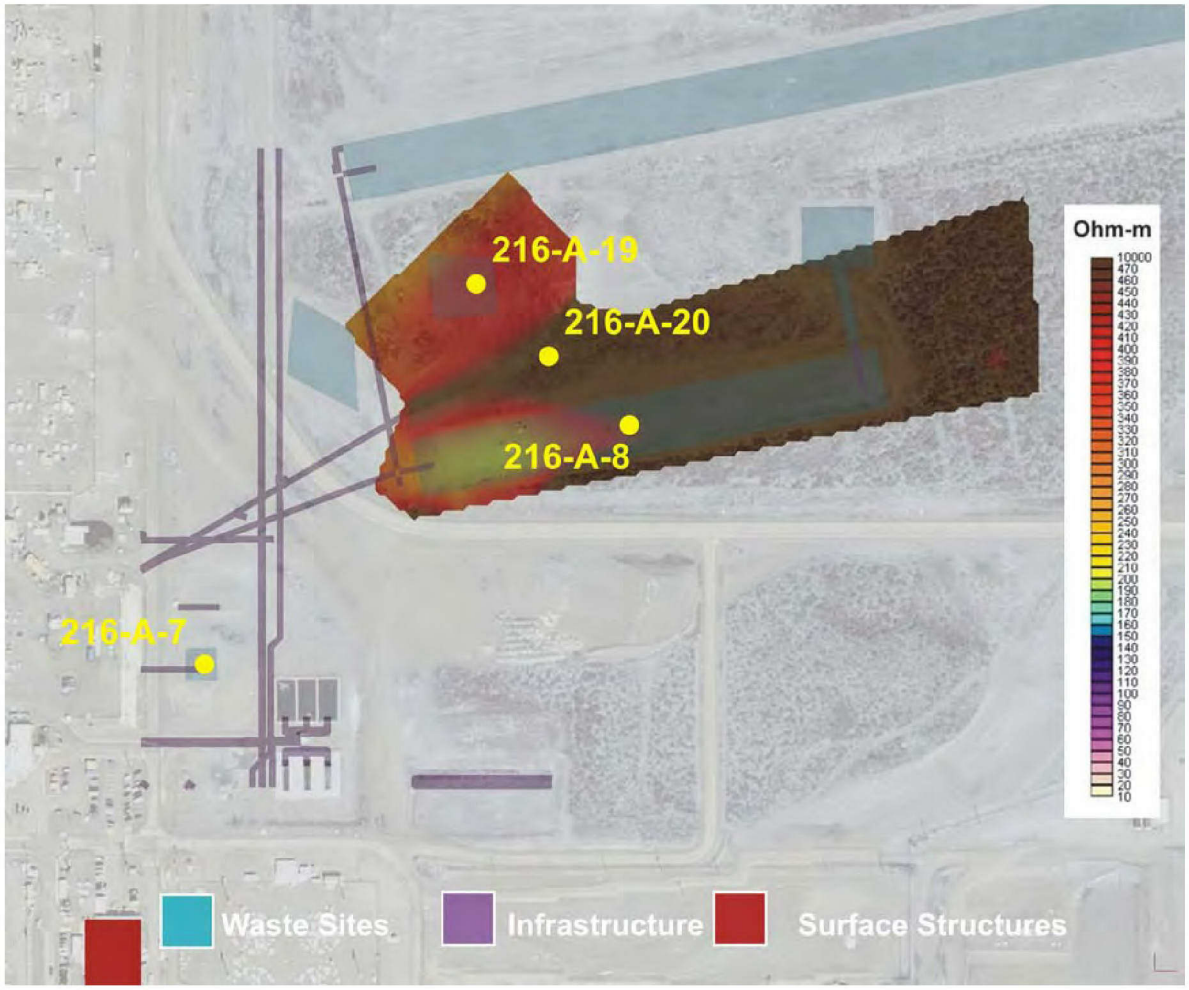

Figure 5-26. Results from the 3D Visualization at a Depth of 75 m BGS.

5.1.3 B-Plant

5.1.3.1 2D Inversion Results

The 2D inversion results of the resistivity survey performed at B-Plant can be viewed in Figures 5-28 through 5-41 below. Figures 5-28 through 5-36 display the results in a cross-sectional format, while Figures 5-37 through 5-41 display the results of a 3D visualization of the same data set. Presenting plan view "depth slices" from the 3D visualization provides a tool for correlating resistivity responses to infrastructure, changes in soil moisture, or changes in soil chemistry.

Ten resistivity lines were acquired at B-Plant; 200EBP01 (Figure 5-28), 200EBP02, 200EBP03 (Figure 5-29), 200EBP04 (Figure 5-30), 200EBP05 (Figure 5-31), 200EBP06 (Figure 5-32), 200EBP07 (Figure 5-33), 200EBP08 (Figure 5-34), 200EBP09 (Figure 5-35), and 200EBP10 (Figure 5-36). Note that while data acquisition was attempted at 200EBP02, no valid data was

acquired as described in Section 4.0. Since data was acquired in lines 200EBP01 and 200EBP03, which flanked either side of 200EBP02, it is suggested that subsurface infrastructure at this location prevented valid data acquisition. Extensive troubleshooting was conducted and resulted in a determination of poor line location given unknown subsurface infrastructure. The resistivity data was processed according to Section 4.3 above using a 2D inversion algorithm (AGI EarthImager 2D). Table 5-3 shows the inversion statistics for goodness of fit in each line at B-Plant. An explanation of the table parameters is discussed in detail within Section 4.3.3.

Table 5-3. Final Inversion Statistics for B-Plant.

Line #	Stage	Trial	Iterations	RMS	L_2
200EBP01	1	1	3	4.86	0.94
200EBP03	3	1	5	6.33	1.60
200EBP04	1	1	2	3.99	0.64
200EBP05	3	3	4	11.56	5.34
200EBP06	1	1	2	3.61	0.52
200EBP07	3	2	6	8.26	2.73
200EBP08	3	2	6	6.62	1.75
200EBP09	3	2	5	6.77	1.84
200EBP10	3	3	6	6.83	1.87

RMS = root-mean-square.

A site specific color scale was developed through a statistical analysis of the apparent resistivity values for all data collected within the B-Plant site with the exception of lines 200EBP07 to 200EBP10, which would distort results, based on the abundance of infrastructure within these lines. A histogram, shown in Figure 5-27, was used to generate a color gradient that is sensitive to the resistivity range.

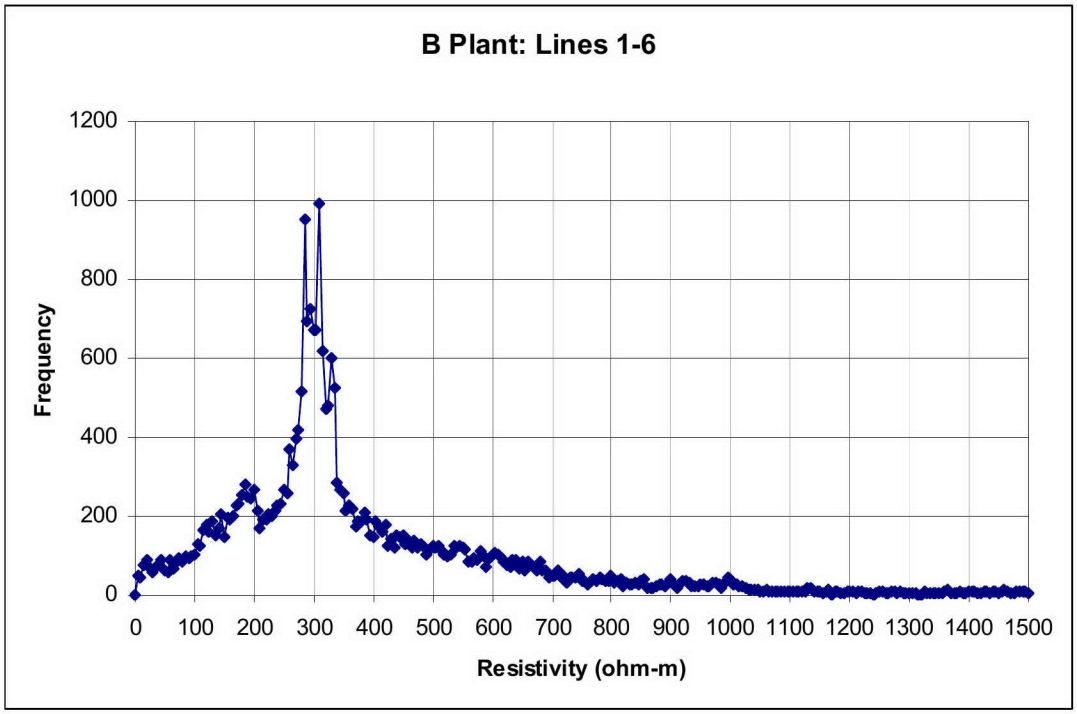

Figure 5-27. Histogram of apparent resistivity data for the B-Plant project site.

Interference from subsurface infrastructure dominates much of the near-surface data at B-Plant. Overall, there is a decrease in resistivity with depth on each of the ten profiles, suggesting an increase in moisture content with depth that is likely to be associated with the water table. Depth to groundwater in the area has been recorded at approximately 94 m BGS. Several of the survey lines show changes in resistivity values at the approximate depth of groundwater. However, where conductive anomalies due to surface infrastructure occur there is a co-mingling of water table and infrastructure response that often distorts both features.

Several unsuccessful attempts to collect data over line 200EB02 were completed but none produced acceptable results. Onsite inspection of the surface soil conditions showed a hard-packed and grouted surface that continued within the fenced 216-B-55 disposal trench. It is suspected that a highly conductive surface coating or grout was used over the area that prevented resistivity data collection. As a result, no contour plot is presented for line 200EB02.

Lines 200EBP01 and 200EBP03 (Figures 5-28 and 5-29) were acquired adjacent to the 216-B-55 waste area. Both lines display a conductive anomaly at the southeastern end of the line. The location of this anomaly correlates with an increased infrastructure area with multiple pipelines and a noted concrete pad. In addition, both lines show a moderately conductive near surface between station 25 and 200 meters that correlates to the location of the 216-B-55 disposal trench. The magnitude and character of the response is not indicative of infrastructure and may be the result of increased soil moisture due to the disposal trench. Lines 200EB03 shows an additional conductive anomaly observed around station 120 m along approximately 10 m BGS. This does

not correlate with provided infrastructure maps or the field notes; however, this location is coincident with a boundary from desert scrub to engineered gravel. The size and character of the feature is indicative of infrastructure. Lines 200EB03 shows another conductive anomaly at station 225 meters that is indicative of infrastructure. The location correlates with a road that is likely to contain subsurface infrastructure that were not present on the supplied maps.

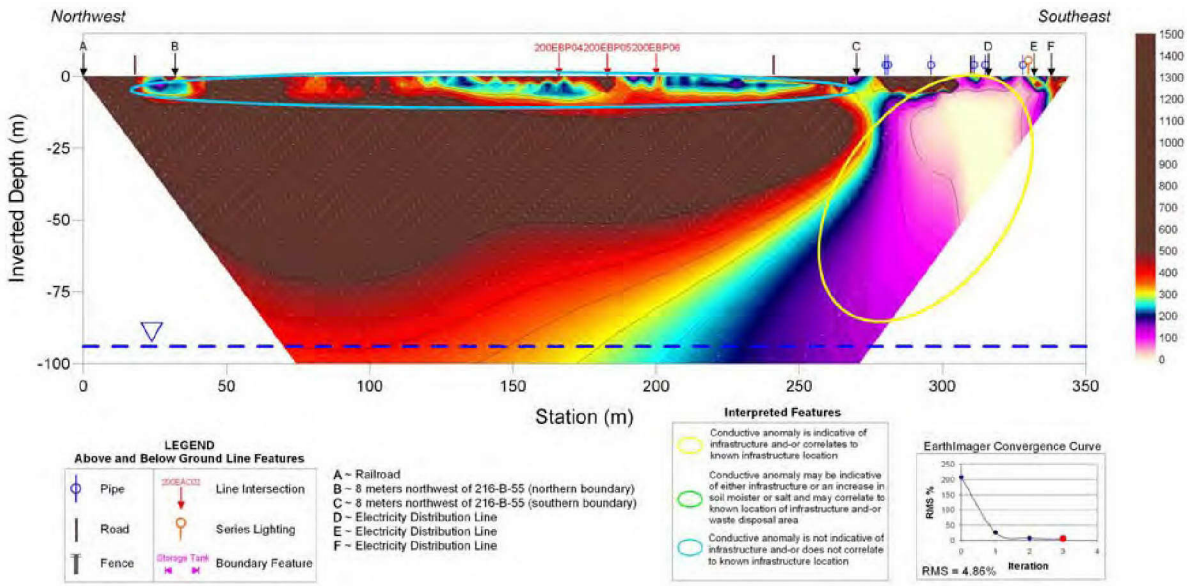

Figure 5-28. Inversion Results for B-Plant Line 200EBP01.

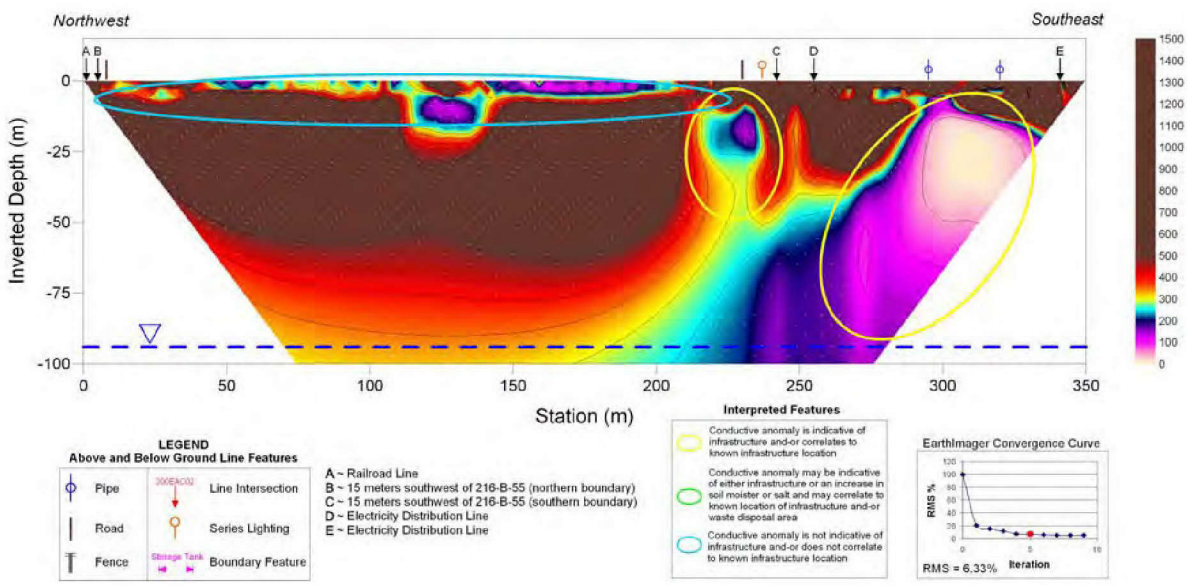

Figure 5-29. Inversion Results for B-Plant Line 200EBP03.

Lines 200EBP04, 200EBP05, and 200EBP06 consistently display a conductive anomaly centered on the lines ranging from 5 to 40 m BGS. Background resistivity values are observed on either side of the conductive anomaly. The depth of the feature suggests that may not be related to infrastructure and could be an increase in soil moisture or a change in soil chemistry. However, line 200EBP05 shows a heavy distortion of the conductive feature that is most likely caused by subsurface infrastructure that is known to exist within the near-surface (less than 4 m). Note that significant quantities of data have been removed from line 200EBP05 prior to inversion based on high error or noise related to infrastructure. The resulting section shows a much deeper conductive anomaly that is clearly influenced by infrastructure. Therefore, it is impossible to separate the effects of infrastructure from a possible increase in soil moisture in this vicinity without additional characterization or 3D inversion. All three lines also show a moderately conductive anomaly in the near surface between station 0 and 60 meters. This correlates with Line 200EBP01 which crosses the three lines just north of the 216-B-55 disposal trench. There is no evidence of infrastructure and the anomaly does not show characteristics and resistivity magnitude of infrastructure. It is possible that the anomaly is the result of increased soil moisture due to the 216-B-55 disposal trench.

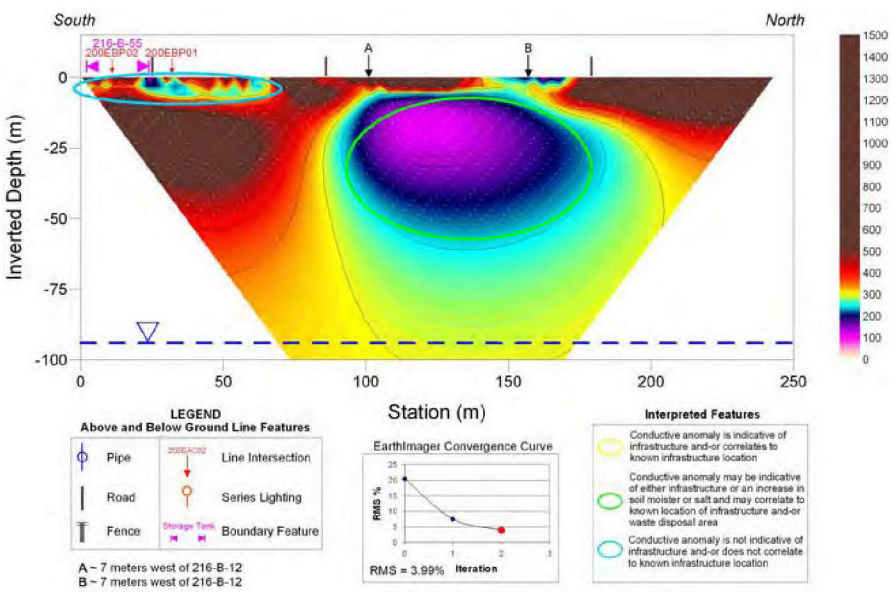

Figure 5-30. Inversion Results for B-Plant Line 200EBP04.

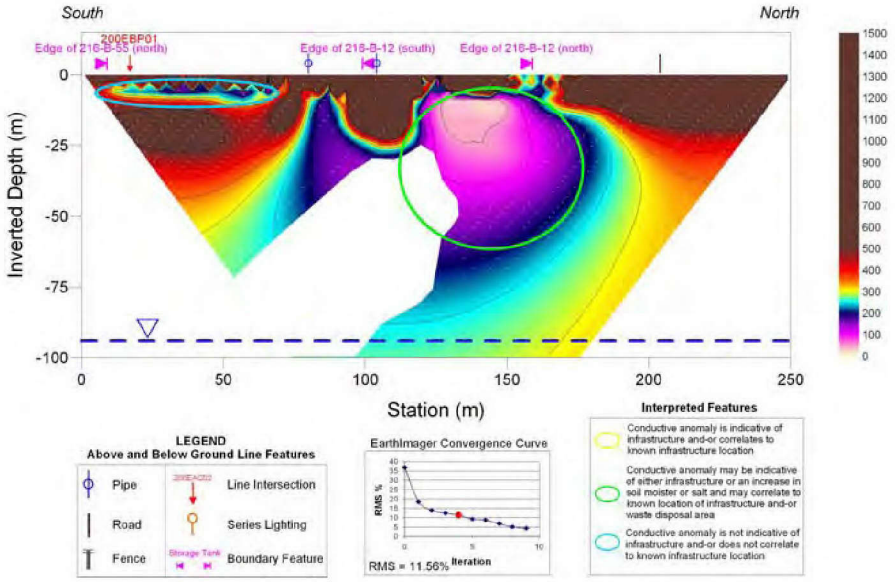

Figure 5-31. Inversion Results for B-Plant Line 200EBP05.

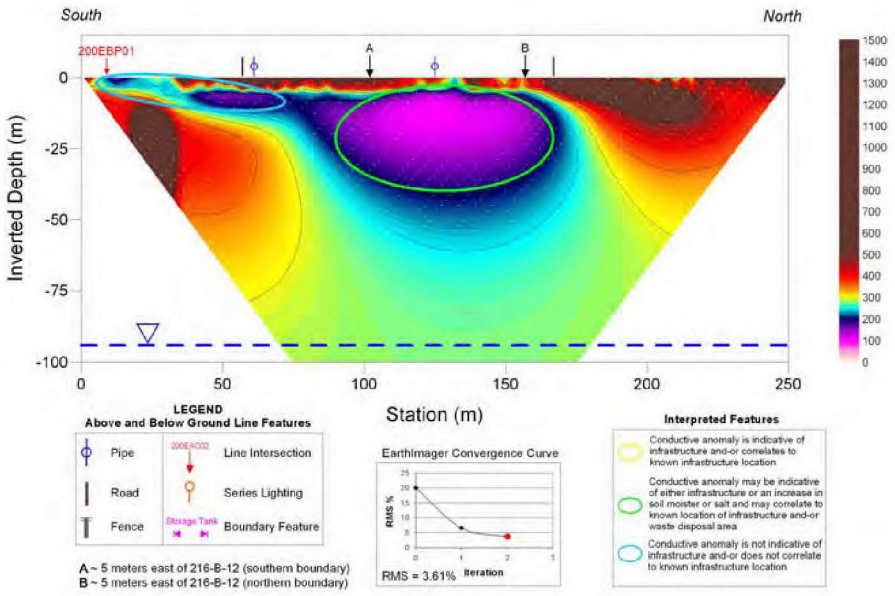

Figure 5-32. Inversion Results for B-Plant Line 200EBP06.

Two-dimensional inversion results for lines 200EBP07, 200EBP08, 200EBP09, and 200EBP10 are indiscernible since they are dominated by subsurface and surface infrastructure. Note that significant quantities of data have been removed from line 200EBP05 prior to inversion based on high error or noise related to infrastructure. The proximity of the resistivity lines to the industrial complex provided an abundance of preferential current pathways that violate the single point

current injection assumption, which makes it impossible to reconstruct based on 2D inversion alone. It is possible that 3D inversion results will be improved but it is unlikely that the results will allow discrimination between infrastructure and disposal volume related moisture increases. The southern ends of both 200EBP09 and 200EBP10 show background resistivity values in the desert scrub areas. They also confirm the location of the pipeline located near the southern end.

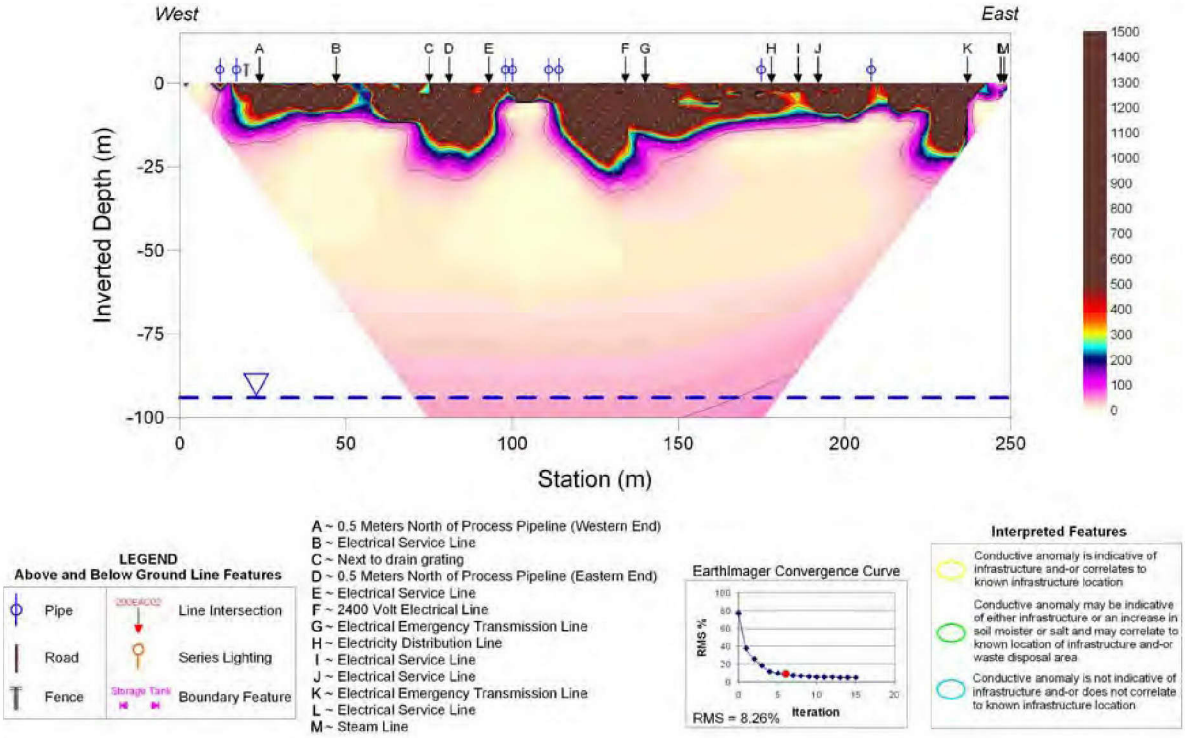

Figure 5-33. Inversion Results for B-Plant Line 200EBP07.

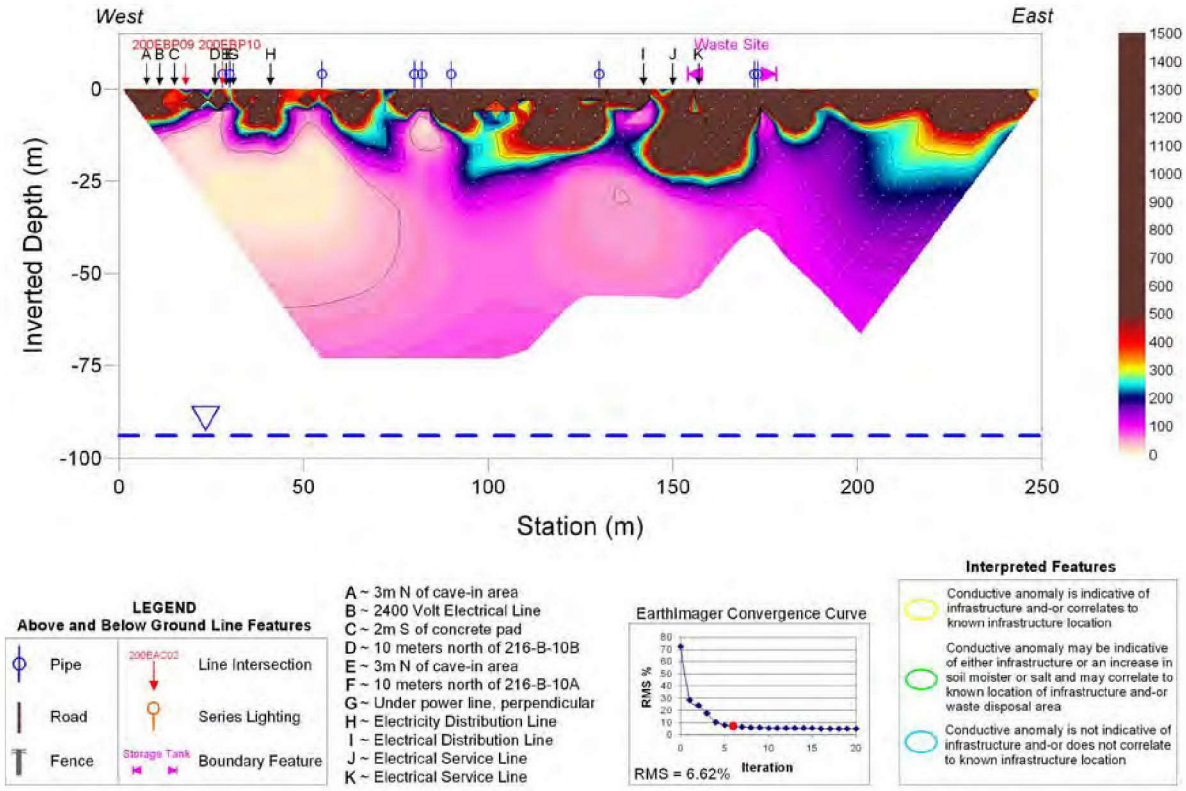

Figure 5-34. Inversion Results for B-Plant Line 200EBP08.

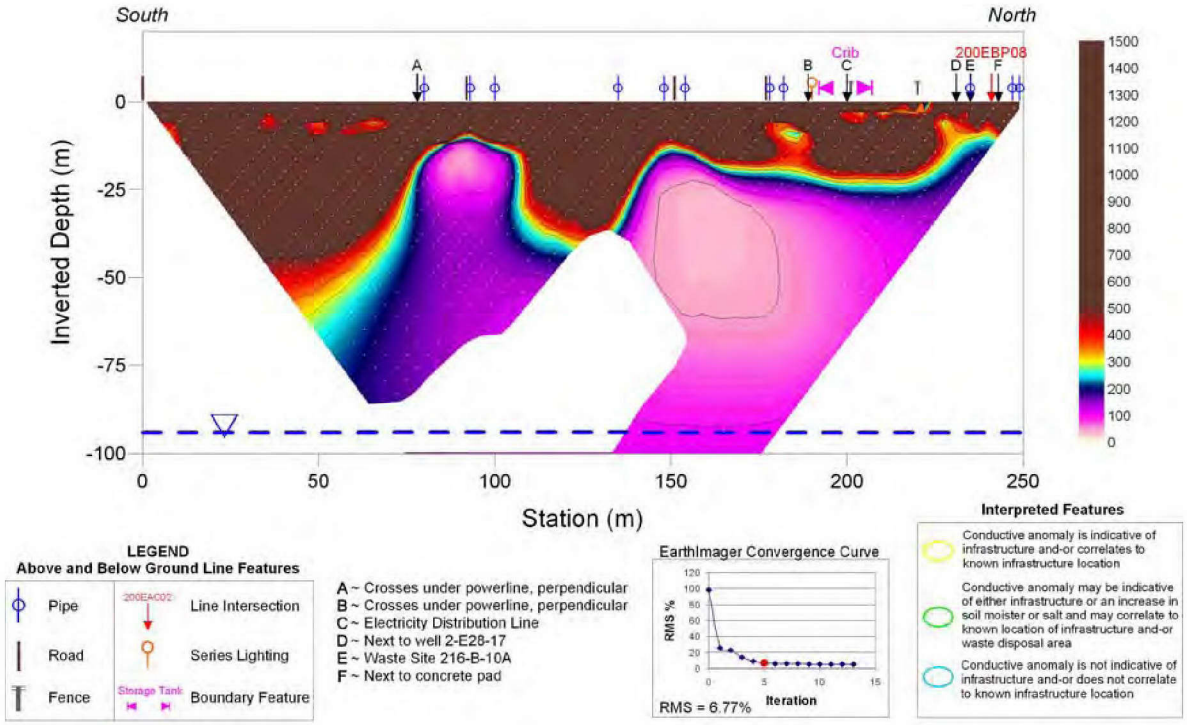

Figure 5-35. Inversion Results for B-Plant Line 200EBP09.

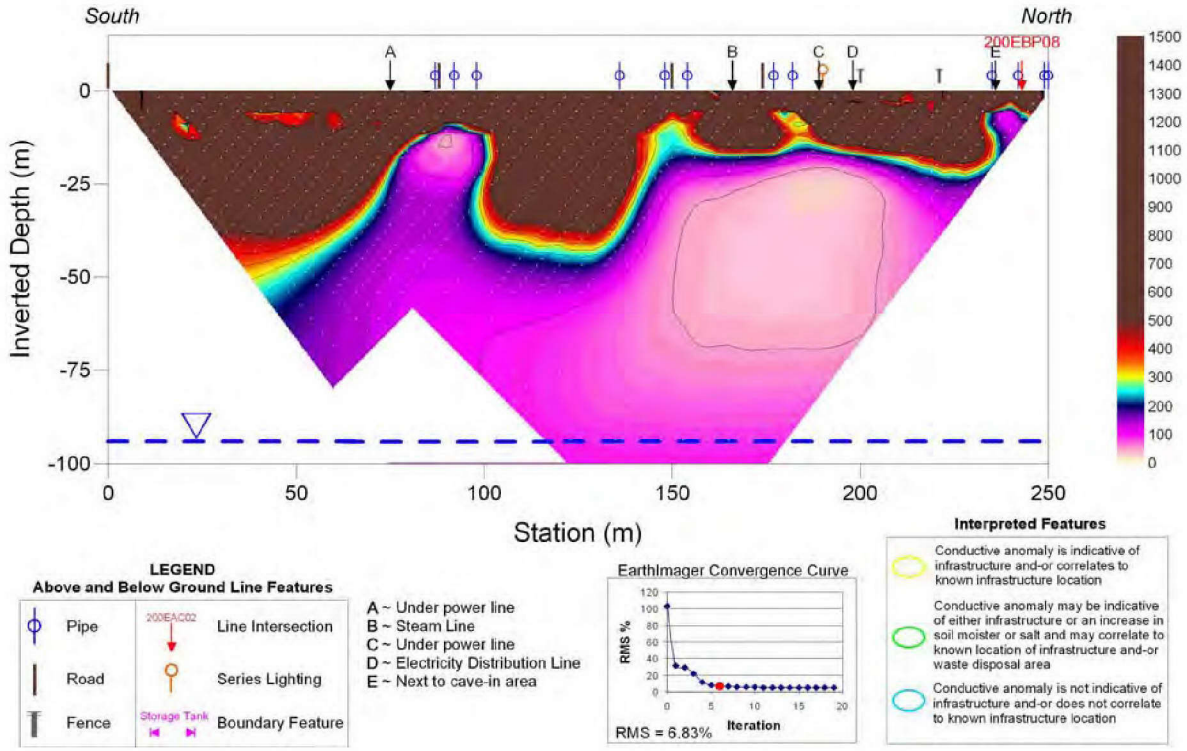

Figure 5-36. Inversion Results for B-Plant Line 200EBP10.

5.1.3.2 3D Rendering of 2D Inversion Results

Figures 5-37 through 5-41 show the plan view resistivity distribution at-depths increasing in 15-meter increments, from 15 to 75 m, respectively. Three-dimensional visualization was not completed for the lines collected south of B-Plant because line layout was not suitable for 3D rendering and the area is dominated by infrastructure. The resulting images would have been misleading and of limited value.

Three-dimensional results for the 216-B-55 and 216-B-12 areas show a large conductivity area in the near-surface towards the southeast of lines 200EBP01 and 200EBP03 that correlates with infrastructure. An additional conductive anomaly is noticeable directly over the 216-B-12 site where 10 to 100 mGal of liquid waste was disposed. The conductivity anomaly is centered at the termination of two external pipelines leading to the location and is most evident on the 30, 45, and 60 m depth slices. The response is heavily distorted due to 2D inversion not being able to resolve the complex 3D target. Note that the contoured results over the 216-B-55 waste site only include results for survey lines 200EBP01 and 200EBP03. However, both lines show little evidence of the 10 to 100 mGal of liquid wasted disposed in the area.

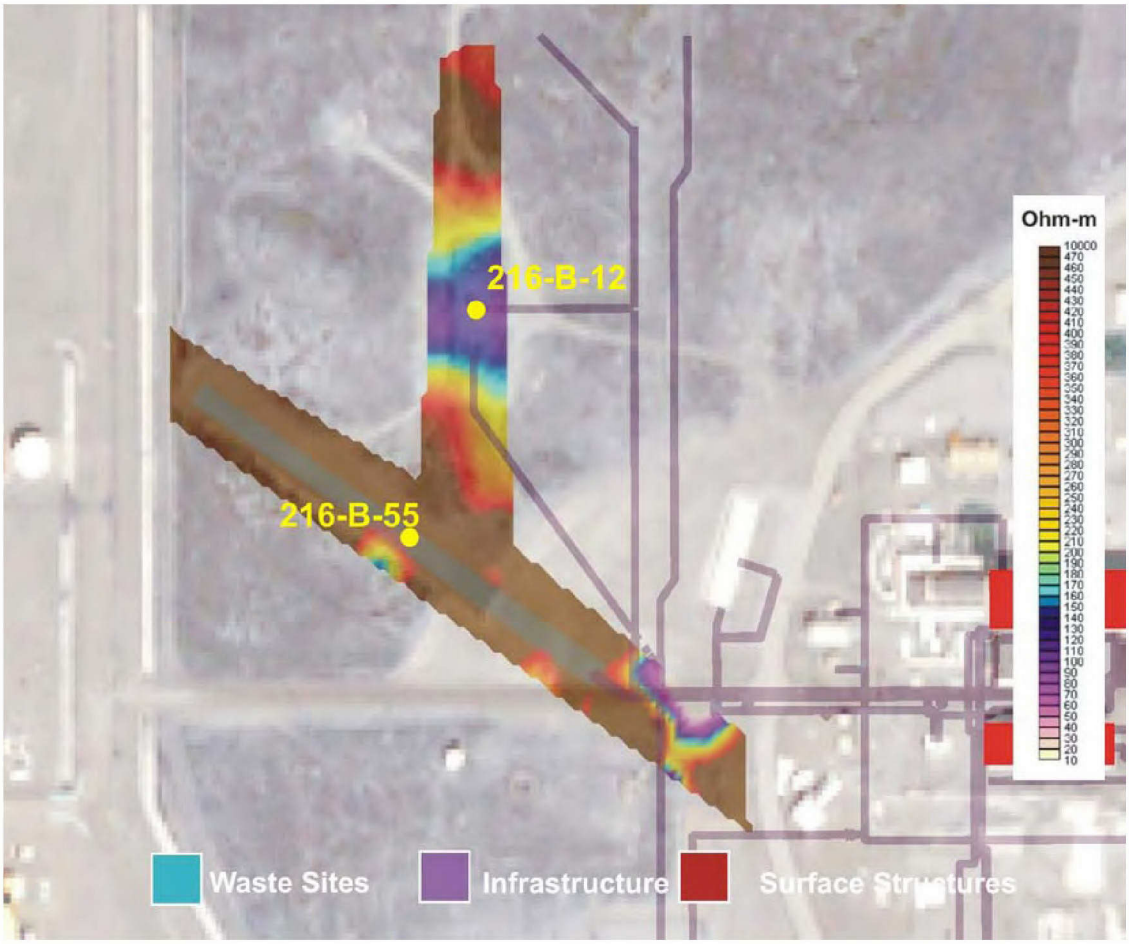

Figure 5-37. Results from the 3D Visualization for B-Plant at a Depth of 15 m BGS.

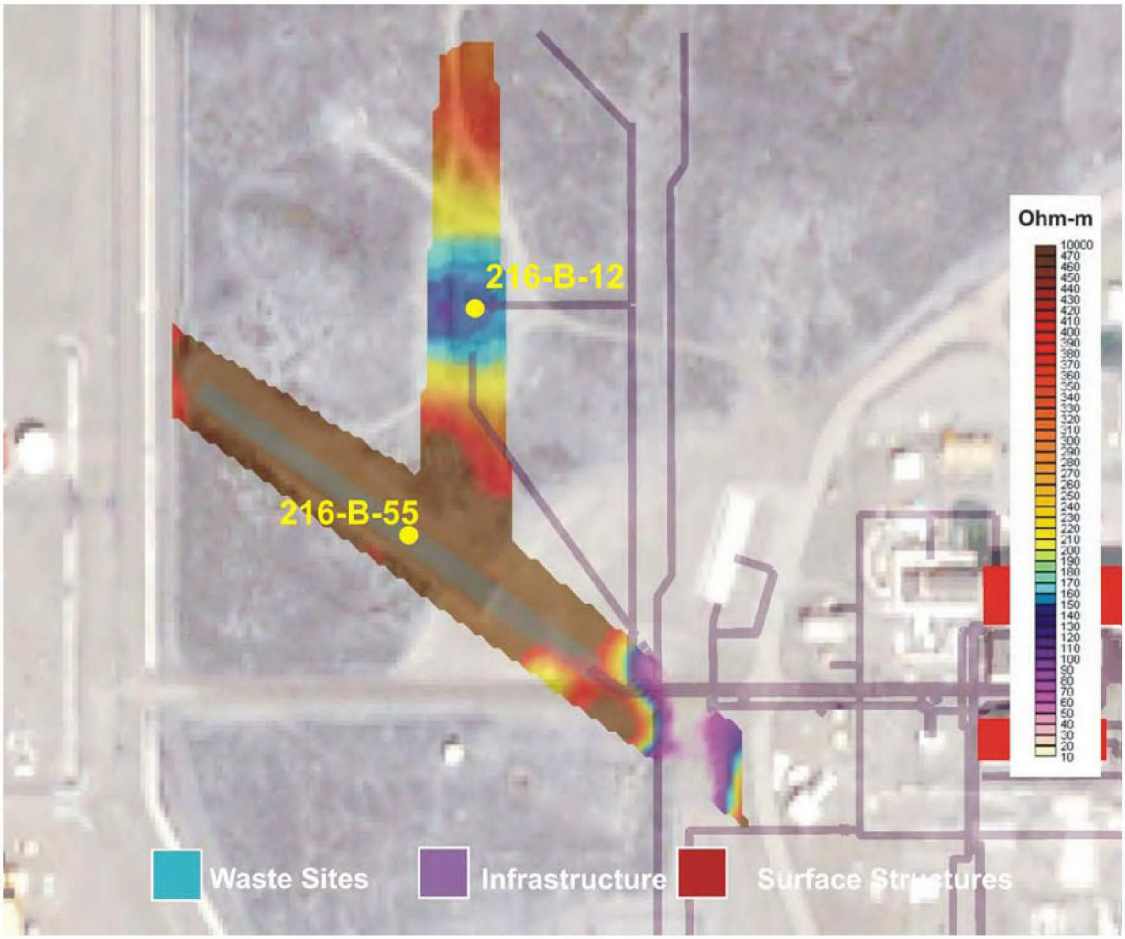

Figure 5-38. Results from the 3D Visualization for B-Plant at a Depth of 30 m BGS.

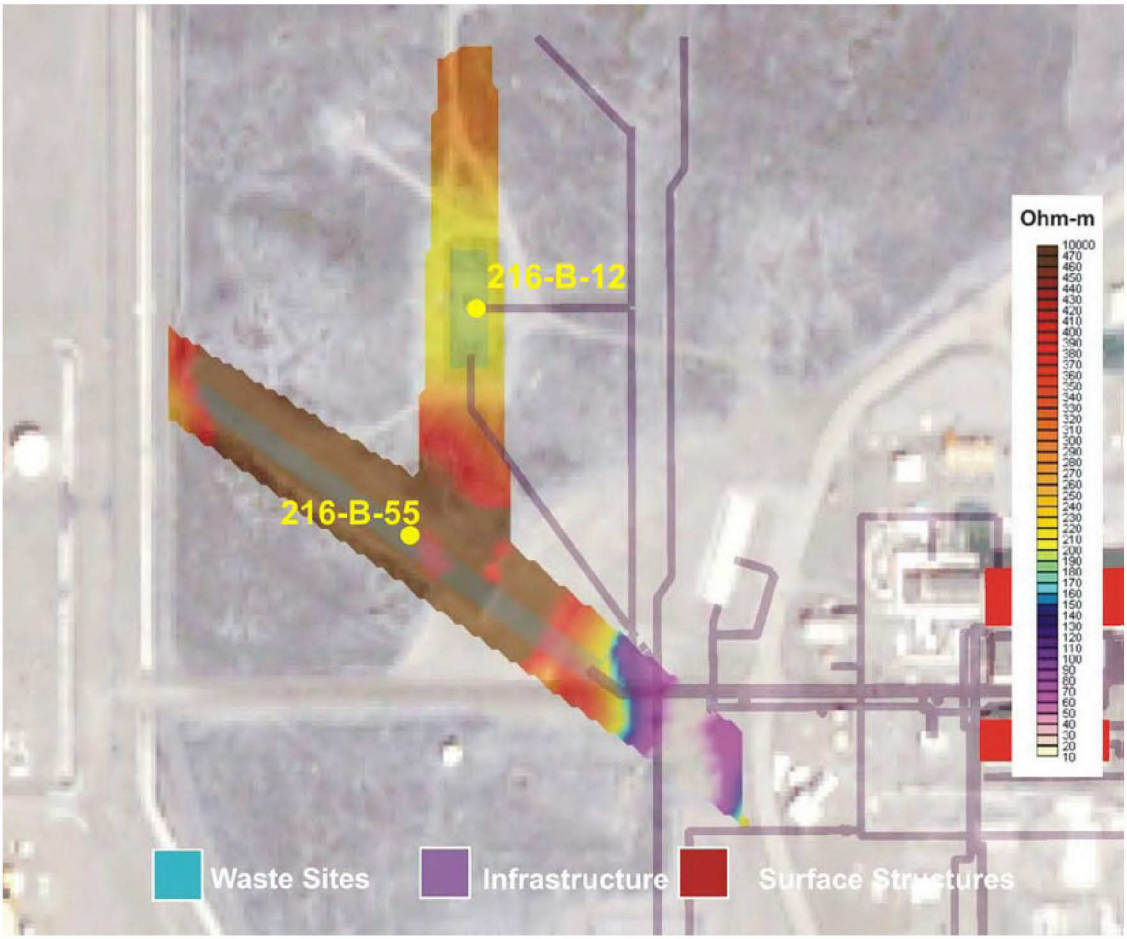

Figure 5-39. Results from the 3D Visualization for B-Plant at a Depth of 45 m BGS.

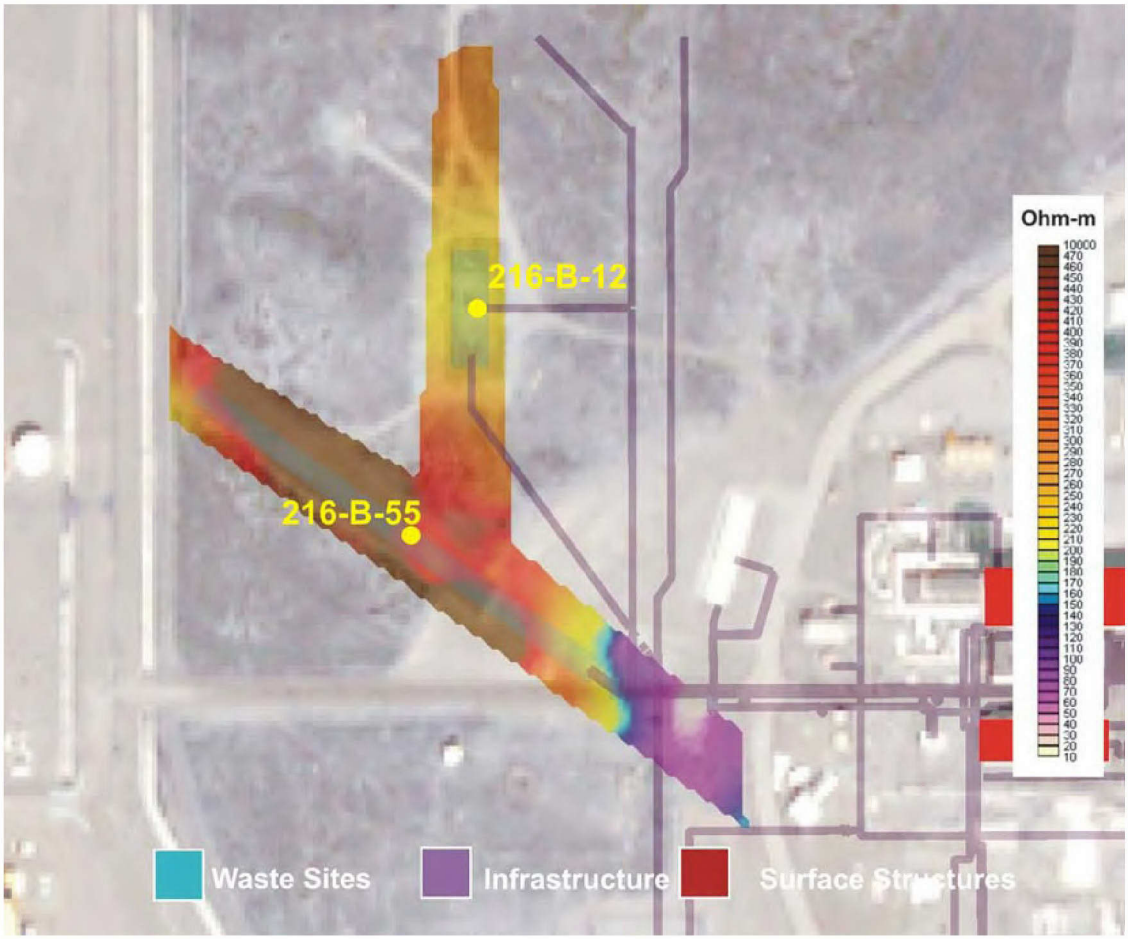

Figure 5-40. Results from the 3D Visualization for B-Plant at a Depth of 60 m BGS.

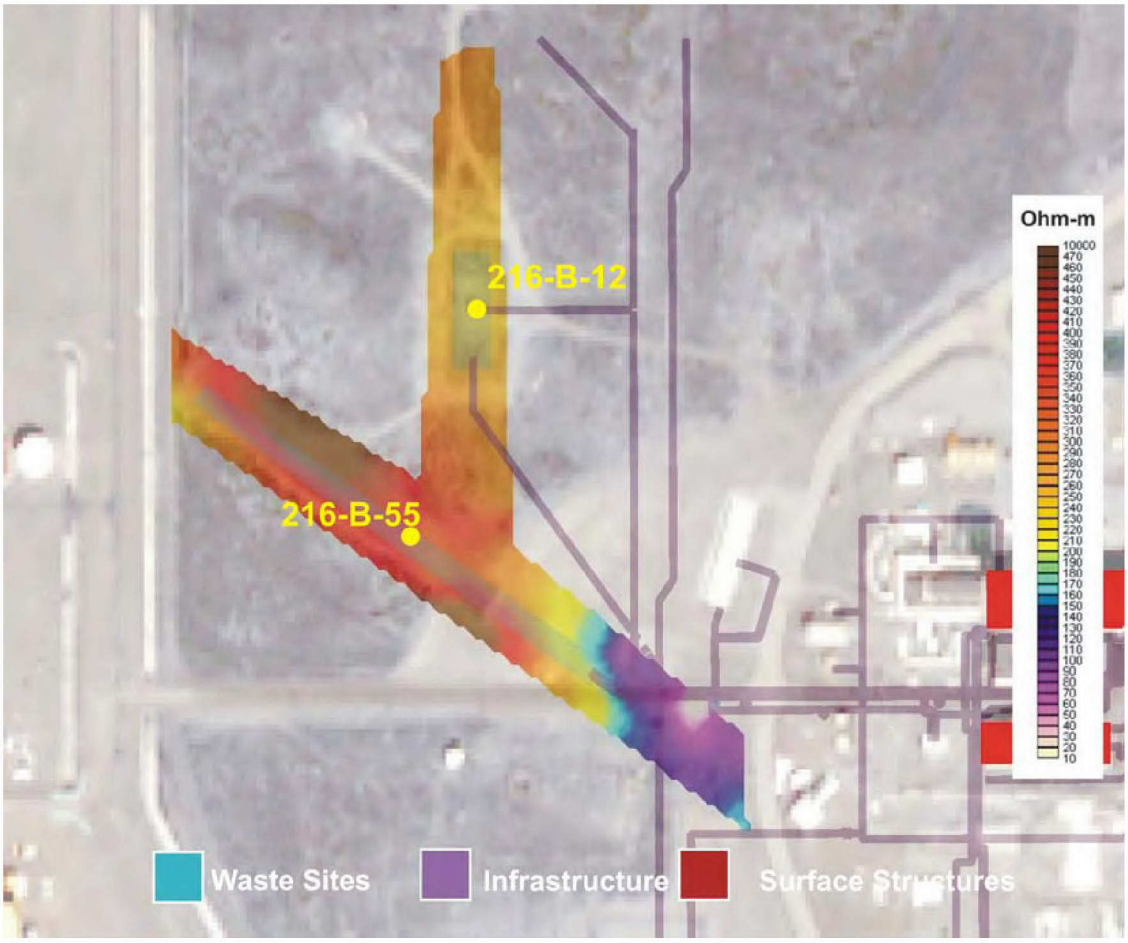

Figure 5-41. Results from the 3D Visualization for B-Plant at a Depth of 75 m BGS.

5.1.4 PUREX Plant

5.1.4.1 2D Inversion Results

The 2D inversion results of the resistivity survey performed at the PUREX site can be viewed in Figures 5-43 through 5-59 below. Figures 5-43 through 5-54 display the results in a cross-sectional format, while Figures 5-55 through 5-59 display the results of a 3D visualization of the same data set. Presenting plan view "depth slices" from the 3D visualization provides a tool for correlating resistivity responses to infrastructure, changes in soil moisture, or changes in soil chemistry.

Figures 5-43 through 5-47 display select results of a previous survey completed at the PUREX site. This data was selected to augment the 3D processing for the current investigation at the PUREX site. Previous projects completed HRR sections and 3D inversion, but not 2D inversion sections. Therefore, the 2D inversion of the old data had to be completed before the data could be used as part of the 3D visualization. An interpretation of the 2D cross-section results for the

previous coverage are not included in this report but remains consistent with the interpreted results of the previously presented HRR sections. Note that the previous SOW for the PUREX site only included 2D HRR presentation and 3D inversion/visualization. This is different to what is conducted as part of this report, which uses 2D inversion and 3D interpolation for visualization.

Seven additional resistivity lines were acquired at PUREX; 200EPX09 (Figure 5-48), 200EPX10 (Figure 5-49), 200EPX11 (Figure 5-50), 200EPX12 (Figure 5-51), 200EPX13 (Figure 5-52), 200EPX14 (Figure 5-53), and 200EPX15 (Figure 5-54). The resistivity data was processed according to Section 4.3 above using a 2D inversion algorithm (AGI EarthImager 2D). Table 5-4 shows the inversion statistics for goodness of fit in each line at B-Plant. An explanation of the table parameters is discussed in detail within Section 4.3.3.

Table 5-4. Final Inversion Statistics for PUREX Plant.

Line #	Stage	Trial	Iterations	RMS	L_2
200EPX02	1	1	2	4.96	0.98
200EPX03	1	1	3	4.28	0.73
200EPX04	1	1	2	3.35	0.45
200EPX06	3	1	4	6.91	1.91
200EPX08	3	1	2	5.56	1.24
200EPX09	3	2	4	5.39	1.16
200EPX10	1	1	4	4.04	0.65
200EPX11	3	1	4	5.61	1.26
200EPX12	1	1	3	4.52	0.82
200EPX13	1	1	3	2.83	0.32
200EPX14	1	1	3	2.74	0.30
200EPX15	1	1	2	4.00	0.64

RMS = root-mean-square.

A site specific color scale was developed through a statistical analysis of the apparent resistivity values for all data collected within the Purex site. A histogram, shown in Figure 5-42, was used to generate a color gradient that is sensitive to the resistivity range.

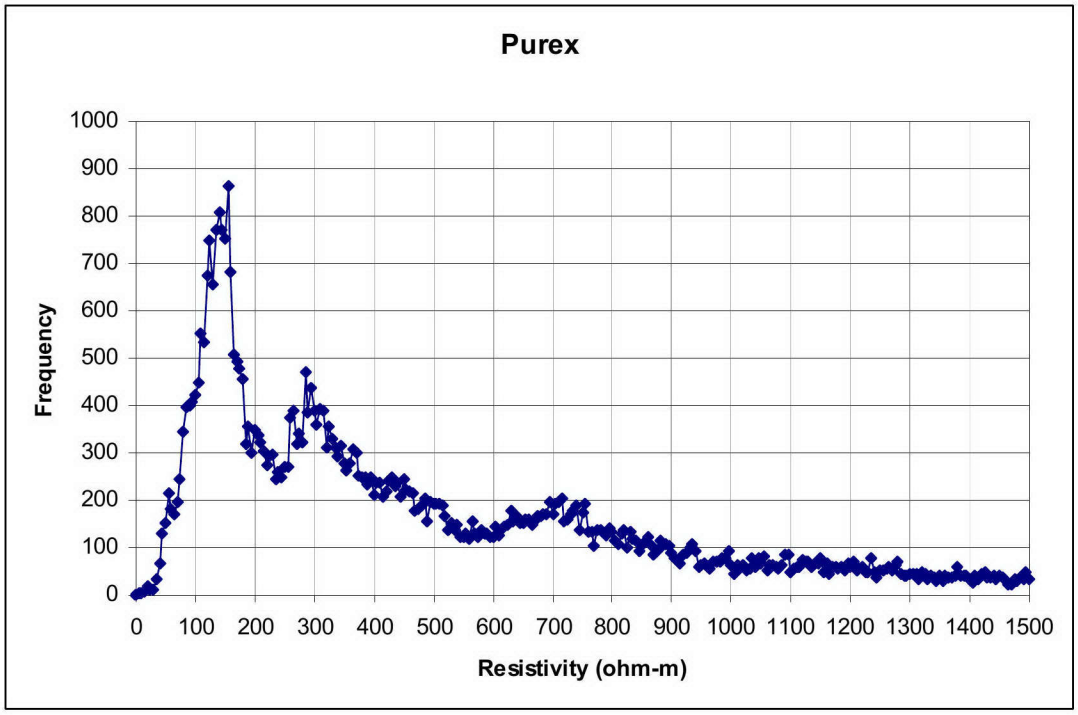

Figure 5-42. Histogram of apparent resistivity data for the Purex project site.

In contrast to several of the other project sites, the PUREX site was relatively free of infrastructure effects. Overall, there is a decrease in resistivity with depth on each of the ten profiles, suggesting an increase in moisture content associated with the water table or salt concentration from historical disposal activities. Depth to groundwater in the area has been recorded at approximately 98 m BGS. However, where conductive anomalies resulting from surface infrastructure occur there is a co-mingling of water table and infrastructure response that often distorts both features.

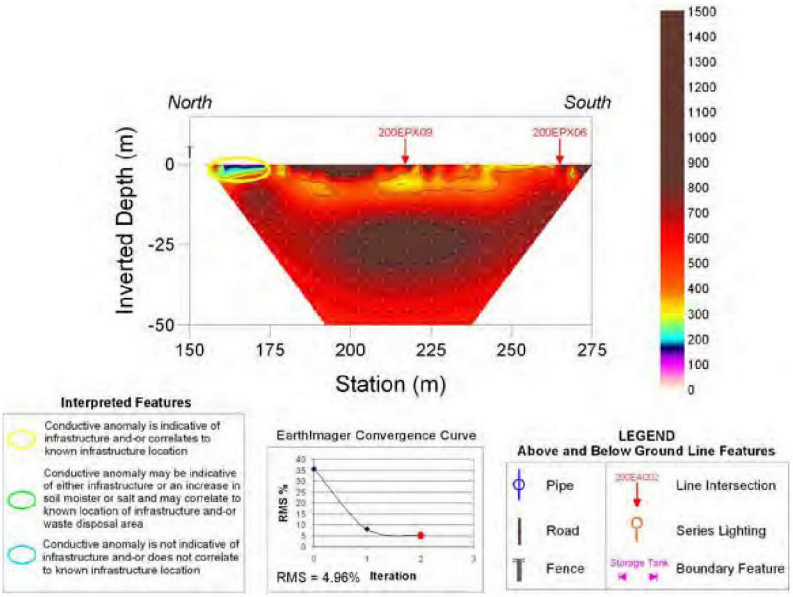

Figure 5-43. Inversion Results for PUREX Line 200EPX02 Old Line 1 and 5.

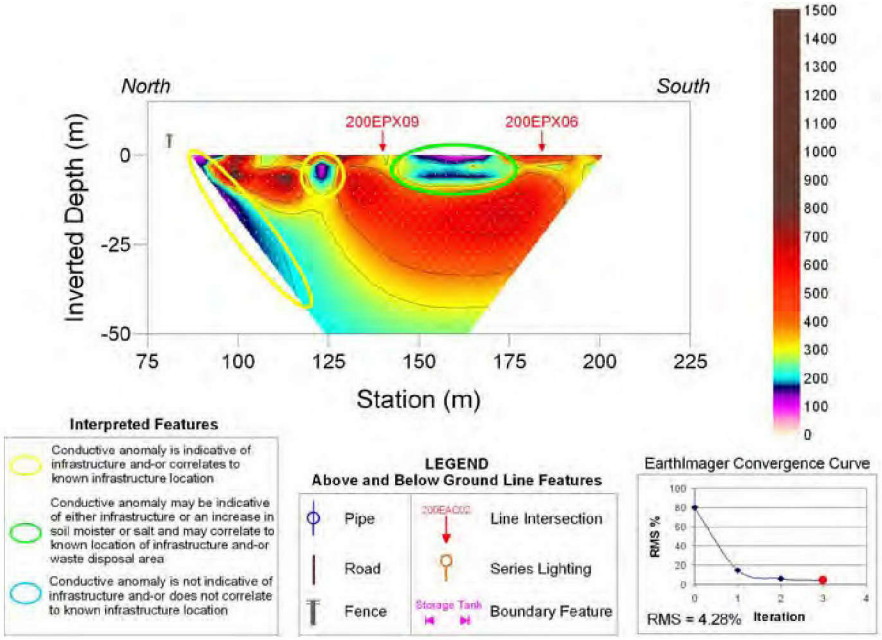

Figure 5-44. Inversion Results for PUREX Line 200EPX03 Old Line 7.

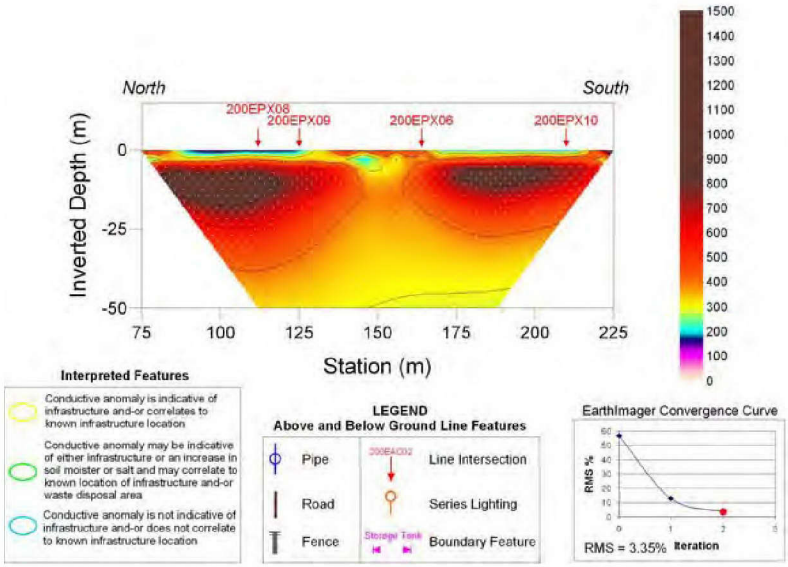

Figure 5-45. Inversion Results for PUREX Line 200EPX04 Old Line 8.

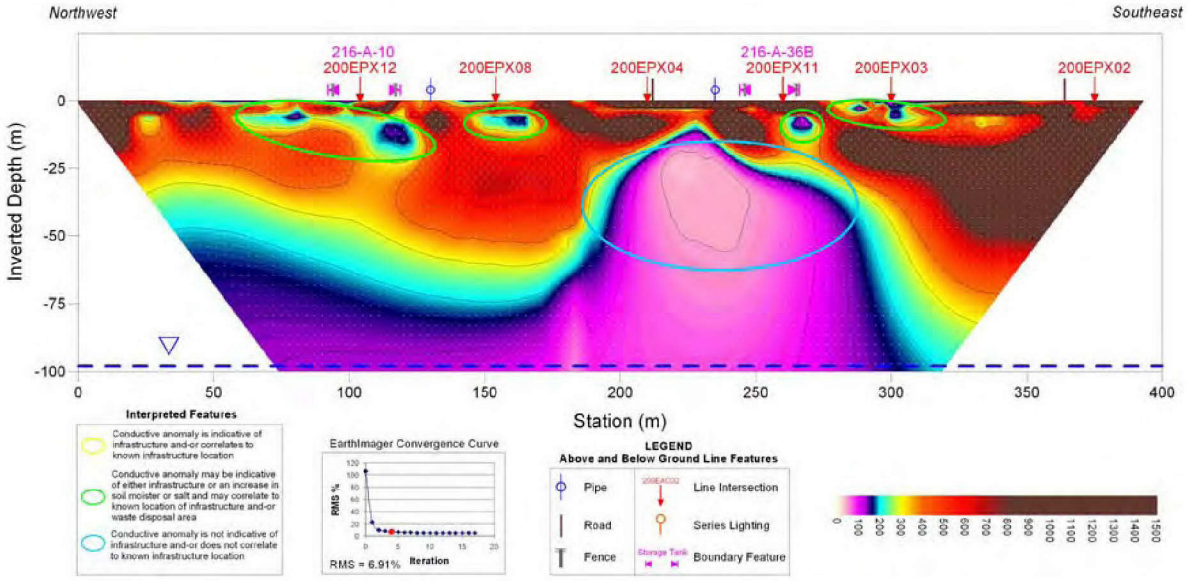

Figure 5-46. Inversion Results for PUREX Line 200EPX06 Old Line 6.

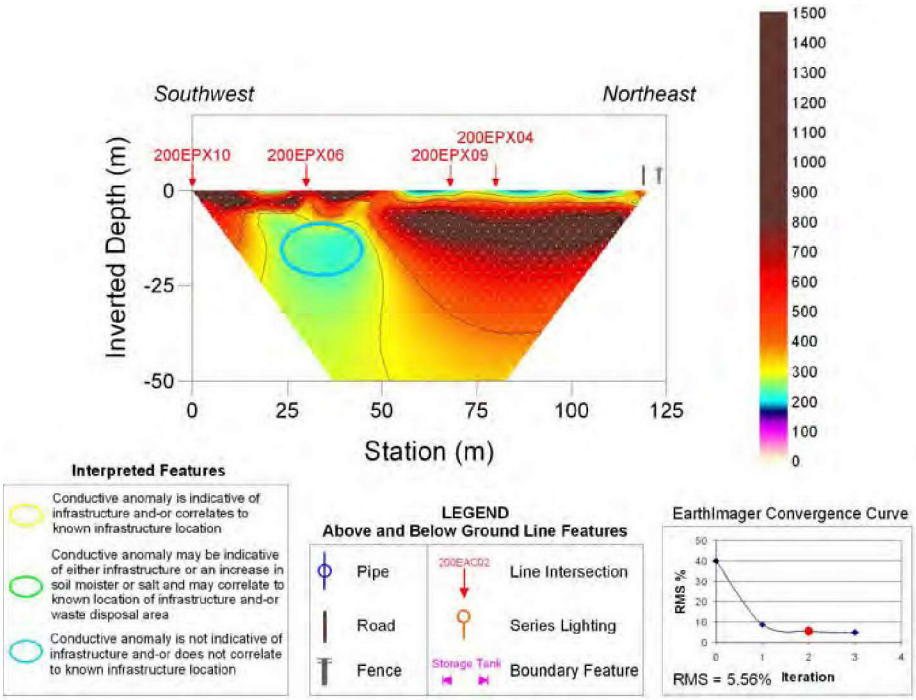

Figure 5-47. Inversion Results for PUREX Line 200EPX08 Old Line 4.

Lines 200EPX09 and 200EPX10 (Figures 5-48 and 5-49) cross-cut the 216-A-36 A/B and 216-A-10 waste areas. Both lines display a conductive anomaly centered near station 175 m that correlates well with the location of the 216-A-36 A/B waste site. This is in agreement with the results obtained from line 200EPX11 which was acquired over the full-length of the waste site. The resolved depth of the conductive anomaly suggests that it is not a result of surface or near-surface infrastructure despite the evidence of a few pipelines beneath the lines. The location of the conductive feature is in close proximity to the disposal of 2500 to 7600 mGal of liquid waste containing large quantities of nitrate. The depth and size of the conductive anomaly is likely distorted by the conductive layer at depth, which is associated with the water table. Both the 2D inversion and 2D contouring process tend to smear or merge separate conductive anomalies. Readers are cautioned not to directly interpret the depth and extent of the anomaly as the depth and extent of an increase in soil moisture. The disturbed area is likely to be smaller than shown on the figures.

Line 200EPX09 shows a small highly conductive feature (approximately 50 Ohm-m) at Station 40 m that correlates spatially to a conductive feature (approximately 100 Ohm-m) on line 200EPX06 at approximately station 120 m. Line 200EPX12, runs in a north-south direction and shows a moderately low conductivity feature (approximately 200 Ohm-m) approximately 10 meters west of lines 200WPX06 and 200WPX09. The three lines show different resistivity values making it challenging to definitively correlate, but all three lines are located over different areas of the localized conductive feature, which may explain the changing resistivity values. This localized response does not correlate with any known infrastructure. The proximity of the conductive feature to the 216-A-10 disposal area, which received over 8200 mGal of liquid

waste, is suspect and may indicate the presence of an increase in soil moisture or salt concentration. Line 200EPX09 also shows a small near surface conductive anomaly (100 to 200 Ohm-m) between station 225 and 275 meters. There is a similar magnitude (150 to 220 Ohm-m) conductive feature in the same geographic location on Line 200EPX06. Line 200EPX03 shows a conductive anomaly (100 to 200 Ohm-m) from station 140 to 165 meters directly between Line 200EPX06 and 200EPX09 that seems to correlate with the same conductive feature. There are no reported infrastructure features and the character of response is not indicative of infrastructure interference.

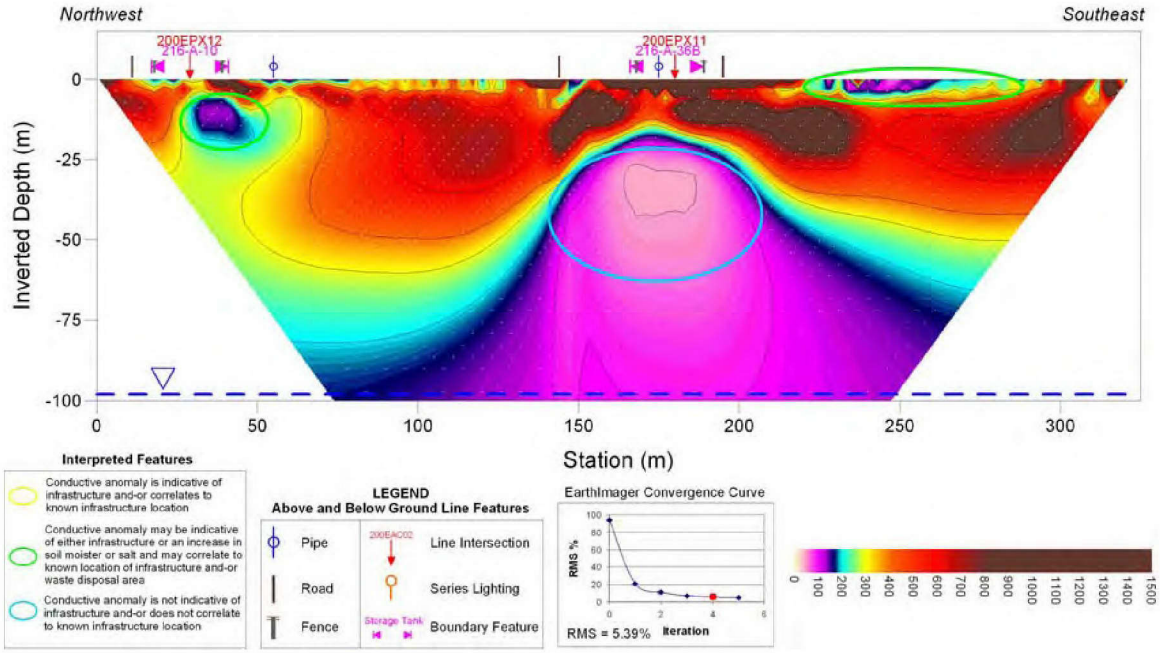

Figure 5-48. Inversion Results for PUREX Line 200EPX09.

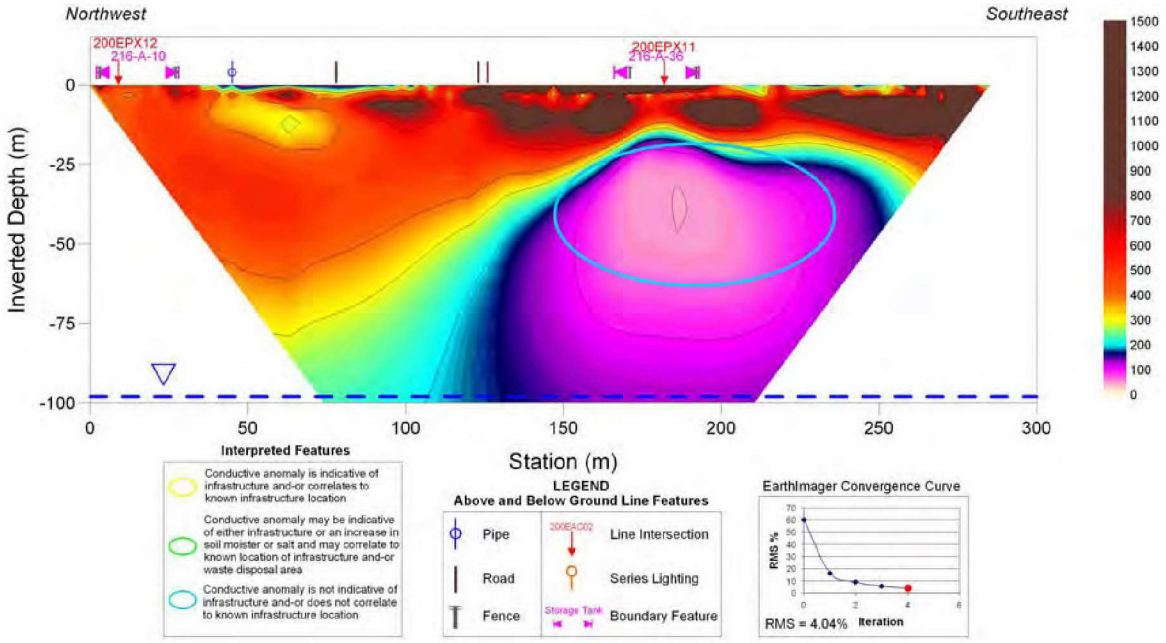

Figure 5-49. Inversion Results for PUREX Line 200EPX10.

Line 200EPX11 shows a highly conductive feature at centered on station 35 meters at a depth of approximately 10 to 15 meters BGS. The anomaly is located at the southern end of the 216-A-36B directly beneath crib infrastructure. It is likely that the response is associated with the crib infrastructure (likely conductive metal) but the proximity to the highly conductive anomaly associated with an increase in soil moisture over most of the line makes it difficult to correlate with certainty. Another highly conductive anomaly is located at the north end of the line near station 230 meters. This location correlates with infrastructure and the end of the 216-A-36A disposal trench. Again, it is likely that the response is associated with pipeline interference but the proximity to the highly conductive anomaly associated with an increase in soil moisture over most of the line makes it difficult to correlate with certainty.

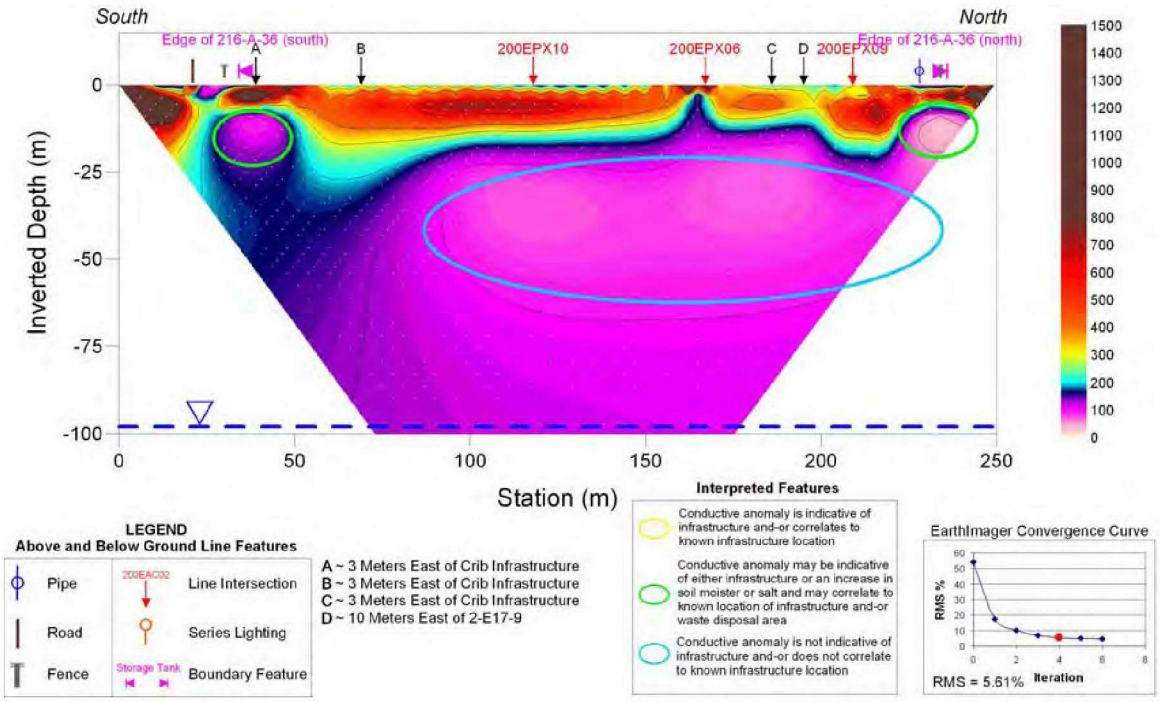

Figure 5-50. Inversion Results for PUREX Line 200EPX11.

Two-dimensional inversion results for line 200EPX12 display a conductive anomaly at approximately 130 m along the line, beginning at a depth of approximately 10 m. The location is in close proximity to well 299-E17-1, which is constructed of steel and may be adversely affecting the inversion model. A moderately conductive anomaly is located between station 150 and 220 meters that correlates with a similar anomaly on lines 200EPX06 and 200EPX09. The area does not correlate with infrastructure and is likely the result of an increase in soil moisture from the 216-A-10 waste disposal trench.

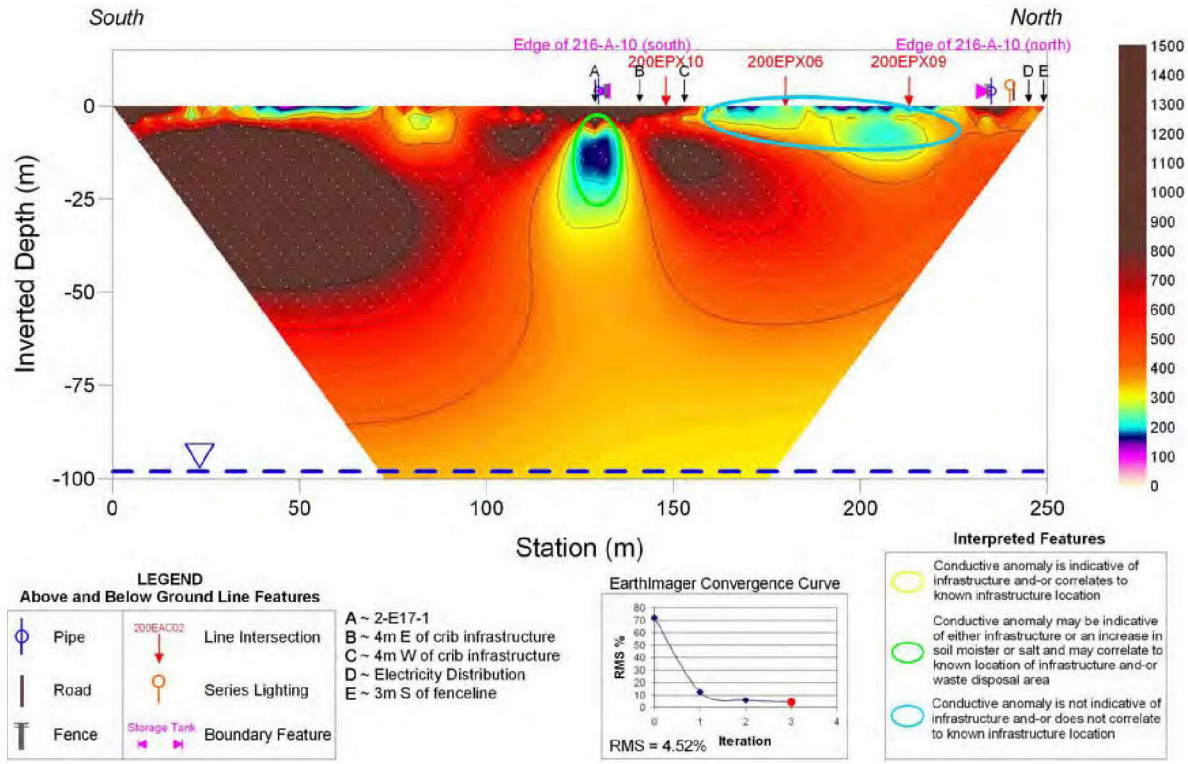

Figure 5-51. Inversion Results for PUREX Line 200EPX12.

Lines 200EPX13, 200EPX14, and 200EPX15 were collected over the 216-A-45 waste area, with line 200EPX14 centered over the waste site. All three lines show a near-surface (approximately 5 to 10 m BGS) conductive layer (150 to 250 Ohm-m), relative to the resistive background. There is clear decrease in resistivity towards the eastern side of the disposal area that is in close proximity to infrastructure, but the feature extends to the west with sufficient distance that it suggests a soil moisture increase or change in soil chemistry is possible. This conductive anomaly is limited to the near surface and has no connection to the water table. Lines 200EPX13 and 200EPX14 show the result of an infrastructure interference between station 150 and 170 associated with a pipeline.

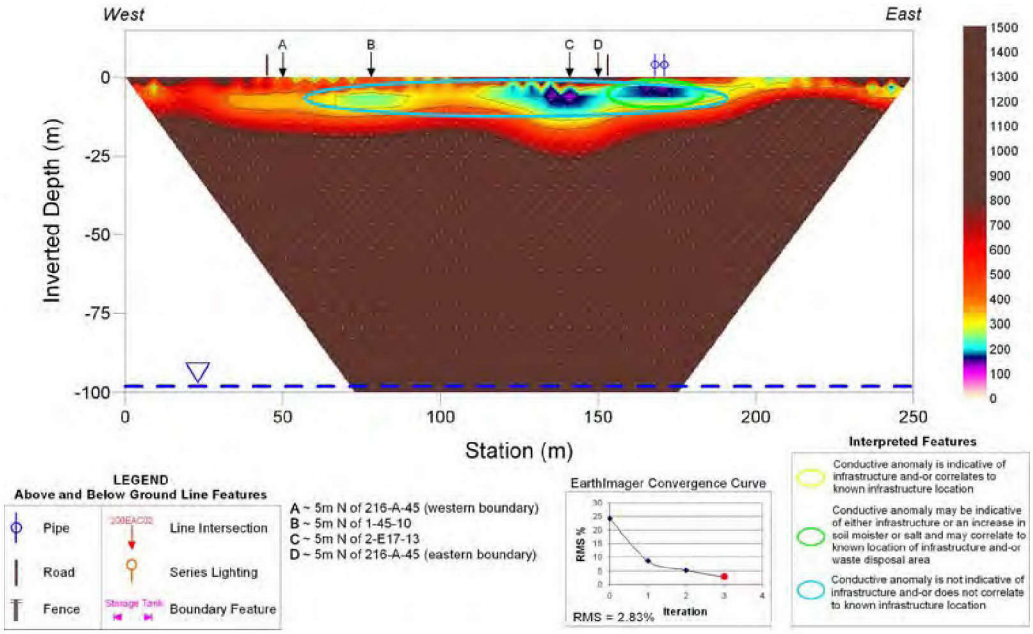

Figure 5-52. Inversion Results for PUREX Line 200EPX13.

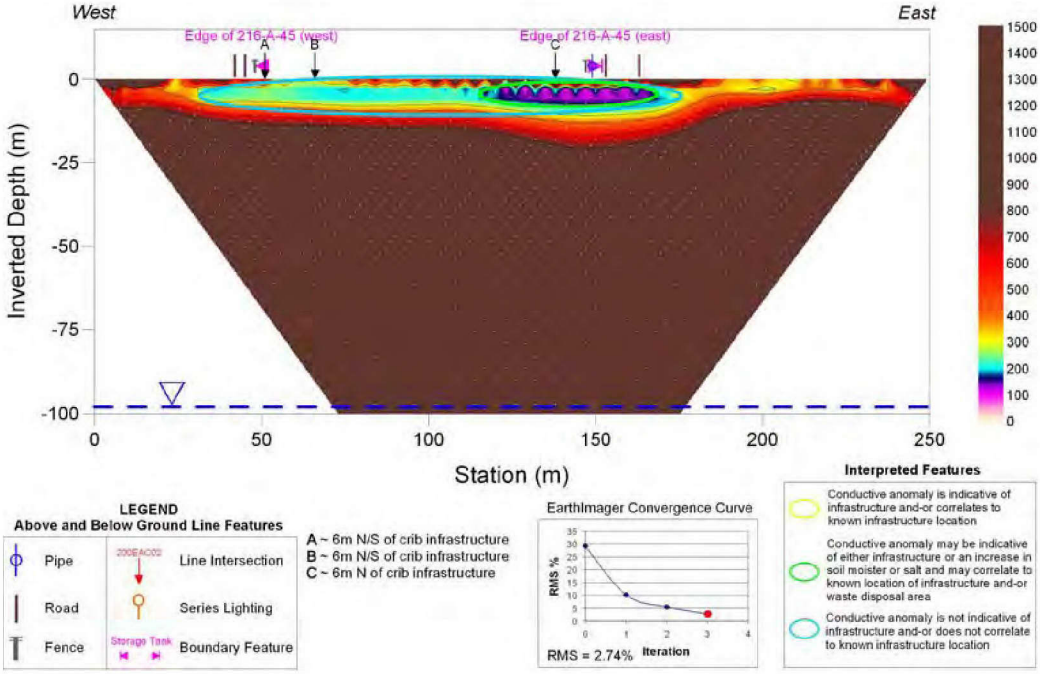

Figure 5-53. Inversion Results for PUREX Line 200EPX14.

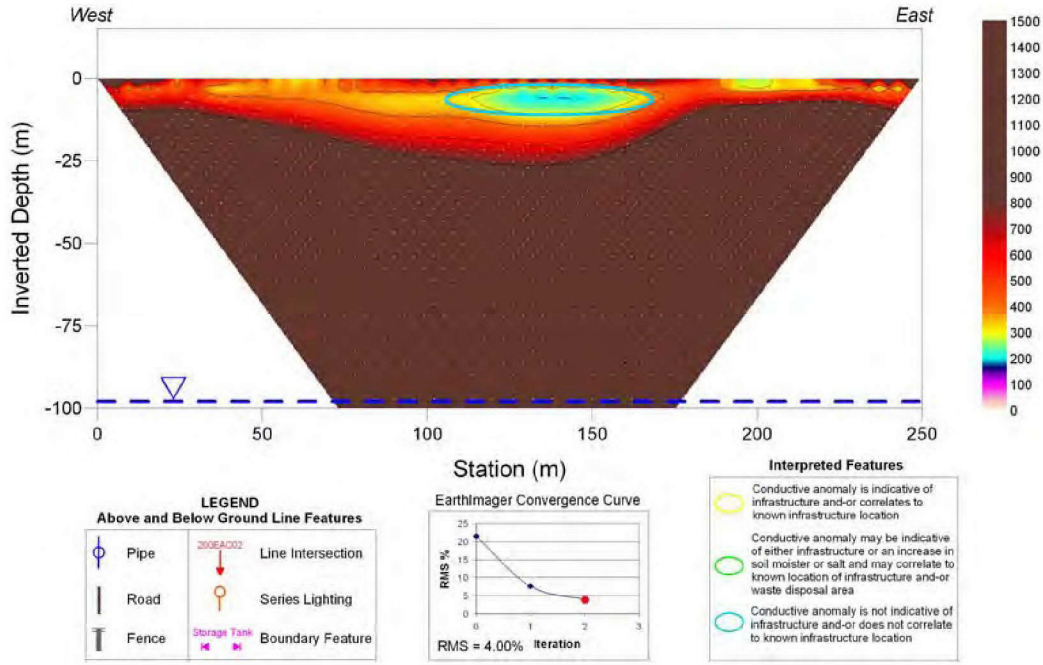

Figure 5-54. Inversion Results for PUREX Line 200EPX15.

5.1.4.2 3D Rendering of 2D Inversion Results

Figures 5-55 through 5-59 show the plan view resistivity distribution at-depths increasing in 15-meter increments, from 15 to 75 m, respectively. Two areas of interest were inverted at the PUREX site; one small area to the southwest of the site over waste area 216-A-45, and one to the northeast of the project site. No data was acquired deeper than 50 m in the southwestern site due to limited line coverage and as such is not presented in deeper sections. It should also be noted that the distance, line layout, and geometry of the survey lines are not optimal for 3D interpolation. However, 3D visualization was still completed according to the project SOW. In addition, inversion results for surface only resistivity measurements tend to vertically merge conductive features, especially where near surface conductive features are found directly above deeper conductive layers which may be caused by the water table. Model layers at the deepest sections tend to appear overly smoothed due to the decrease in sensitivity inherent when resistivity measurements are collected from only surface electrodes. If available, additional depth or borehole electrodes can be used to increase the sensitivity of the lower model layers by adding data more proximal to the water table. Readers are cautioned to be suspicious of depth slices bellow a depth of 40 meters BGS.

Depth slices from the 3D imaging over the northeastern portion of the site show conductivity feature located within the 216-A-36 A/B waste site. The feature extends the full length of the waste area and increases in size with depth. This correlates well with previous survey conducted at PUREX where only one survey line was conducted near the 216-A-36A and -B waste areas. The resistivity low extends beyond 75 m and is likely to be in contact with groundwater.

An additional, conductive response was observed in the far northwestern portion of the 45, 60, and 75 m depth slices. This feature is attributed to a distortion due to the large pipeline in the vicinity. Two small conductive features are visible near the 216-A-10 waste area but are limited to the near-surface. There is insufficient data to determine the possible cause of the anomalies. Relative to these features the remainder of the information is relatively inconsequential, although the 2D inversion sections show some conductive features over the 216-A-45 waste area. By comparison, a similar feature was observed on previous PUREX surveys, where the limited coverage in the area shows a target at-depth rather than the near-surface.

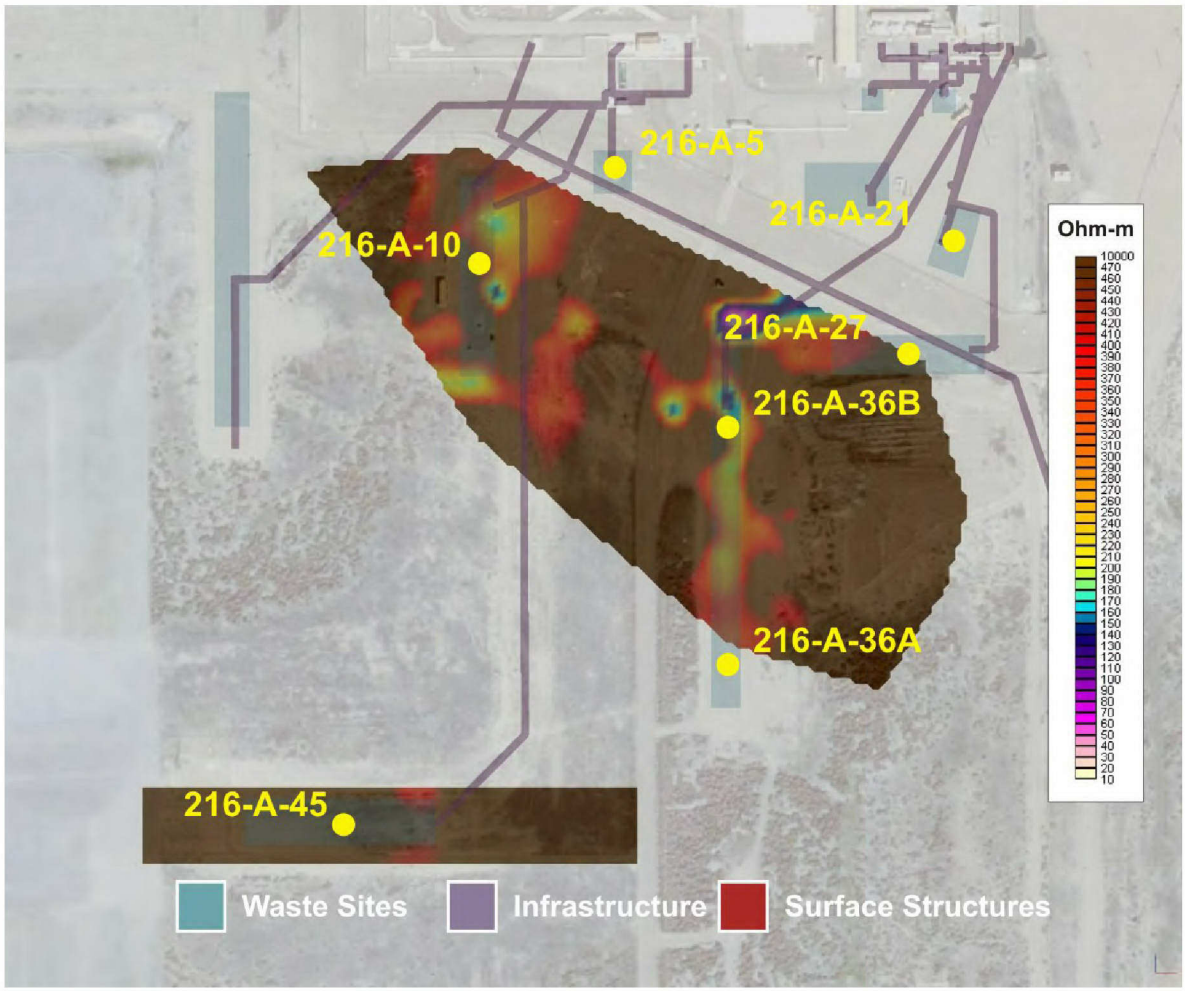

Figure 5-55. Results from the 3D Visualization for PUREX at a Depth of 15 m BGS.

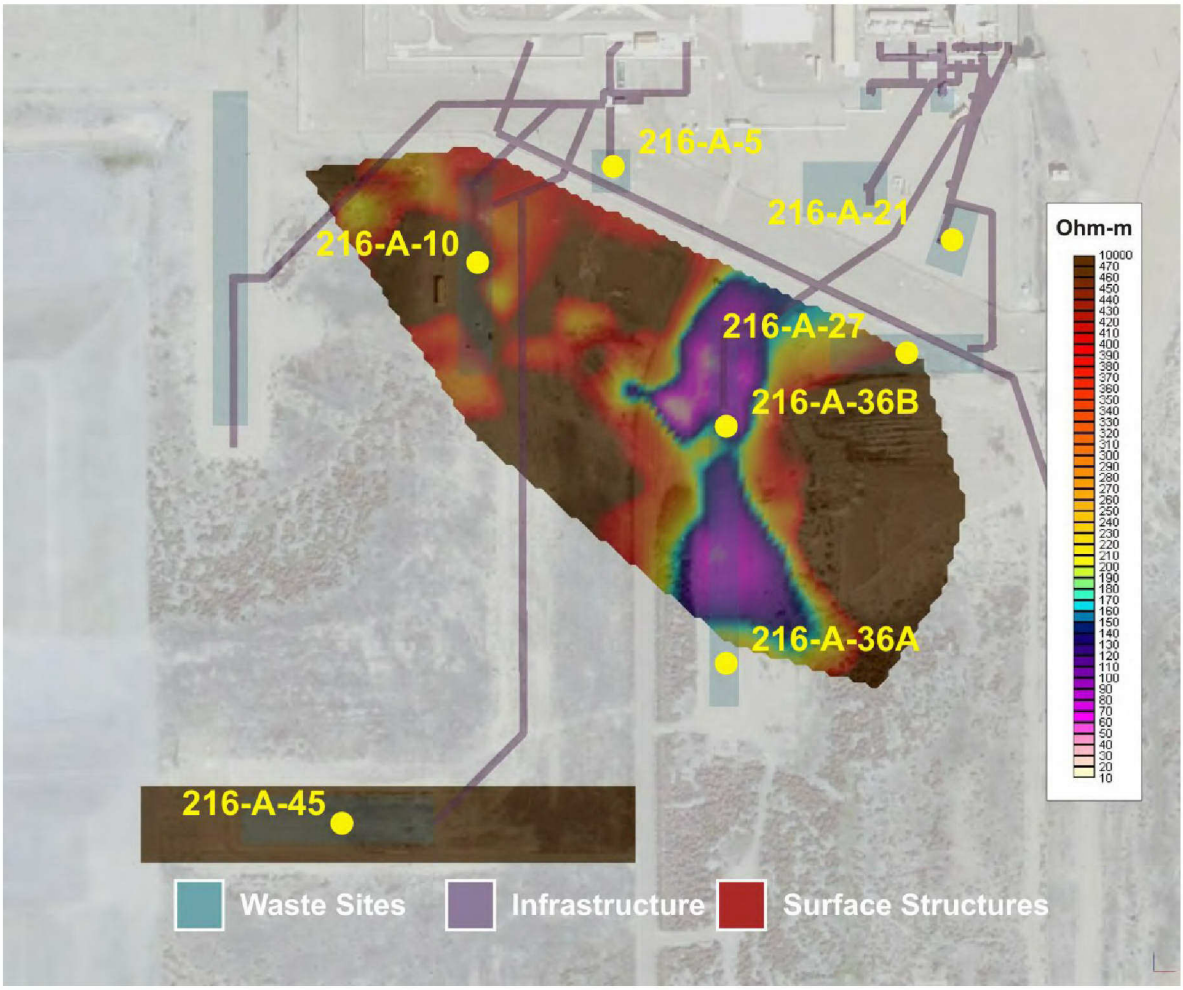

Figure 5-56. Results from the 3D Visualization for PUREX at a Depth of 30 m BGS.

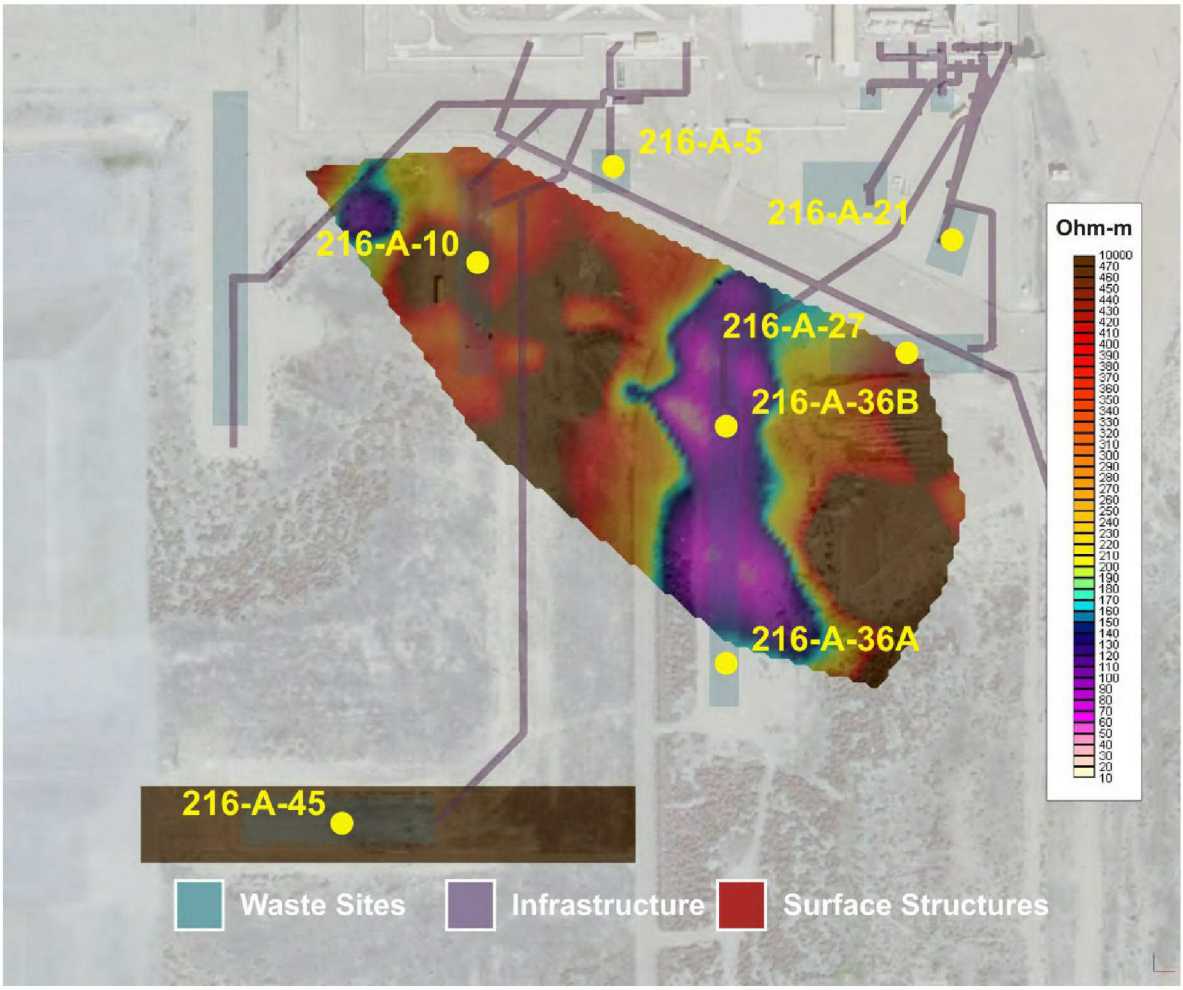

Figure 5-57. Results from the 3D Visualization for PUREX at a Depth of 45 m BGS.

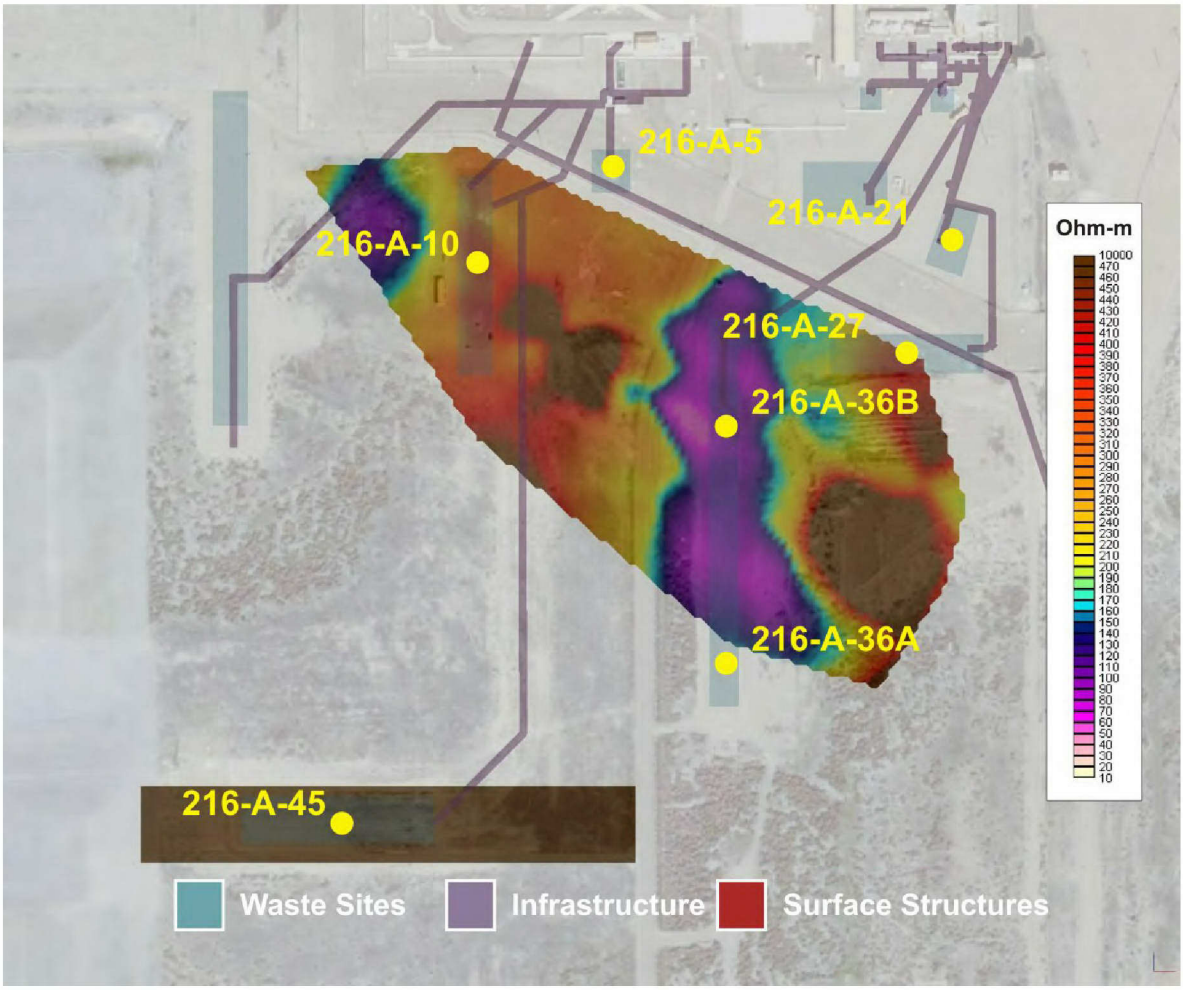

Figure 5-58. Results from the 3D Visualization for PUREX at a Depth of 60 m BGS.

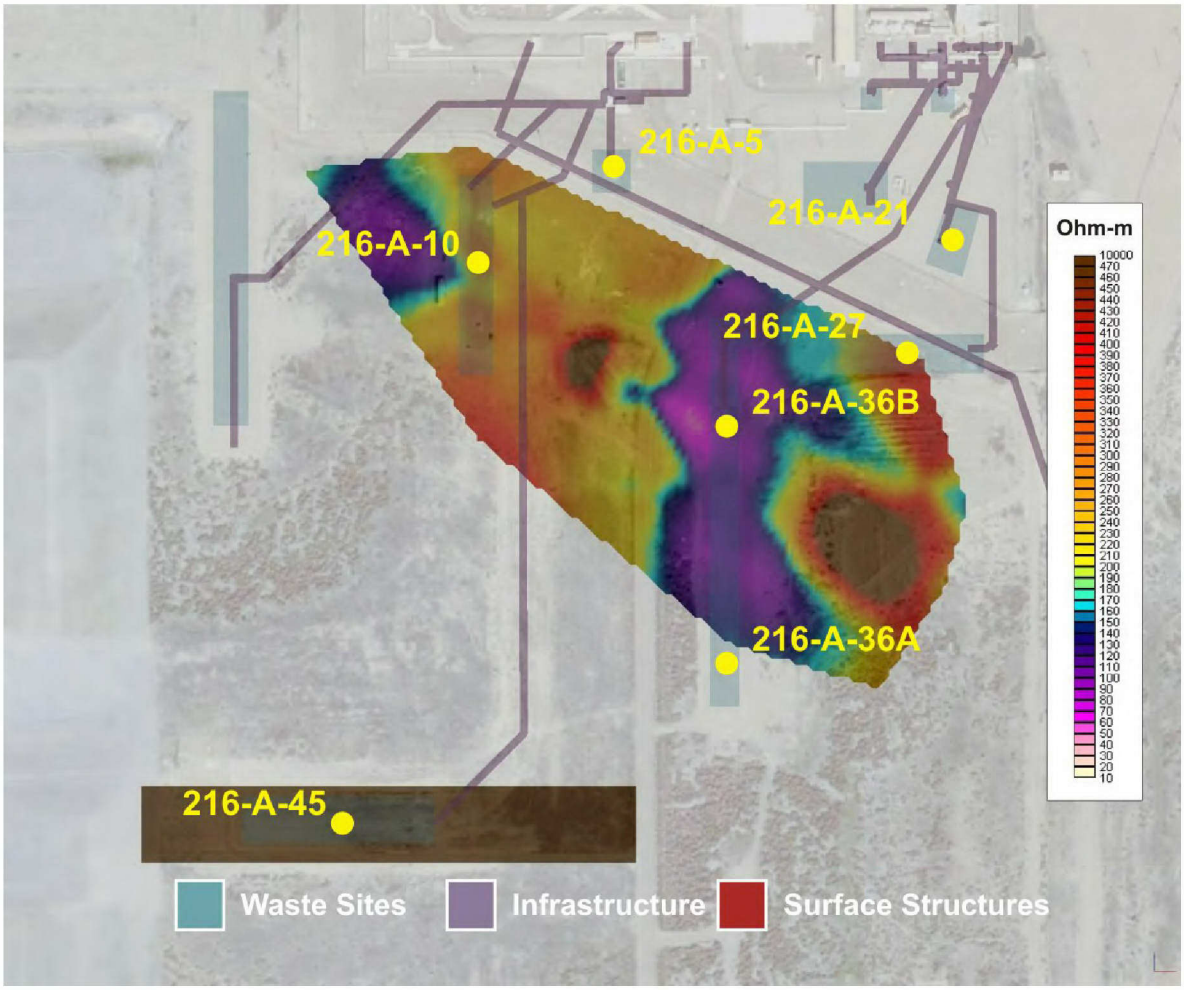

Figure 5-59. Results from the 3D Visualization for PUREX at a Depth of 75 m BGS.

5.2 200 WEST

5.2.1 S-Complex

5.2.1.1 2D Inversion Results

The 2D inversion results of the resistivity survey performed at S-Complex are displayed in Figures 5-61 through 5-76 below. Figures 5-61 through 5-66 display the results in a cross-sectional format, while Figures 5-67 through 5-76 displays the results of two separate 3D visualizations conducted for S-Complex. Presenting plan view "depth slices" from the 3D visualization provides a tool for correlating resistivity responses to infrastructure, changes in soil moisture, or changes in soil chemistry.

Six resistivity lines were acquired at S-Complex; 200WSC01 (Figure 5-61), 200WSC02 (Figure 5-62), 200WSC03 (Figure 5-63), 200WSC04 (Figure 5-64), 200WSC05 (Figure 5-65),

and 200WSC06 (Figure 5-66). The resistivity data was processed according to Section 4.3 above using a 2D inversion algorithm (AGI EarthImager 2D). Table 5-5 shows the inversion statistics for goodness of fit in each line at S-Complex. An explanation of the table parameters is discussed in detail within Section 4.3.3.

Table 5-5. Final Inversion Statistics for S-Complex.

Line #	Stage	Trial	Iterations	RMS	L_2
200WSC01	3	2	5	7.18	2.06
200WSC02	1	1	4	4.44	0.77
200WSC03	3	1	4	5.90	1.39
200WSC04	3	2	4	5.58	1.24
200WSC05	1	1	4	4.81	0.92
200WSC06	1	1	4	4.48	0.80

RMS = root-mean-square.

A site specific color scale was developed through a statistical analysis of the apparent resistivity values for all data collected within the S-Complex site. A histogram, shown in Figure 5-60, was used to generate a color gradient that is sensitive to the resistivity range.

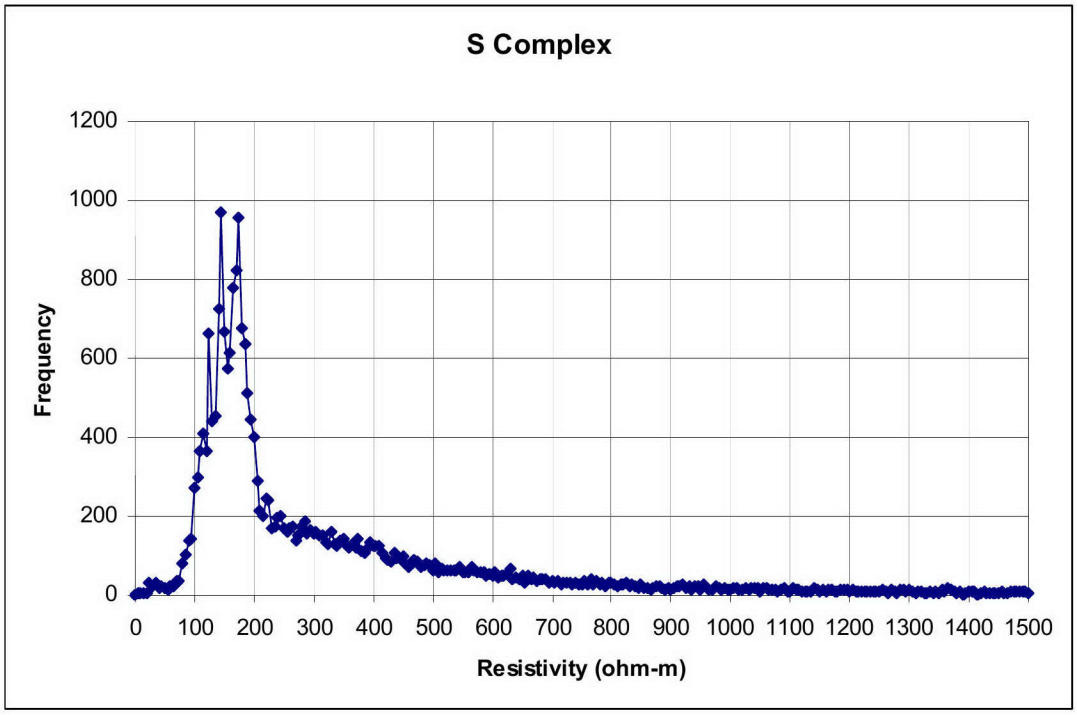

Figure 5-60. Histogram of apparent resistivity data for the Purex project site.

Interference from subsurface infrastructure dominates much of the near-surface data at S-Complex. All six lines cross at least two known pipelines. Overall, there is a decrease in resistivity with depth on each of the three profiles, suggesting an increase in moisture content that is associated with the water table. Depth to groundwater in the area has been recorded at approximately 73 m BGS.

Lines 200WSC01, 200WSC02, and 200WSC03 start in the south and are located under an above ground pipeline and over subsurface utility lines. Line 200WSC01 shows two highly conductive anomalies at approximately 150 m and 225 m along the line that are indicative of underground pipeline interference. An extension of a known pipeline parallels the resistivity line in close proximity. In addition, a steel cased monitoring well (2-E17-13) is located near station 45 m. The contouring process tends to smear or merge the conductive feature at-depth (water table) with the anomalies that are likely caused by pipelines. The resulting conductive feature is therefore larger than one would expect if the section were not complicated by modeling and infrastructure interference.

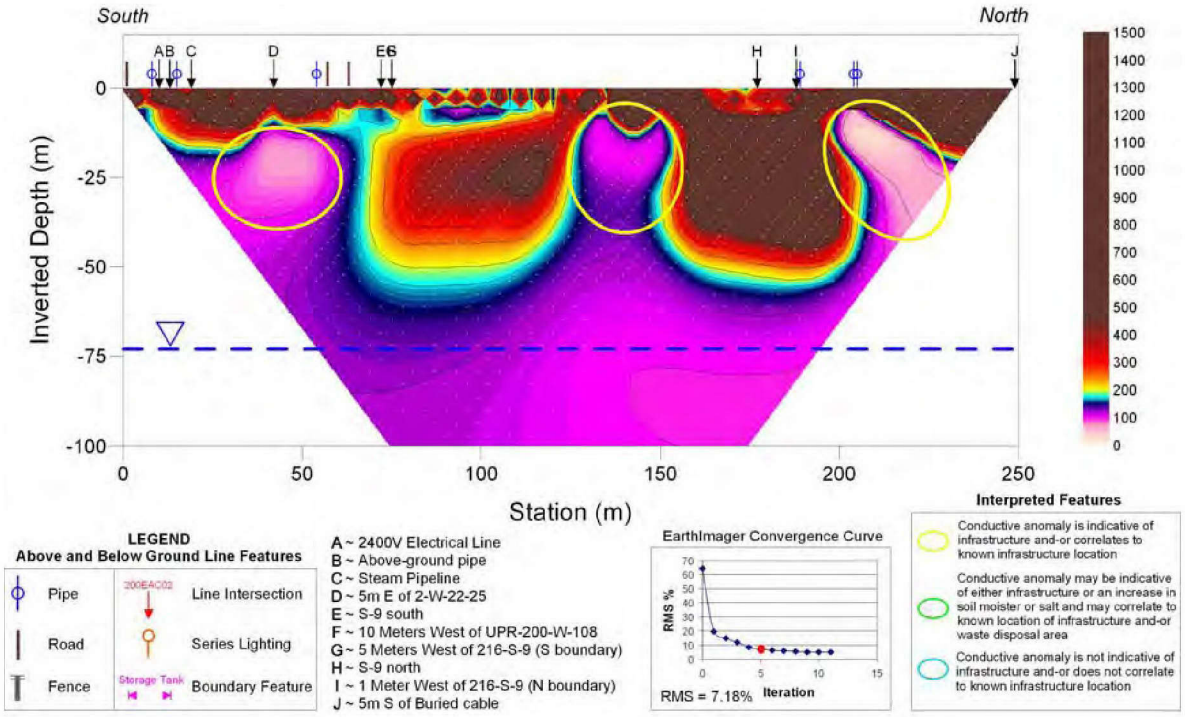

Figure 5-61. Inversion Results for S-Complex Line 200WSC01.

There is a distinct pipeline response on Line 200WSC02 and Line 200WSC03 at approximately 230 m along each line. The conductive anomaly on the southern end of each line is likely an effect from the pipeline. Line 200WSC03 shows a smaller conductive anomaly located at approximately 90 m along the line. This correlates with another steel cased monitoring well 299-W22-26.

All three resistivity lines centered over the 216-S-9 waste disposal trench show scattered pipeline related anomalies and the water table at depth. However, besides the conductive pipeline interference the area, above the water table (approximately 75 m), is dominated by a high resistivity (500 to 1500 Ohm-m) zone that shows no evidence of increased soil moisture or a change in soil chemistry due to the 216-S-9 waste disposal trench.

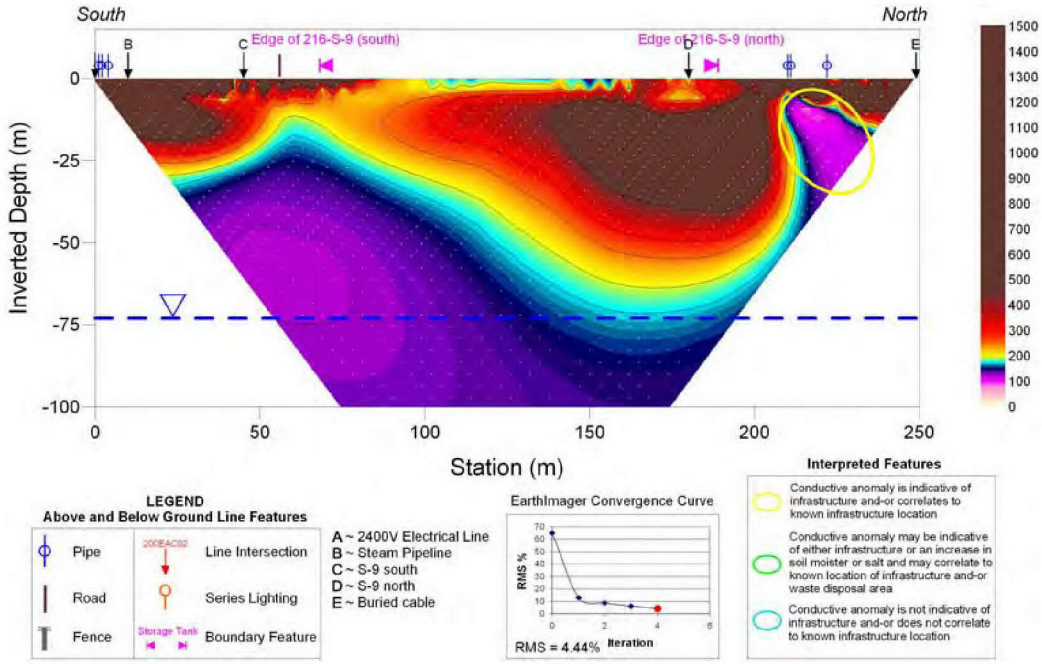

Figure 5-62. Inversion Results for S-Complex Line 200WSC02.

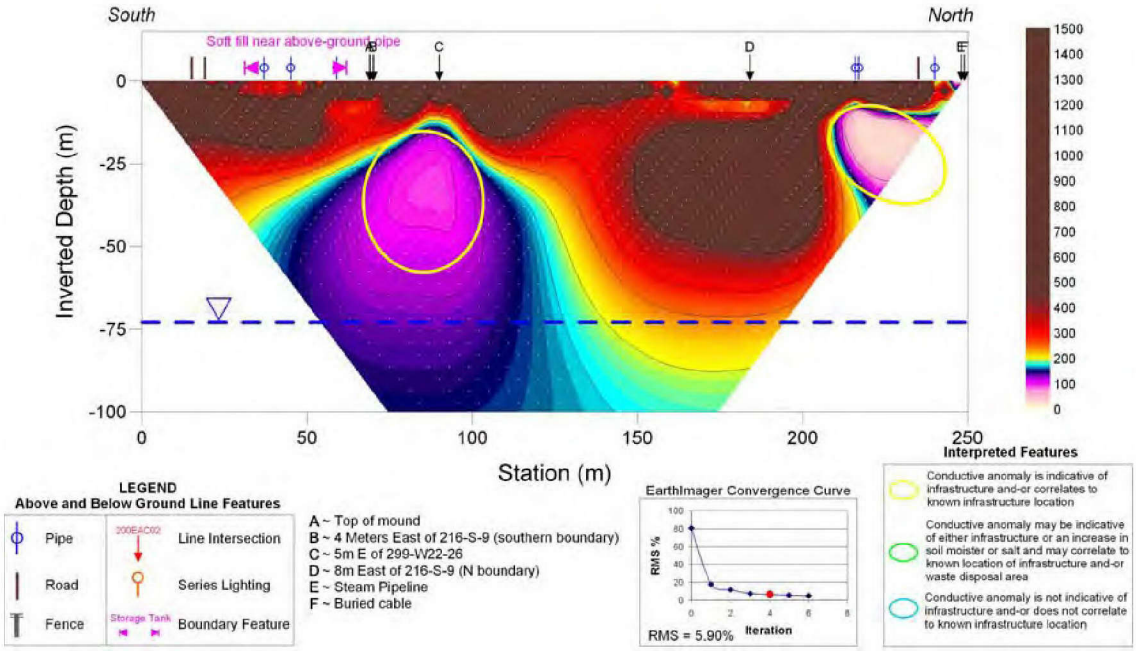

Figure 5-63. Inversion Results for S-Complex Line 200WSC03.

Lines 200WSC04 and 200WSC05 display a conductive anomaly associated with pipelines at approximately 150 m along the line. Line 200ESC06 shows a moderately conductive anomaly (approximately 150 to 200 Ohm-m) at a depth of approximately 15 to 25 meters. There is no evidence of pipeline interference at this location. The depth of the anomaly is likely to be distorted by the contouring process, which tends to smear or merge the conductive surface feature with the moderately conductive feature at depth that is likely caused by the water table. The relatively moderate conductivity and deep location makes it is difficult to determine if the large conductive anomaly is related to a pipeline or the disposal of 1.3 mGal of liquid waste at the 216-S-13 that contained high amounts of nitrate.

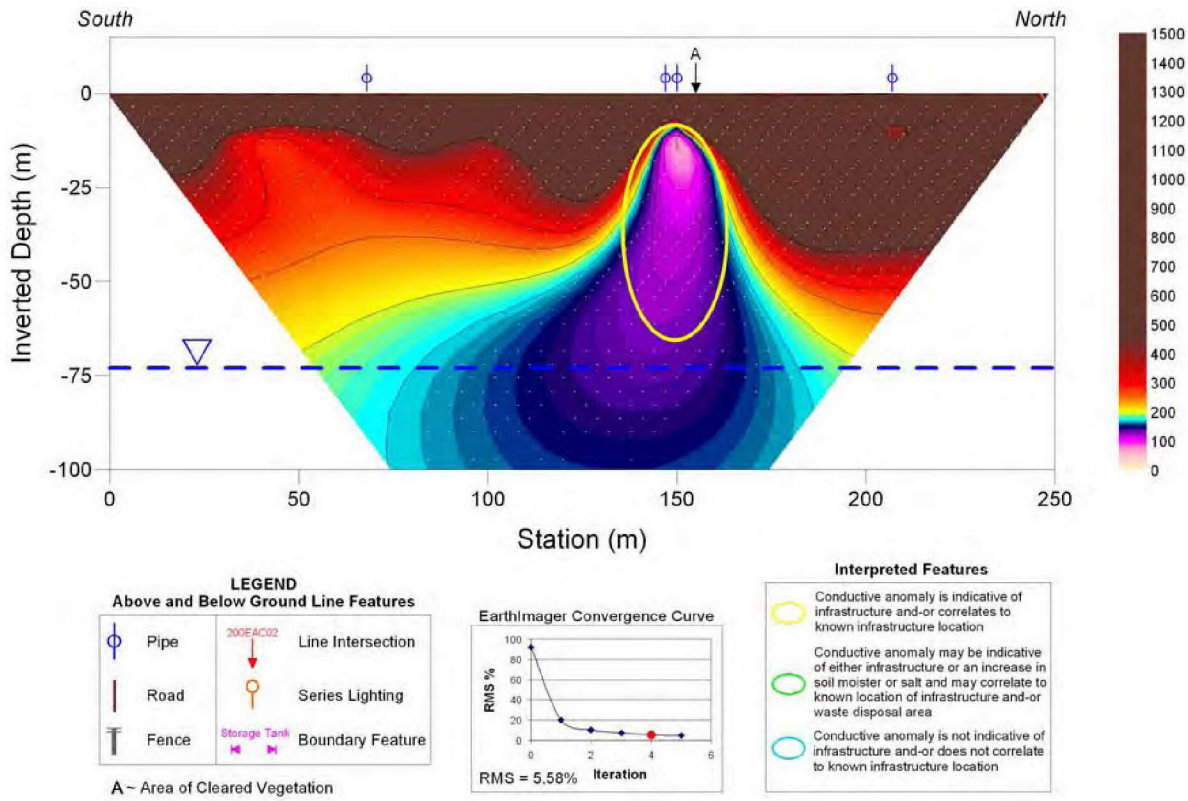

Figure 5-64. Inversion Results for S-Complex Line 200WSC04.

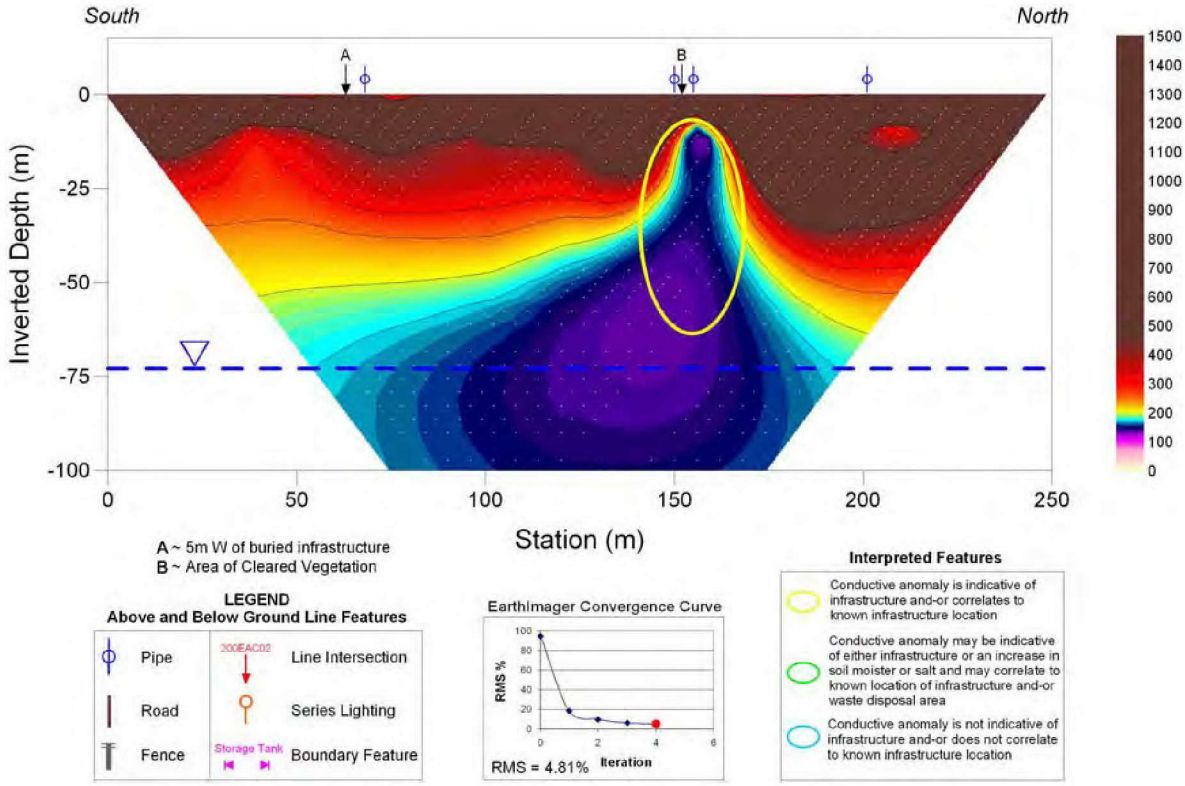

Figure 5-65. Inversion Results for S-Complex Line 200WSC05.

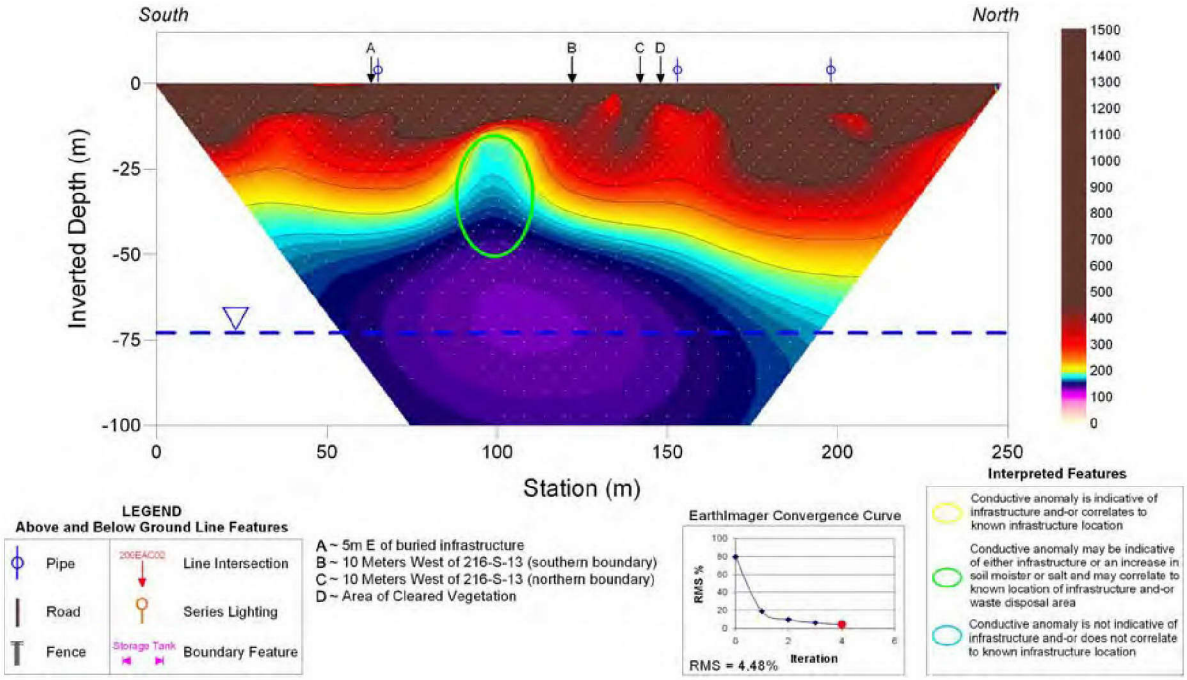

Figure 5-66. Inversion Results for S-Complex Line 200WSC06.

5.2.1.2 3D Rendering of 2D Inversion Results

For purposes of 3D visualization the site was divided into two sub-sites; S-Complex A which is comprised of the three resistivity lines acquired in the northern portion of the site (Figures 5-67 through 5-71), and S-Complex B which consists of the three resistivity lines completed in the southern portion of the site (Figures 5-72 through 5-76).

Both S-Complex A and B show an overall decreasing resistivity with depth as the slices approach the water table. The pipe features and steel cased wells mentioned in the above 2D section can be seen as resistive lows throughout the images. The features, as in the 2D image, increase laterally with depth. Eventually, with depth, the sections display a regional decrease in resistivity, associated with the increased moisture due to the water table.

Lines 200WSC01, 200EC102, and 200EC103 all display correlations with pipeline features and a relative increase in conductivity with depth. Interspersed between the pipeline features are relative high resistivity areas that represent background. Near-surface features are heavily dominated by infrastructure making accurate correlations with non-infrastructure related features difficult.

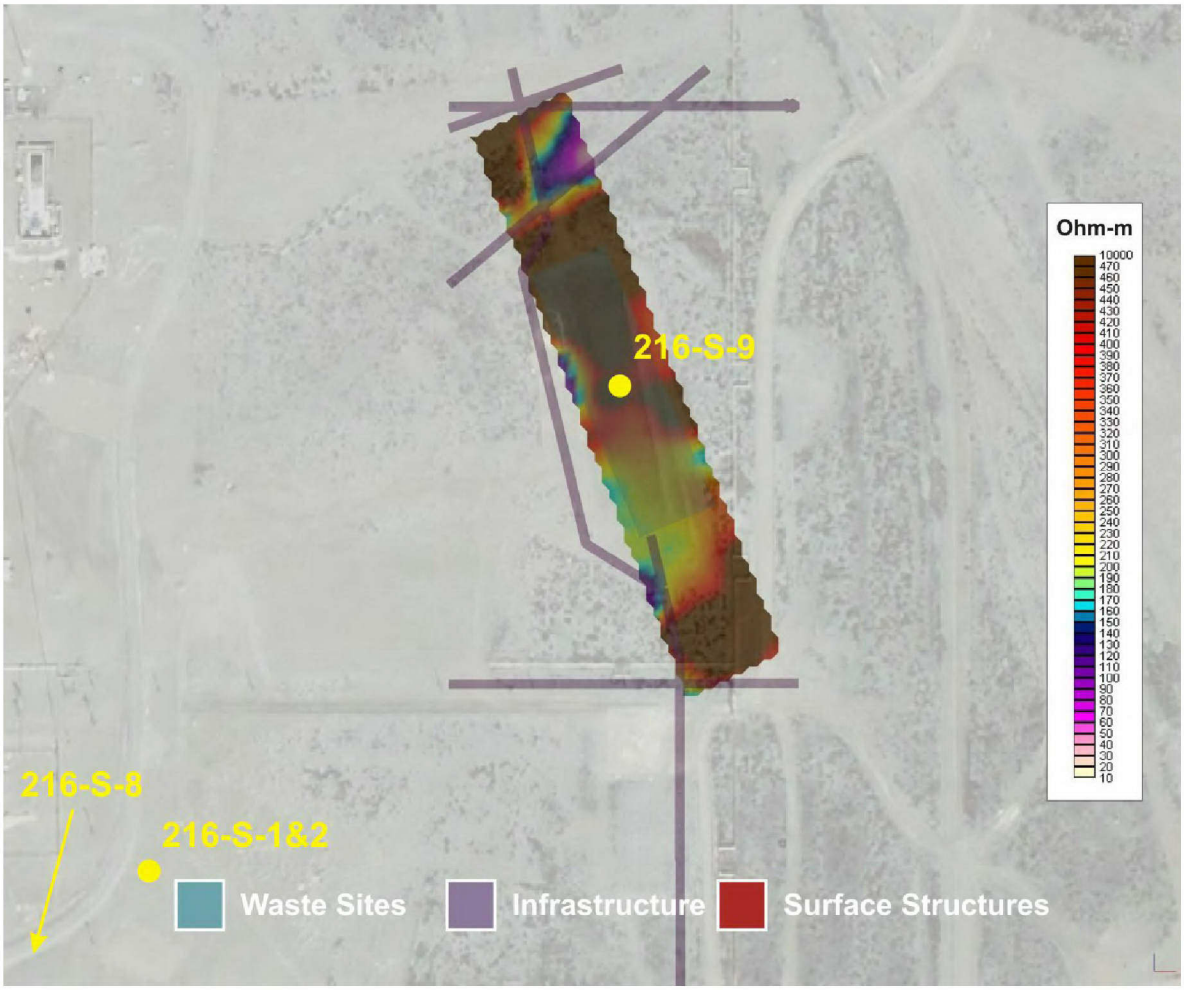

Figure 5-67. Results from the 3D Visualization for S-Complex A at a Depth of 15 m BGS.

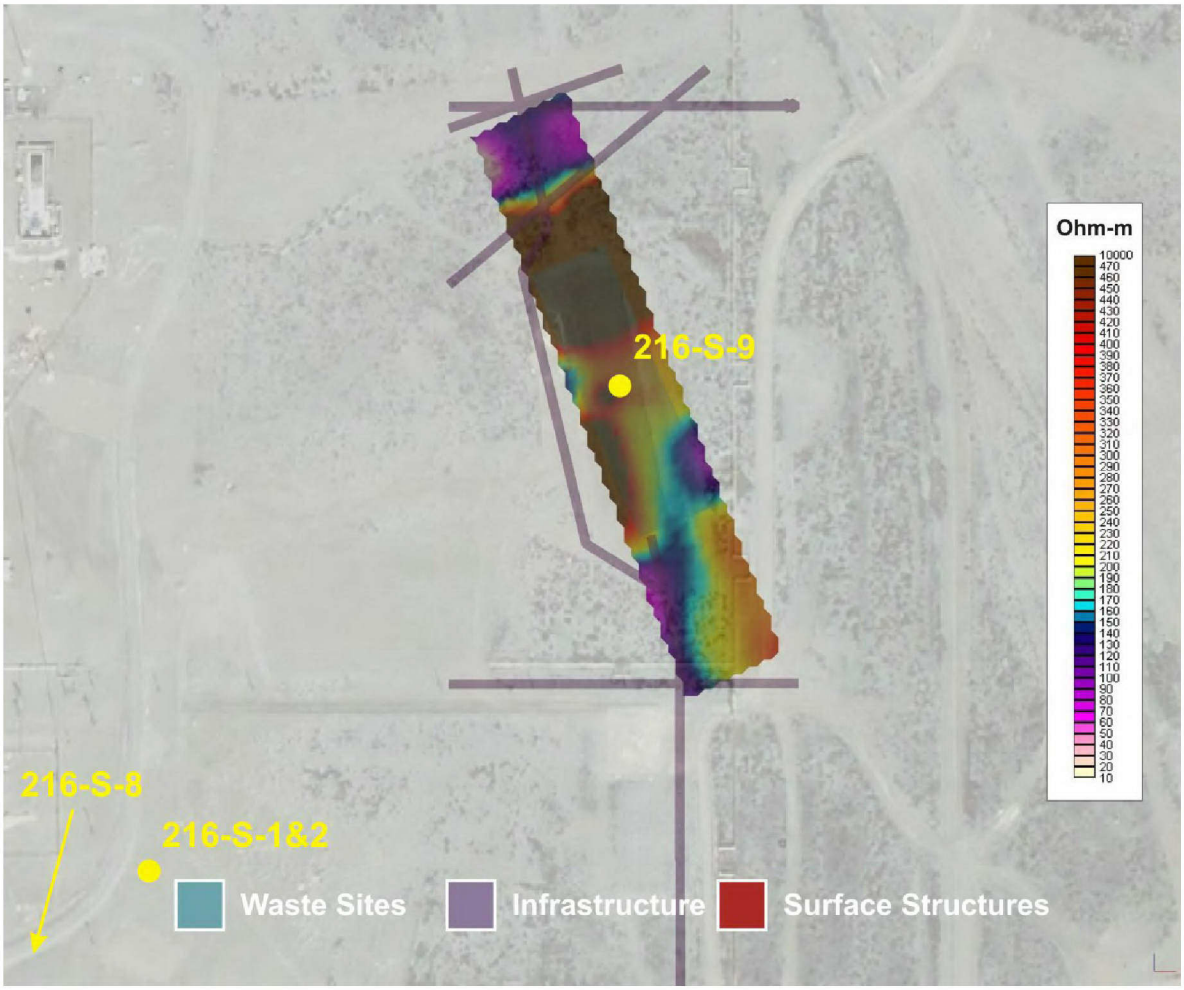

Figure 5-68. Results from the 3D Visualization for S-Complex A at a Depth of 30 m BGS.

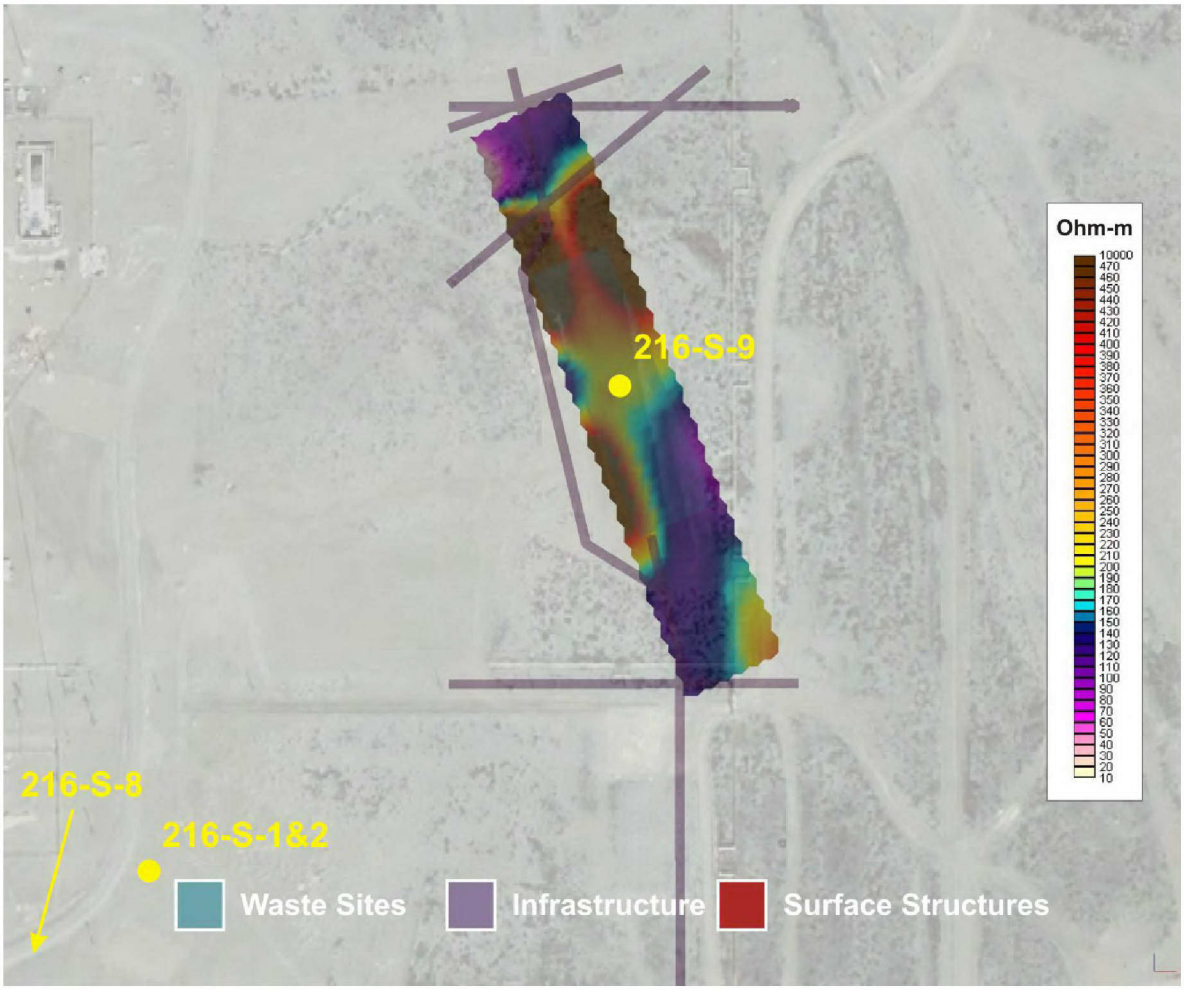

Figure 5-69. Results from the 3D Visualization for S-Complex A at a Depth of 45 m BGS.

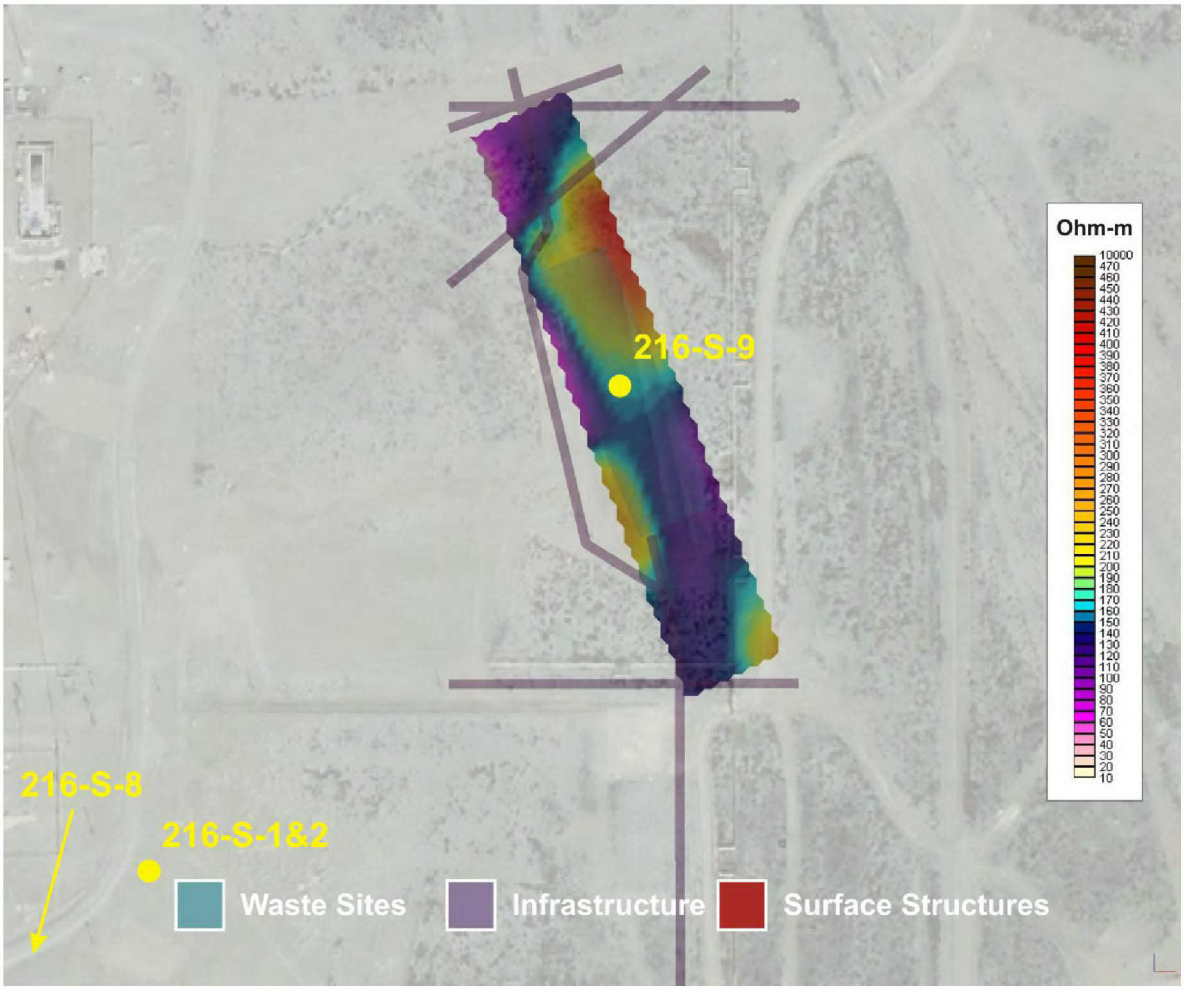

Figure 5-70. Results from the 3D Visualization for S-Complex A at a Depth of 60 m BGS.

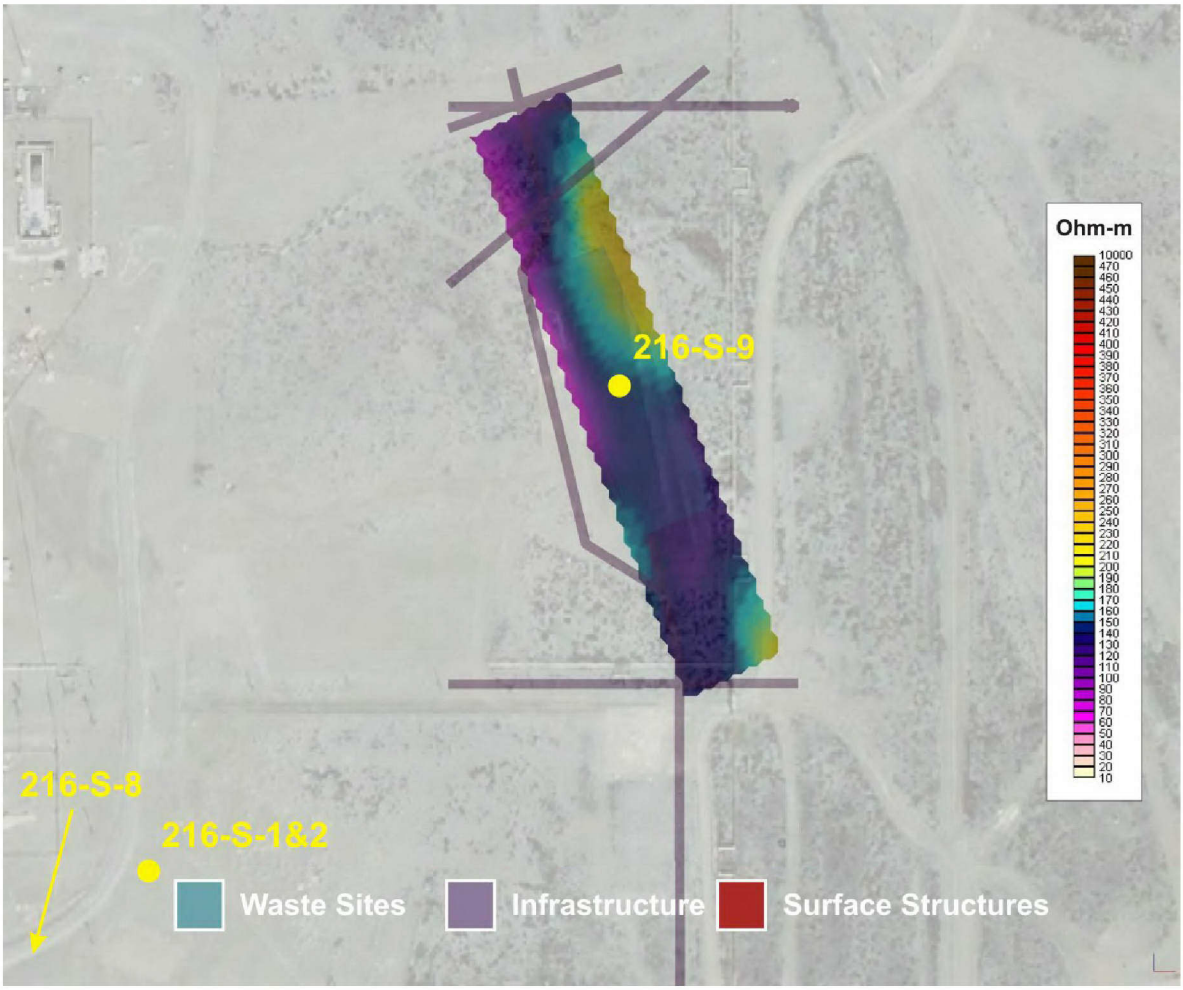

Figure 5-71. Results from the 3D Visualization for S-Complex A at a Depth of 75 m BGS.

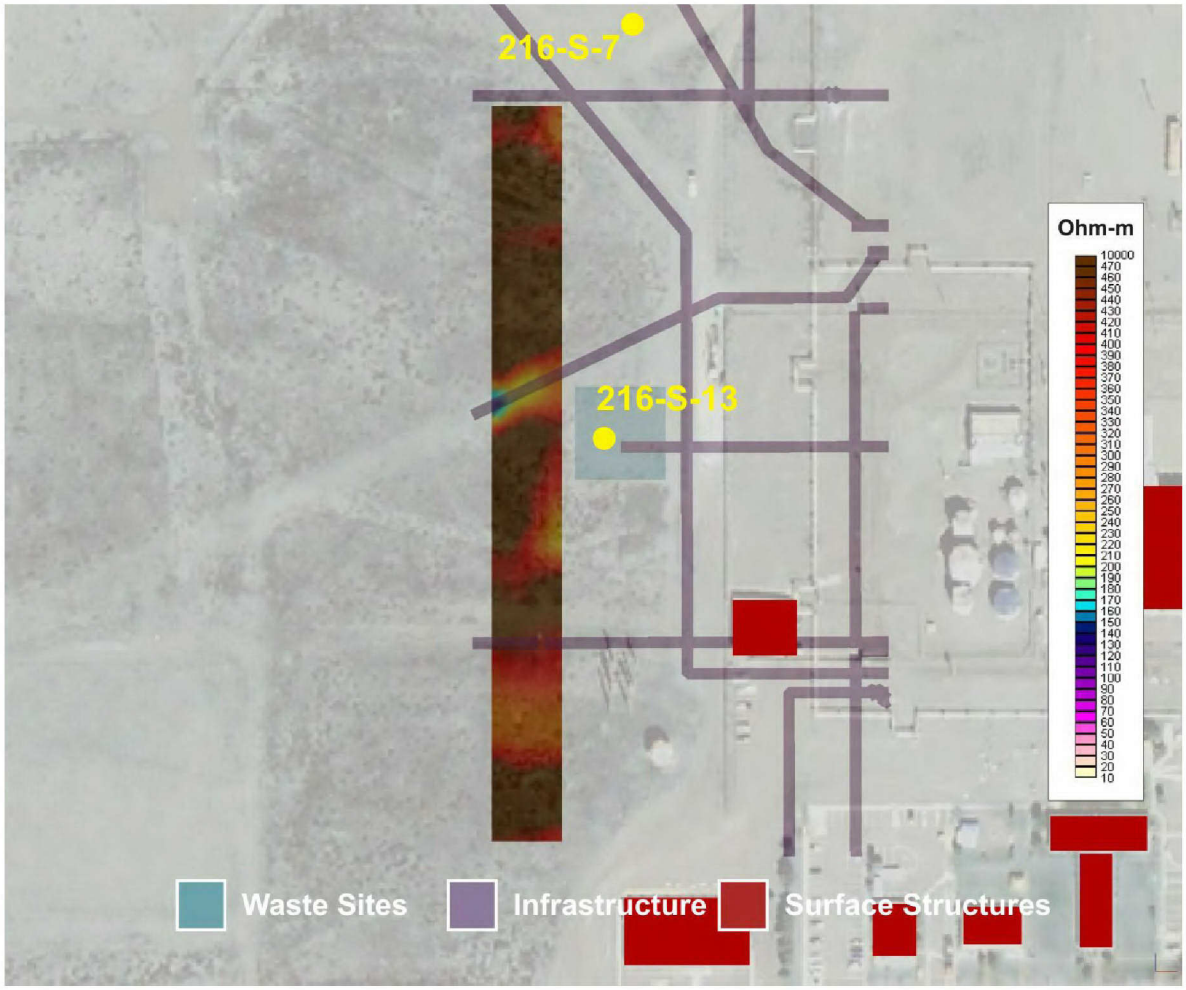

Figure 5-72. Results from the 3D Visualization for S-Complex B at a Depth of 15 m BGS.

The results of the 3D visualization images for the southern portion of the S-Complex site show conductive features that correlate with infrastructure. There is a conductive feature on the eastern edge that increases with depth that is in close proximity to the 216-S-13 disposal site. It is possible that the response is due to the increased soil moisture from the liquid waste. Additional survey coverage between line 200WSC06 and the 216-S-13 waste site is needed to further delineate the local contributions to the low resistivity anomaly.

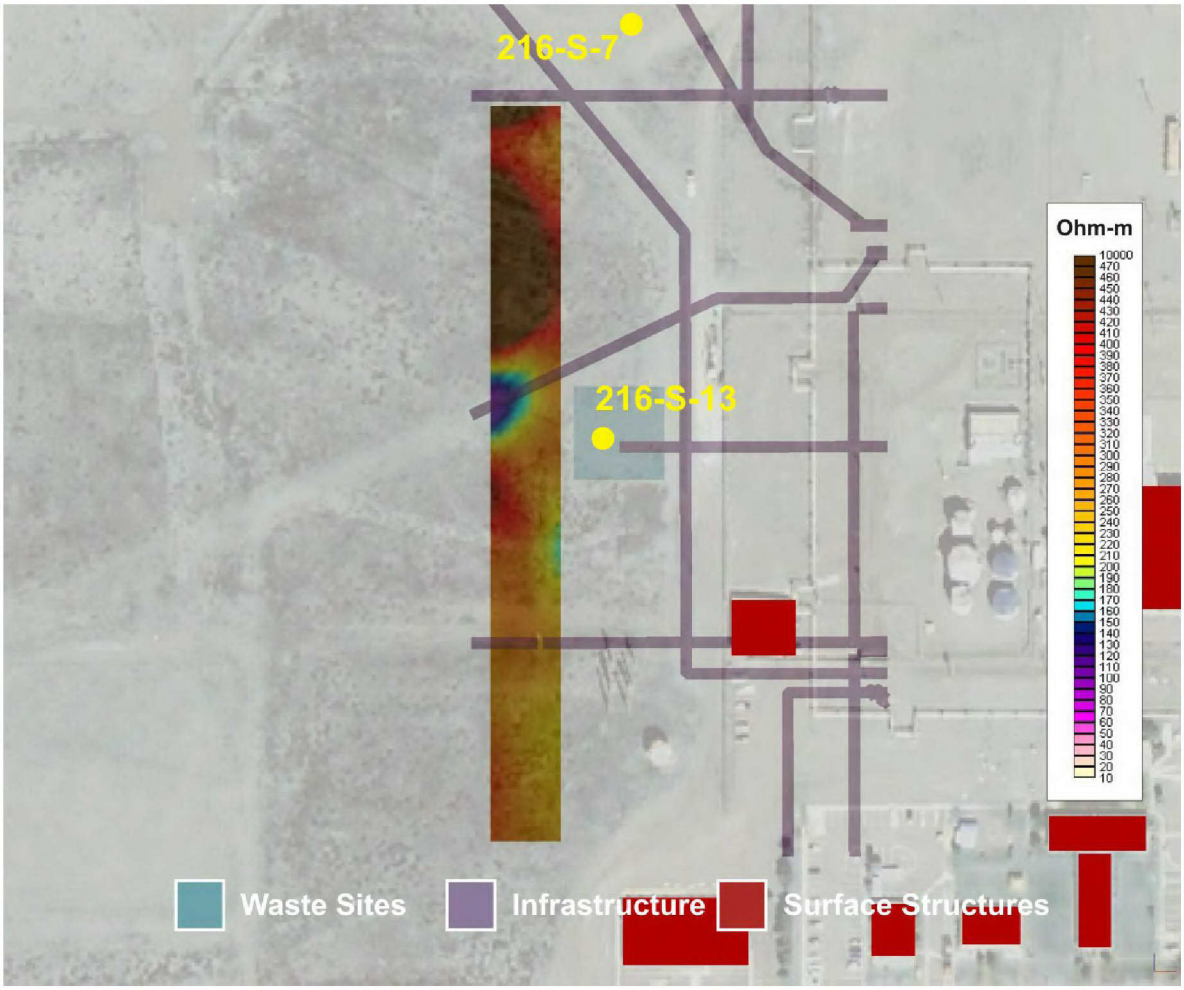

Figure 5-73. Results from the 3D Visualization for S-Complex B at a Depth of 30 m BGS.

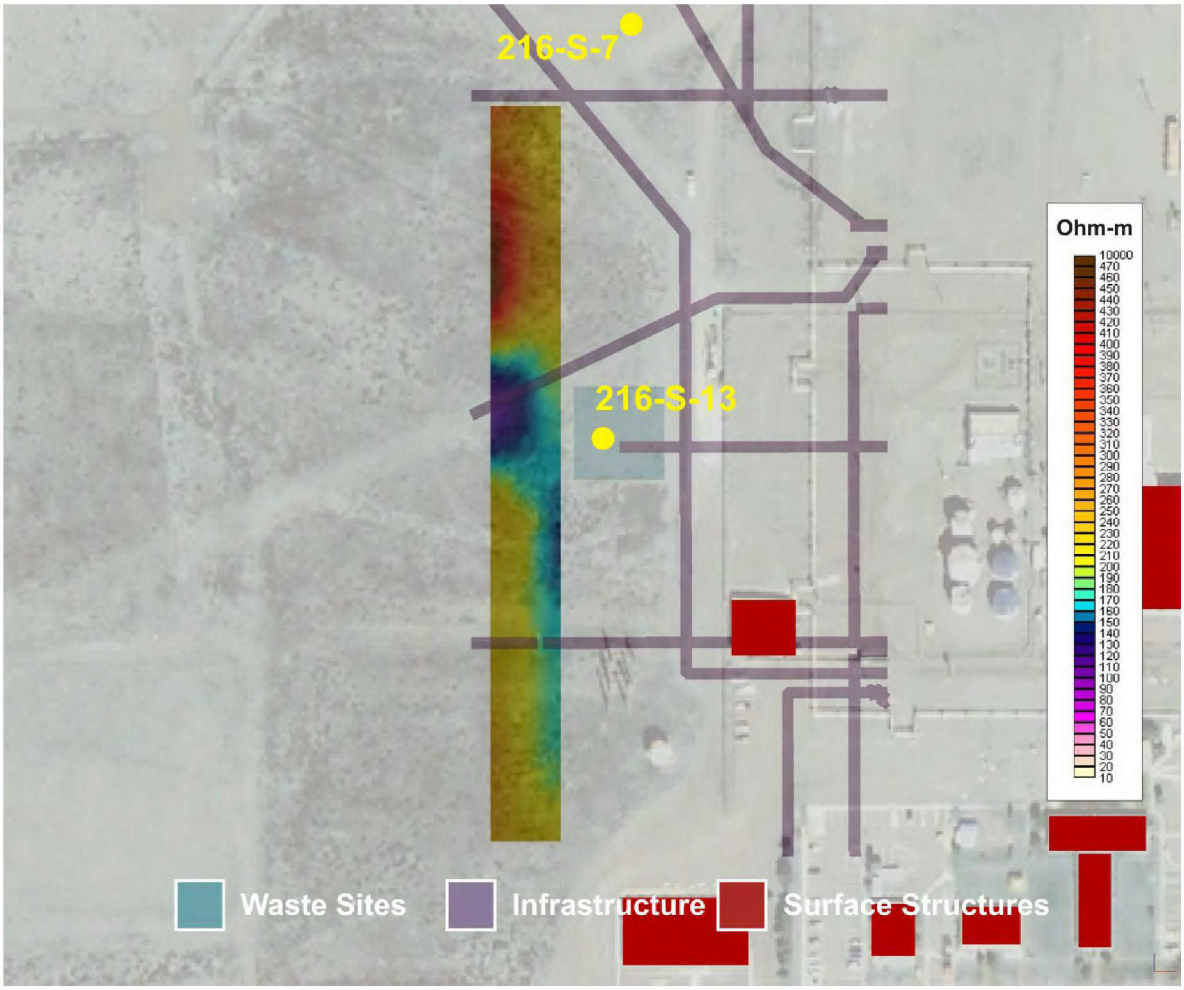

Figure 5-74. Results from the 3D Visualization for S-Complex B at a Depth of 45 m BGS.

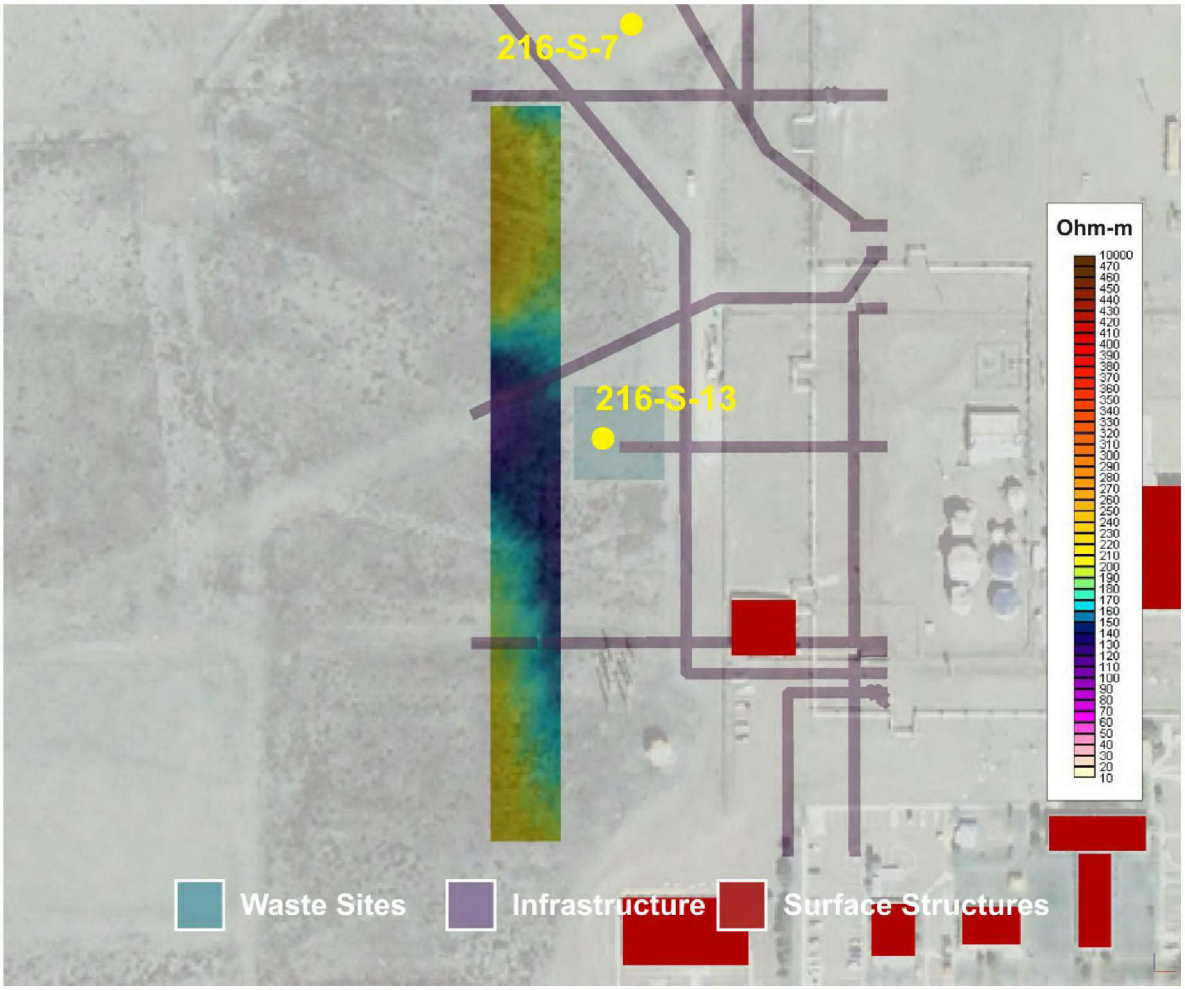

Figure 5-75. Results from the 3D Visualization for S-Complex B at a Depth of 60 m BGS.

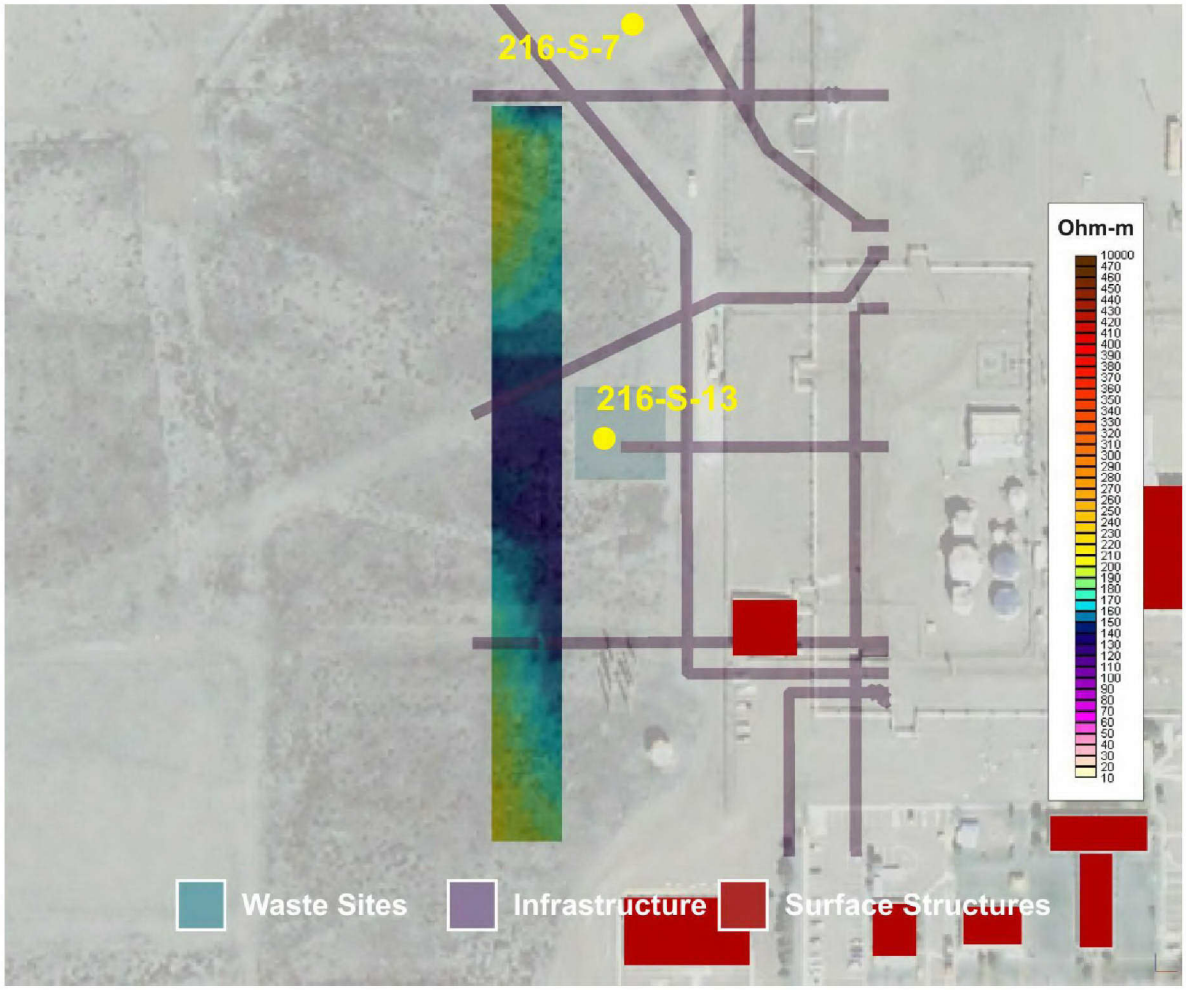

Figure 5-76. Results from the 3D Visualization for S-Complex B at a Depth of 75 m BGS.

5.2.2 T-Plant

5.2.2.1 2D Inversion Results

The 2D results of the resistivity survey performed at T-Plant can be viewed in Figures 5-78 through 5-97 below. Figures 5-78 through 5-87 display the results in a cross-sectional format, while Figures 5-88 through 5-97 display the results of a 3D visualization of the same data set. Presenting plan view "depth slices" from the 3D visualization provides a tool for correlating resistivity responses to infrastructure, changes in soil moisture, or changes in soil chemistry.

Ten resistivity lines were acquired at T-Plant; 200WTP01 (Figure 5-78), 200WTP02 (Figure 5-79), 200WTP03 (Figure 5-80), 200WTP04 (Figure 5-81), 200WTP05 (Figure 5-82), 200WTP06 (Figure 5-83), 200WTP07 (Figure 5-84), 200WTP08 (Figure 5-85), 200WTP09 (Figure 5-86), and 200WTP10 (Figure 5-87). The resistivity data was processed according to Section 4.3 above using a 2D inversion algorithm (AGI EarthImager 2D). Table 5-6 shows the

inversion statistics for goodness of fit in each line at B-Plant. An explanation of the table parameters is discussed in detail within Section 4.3.3.

Table 5-6. Final Inversion Statistics for T-Plant.

Line #	Stage	Trial	Iterations	RMS	L_2
200WTP01	1	1	3	3.05	0.37
200WTP02	1	1	3	3.04	0.37
200WTP03	1	1	3	3.93	0.62
200WTP04	3	2	5	7.70	2.37
200WTP05	3	2	6	8.96	3.21
200WTP06	3	3	5	6.59	1.74
200WTP07	1	1	3	4.60	0.85
200WTP08	1	1	4	4.96	0.98
200WTP09	3	2	5	7.61	2.32
200WTP10	1	1	3	4.74	0.90

RMS = root-mean-square.

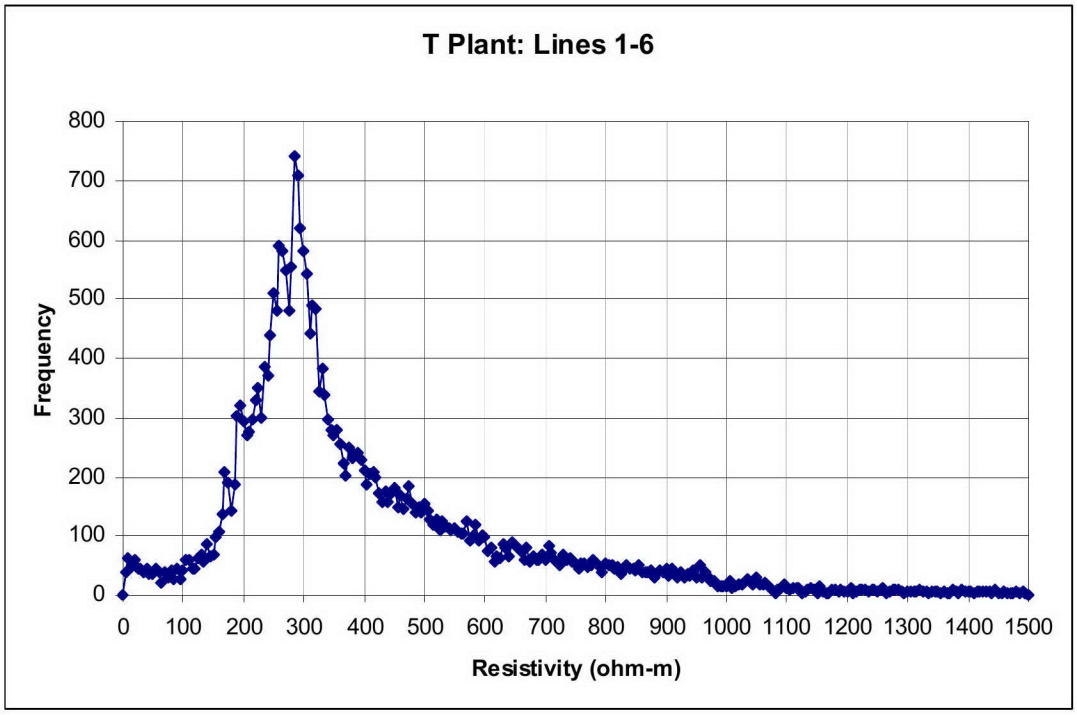

Figure 5-77. Histogram of apparent resistivity data for the T-Plant project site.

A site specific color scale was developed through a statistical analysis of the apparent resistivity values for all data collected within the T-Plant site with the exception of lines 200ETP07 to 200ETP10, which would distort results, based on the abundance of infrastructure within these lines. A histogram, shown in Figure 5-77, was used to generate a color gradient that is sensitive to the resistivity range

Interference from subsurface infrastructure dominates much of the near-surface resistivity data at 216-T-6 trench near T-Plant. The southern portions of the lines near 216-T-34 and 216-T-35 trenches show an overall decrease in resistivity with depth on each of the profiles, suggesting an increase in moisture content associated with the water table. Depth to groundwater in the area has been recorded at approximately 82 m BGS.

Lines 200WTP01, 200WTP02, and 200WTP03 were centered over the 216-T-35 waste site. All three lines show a small near-surface decrease in resistivity in the upper 30 m of the section, between station 40 and 100 m along the line. This correlates with the southern border of the waste site and is likely indicative of an increase in soil moisture or a change in soil chemistry. The southern portions of the lines show relatively high resistivity values falling within the observed range of background geology. The northern sections of lines 200WTP01 and 200WTP03, from station 150 to 200 meters, show a low resistivity near-surface that appears to merge with the water table at-depth. A pipeline interference is visible near station 200 m along line 200WTP03. It is unlikely, however, that the near-surface low resistivity anomaly is in physical contact with the water table and more likely an artifact of the contouring process that

tends to smear and merge separate conductive features. Line 200WTP02 shows a conductive near surface at the same location (station 150 to 220 meters) as the deeper anomaly along liens 200WTP01 and 200WTP03. It is possible that the proximity of the line to the center of the disposal trench has interference effects, but the anomaly is likely to be continuous with the neighboring lines. Line 200WTP02 shows a distinct pipeline interference conductive anomaly at station 220 meters that appears to extend to the water table. The vertical extension is an artifact of the inversion and contouring process and is likely pulling the water table conductive anomaly higher than is reasonable. Line 200WPT03 shows a small vertical conductive anomaly located at station 110 meters. The size and magnitude of the anomaly is indicative of infrastructure, but there is no evidence of infrastructure in the vicinity. The conductive anomaly associated with the water table along line 200WTP03 is significantly higher in elevation than it should be and appears to be the result of superposition of the near surface conductive anomalies with the conductive feature at depth.

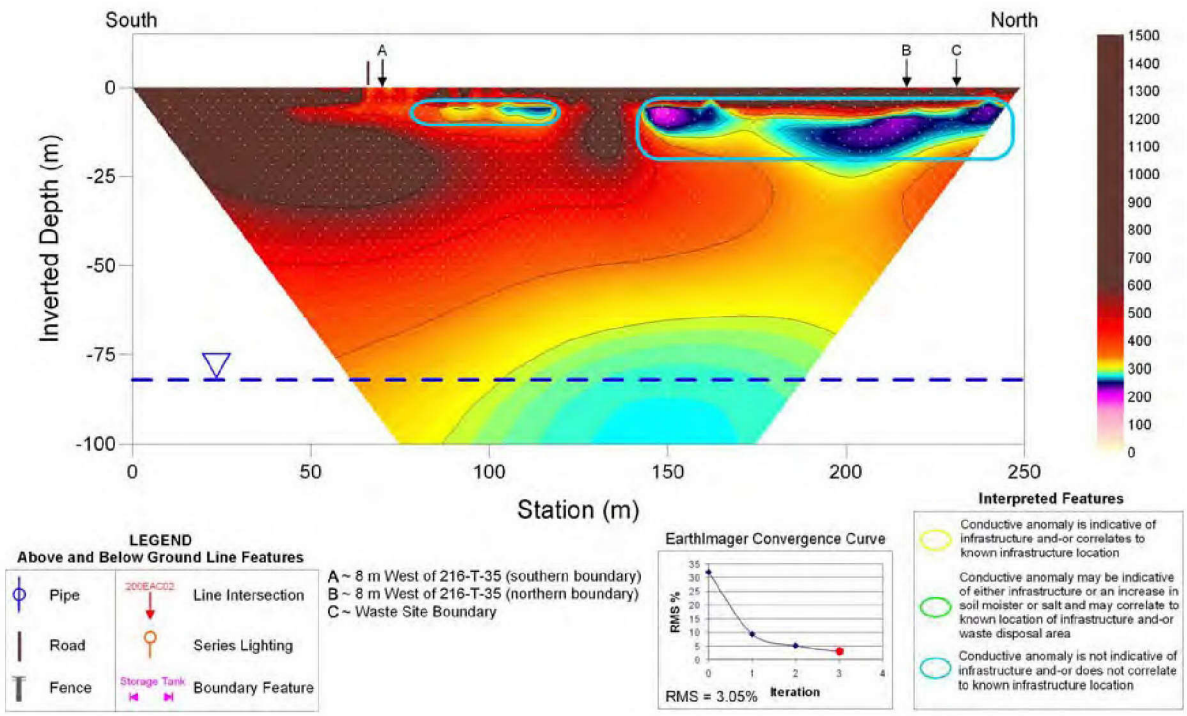

Figure 5-78. Inversion Results for T-Plant Line 200WTP01.

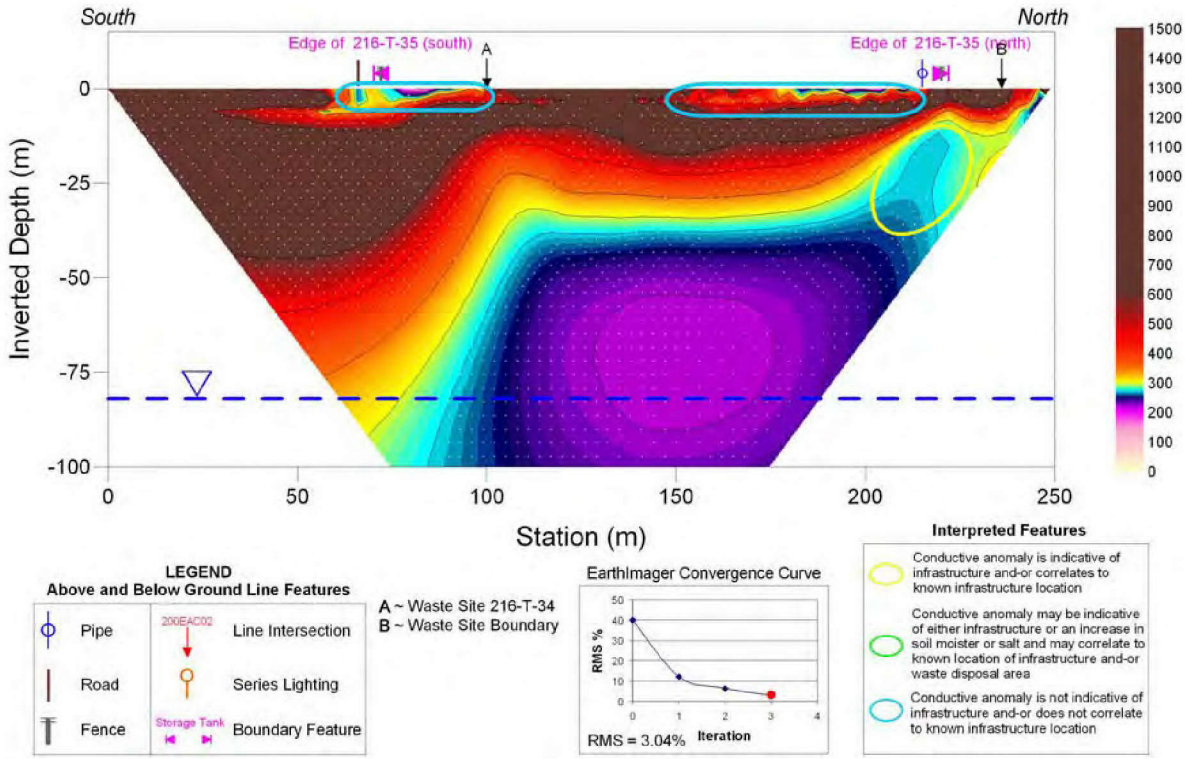

Figure 5-79. Inversion Results for T-Plant Line 200WTP02.

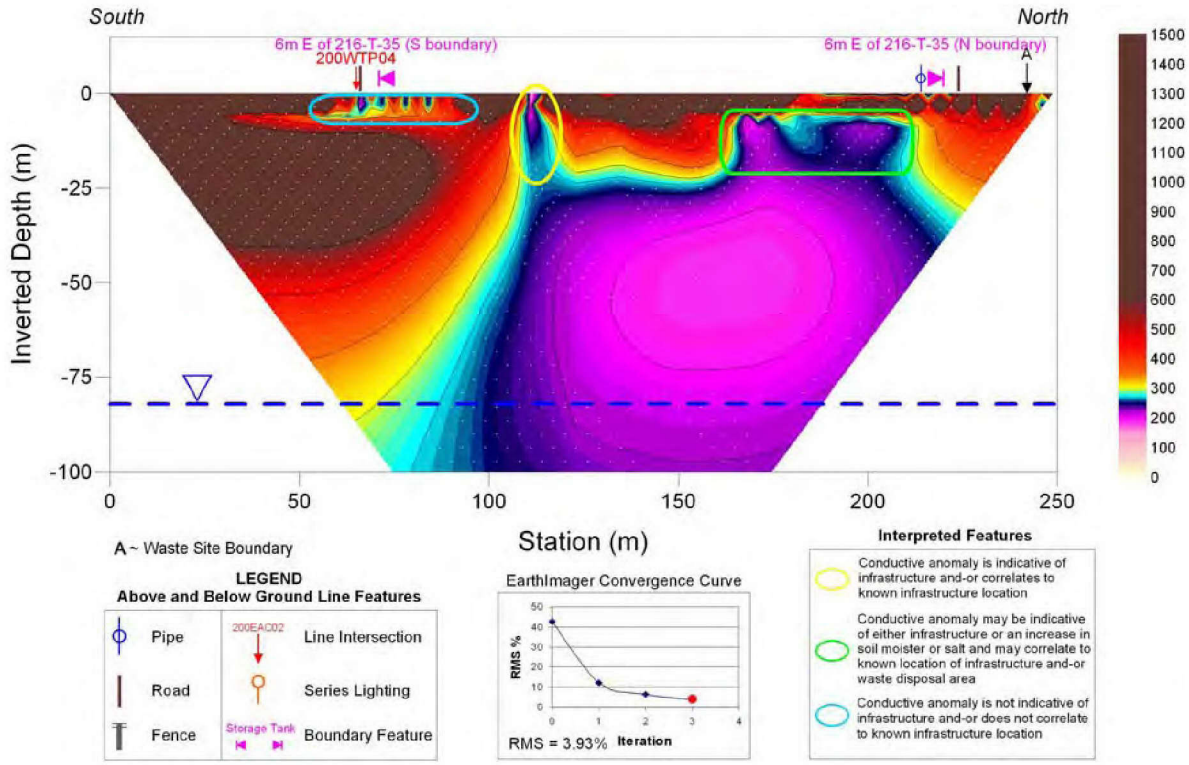

Figure 5-80. Inversion Results for T-Plant Line 200WTP03.

Lines 200WTP04, 200WTP05, and 200WTP06 are directly adjacent and to the east of the first three lines and are centered over the 216-T-34 waste site. The northern sections of the three lines from station 130 m onward is dominated by a highly conductive anomaly resulting from the railroad and pipelines. The northern area is not suitable for data interpretation even under 3D inversion. However, the southern portion of the lines combined with data collected over 216-T-35 trench and a few orthogonal lines could be incorporated into a larger 3D inversion study.

Lines 200WTP04 and 200WTP05 exhibit a subsurface linear conductive feature at approximately 100 m along the line. This correlates spatially with the start of the waste area, but is more characteristic of the pipeline responses seen in this study. However, review of local pipeline locations, shows no evidence of infrastructure at this location. The resistivity magnitude correlation between the lines is challenging because the resistivity value changes from approximately 50 Ohm-m on line 200WTP04 to approximately 300 Ohm-m on line 200WTP05. However, the response magnitude on line 200WTP04 is too great to be associated with an increase in soil moisture alone. Additional survey lines south of the railway area set perpendicular to the three lines might allow additional characterization. The water table and the associated decrease in resistivity values is present on all three lines but is distorted due to surface infrastructure response. Where infrastructure disturbances are not present, resistivity values are

greater between 600 and 1500 Ohm-m, indicative of background, which would suggest little evidence of moisture increase associated with waste disposal.

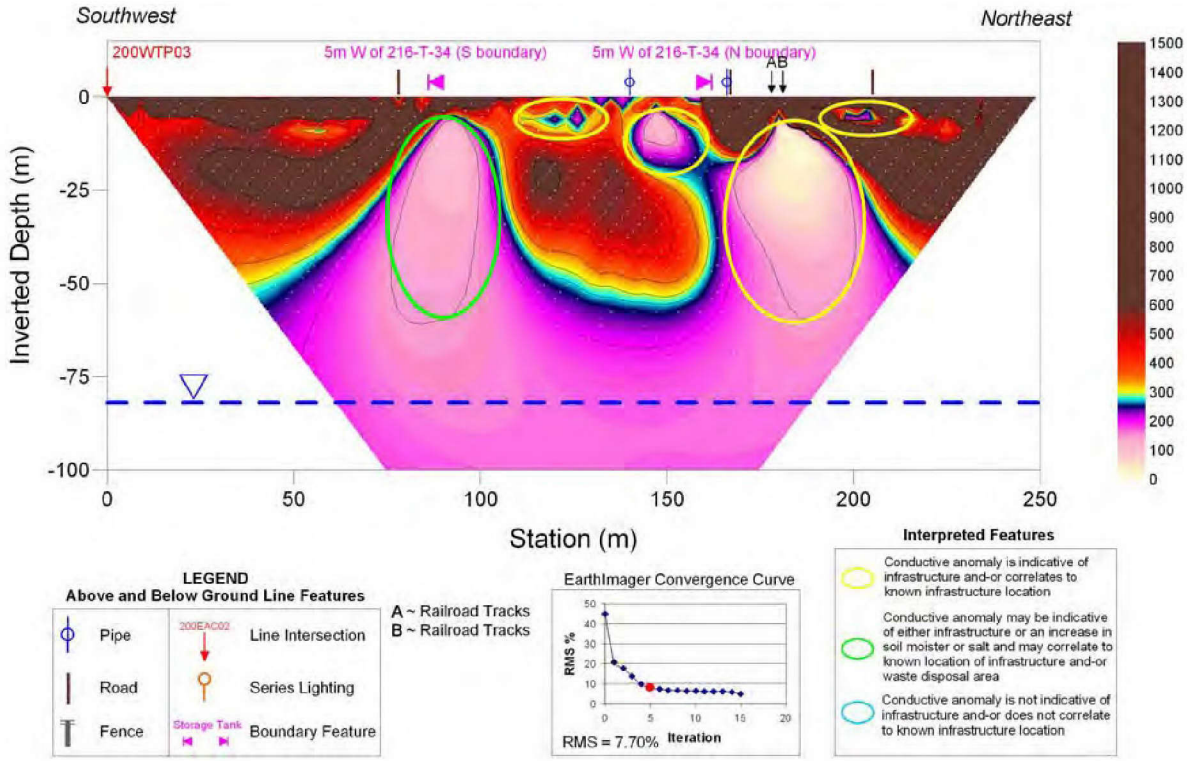

Figure 5-81. Inversion Results for T-Plant Line 200WTP04.

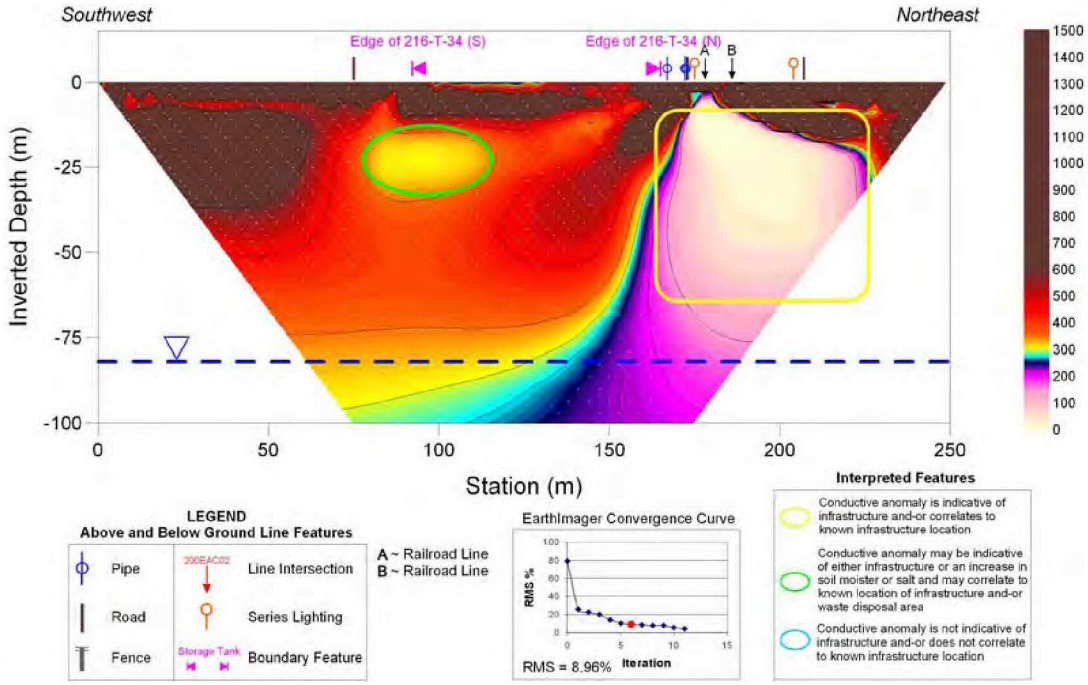

Figure 5-82. Inversion Results for T-Plant Line 200WTP05.

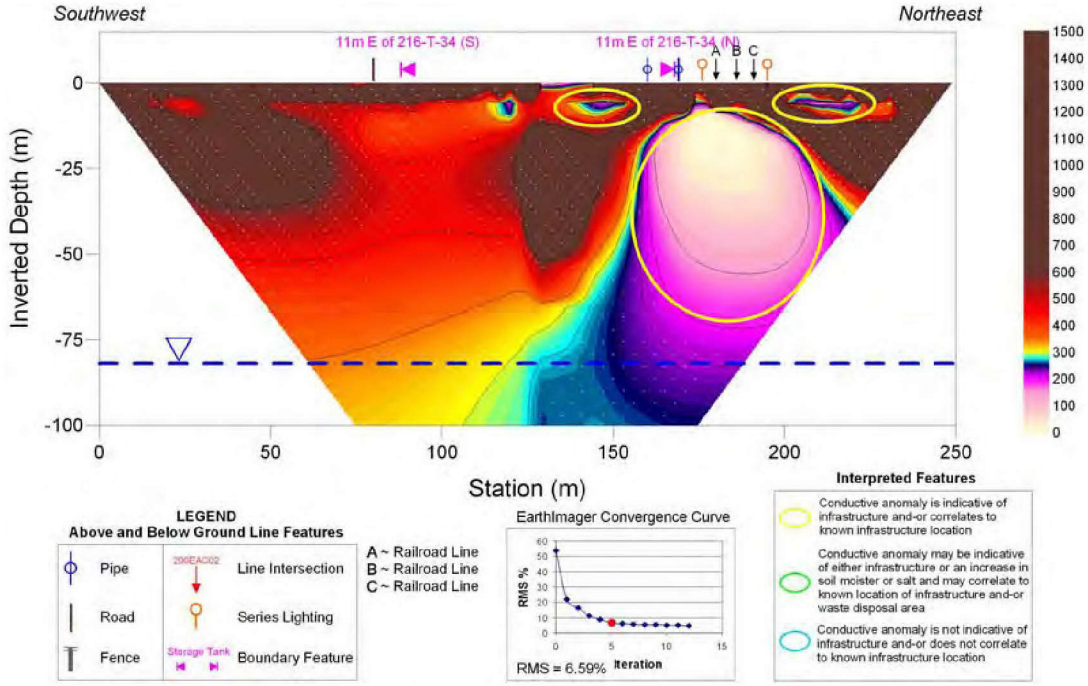

Figure 5-83. Inversion Results for T-Plant Line 200WTP06.

Lines 200WTP07, 200WTP08, 200WTP09, and 200WTP10 were acquired in the southern portion of the T-Plant site centered over the 216-T-6 waste site. The results of line 200WTP07 are relatively free of infrastructure responses despite the close proximity to several pipes and structures. As with the majority of the results collected within this study there is a consistent increase in conductivity with depth as a result of proximity to groundwater. The conductivity feature approximately 175 m along the line is correlates spatially with liquid waste disposal from 216-T-3. However, there is a near surface conductive feature at station 175 m on line 200WTP08 that is indicative of pipeline interference. The proximity to the water table and the associated low resistivity response tends to smear or merge the near surface and deeper conductive zones resulting in a disproportionately large area. Therefore, it is not possible to conclude whether the anomaly is due to liquid waste disposal or a pipeline interference. Line 200WTP07, 2000WTP08 and 200WTP09 all show a conductive linear feature at approximately 20 m along the line that corresponds with the railroad.

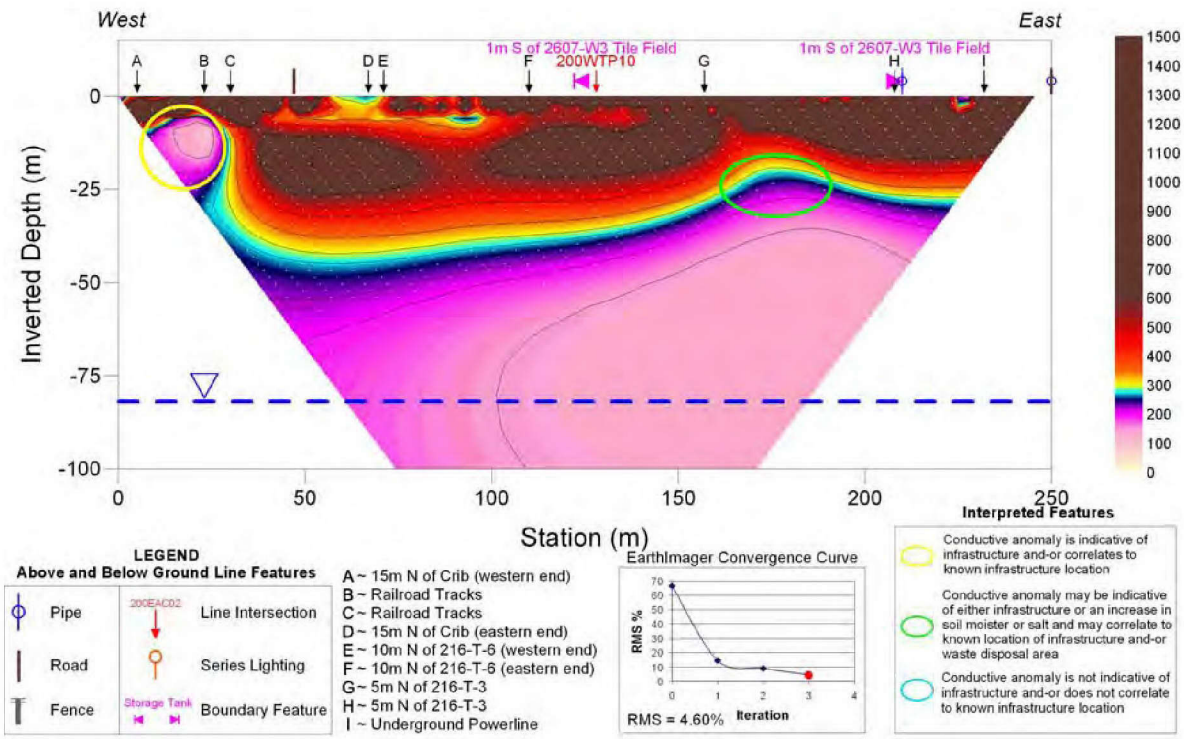

Figure 5-84. Inversion Results for T-Plant Line 200WTP07.

Line 200WTP08 displays another conductive anomaly at 100 m. The feature correlates to infrastructure or exhibit features indicative of infrastructure. The conductive feature at station 175 m on line 200ETP07 is also visible on line 200WTP08 despite the infrastructure distortions. The area beneath the 216-T-6 waste site is relatively resistive in comparison to the area beneath

the neighboring 216-T-3 waste site. The resistive zone shows little evidence of increased in soil moisture due to waste disposal at the 216-T-6 waste disposal site. Line 200WTP09 was completed directly over and parallel to a conductive pipeline. This provides a preferential current flow pathway making the data unsuitable for interpretation. There appears to be some correlation to line 200WTP08, but the extreme conductive feature due to the pipeline dominates.

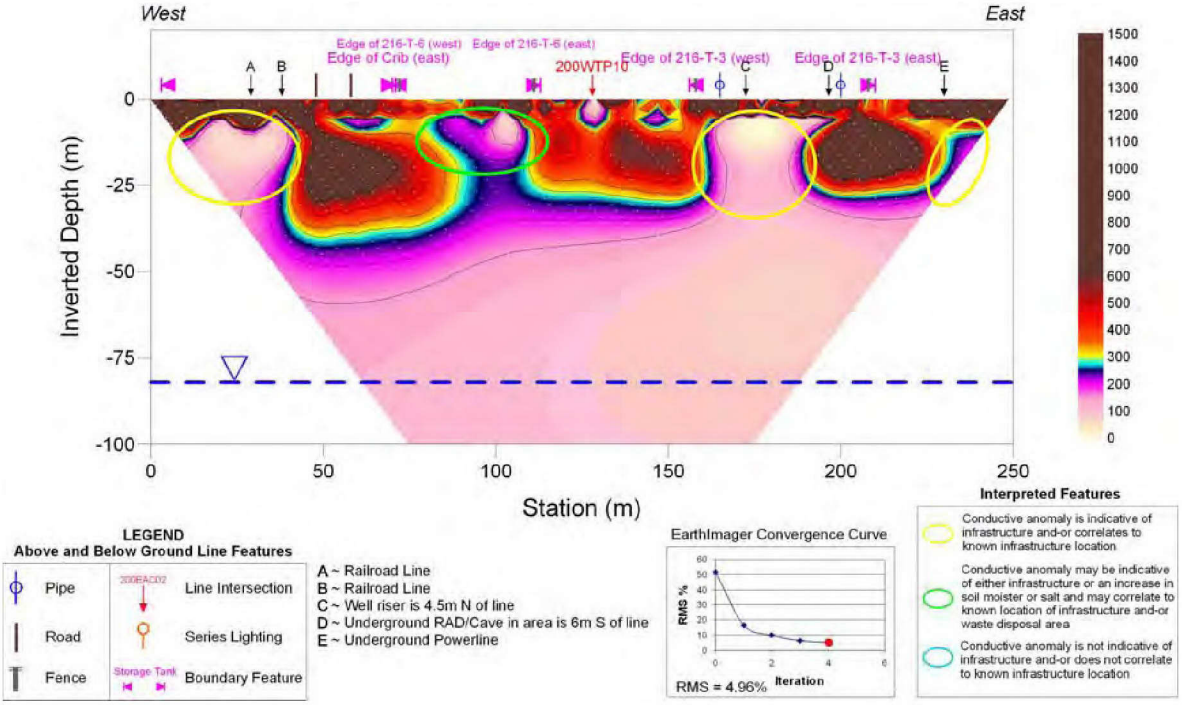

Figure 5-85. Inversion Results for T-Plant Line 200WTP08.

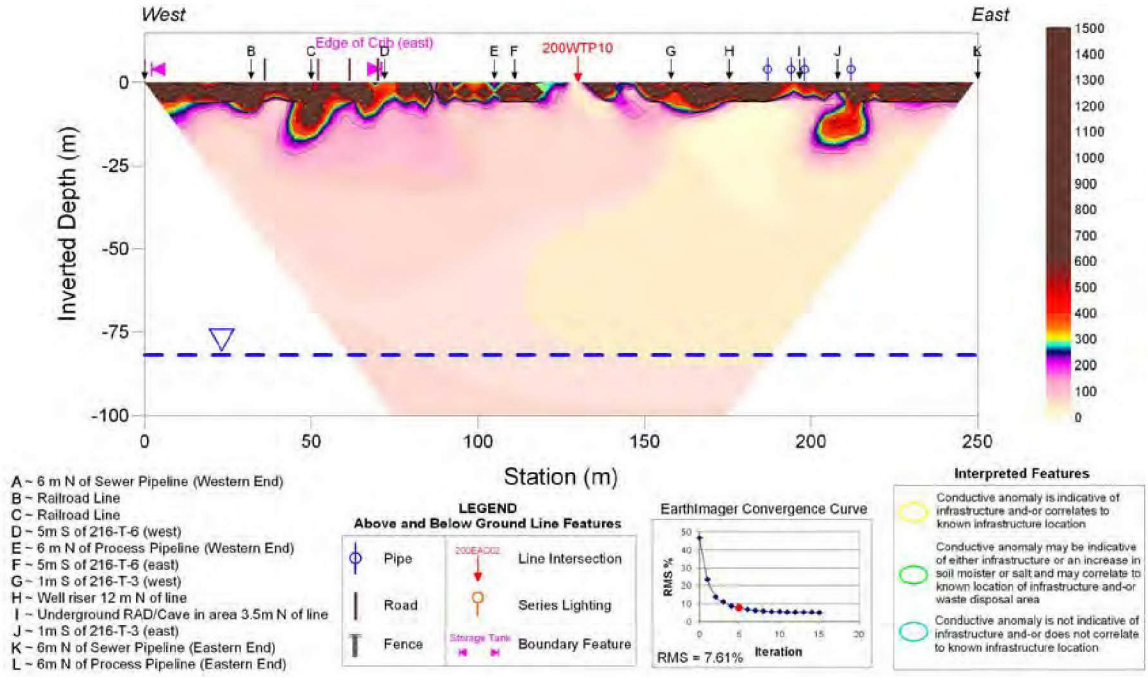

Figure 5-86. Inversion Results for T-Plant Line 200WTP09.

Line 200WTP10 shows minimal interference from infrastructure with the exception of the pipeline response at the start of the line. Note the location of line 200WTP09 which is directly over the conductive feature. The remainder of the line is relatively free of anomalies displaying the previously mentioned increase in conductivity with depth and moisture content. The intersection of line 200WTP10 with lines 200WTP07 and 200WTP08 suggests that the conductive anomaly seen in approximately 175 m along the line is an off-line 3D effect from a nearby target to the south. There is a near surface conductive anomaly from station 200 to 250 meters that correlates with the perimeter fence of a lay-down yard. The resulting anomaly is likely caused by the conductive metallic fence line.

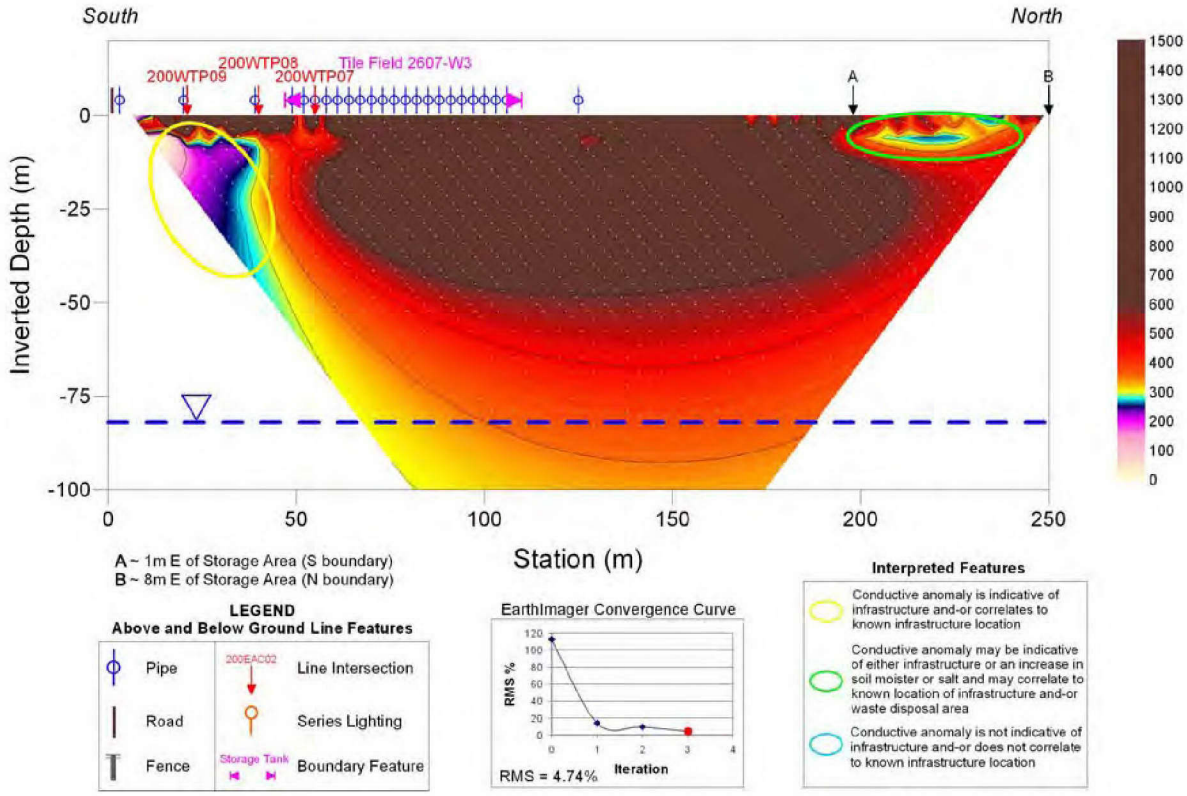

Figure 5-87. Inversion Results for T-Plant Line 200WTP10.

5.2.2.2 3D Rendering of 2D Inversion Results

For purposes of 3D visualization, the site was divided into two sub-sites (i.e., T-Plant A and T-Plant B). T-Plant A is comprised of the six-resistivity lines acquired in the northern portion of the site (Figures 5-88 through 5-92). T-Plant B consists of the three of the four resistivity lines completed in the southern portion of the site (Figures 5-93 through 5-97). Line 200WTP10 was omitted, as it is not conducive to 3D visualization.

Both T-Plant A and B show an overall decreasing resistivity with depth as the slices approach the water table. The pipe features mentioned in the above 2D section can be seen as resistive lows throughout the images. The features, as in the 2D image, increase laterally with depth.

T-Plant A shows an increase in conductivity near the 216-T-35 waste. This suggests an increase in moisture content relative to the surrounding background material. This is best displayed in Figures 5-89 and 5-90 at-depths 30 and 45 m, respectively. Anomalies observed over the 216-T-34 waste site are indicative of conductive infrastructure and do not appear to be associated with increased moisture content or a change in soil chemistry.

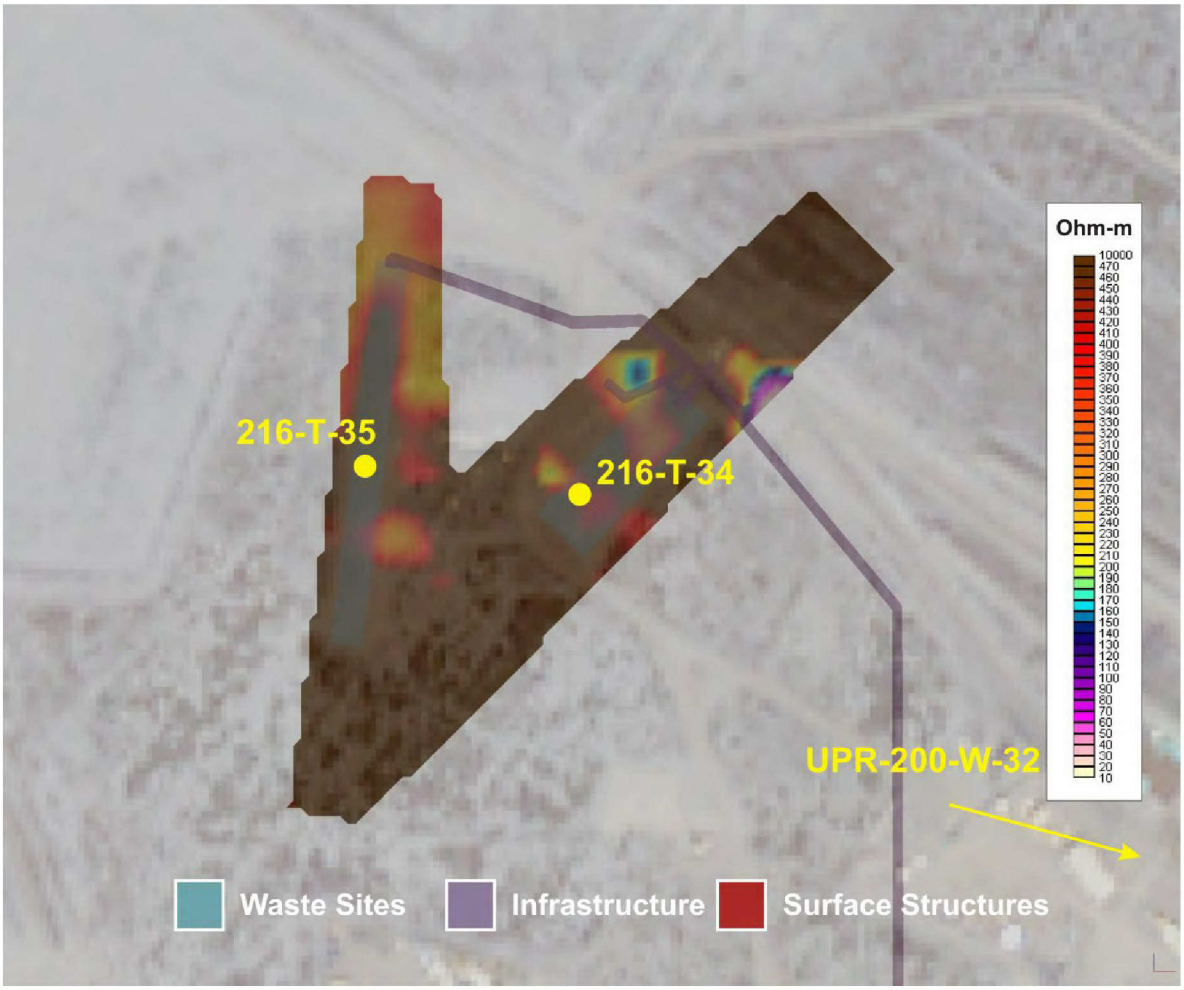

Figure 5-88. Results from the 3D Visualization for T-Plant A at a Depth of 15 m BGS.

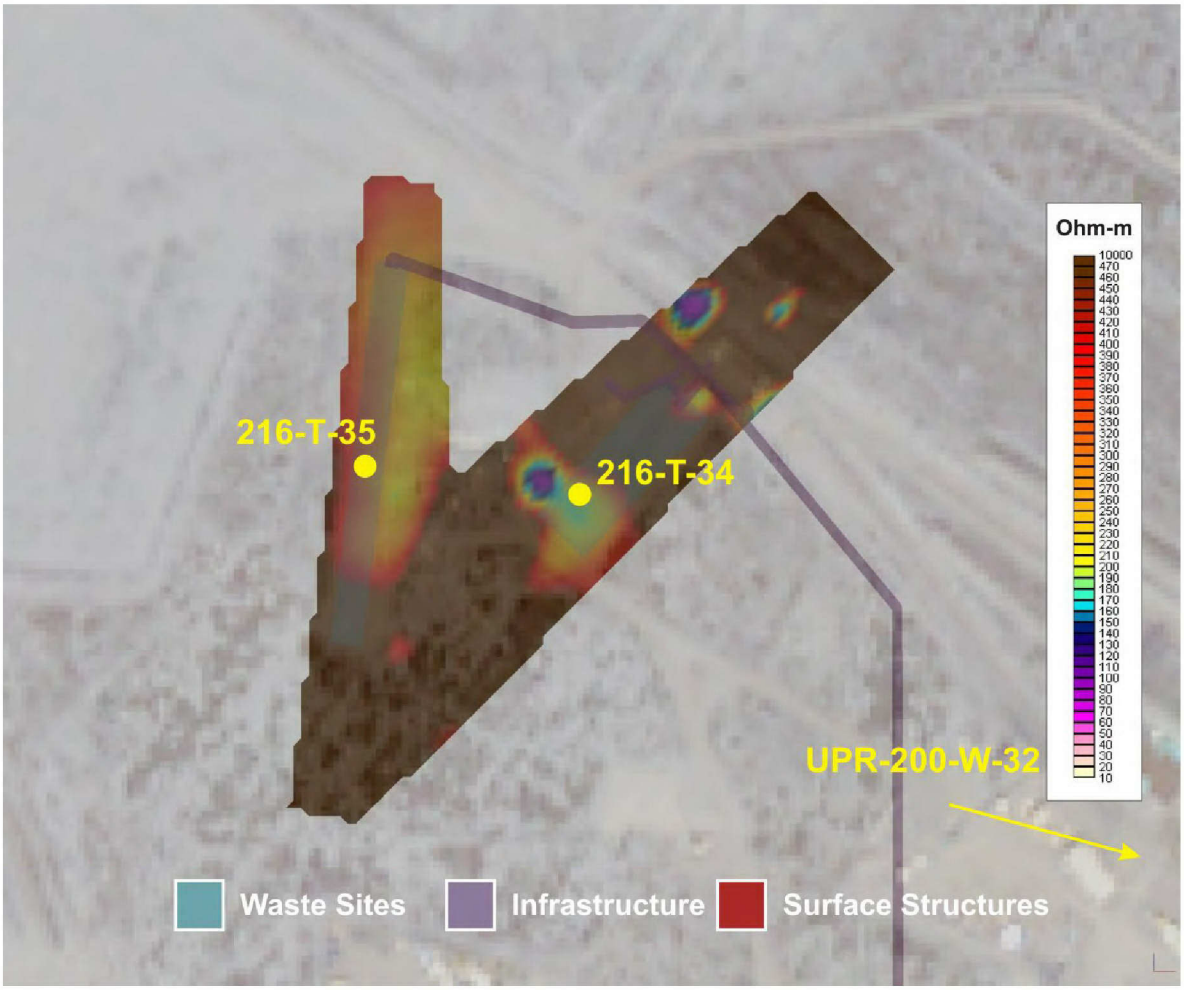

Figure 5-89. Results from the 3D Visualization for T-Plant A at a Depth of 30 m BGS.

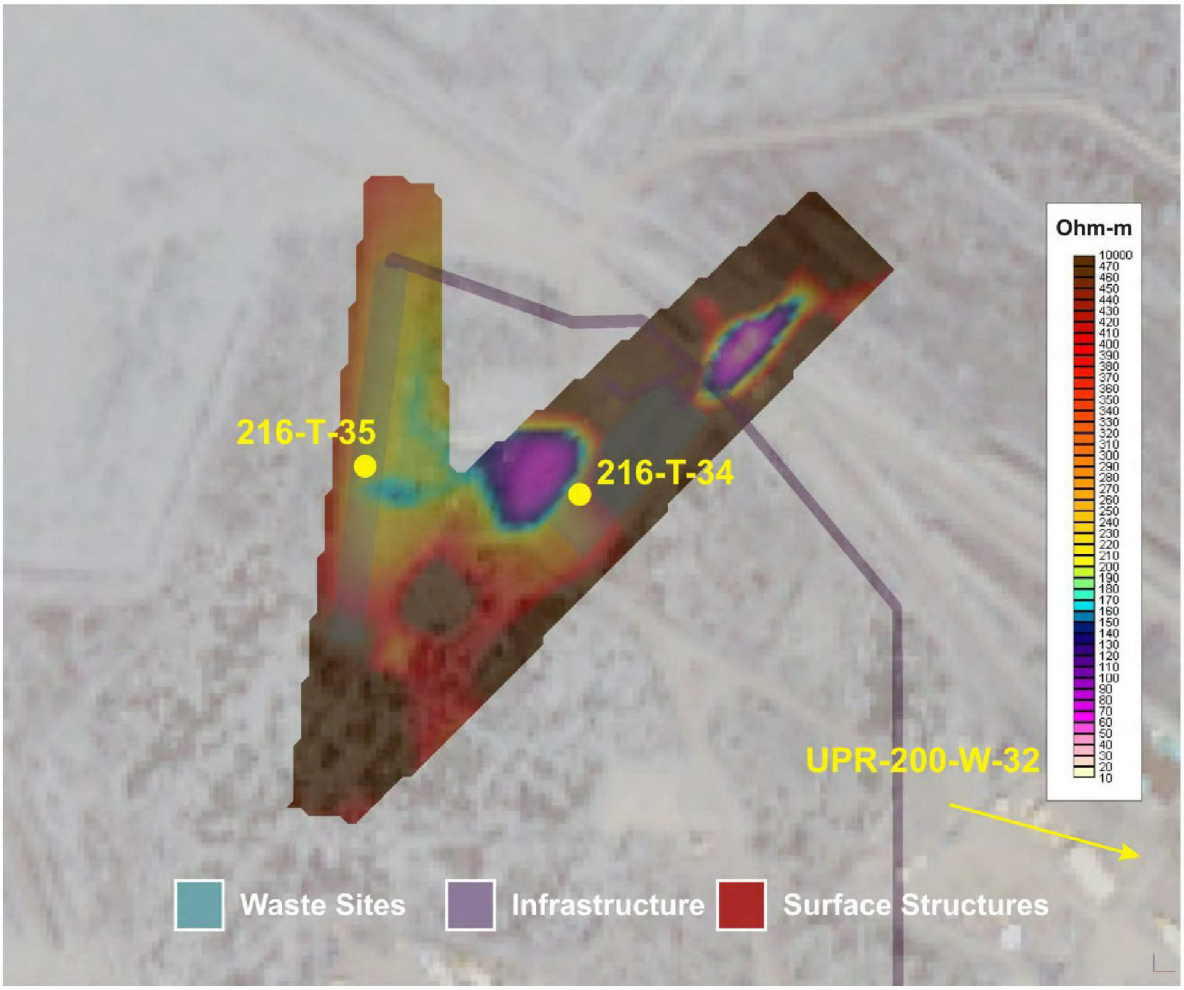

Figure 5-90. Results from the 3D Visualization for T-Plant A at a Depth of 45 m BGS.

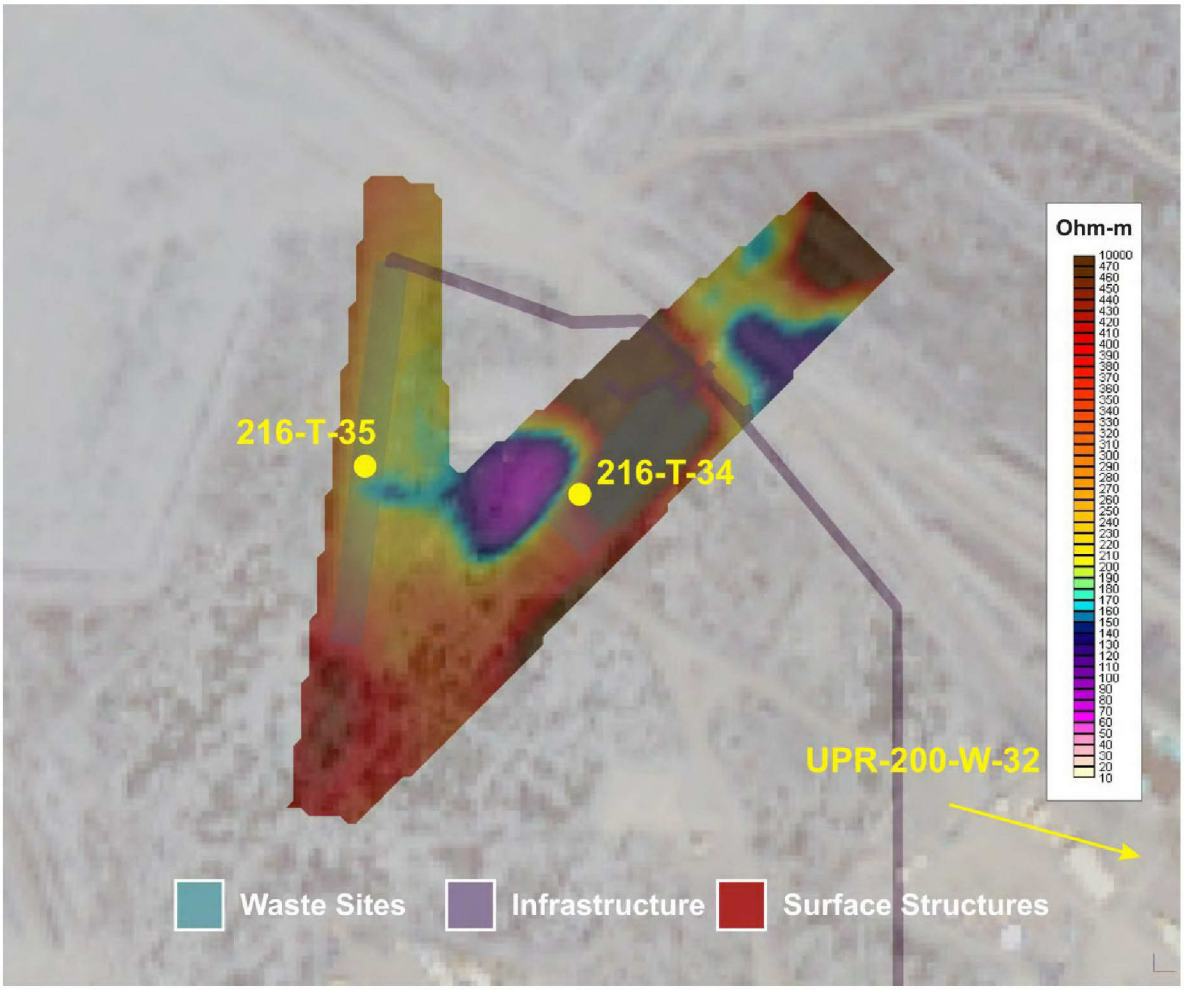

Figure 5-91. Results from the 3D Visualization for T-Plant A at a Depth of 60 m BGS.

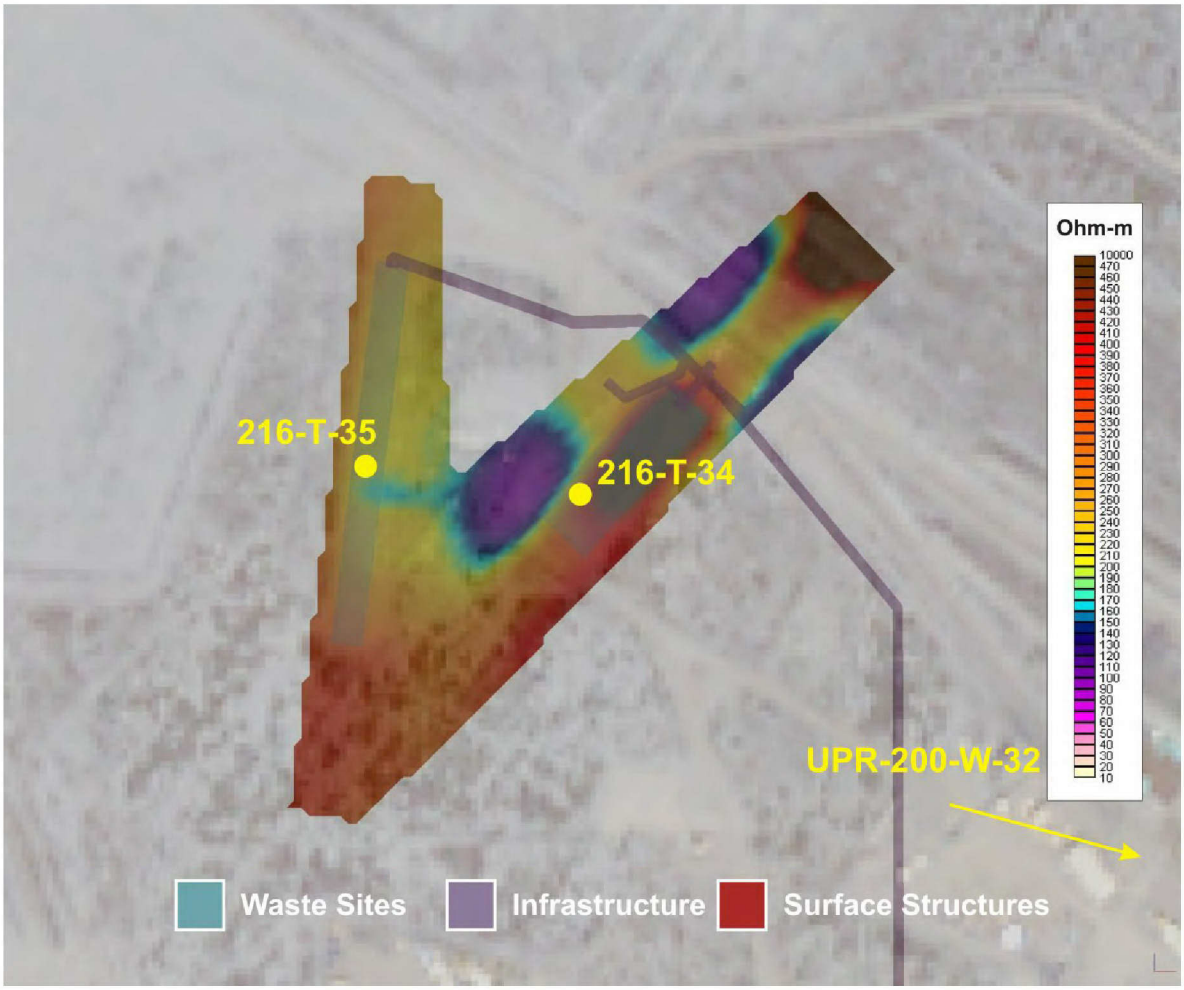

Figure 5-92. Results from the 3D Visualization for T-Plant A at a Depth of 75 m BGS.

The results for 3D visualization for T-Plant B show the southern portion dominated by infrastructure. A linear conductive feature can be seen on the western portion of Figure 5-93 that is associated with the railway lines. Background resistivity values are observed in the northern portion of Figure 5-93. Overall resistivity decreases with depth, with the exception of a resistive lobe centered in the coverage area. The significant quantity of subsurface and surface infrastructure precludes the ability to detect possible features associated with waste disposal. As a result, this area is not suitable for additional resistivity characterization.

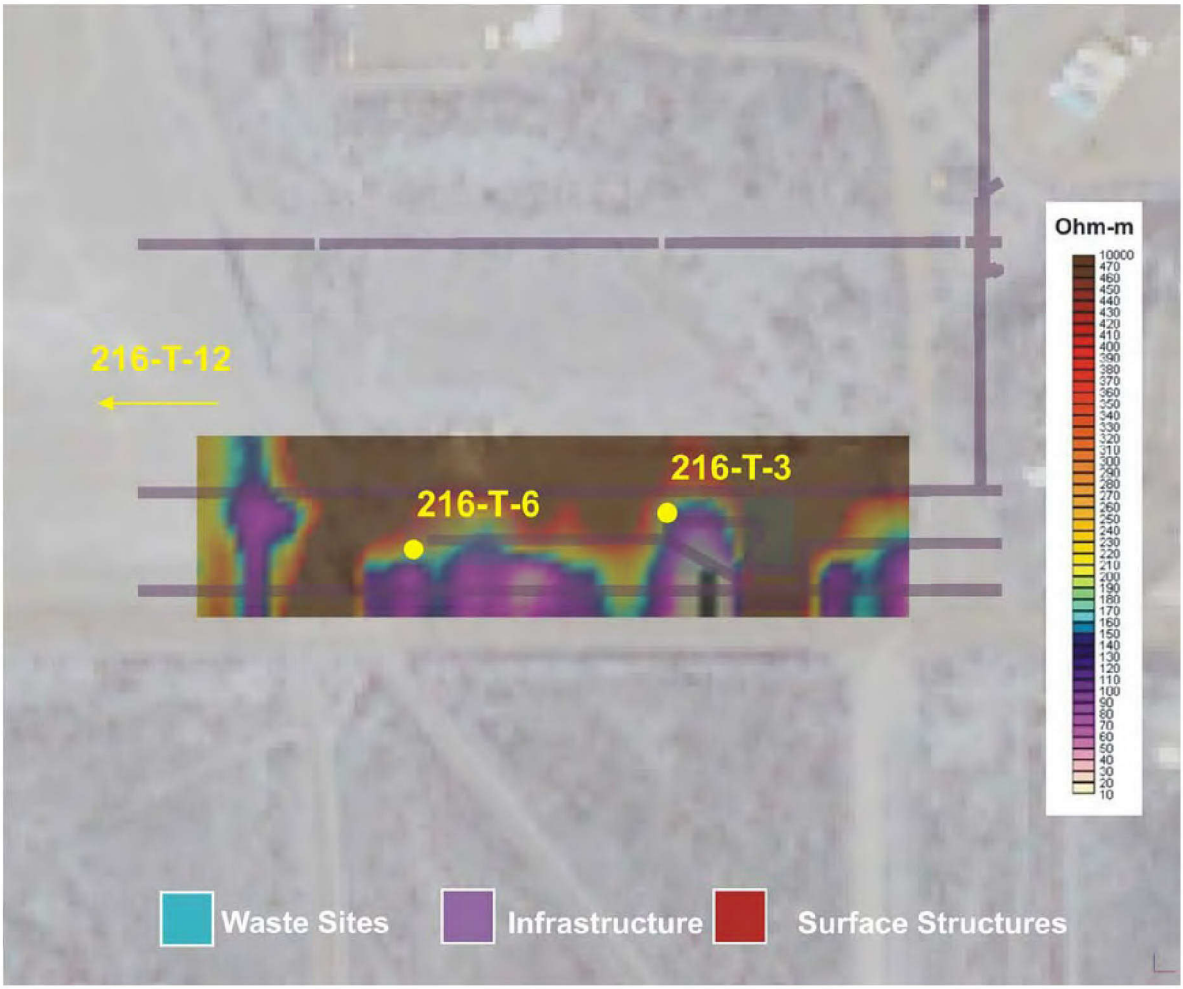

Figure 5-93. Results from the 3D Visualization for T-Plant B at a Depth of 15 m BGS.

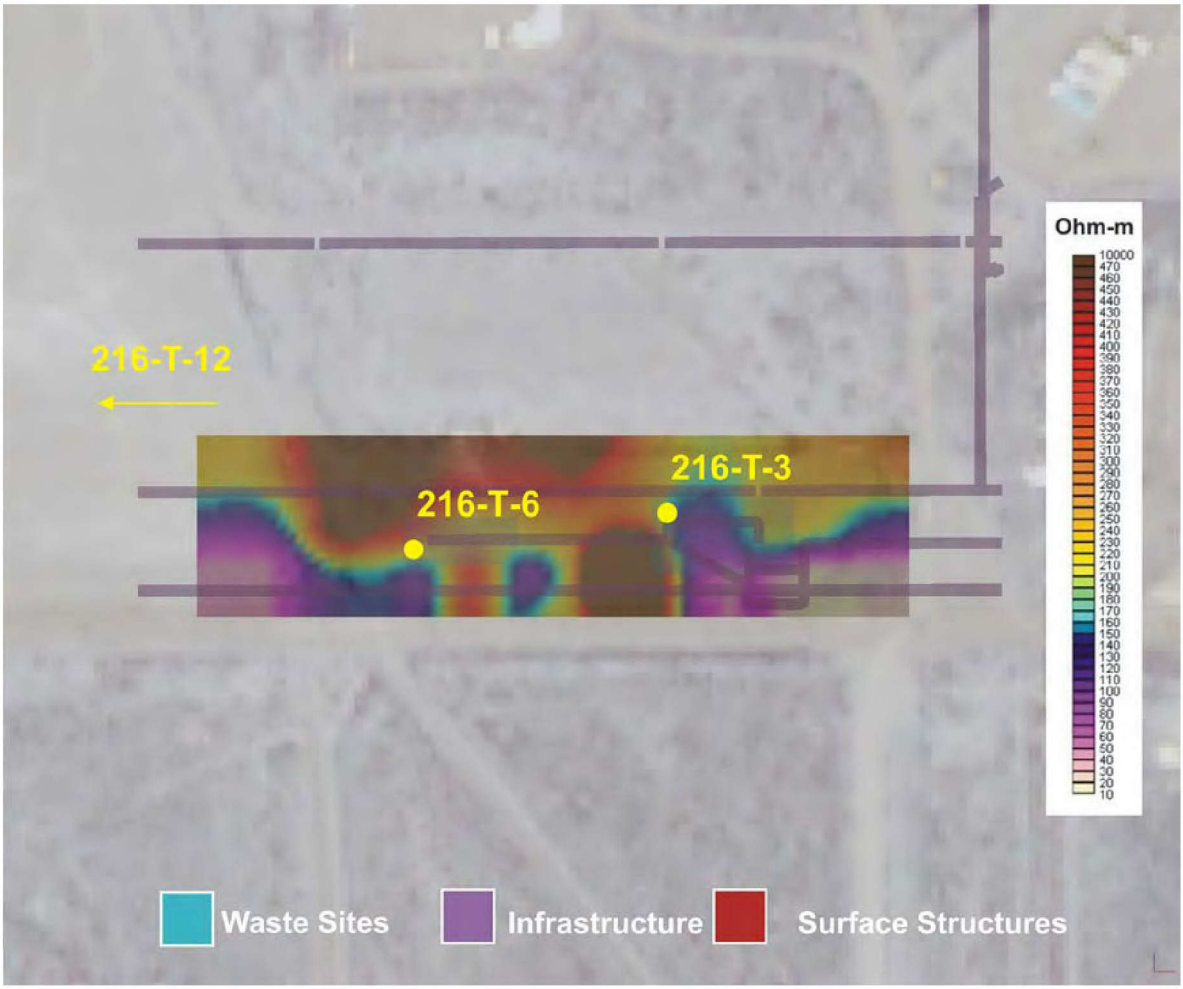

Figure 5-94. Results from the 3D Visualization for T-Plant B at a Depth of 30 m BGS.

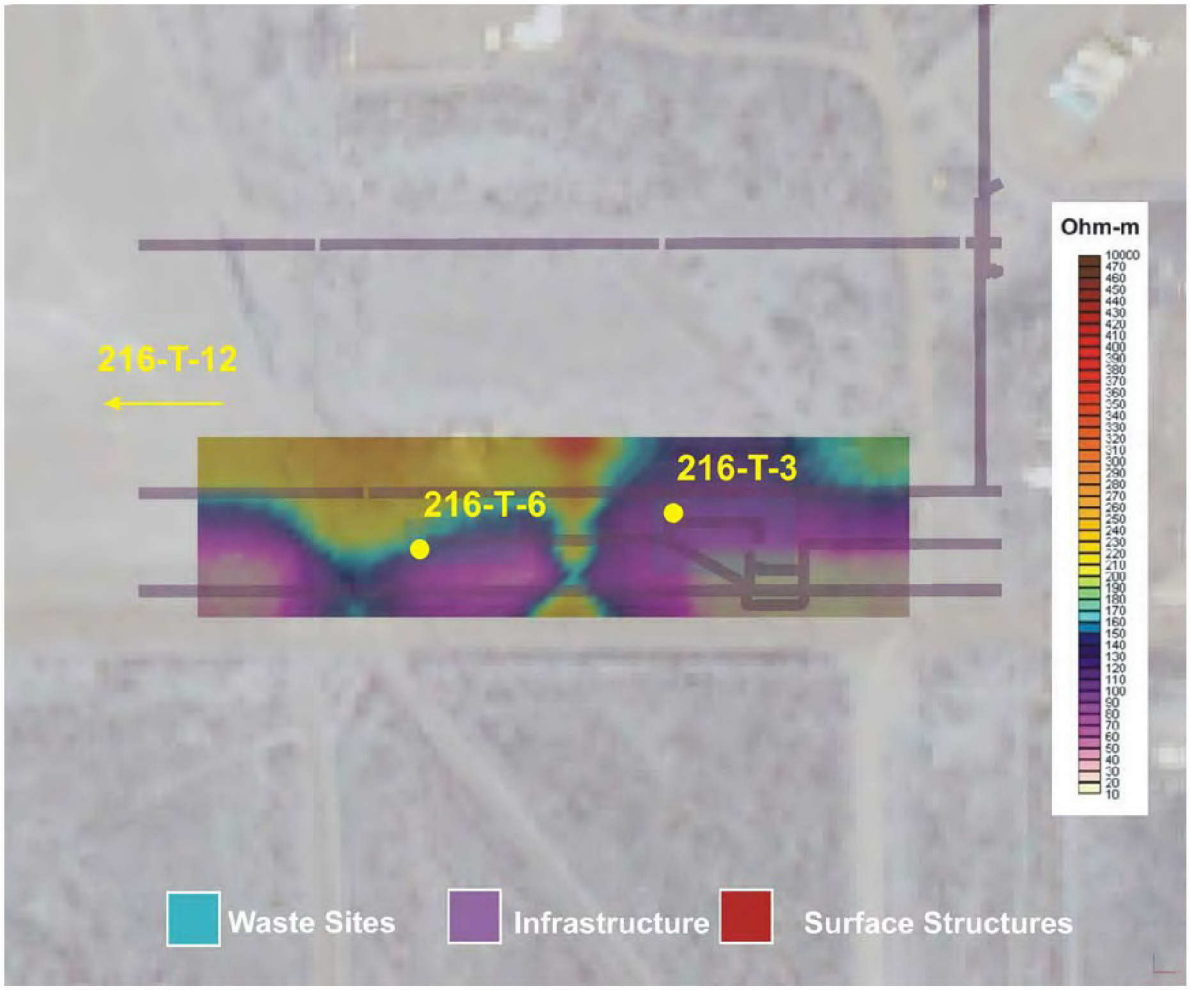

Figure 5-95. Results from the 3D Visualization for T-Plant B at a Depth of 45 m BGS.

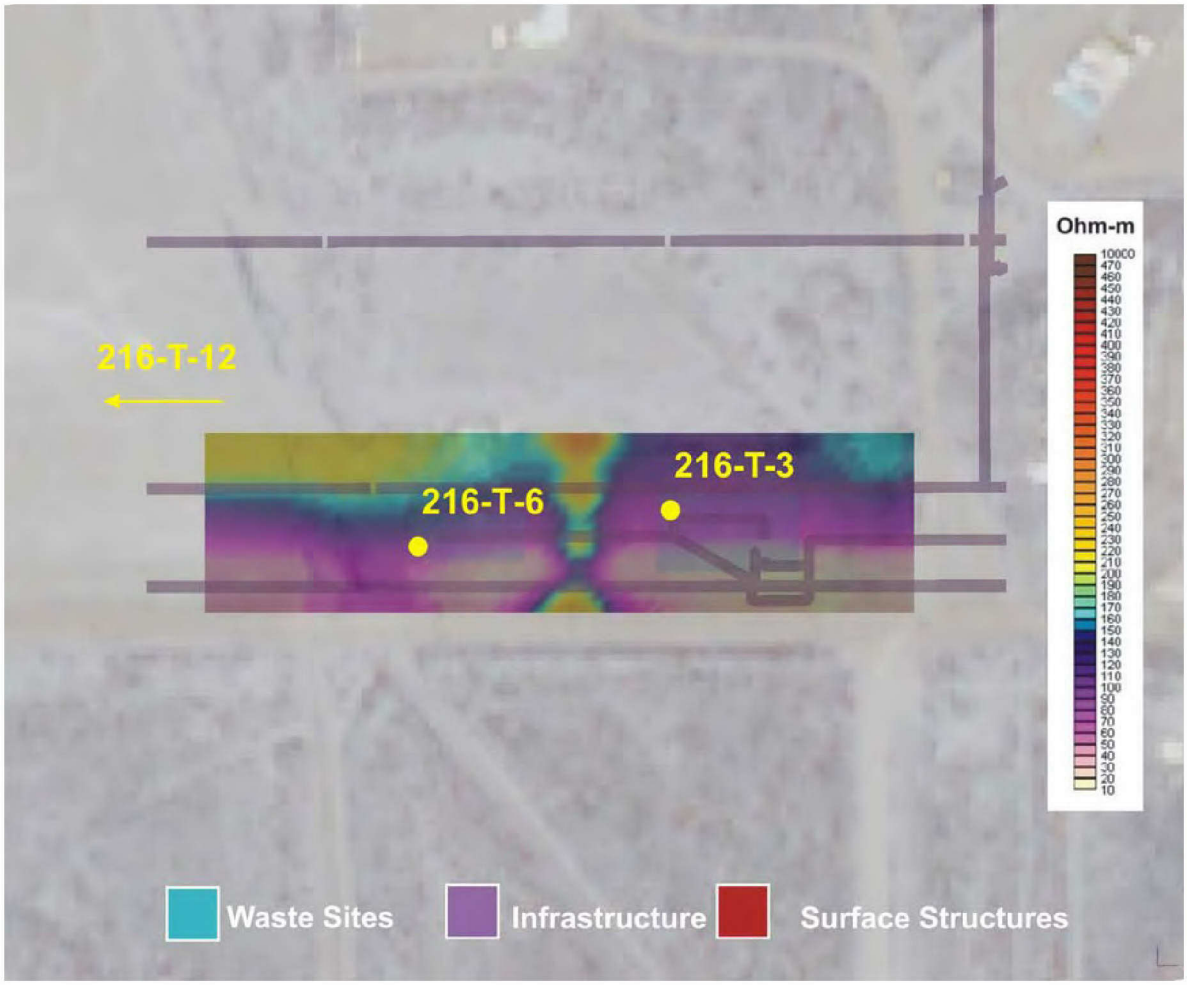

Figure 5-96. Results from the 3D Visualization for T-Plant B at a Depth of 60 m BGS.

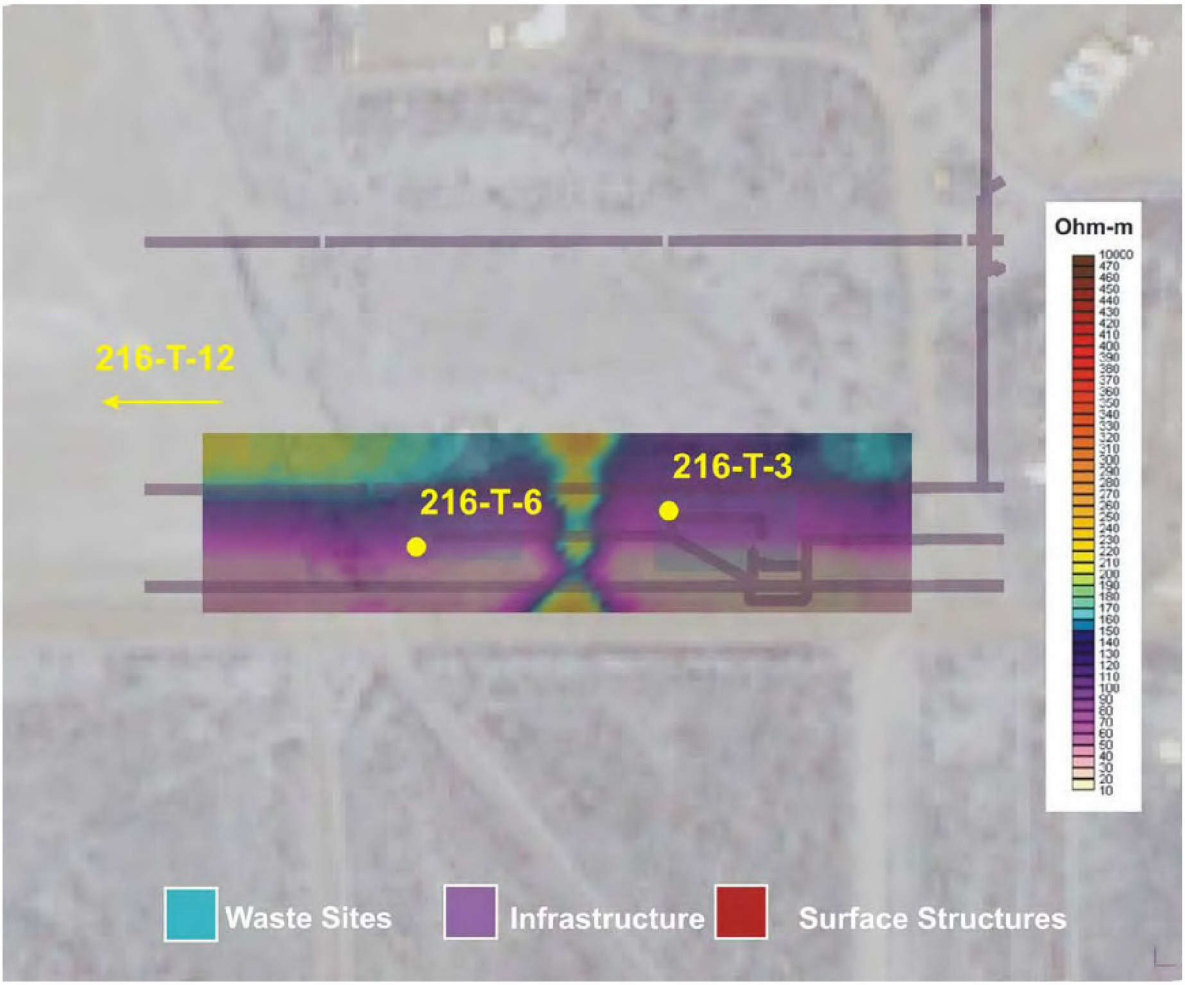

Figure 5-97. Results from the 3D Visualization for T-Plant B at a Depth of 75 m BGS.

5.2.3 216-Z-16 Trench

5.2.3.1 2D Inversion Results

The 2D inversion results of the resistivity survey performed at 216-Z-16 Trench can be viewed in Figures 5-99 through 5-106 below. Figures 5-99 through 5-101 display the results in a cross-sectional format, while Figures 5-102 through 5-106 display the results of a 3D visualization of the same data set. Presenting plan view "depth slices" from the 3D visualization provides a tool for correlating resistivity responses to infrastructure, changes in soil moisture, or changes in soil chemistry.

Three resistivity lines were acquired at the 216-Z-16 Trench site; 200WZT01 (Figure 5-99), 200WZT02 (Figure 5-100), and 200WZT03 (Figure 5-101). The resistivity data was processed according to Section 4.3 above using a 2D inversion algorithm (AGI EarthImager 2D).

Table 5-7 shows the inversion statistics for goodness of fit in each line at the 216-Z-16 Trench waste site. An explanation of the table parameters is discussed in detail within Section 4.3.3.

Table 5-7. Final Inversion Statistics for the 216-Z-16 Trench Waste Site.

Line #	Stage	Trial	Iterations	RMS	L_2
200WZT01	1	1	4	4.79	0.92
200WZT02	1	1	3	4.56	0.83
200WZT03	1	1	4	4.70	0.89

RMS = root-mean-square.

A site specific color scale was developed through a statistical analysis of the apparent resistivity values for all data collected within the 216-Z-16 site. A histogram, shown in Figure 5-98, was used to generate a color gradient that is sensitive to the resistivity range

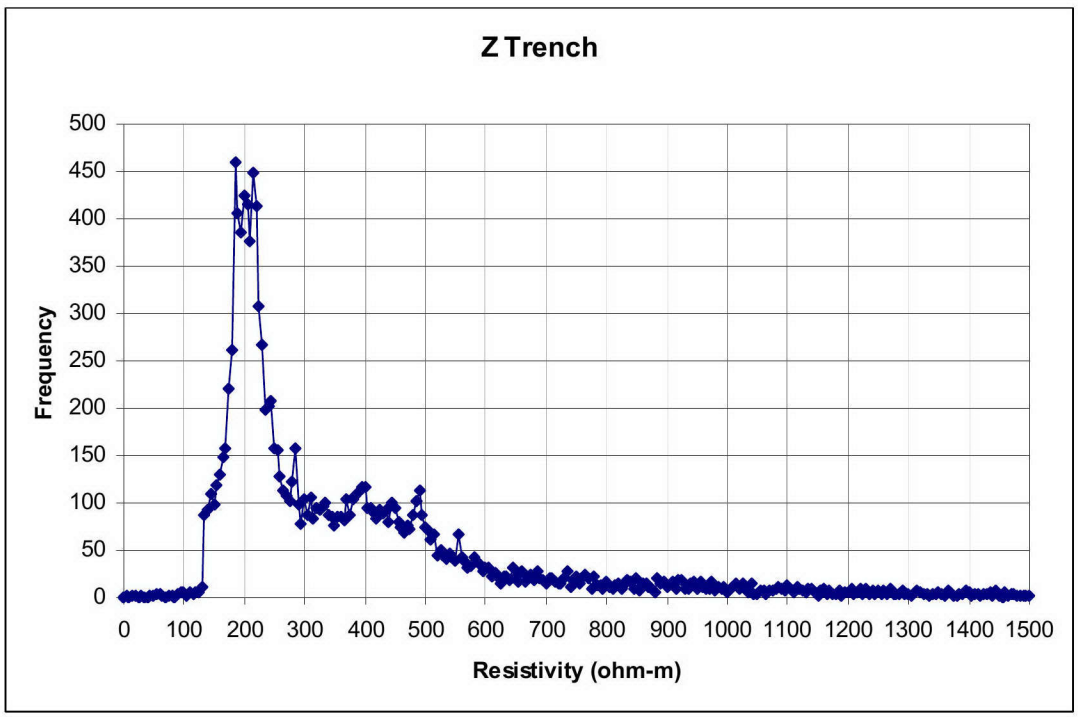

Figure 5-98. Histogram of apparent resistivity data for the 216-Z-16 project site.

Minimal interference from subsurface infrastructure was observed at the 216-Z-16 Trench Site. Despite the presence of several steel pipes rising to the surface from within the trench area. It is possible that considerable amount of subsurface infrastructure exists at depth within the disposal trench. A magnetic and electromagnetic survey could provide much needed information. There

is a large conductive anomaly (approximately 150 Ohm-m) centered at approximately 160 m along line 200WZT01; located at a depth of approximately 40 m BGS). Pipeline features tend to be of higher magnitude and are typically located ad a shallower depth. However, the relatively close proximity of the water table and the associated low resistivity response tend to smear or merge the two anomalies. As a result, it is difficult to determine if the feature is related to infrastructure interference or is associated with 216-Z-16 waste site disposal volume of approximately 2.7 mGal of waste. Overall, there is a decrease in resistivity with depth on each of the three profiles, suggesting an increase in moisture content or salt concentration with depth. Depth to groundwater in the area has been recorded at approximately 72 m BGS. The conductive feature at-depth correlates with the known depth to groundwater. Where conductive anomalies resulting from near-surface infrastructure occur there is a co-mingling of water table and infrastructure response that often distorts both features.

A near the surface moderately conductive anomaly from approximately 10 to 20 m BGS can be seen on lines 200WZT02 and 200WZT03 near station 75 m . This is a small feature that is more conductive (around 300 ohm-m) than the observed background resistivity of the Hanford formation (> 400 Ohm-m), suggesting a relative increase in moisture content or salt concentration. It should be noted that this coverage is insufficient for a true background comparison, as the coverage is limited to the area of disturbed soil. Additionally, background resistivity values can vary from site to site.

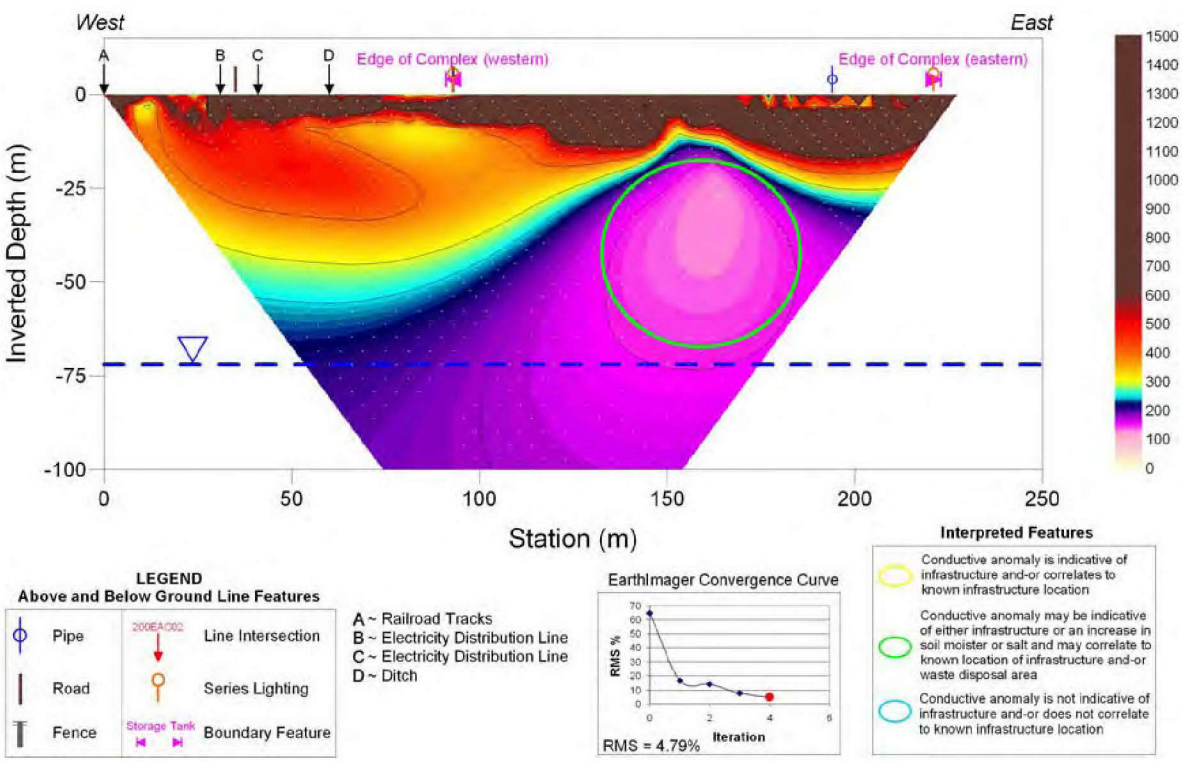

Figure 5-99. Inversion Results for 216-Z-16 Trench Line 200WZT01.

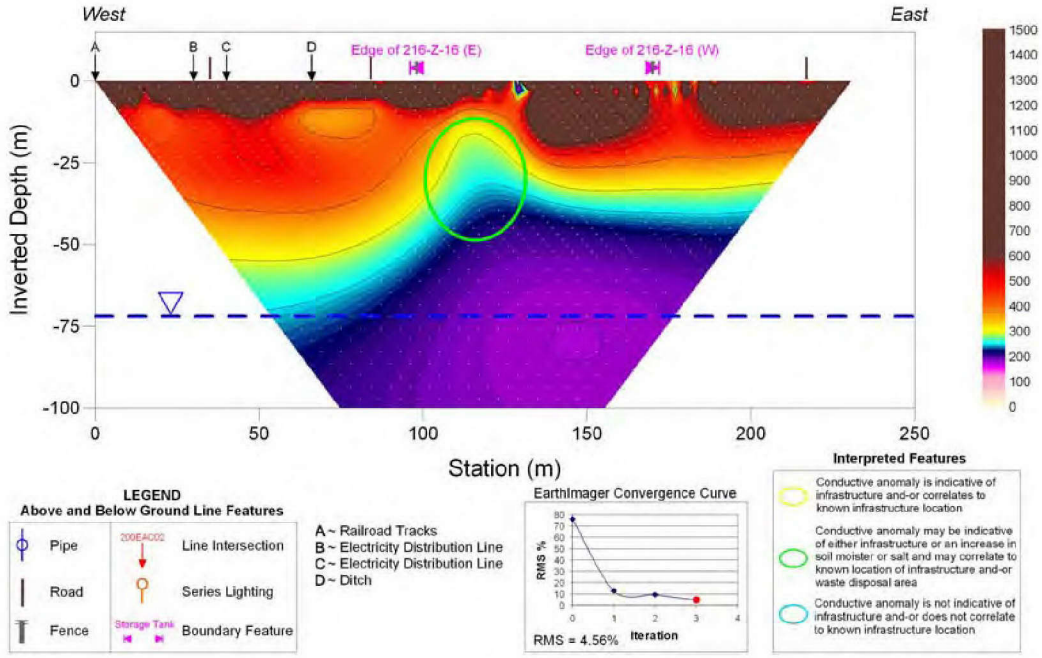

Figure 5-100. Inversion Results for 216-Z-16 Trench Line 200WZT02.

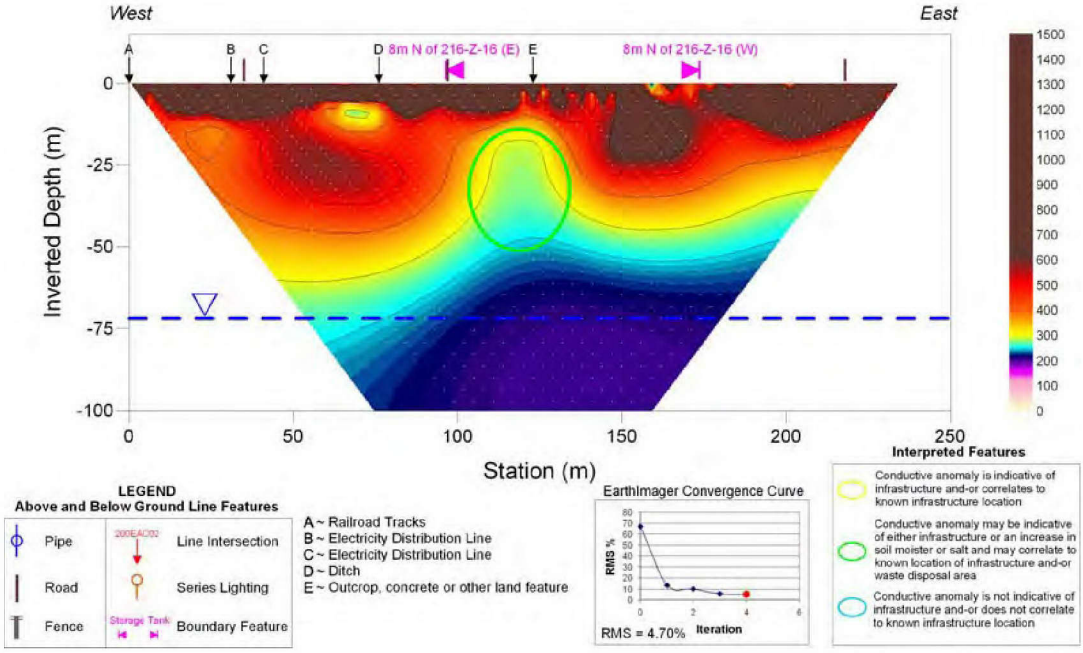

Figure 5-101. Inversion results for 216-Z-16 Trench Line 200WZT03.

5.2.3.2 3D Rendering of 2D Inversion Results

Figures 5-102 through 5-106 show the plan view resistivity distribution at-depths increasing in 15-meter increments, from 15 to 75 m. Note the predictable decreasing resistivity with depth. The infrastructure mentioned in the above 2D section can be seen as resistivity lows throughout the depth slices. The feature, as in the 2D image, increases laterally with depth. However, the extrapolated geometries of the associated resistivity lows vary. Eventually, the sections display a regional decrease in resistivity with depth, associated with the increased moisture content at-depth (Figure 5-106) most likely associated with the water table.

Additionally, on the western portion of the image there is very good correlation with the desert scrub areas and higher resistivity values. This may be a background resistivity value, although it is difficult to surmise with the limited coverage. Also, note that boundary of the sage area, or transition to the gravel access road correlates with a decrease in resistivity.

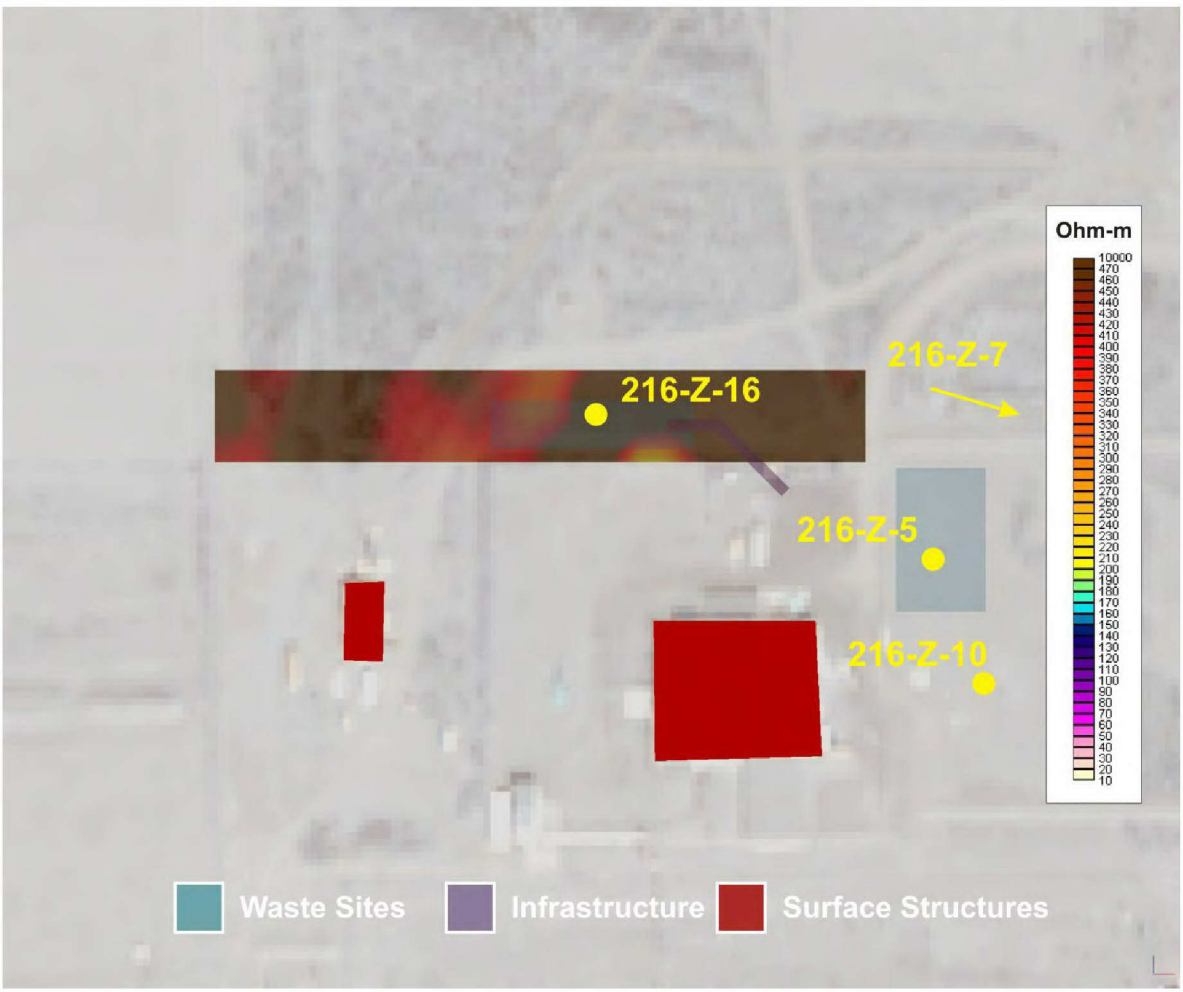

Figure 5-102. Results from the 3D Visualization at a Depth of 15 m BGS.

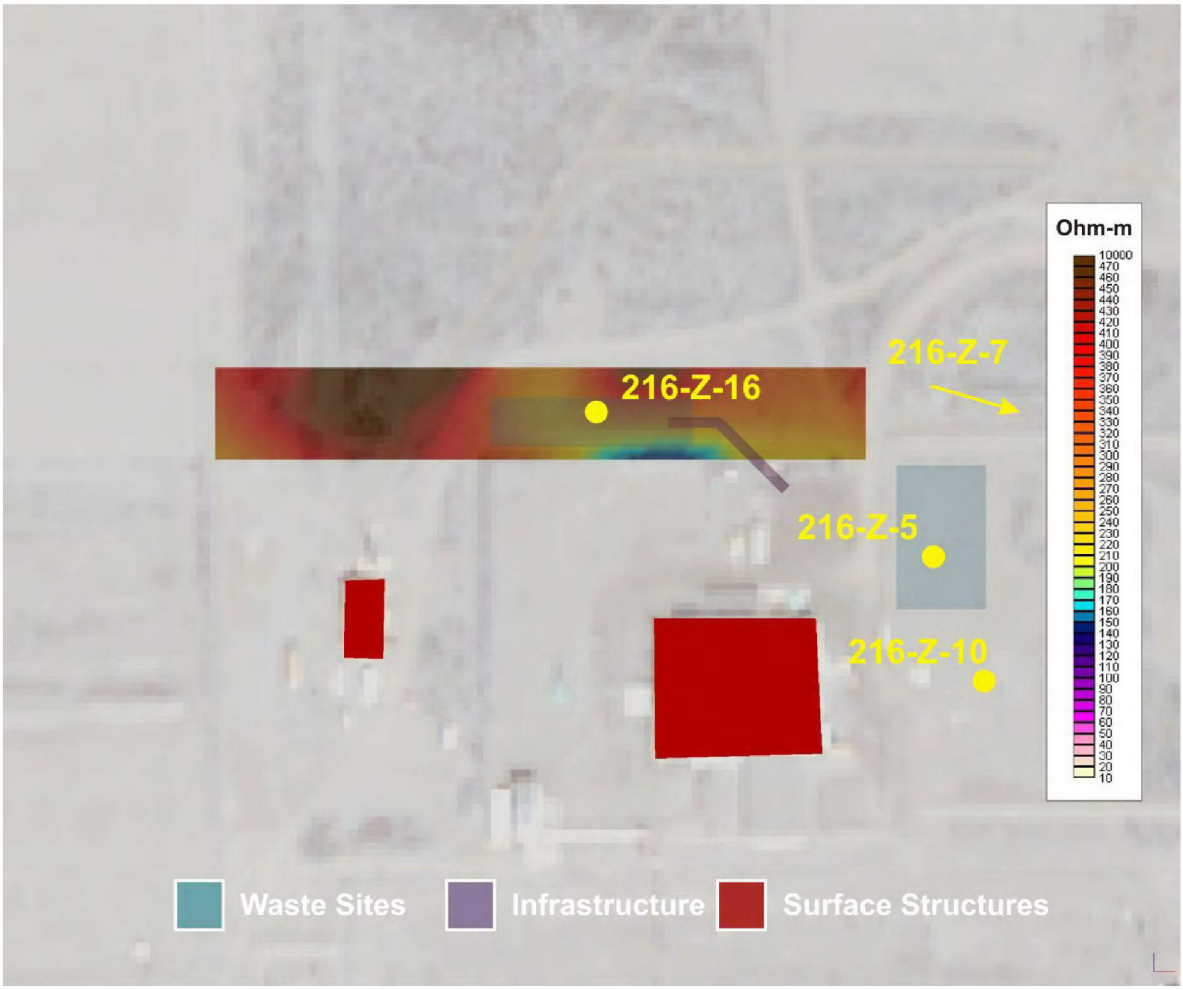

Figure 5-103. Results from the 3D Visualization at a Depth of 30 m BGS.

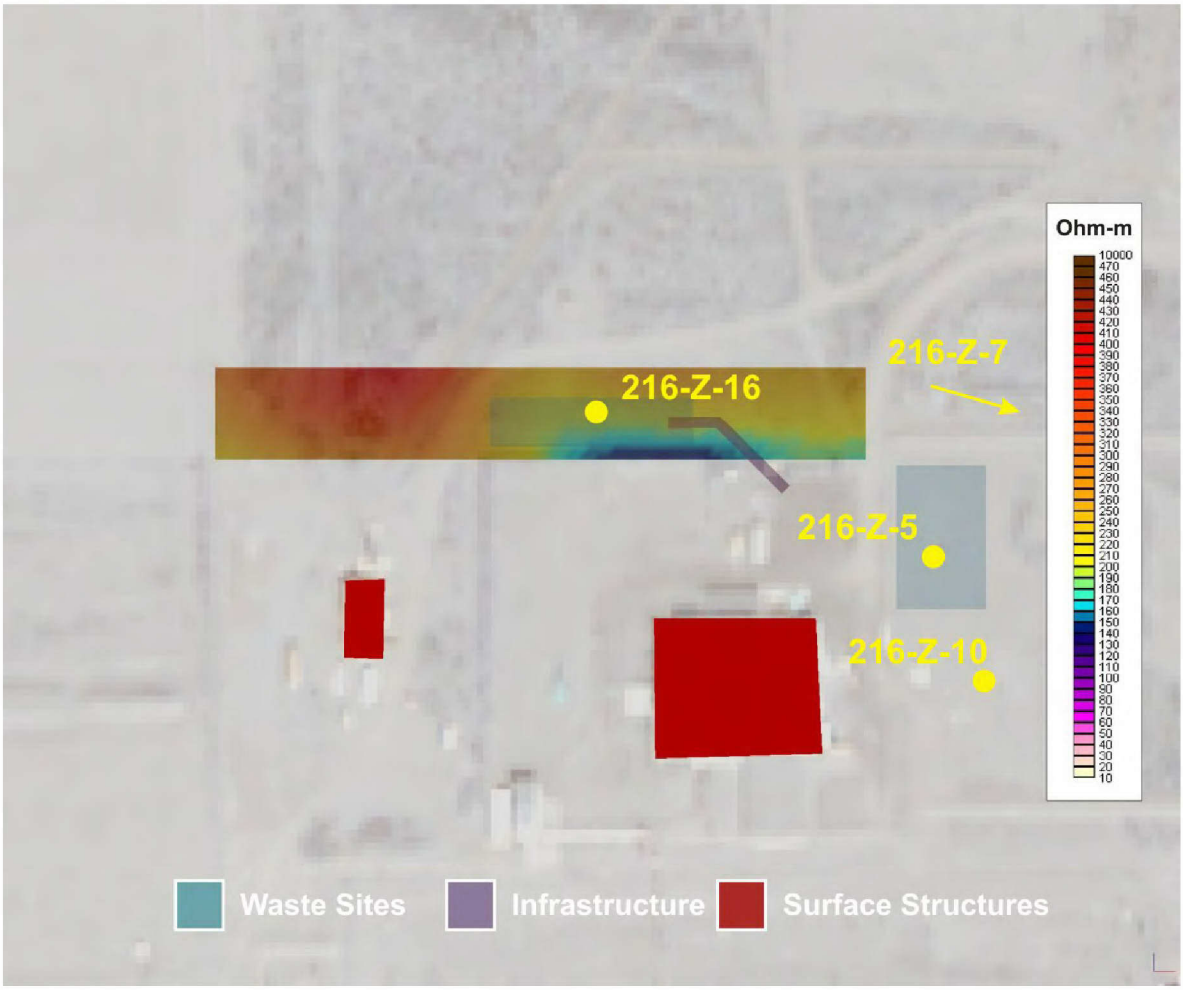

Figure 5-104. Results from the 3D Visualization at a Depth of 45 m BGS.

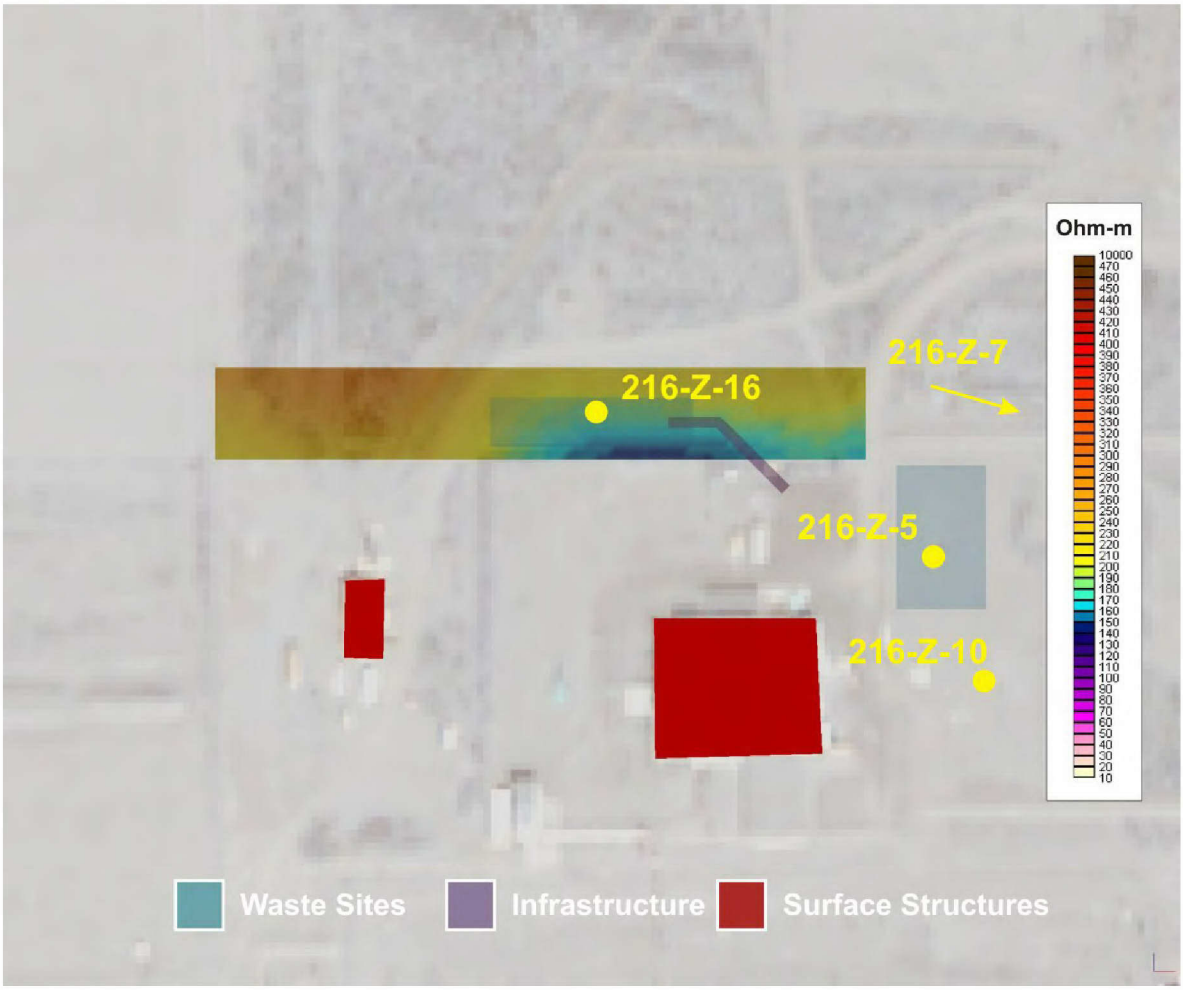

Figure 5-105. Results from the 3D Visualization at a Depth of 60 m BGS.

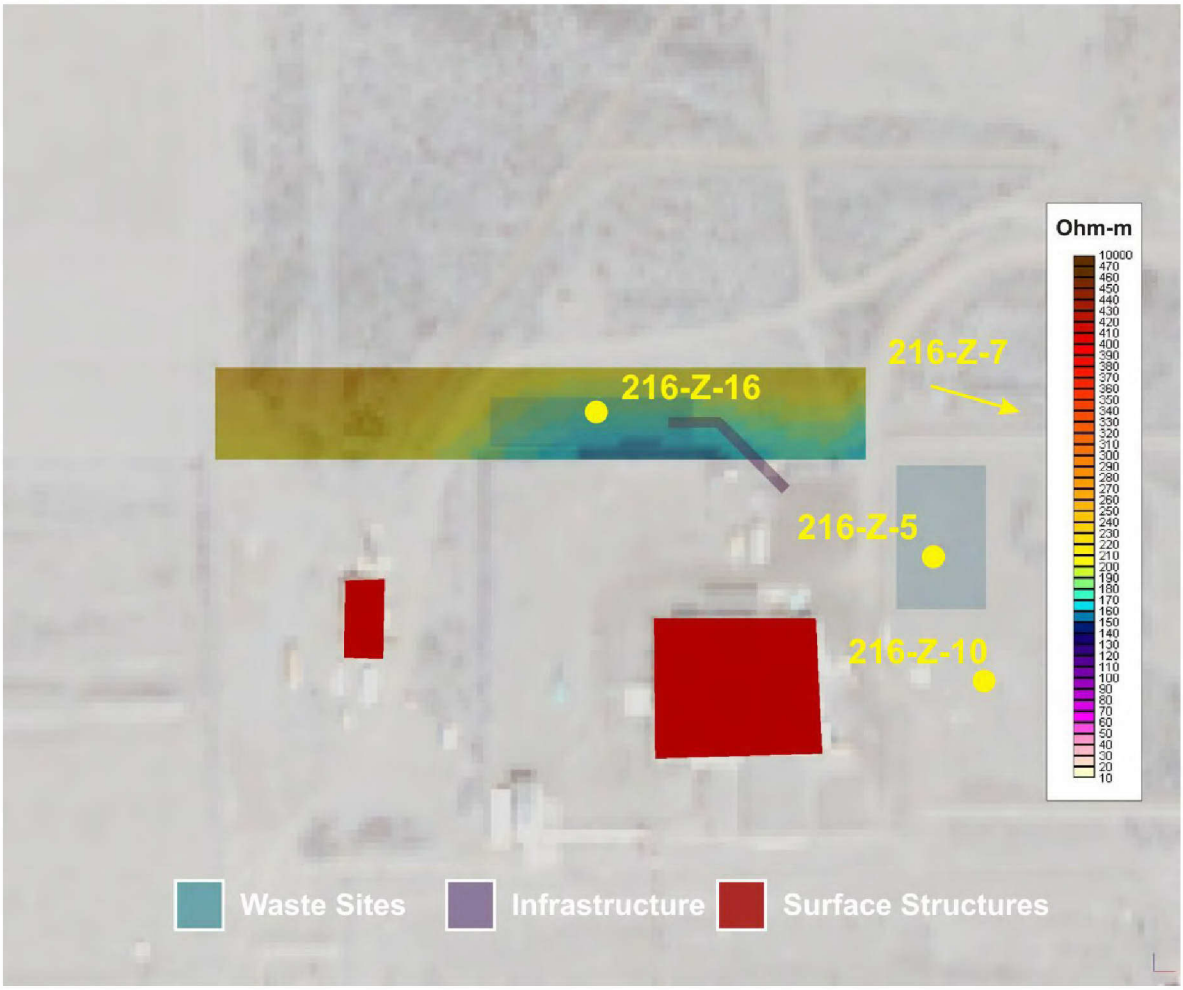

Figure 5-106. Results from the 3D Visualization at a Depth of 75 m BGS.

6.0 CONCLUSIONS

A non-invasive geophysical survey was conducted over select waste disposal facilities within both the 200 West and 200 East areas of the Hanford Site. Sites within the 200 East area selected for this investigation included four resistivity lines at 216-C-1, nine resistivity lines at A-Complex, ten resistivity lines at B-Plant, and seven resistivity lines at PUREX. Sites within the 200 West area selected for this investigation included six resistivity lines at S-Complex, ten resistivity lines at T-Plant, and three resistivity lines at 216-Z-16 Trench.

The goal of the project was to define the extent of possible subsurface conductive anomaly areas associated with waste disposal volumes. Interpretation of the results was designed to be aided by independent soil borings, which were not available at the time of this report preparation.

The resistivity data were processed using 2D electrical resistivity inversion. The resistivity inversion technique uses an optimization routine to iteratively calculate the best representation of the true resistivity of the subsurface. The objective of the inversion is to calculate a spatial distribution of resistivity that most closely match measured field data. The difference between the modeled and measured resistivity is captured by the RMS error parameter, which was less than 5 percent for each modeled section.

The resistivity results showed that survey areas that contained limited infrastructure had good correlation to known disposal volumes and the application of data inversion to electrical resistivity data helped constrain targets related to increased moisture or increased salts. This is most evident at the PUREX project site where the results from this survey reduced the footprint of conductive features that were detected on previous resistivity surveys. The combination of additional survey coverage and 2D inversion and correlation to infrastructure has enhanced the understanding of subsurface conditions. The use of resistivity in this area could be greatly enhanced by acquiring a few more strategically placed resistivity lines and inverting the entire data set in three dimensions.

Several of the survey areas suffered from electrical interference due to subsurface and surface infrastructure. In these areas, the highly conductive infrastructure comprised mainly of pipes or pipe networks provided a preferential electric current pathway that could not be resolved by the 2D inversion software. In a few places, the anthropogenic conductive features caused by infrastructure merged with the conductive region at-depth caused by the water table. The contouring process tends to smear or merge the two anomalies and the resulting conductive feature is therefore larger than one would expect if the section was not complicated by modeling and infrastructure interference. To help separate or interpret the infrastructural affects in the resistivity data from those of past waste disposal practices, an intensive digitizing effort was performed to visualize the geo-referenced infrastructure with the resistivity results. The visualization allowed direct correlation of resistivity anomalies to the responsible infrastructure. Where infrastructure was less abundant, this graphical correlation allowed interpretation of subsurface soil properties despite the infrastructure disturbances. Where infrastructure was pervasive, the resulting models showed unrealistic results that had little correlation to geology or hydrology. It is possible that 3D inversion could reduce the effect of the infrastructure in these areas, but it would require a combination of forward modeling to evaluate pipeline geometry and

inversion using a-priori pipeline parameters. In addition, several infrastructure dominated areas could be enhanced by additional well-planned resistivity lines that would improve data point density and geometry. The planning should also include an electromagnetic and magnetic reconnaissance survey over the area to understand more fully the exact placement of buried infrastructure. Any new resistivity lines should avoid the infrastructure as much as possible.

216-C-1 Project Site: The 216-C-1 site was one of the most heavily infrastructure-dominated project sites. Despite the severe infrastructure, the data revealed a few interesting resistivity anomalies where the displayed values appeared too conductive to represent saturated soil, yet the character did not resemble a typical infrastructure response. This may suggest a combination of increased soil moisture and infrastructure, where 2D inversion is not suitable for the complexity of the subsurface. Three-dimensional offline effects, caused by subsurface metallic items near the survey line, also distorted inversion results and may be improved by 3D inversion. It is unlikely that additional surface resistivity will improve imaging results due to the abundance of infrastructure that would prevent beneficial placement of supporting surface survey lines. A borehole-based ERT survey, where resistivity data are acquired between two vertical set of electrodes placed in parallel boreholes, would likely result in usable resistivity data for interpretation of a plume resulting from liquid waste disposal.

A-Complex Project Site: The A-Complex site showed near-surface conductive features that correlate well with the boundary of the 216-A-19 and -20 waste sites. The conductive feature is limited to the first 15 m of the subsurface and does not contact the water table. The shape and magnitude of the feature is not characteristic of infrastructure and is therefore likely to be the result of an increase in soil moisture or salt concentration. Survey lines over the 216-A-8 disposal trench showed a low resistivity anomaly associated with the termination of the inflow pipeline. However, there is evidence of conductive material within the first 10 m that is characteristic of liquid waste disposal. The two survey lines conducted between the 216-A-7 waste site and the 207-A-North and -South ponds were greatly impacted by infrastructure. It is unlikely that additional surface survey coverage or processing using 3D inversion would produce additional information in this area due to the infrastructure complexity. An ERT survey straddling the 216-A-7 crib may result in usable resistivity data for interpretation of a plume resulting from liquid waste disposal.

B-Plant Project Site: The B-Plant site includes three characterization targets, the 216-B-55 trench, the 216-B-12 crib, and the area south of the B-Plant industrial complex. Characterization efforts for one survey line placed directly over the 216-B-55 trench were challenged by unknown subsurface conditions that prevented collection of usable data. Nevertheless, the two survey lines adjacent to the trench provide acceptable data that shows little evidence of a change in soil moisture or chemistry associated with the past liquid waste disposal. By contrast, results over the 216-B-12 crib showed a conductive feature directly over the crib within the first 5 to 40 m. The depth and magnitude of the feature suggests the presence of increased soil moisture or salt concentration. However, the survey line completed directly over the crib shows a heavy distortion of the conductive feature that is most likely caused by subsurface infrastructure within the crib. Therefore, the conductive feature may be the result of either soil moisture or infrastructure, or both. Three-dimensional inversion processing would provide additional constraints to the model and additional survey coverage perpendicular to the current lines would

provide a more suitable geometry. Survey results for the area south of B-Plant were heavily distorted due to infrastructure and provided no useable results pursuant to the characterization of disposal volumes. It is unlikely that additional surface resistivity surveying will produce better results in this area. However, an ERT survey would greatly enhance the utility of resistivity characterization in this area.

PUREX Project Site: Additional survey coverage over the PUREX site was conducted as part of this project to help refine interpretation of conductive anomalies that were detected on previous resistivity surveys. The increased survey coverage and 2D inversion processing produced a more refined representation of subsurface conditions. Distortions due to infrastructure were present but correlation of features to digitized pipelines allowed for separation of increased moisture areas from infrastructure. The most significant conductive feature is located over the extent of the 216-A-36 A/B waste site and increases in size with depth. The resistivity low extends beyond 75 m and is likely to be in contact with groundwater. Two small near-surface conductive features are visible near the 216-A-10 waste area, but there is insufficient data to determine the possible cause of the anomalies. Additional survey coverage would greatly benefit in the characterization of this area. Two-dimensional inversion sections show some conductive features over the 216-A-45 waste area within the first 10 m of the ground surface. Enhancement of the resistivity results could be accomplished by completing a 3D inversion model with additional data. This might provide a better volumetric assessment of detected features.

S-Complex Project Site: The S-complex project site included two characterization areas, 216-S-13 to the south and 216-S-9 to the north. Each site consisted of three survey lines and contained several intersecting and paralleling infrastructure features that adversely affected inversion results. However, there is a conductive feature on the eastern edge of the 216-S-13 survey area that increases with depth and is in close proximity to the 216-S-13 disposal site. The shape and magnitude of the response is not necessarily indicative of infrastructure and could be due to the increased soil moisture or salt concentration from the liquid waste disposal site to the east. Additional survey coverage between the eastern survey line and the 216-S-13 waste site is needed to further delineate the local contributions to the low resistivity anomaly. The 216-S-9 characterization area is greatly hampered by pipeline disturbances. However, besides the pipeline induced anomalies and the water table, there is little evidence of increased soil moisture or a change in soil and water chemistry as supported by the high resistivity values shown in the near-surface that are adjacent to the pipeline responses. Two-dimensional inversion may be poorly suited for reconstruction of this complex area. Three-dimensional inversion may provide additional characterization results by constraining the pipeline features. Additional surveying perpendicular to the survey lines will improve electrode geometry. Additionally, an ERT survey would greatly enhance the utility of resistivity characterization in this area.

T-Plant Project Site: The T-Plant resistivity project site included two characterization areas centered over the 216-T-34 and -35 trenches and the 216-T-3 waste site. Results for the 216-T-34 and -35 areas showed a significant distortion due to the railway lines and subsurface pipes. Despite the distortions, there was a noticeable increase in conductivity near the 216-T-35 trench that is likely caused by an increase in moisture content or salt concentration relative to the surrounding background material. However, it is unlikely that the near-surface low resistivity

anomaly is in physical contact with the water table. There is little evidence of an increase in soil moisture over the 216-T-34 trench. However, the inversion model appears to suffer from offline 3D effects from the 216-T-34 trench. Three-dimensional inversion and additional survey coverage perpendicular to the current survey lines as well as ERT data would be beneficial in resolving this area.

216-Z-16 Trench Project Site: 216-Z-16 Trench results were relatively free of adverse infrastructure anomalies despite the presence of observed infrastructure. While lower resistivity values are associated with the 216-Z-16 Trench site, they are weak in comparison to features representing disposal volumes at other sites. Of interest is a small conductive feature that occurs on the southeastern edge of the survey area that increases with depth starting at 30 BGS. Although not shown on the maps, visual observation onsite showed several structures and electrical boxes in the vicinity.

7.0 LESSONS LEARNED & RECOMMENDATIONS

This section presents lessons learned and recommendations in association with data acquisition, data quality, and data processing that were gained as part of this resistivity characterization effort. A lessons-learned meeting was held following completion of data collection and processing activities. Personnel directly involved in the planning and executing the data collection and processing attended the lessons-learned meeting. From the lessons learned, a series of recommendations were developed to improve future deployment of resistivity characterization. Suggestions for future work to help refine or improve the geophysical characterization of a contaminant plume are as follows:

7.1 SURVEY DESIGN

Many of the sites presented infrastructure challenges in the same regions as potential resistivity lows. It is recommended that for future projects a reconnaissance survey using electromagnetic induction and magnetic gradiometry be conducted prior to the resistivity survey design. The electromagnetic and magnetic survey would be used in conjunction with available infrastructure maps to locate areas that are not suitable for resistivity imaging.

A survey design should be conducted prior to surveying that includes a map inspection of subsurface infrastructure, surface infrastructure, and site logistical limitations. Inspection of site parameters should be conducted using available maps, geophysical reconnaissance surveys, and onsite verification. From the analysis, forward modeling of the project areas should be conducted to determine the optimal line location and spacing. The results of the analysis should be drafted into a survey design document that describes equipment, line geometry, and processing.

Where possible, placement of resistivity survey lines should be limited to areas that do not contain an abundance of subsurface or surface infrastructure that adversely affect resistivity results. If avoiding infrastructure areas is not possible, then a graded approach should be considered, including:

1. Reconnaissance mapping of features to help with placement of survey lines and resistivity interpretation.
2. Complete one test line to fully assess data quality in the selected location.
3. Complete an assessment as to the effectiveness of resistivity imaging at the specified location based on the test line.

In areas that do contain substantial infrastructure, resistivity data can still be useful if acquired using a borehole-based ERT survey. ERT data are acquired between two vertical sets of electrodes placed in parallel boreholes. The electrodes would be placed far below the infrastructure allowing imaging of increased soil moisture or salt concentration.

7.2 DATA ACQUISITION

The use of ATVs and four-wheel drive trucks greatly improved data acquisition efficiency and decreased the risk of injury. Increased usage of such vehicles will improve efficiency and reduce project costs.

The time required to setup remote reference electrode arrays is significant due to site logistics and access limitations. It is recommended that on future projects remote reference electrode arrays be catalogued, surveyed, cordoned off, and allowed to remain onsite to reduce data acquisition time for future projects.

Performing data collection in high traffic areas on weekend, or at night, worked well and avoided potential interference, safety problems, and inconvenience issues associated with routing sensitive equipment in high traffic areas.

Some disposal areas are known to be dynamic systems with possible transient plume movement in both the vadose zone and groundwater. For example, nitrate concentrations in groundwater around the T Waste Management Area have shown significant increases within the last several years. To capture these dynamics, we recommend that the subsurface in vicinity of selected disposal areas be evaluated with a successive time-series of resistivity data acquisition campaigns. From an acquisition standpoint, data quality would be improved if permanent resistivity electrodes were left in place so exact, and direct, comparison of analysis results from each of the data acquisition could be made.

For this effort, no well-to-well (WTW) data were acquired. WTW data have proved to be invaluable to plume mapping for other projects within the Hanford Site. It is recommended that WTW measurements be acquired on future deployments, where sufficient well distributions are available. The disadvantage of the WTW data is that-depth information is lost. Therefore, it is recommended that as many deep electrodes be placed the target waste area as possible and be distributed at a low spatial density. Additionally, several deep electrodes could be nested in a single hole. Deep electrodes can be installed as part of sampling boreholes with little modification to current hardware and techniques.

The AGI SuperSting R8 is limited to a 400-watt transmitter. The resolution of the data acquisition card is limited to a maximum of 30 nano-volts. The limited surface electrode grounding (less than 11 inches [28 centimeters]) proved difficult in transmission with only a 400-watt system. Since the grounding condition of the electrode cannot be changed without an excavation permit, the only method for improving signal-to-noise is to increase the signal (transmitted power) or improving the data acquisition card resolution.

7.3 DATA PROCESSING AND MODELING

The location of several characterization sites discussed within this report centered over cribs, trenches, and vaults that contain significant quantities of metal. The disposal site infrastructure creates a 3D response that cannot be adequately imaged using 2D data collection. It is

recommended that, where possible, 3D resistivity data collection is conducted to reduce the 3D effect of disposal site infrastructure.

Since the resistivity data were interpolated over large areas, caution must be exercised when trying to use the data for quantitative purposes. As one moves away from a resistivity line, the degree of confidence in the interpolated values decrease. If the data are to be used for a well citing, for example, then we suggest staying close to where data were acquired.

As specified in the contracted SOW, the inversion processing completed for this data was implemented using a 2D inversion algorithm. Resistivity is a 3D volumetric property, which can be greatly influenced by subsurface features near survey lines in addition to directly beneath the survey lines. The interpretation of the data sets is likely to improve with a more suited 3D inversion processing technique. However, in order to perform 3D inversion, suitable survey design (line location, spacing, geometry) is required.

Areas with substantial infrastructure presented the most difficulties with regard to inversion modeling and associated interpretation of estimated resistivity distributions. It is recommended that new models be developed to more effectively deal with the effect of the infrastructure on inversion modeling results. The new models should make use different modeling methods, such as the analytic element method, filtering, or some other technique that would help to approximate the effects of infrastructure in inversion models.

8.0 REFERENCES

29 CFR 1910.120, "Hazardous Waste Operations and Emergency Response," *Code of Federal Regulations*, as amended.

Barker, R.D., 1989, "Depth of investigation of collinear symmetrical four-electrode arrays," *Geophysics*, 54(8):1031-1037.

Battelle Press, 2003, "Hanford Site Historic District: History of the Plutonium Production Facilities 1943-1990," *Battelle Press*, Columbus, Ohio.

Corbin R.A., B.C. Simpson, M.J. Anderson, W.F. Danielson, III, J.G. Field, T.E. Jones, and C.T. Kincaid, 2005, *Hanford Soil Inventory Model, Rev. 1,* PNNL-15367 and RPP-26744, Rev. 0, CH2M HILL Hanford Group, Inc., Richland, Washington.

Dahlin, T. and Zhou, B., 2004, "A numerical comparison of 2D resistivity imaging with 10 electrode arrays," *Geophysical Prospecting*, 52(5): 379-398.

deGroot-Hedlin, C. and Constable, S., 1990, "Occam's inversion to generate smooth, two-dimensional models from magnetotelluric data," *Geophysics*, 55(12): 1613-1624.

deGroot-Hedlin, C. and Constable, S., 2004, "Inversion of magnetotelluric data for 2D structure with sharp resistivity contrasts," *Geophysics*, 69(1): 78-86.

Dey, A. and H.F. Morrison, 1979, "Resistivity modeling for arbitrarily shaped three-dimensional structures," *Geophysics*, 44(4): 753-780.

Edwards, L. S., 1977, "A Modified Pseudo-Section for Resistivity and IP," *Geophysics*, 43(5): 1020-1036.

Fink, J.B., 1980, "Logarithmic Pseudo-Sections," Abstract, Proceedings of the 50th Ann. Mtg. Soc. Expl. Geophysicists.

Gephart, R.E., 2003, "Hanford: A Conversation about Nuclear Waste and Cleanup," *Battelle Press*, Columbus, Ohio.

Hallof, P.G., 1957, "On the interpretation of resistivity and induced polarization measurements," Ph.D. Thesis, Massachusetts Institute of Technology.

Koefoed, O., 1972, "Discussion on 'Depth of investigation in direct current methods' by A. Roy and A. Apparao," *Geophysics*, 37(5):703-704.

LaBrecque, D.J., Miletto, M., Daily, W., Ramirez, A. and Owen, E., 1996, "Effects of noise on Occam's inversion of resistivity tomography data," *Geophysics*, 61(2): 538-548.

Li, Y. and D.W. Oldenburg, 1994, "Inversion of 3-D DC resistivity data using an approximate inverse mapping," *Geophysical Journal International*, 116:527-537.

Loke, M.H., Acworth, I. and Dahlin, T., 2003, "A comparison of smooth and blocky inversion methods in 2D electrical imaging surveys," *Exploration Geophysics*, 34(3): 182-187.

Loke, M.H. and Barker, R.D., 1996b, "Rapid least-squares inversion of apparent resistivity pseudo-sections by a quasi-Newton method," *Geophysical Prospecting*, 44(1): 131-152.

Oldenburg, D.W. and Li, Y., 1999, "Estimating depth of investigation in dc resistivity and IP surveys," *Geophysics*, 64(2): 403-416.

Robain, H. et al., 1999, "Location of infinite electrodes in pole-pole electrical surveys: Consequences for 2D imaging," *Journal of Applied Geophysics*, 41(4): 313-333.

Roy, A. and A. Apparao, 1971, "Depth of investigation in direct current methods," *Geophysics*, 36(5):943-959.

Roy, A., 1972, "Depth of investigation in Wenner, three-electrode, and dipole-dipole DC resistivity methods," *Geophysical Prospecting*, 20:329-340.

Telford, W.M., L.P. Geldart, and R.E. Sheriff, 1990, "Applied Geophysics," Cambridge University Press, Cambridge, United Kingdom.

APPENDIX A

SUPPLEMENTAL TWO-DIMENSIONAL INVERSION RESULTS

LIST OF FIGURES

Figure A-1. Inversion Results for Line 200EC101 ..... A-1
Figure A-2. Inversion Results for Line 200EC102 ..... A-1
Figure A-3. Inversion Results for Line 200EC103 ..... A-2
Figure A-4. Inversion Results for Line 200EC104 ..... A-2
Figure A-5. Inversion Results for Line 200EAC01 ..... A-3
Figure A-6. Inversion Results for Line 200EAC02 ..... A-3
Figure A-7. Inversion Results for Line 200EAC03 ..... A-4
Figure A-8. Inversion Results for Line 200EAC04 ..... A-4
Figure A-9. Inversion Results for Line 200EAC05 ..... A-5
Figure A-10. Inversion Results for Line 200EAC06 ..... A-5
Figure A-11. Inversion Results for Line 200EAC07 ..... A-6
Figure A-12. Inversion Results for Line 200EAC08 ..... A-6
Figure A-13. Inversion Results for Line 200EAC09 ..... A-7
Figure A-14. Inversion Results for Line 200EBP01 ..... A-8
Figure A-15. Inversion Results for Line 200EBP03 ..... A-8
Figure A-16. Inversion Results for Line 200EBP04 ..... A-9
Figure A-17. Inversion Results for Line 200EBP05 ..... A-9
Figure A-18. Inversion Results for Line 200EBP06 ..... A-10
Figure A-19. Inversion Results for Line 200EBP07 ..... A-10
Figure A-20. Inversion Results for Line 200EBP08 ..... A-11
Figure A-21. Inversion Results for Line 200EBP09 ..... A-11
Figure A-22. Inversion Results for Line 200EBP10 ..... A-12
Figure A-23. Inversion Results for Line 200EPX02 South A-13
Figure A-24. Inversion Results for Line 200EPX03 ..... A-13
Figure A-25. Inversion Results for Line 200EPX04 ..... A-14
Figure A-26. Inversion Results for Line 200EPX06 ..... A-14
Figure A-27. Inversion Results for Line 200EPX08 ..... A-15
Figure A-28. Inversion Results for Line 200EPX09 ..... A-15
Figure A-29. Inversion Results for Line 200EPX10 ..... A-16
Figure A-30. Inversion Results for Line 200EPX11 ..... A-16

Figure A-31. Inversion Results for Line 200EPX12. ..... A-17
Figure A-32. Inversion Results for Line 200EPX13. ..... A-17
Figure A-33. Inversion Results for Line 200EPX14. ..... A-18
Figure A-34. Inversion Results for Line 200EPX15. ..... A-18
Figure A-35. Inversion Results for Line 200WSC01. ..... A-19
Figure A-36. Inversion Results for Line 200WSC02. ..... A-19
Figure A-37. Inversion Results for Line 200WSC03. ..... A-20
Figure A-38. Inversion Results for Line 200WSC04. ..... A-20
Figure A-39. Inversion Results for Line 200WSC05. ..... A-21
Figure A-40. Inversion Results for Line 200WSC06. ..... A-21
Figure A-41. Inversion Results for Line 200WTP01. ..... A-22
Figure A-42. Inversion Results for Line 200WTP02. ..... A-22
Figure A-43. Inversion Results for Line 200WTP03. ..... A-23
Figure A-44. Inversion Results for Line 200WTP04. ..... A-23
Figure A-45. Inversion Results for Line 200WTP05. ..... A-24
Figure A-46. Inversion Results for Line 200WTP06. ..... A-24
Figure A-47. Inversion Results for Line 200WTP07. ..... A-25
Figure A-48. Inversion Results for Line 200WTP08. ..... A-25
Figure A-49. Inversion Results for Line 200WTP09. ..... A-26
Figure A-50. Inversion Results for Line 200WTP10. ..... A-26
Figure A-51. Inversion Results for Line 200WZT01. ..... A-27
Figure A-52. Inversion Results for Line 200WZT02. ..... A-27
Figure A-53. Inversion Results for Line 200WZT03. ..... A-28

OUTPUT FROM AGI EARTHIMAGER 2D OF INVERSION RESULTS FOR SELECT SITES IN THE 200 EAST AND 200 WEST AREAS

200 EAST: 216-C-1

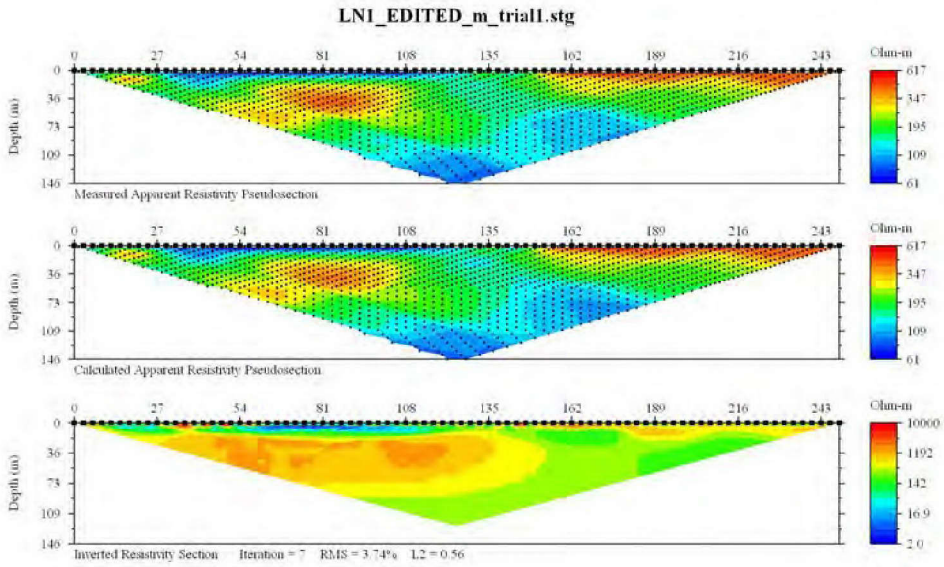

Figure A-1. Inversion Results for Line 200EC101.

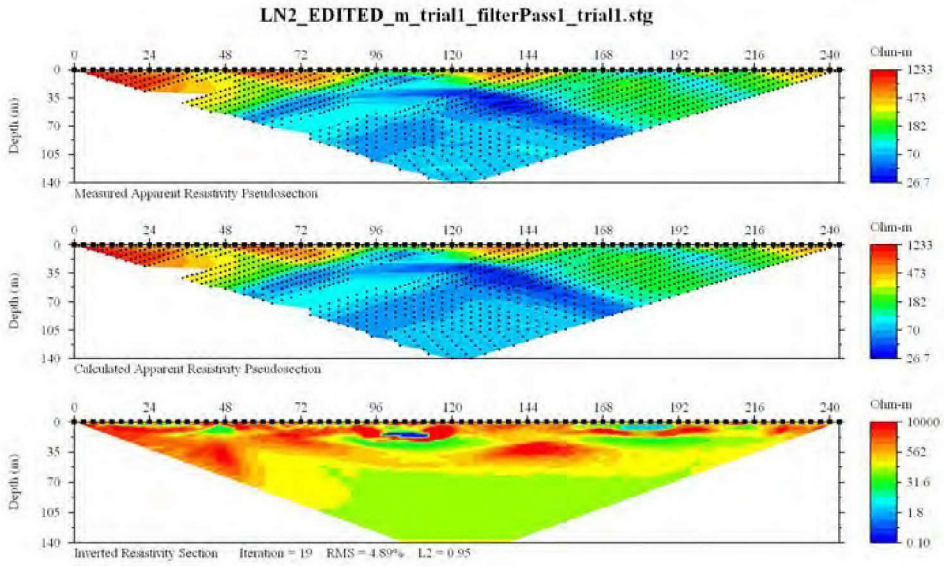

Figure A-2. Inversion Results for Line 200EC102.

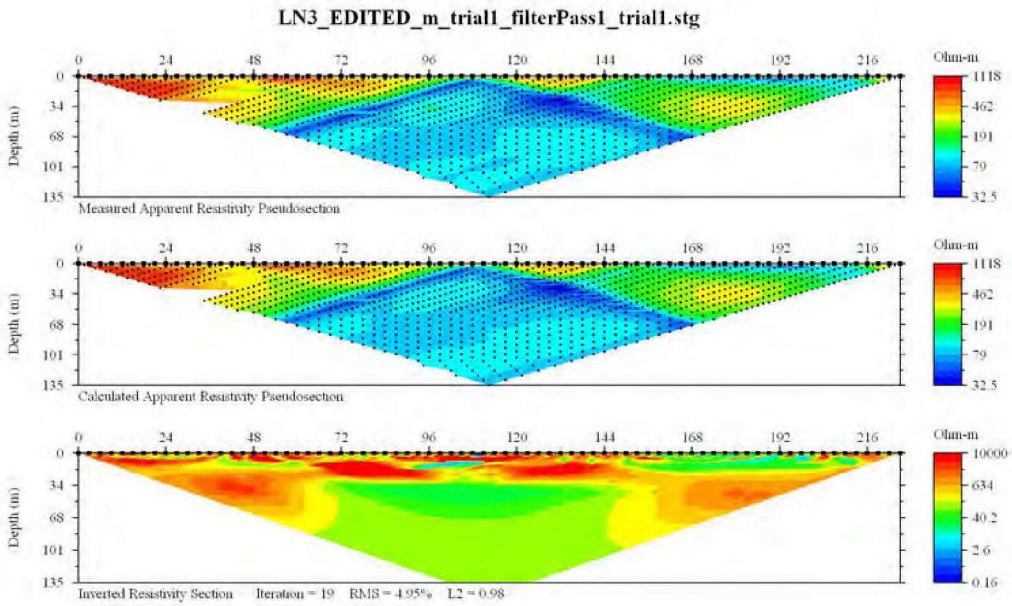

Figure A-3. Inversion Results for Line 200EC103.

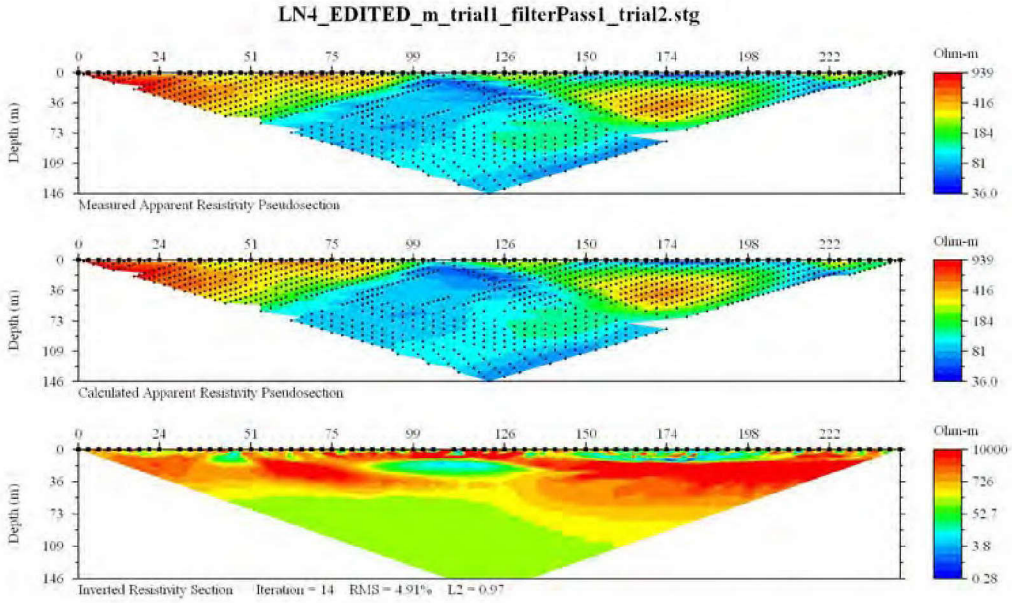

Figure A-4. Inversion Results for Line 200EC104.

200 EAST: A-COMPLEX

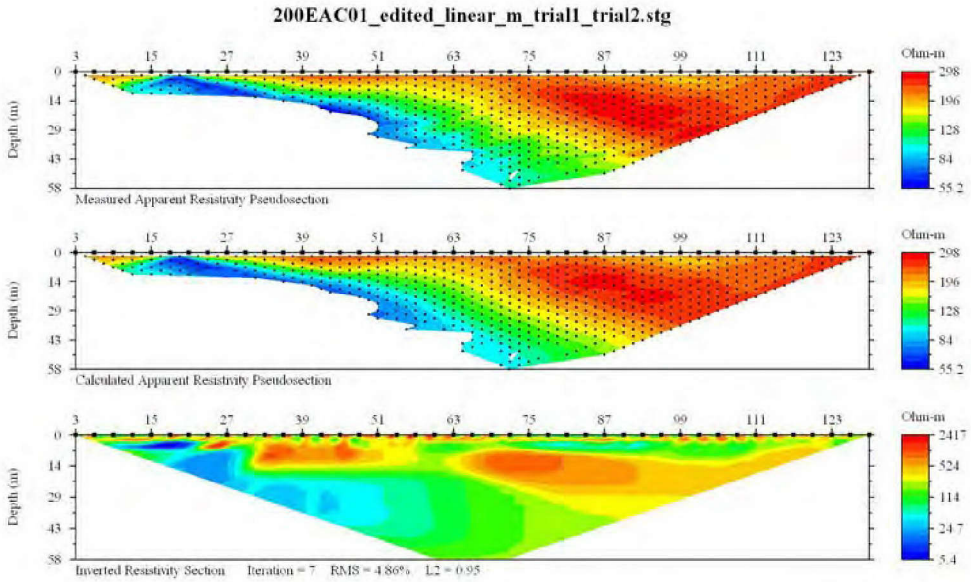

Figure A-5. Inversion Results for Line 200EAC01.

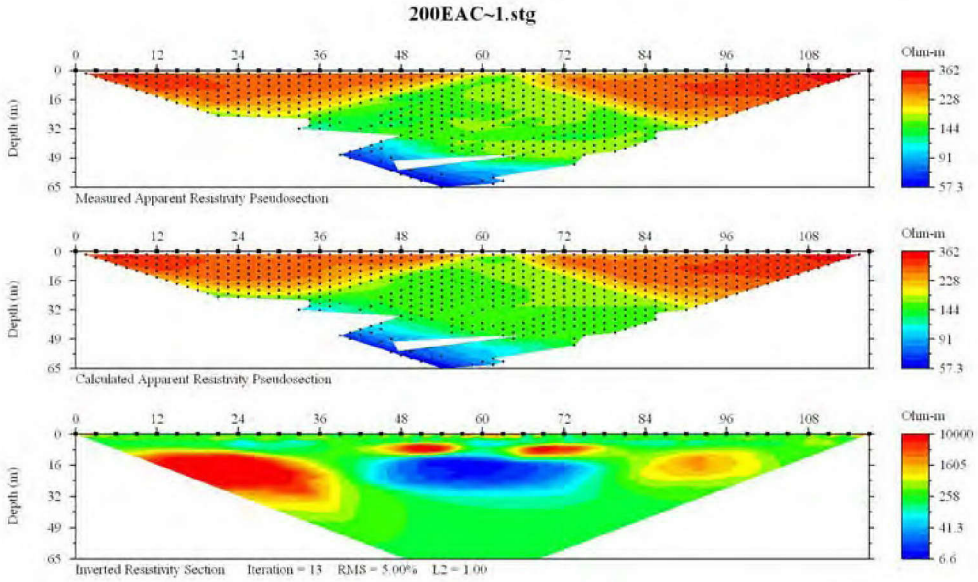

Figure A-6. Inversion Results for Line 200EAC02.

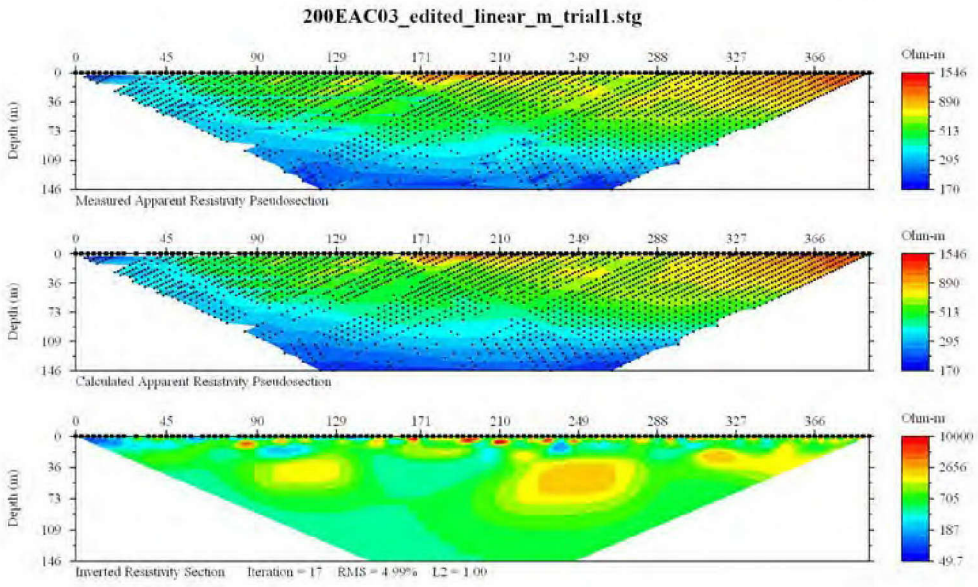

Figure A-7. Inversion Results for Line 200EAC03.

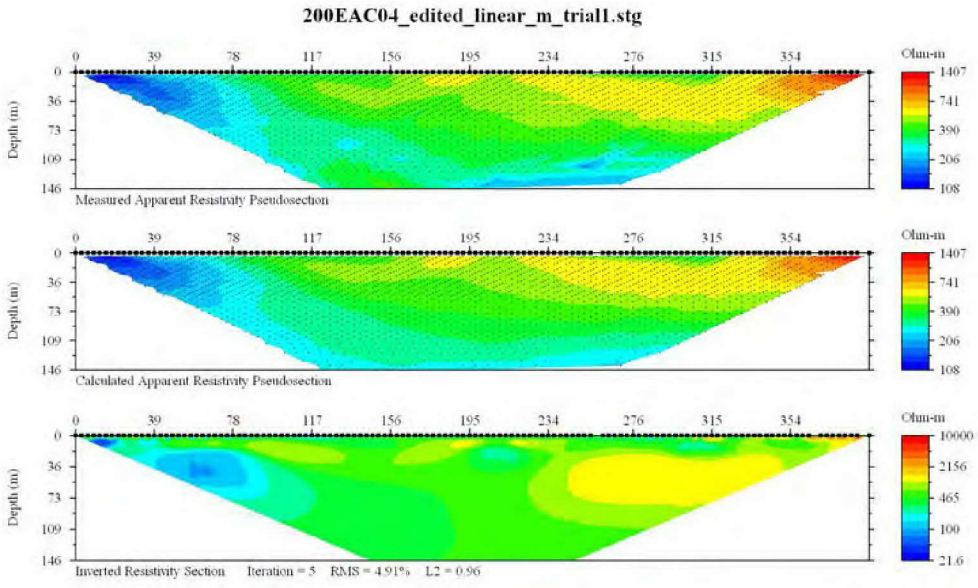

Figure A-8. Inversion Results for Line 200EAC04.

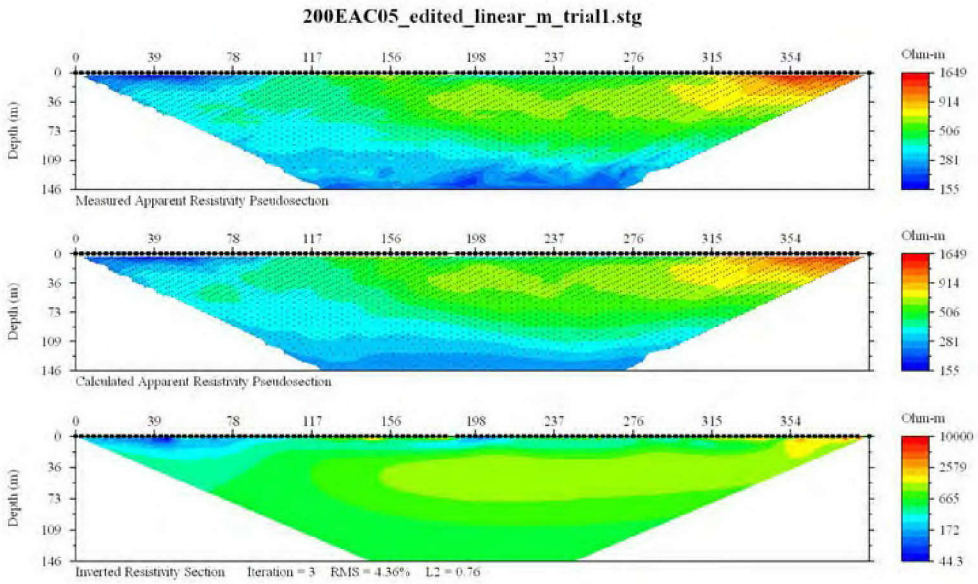

Figure A-9. Inversion Results for Line 200EAC05.

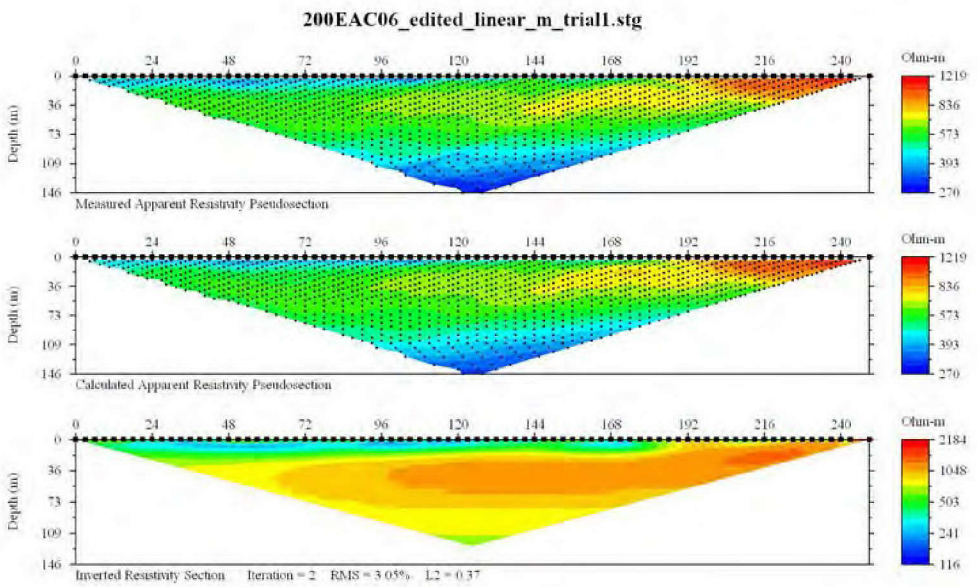

Figure A-10. Inversion Results for Line 200EAC06.

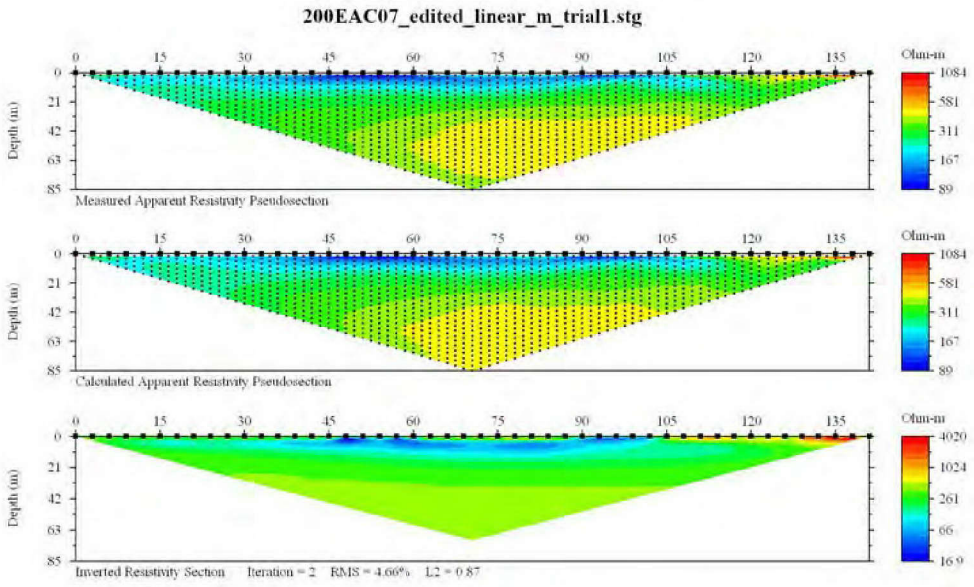

Figure A-11. Inversion Results for Line 200EAC07.

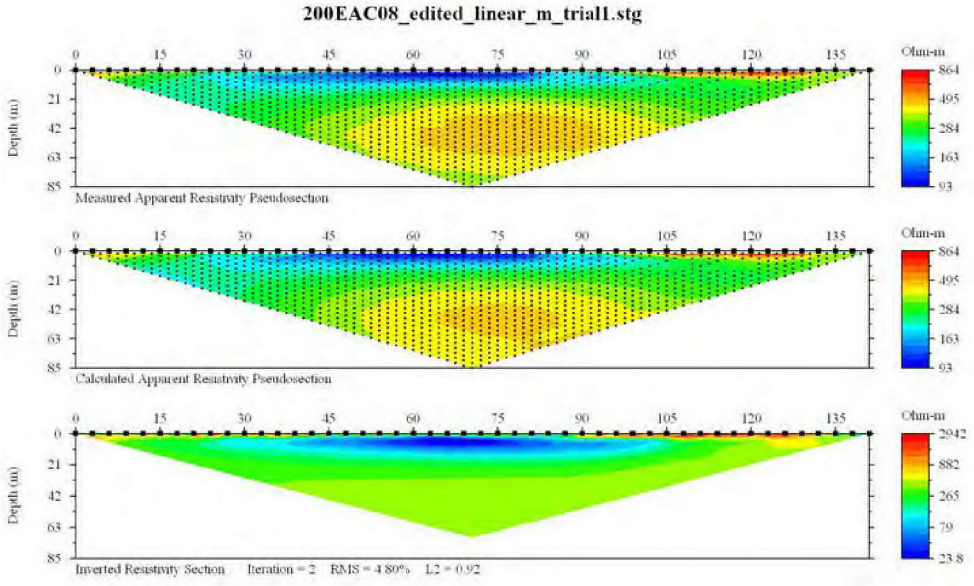

Figure A-12. Inversion Results for Line 200EAC08.

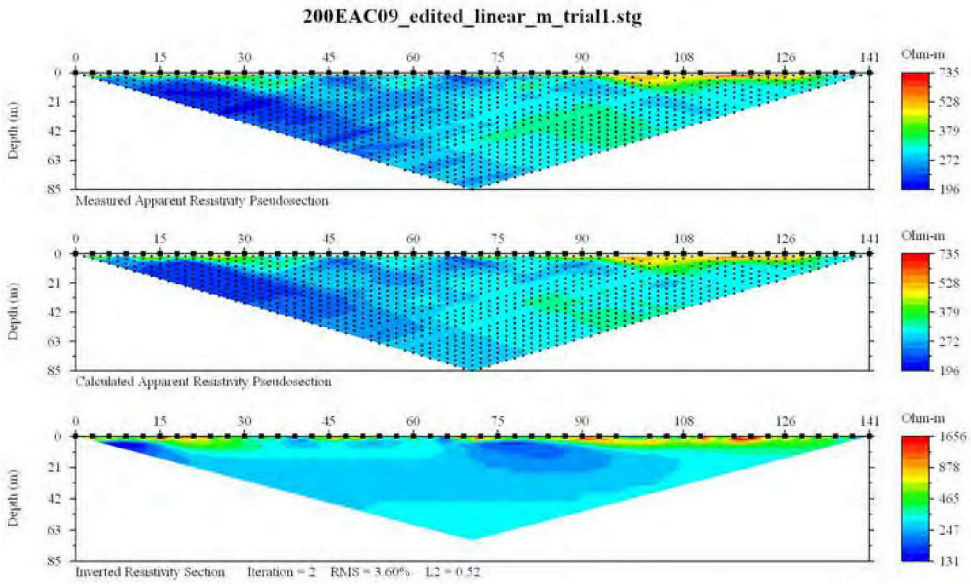

Figure A-13: Inversion Results for Line 200EAC09.

200 EAST: B-PLANT

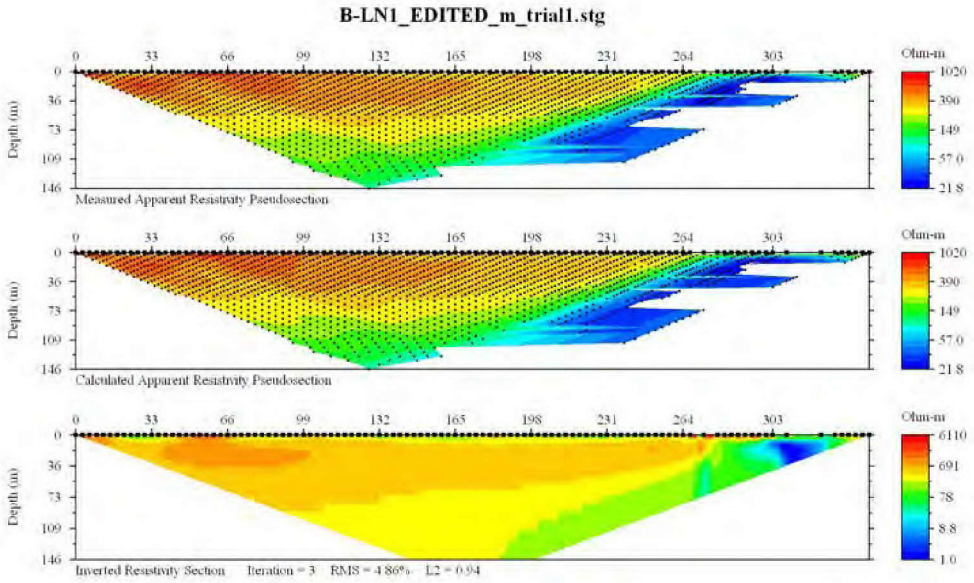

Figure A-14. Inversion Results for Line 200EBP01.

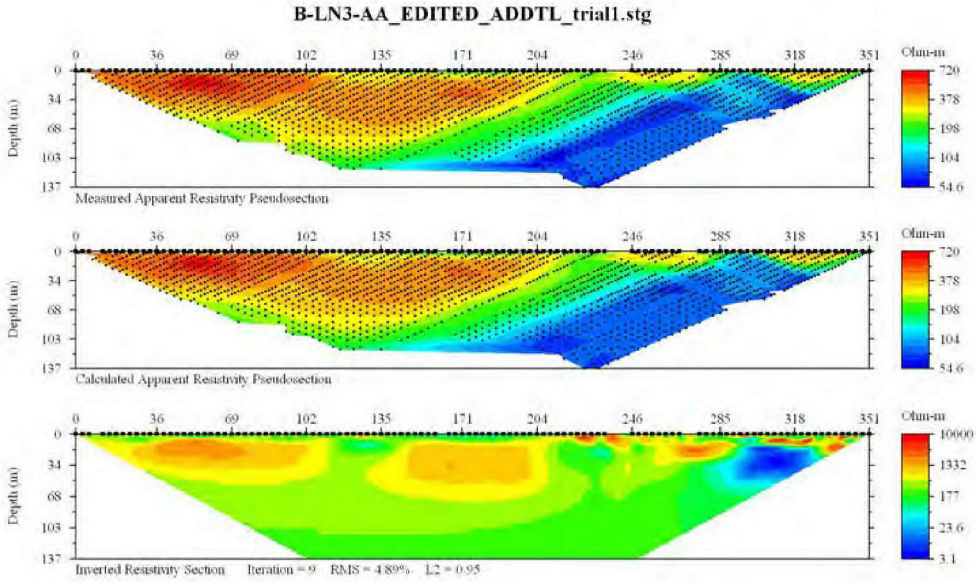

Figure A-15. Inversion Results for Line 200EBP03.

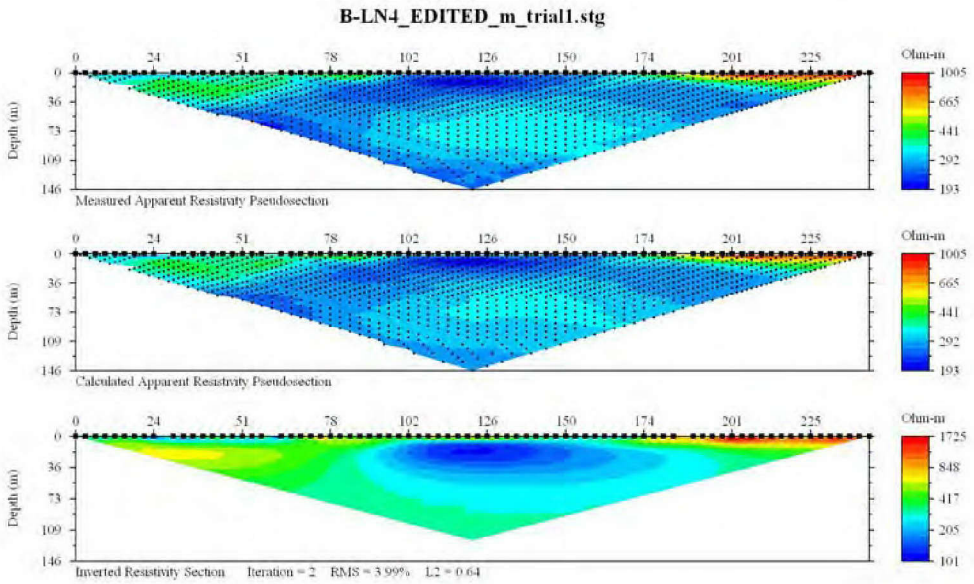

Figure A-16. Inversion Results for Line 200EBP04.

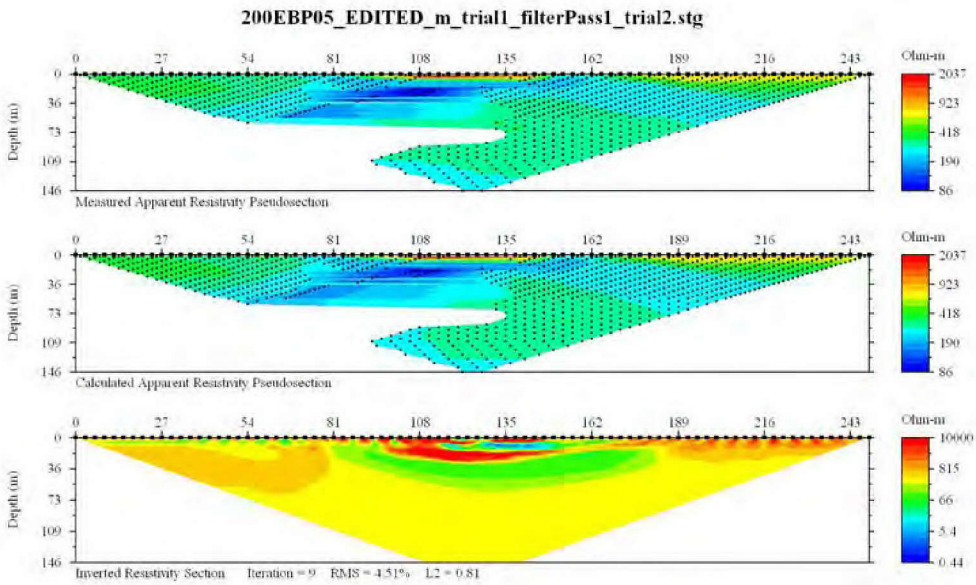

Figure A-17. Inversion Results for Line 200EBP05.

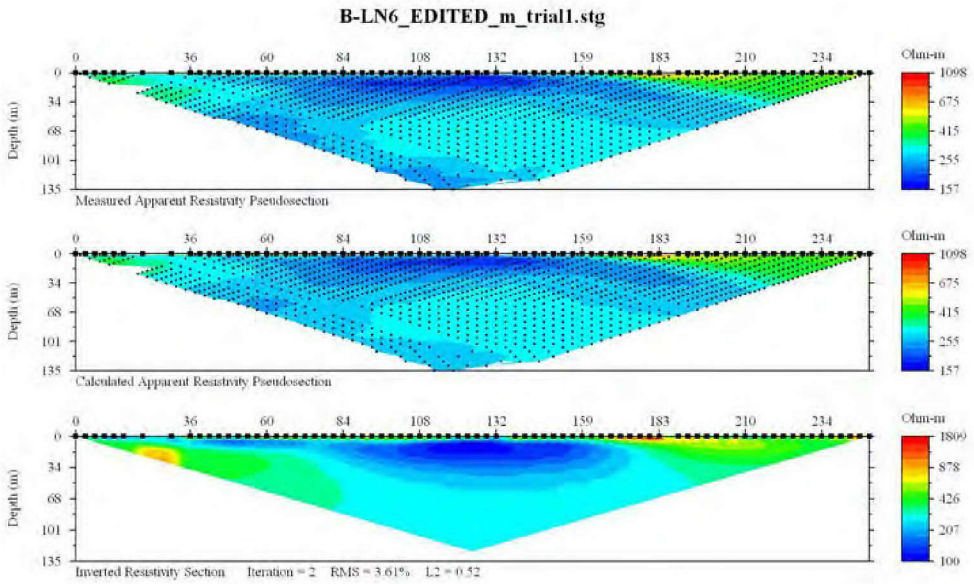

Figure A-18. Inversion Results for Line 200EBP06.

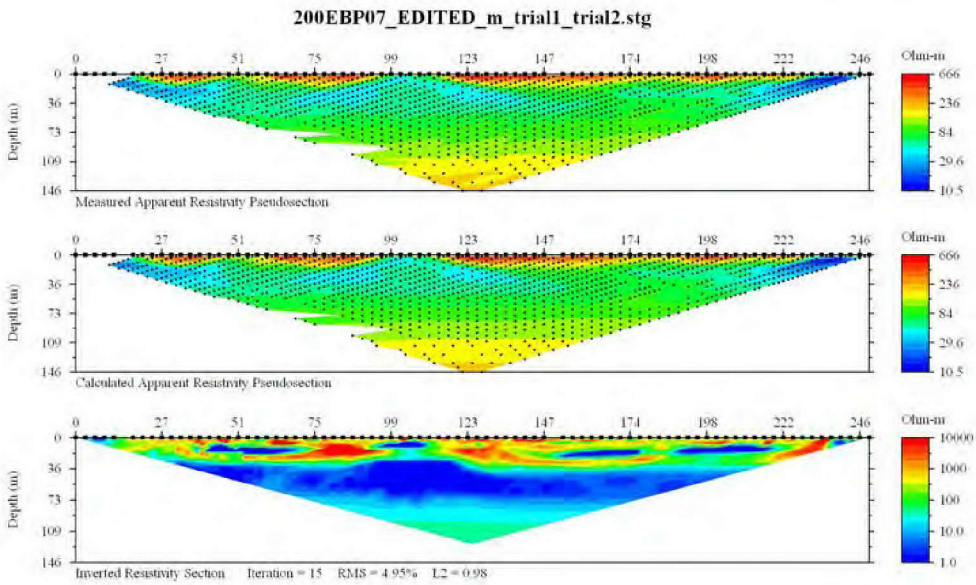

Figure A-19. Inversion Results for Line 200EBP07.

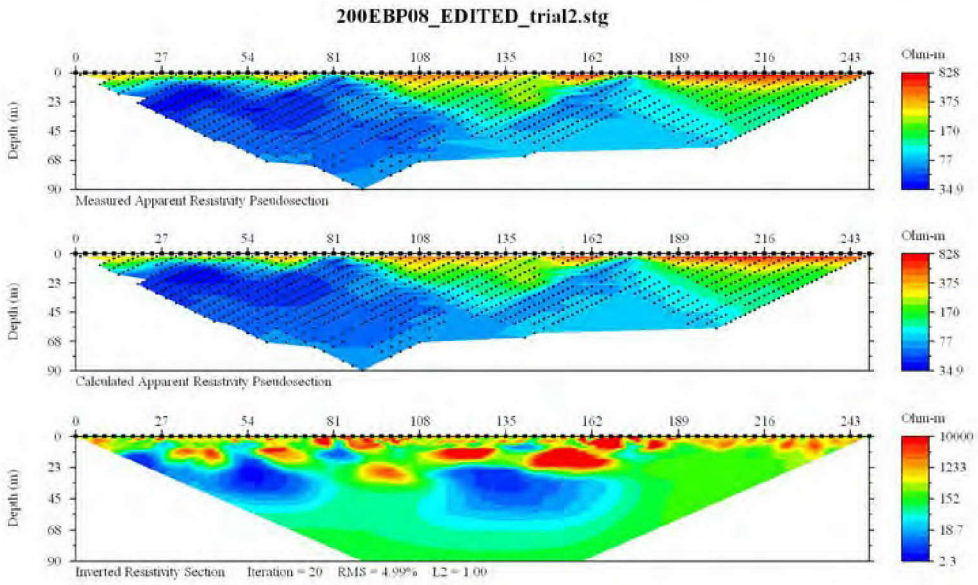

Figure A-20. Inversion Results for Line 200EBP08.

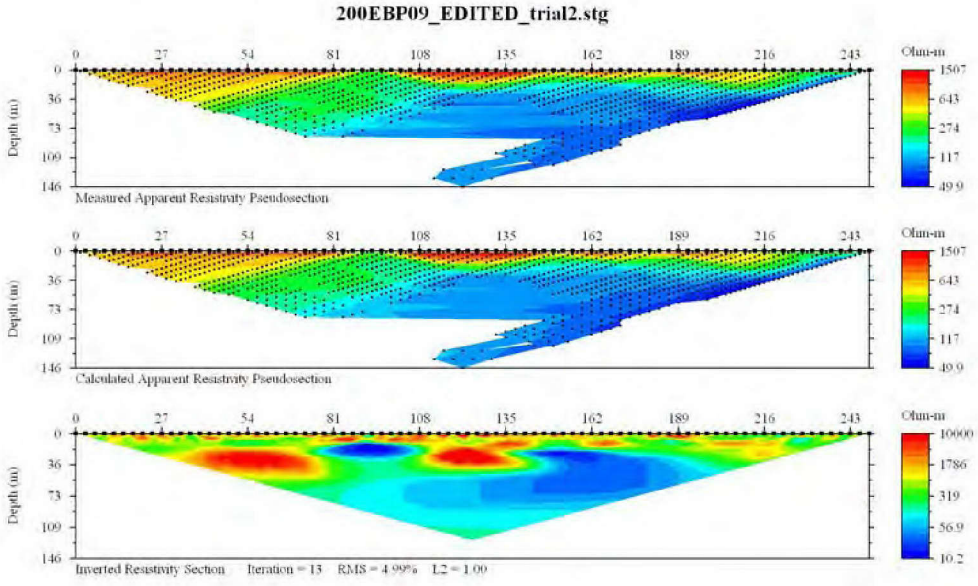

Figure A-21. Inversion Results for Line 200EBP09.

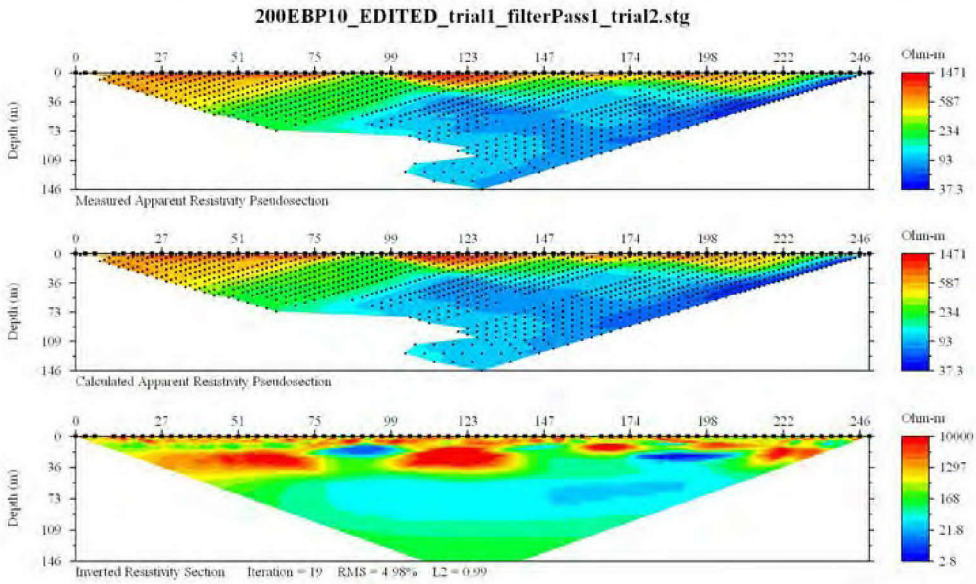

Figure A-22. Inversion Results for Line 200EBP10.

200 EAST: PUREX PLANT

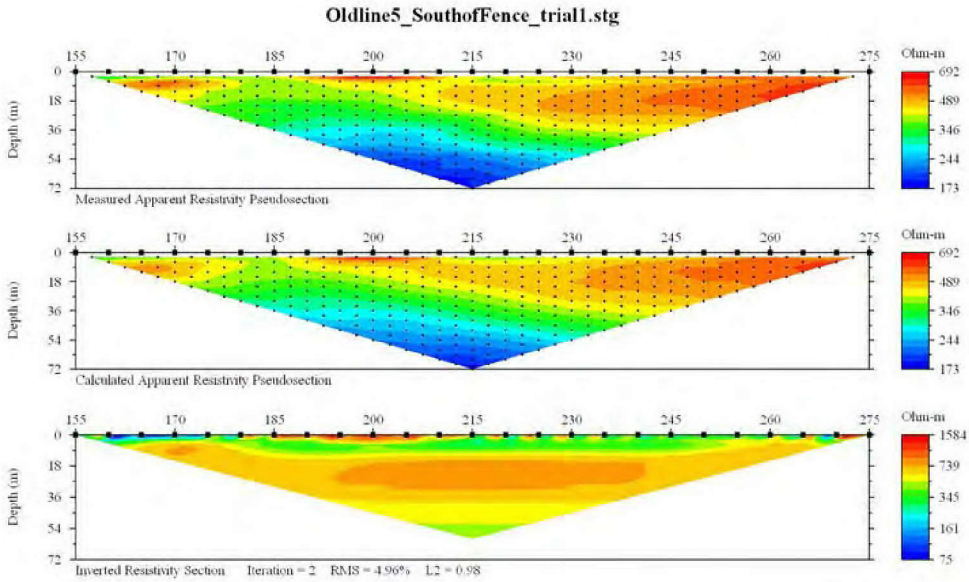

Figure A-23. Inversion Results for Line 200EPX02 South.

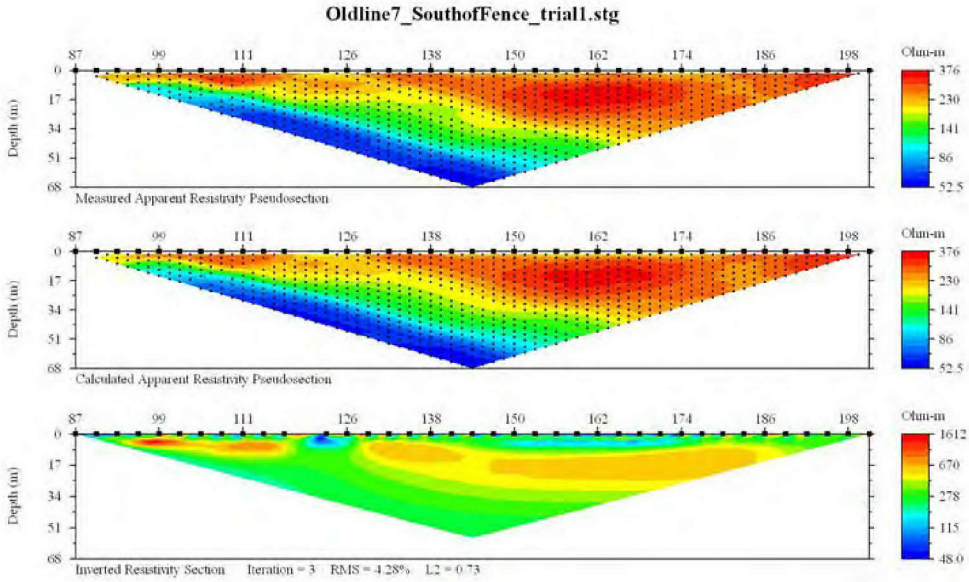

Figure A-24. Inversion Results for Line 200EPX03.

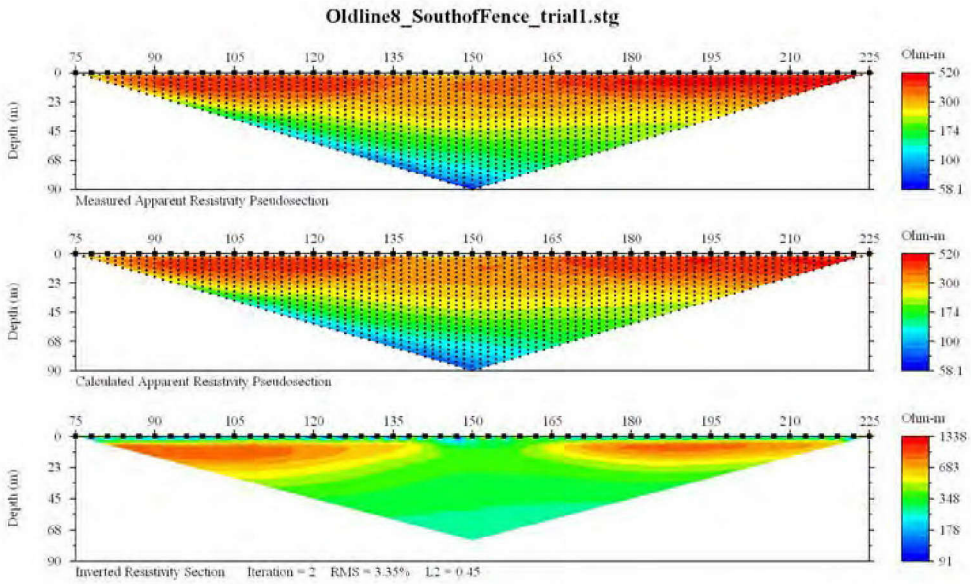

Figure A-25. Inversion Results for Line 200EPX04.

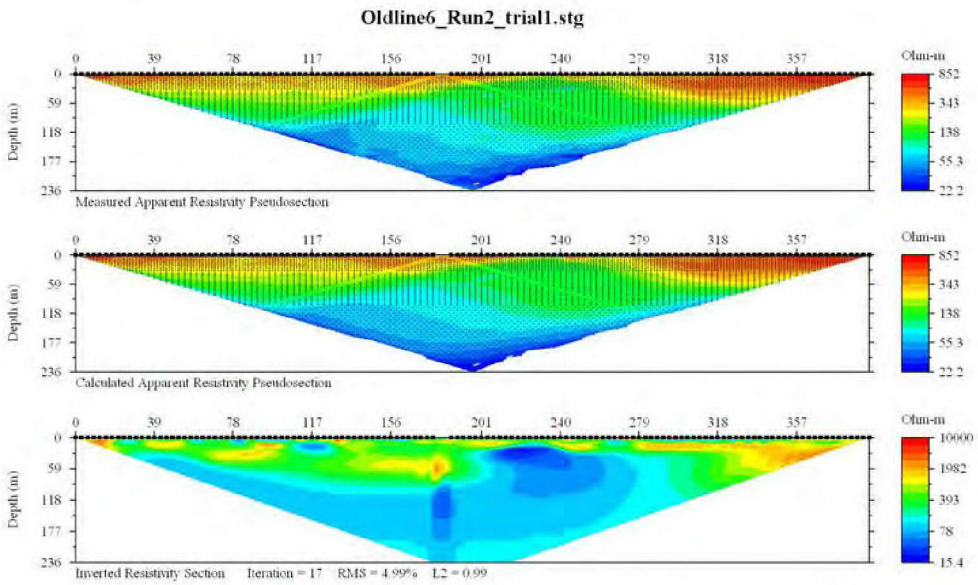

Figure A-26. Inversion Results for Line 200EPX06.

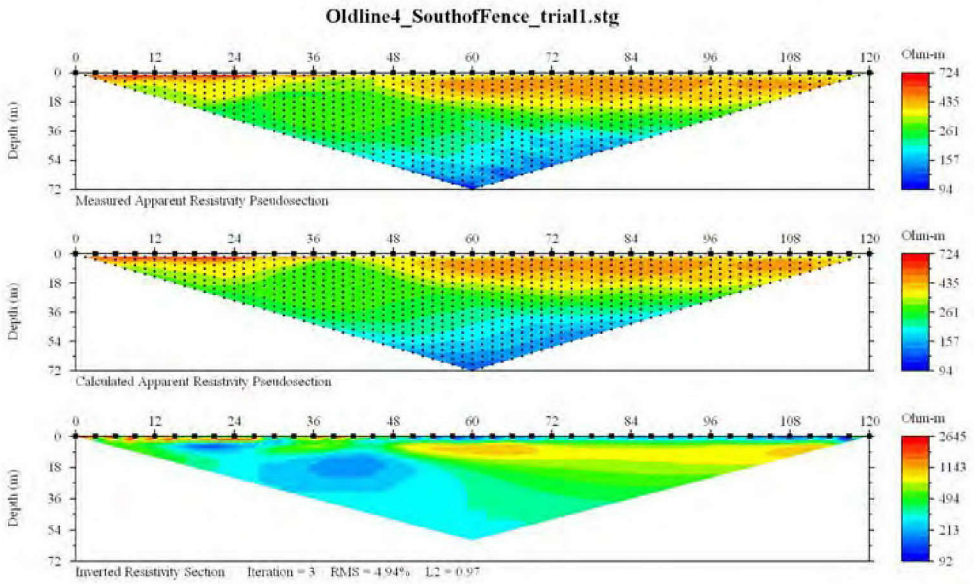

Figure A-27. Inversion Results for Line 200EPX08.

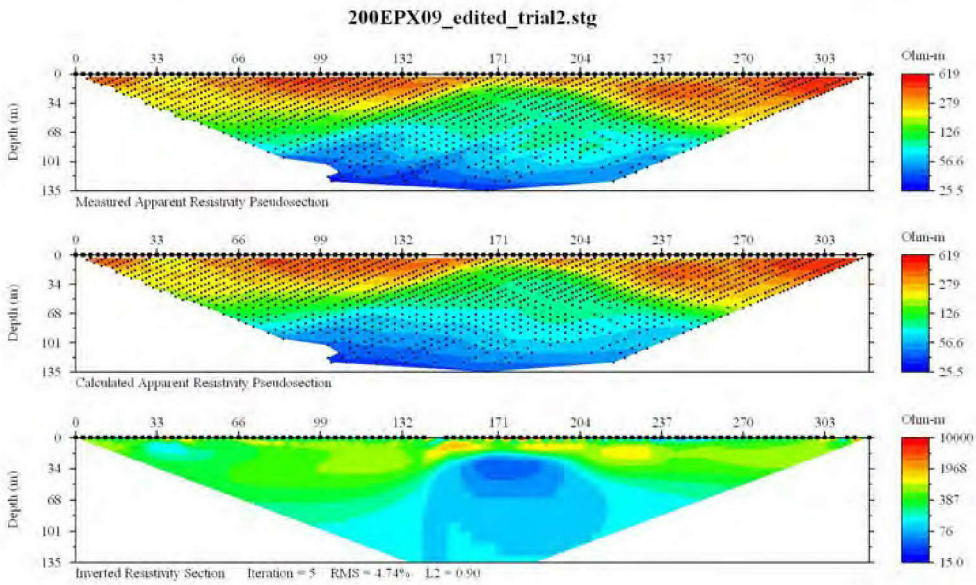

Figure A-28. Inversion Results for Line 200EPX09.

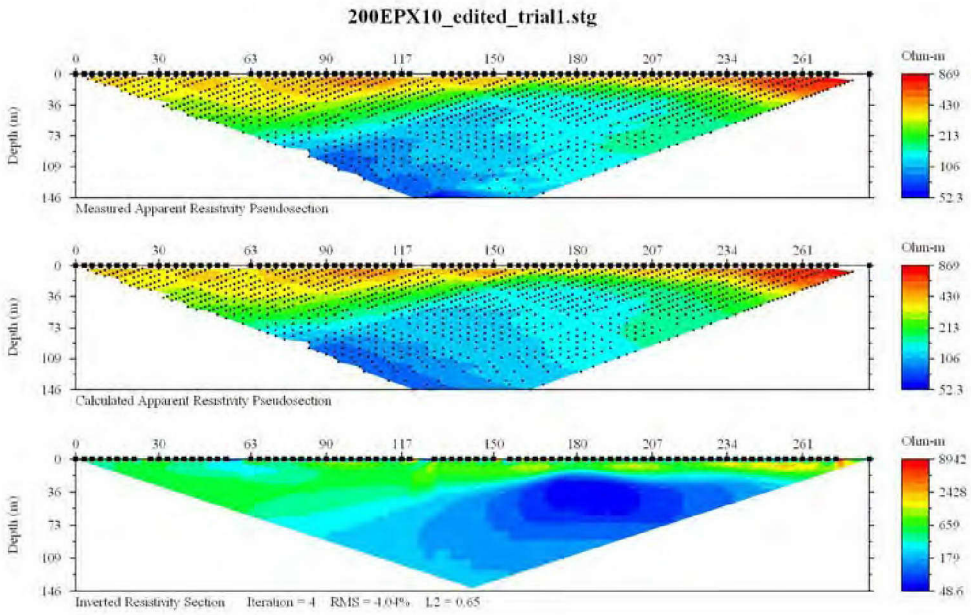

Figure A-29. Inversion Results for Line 200EPX10.

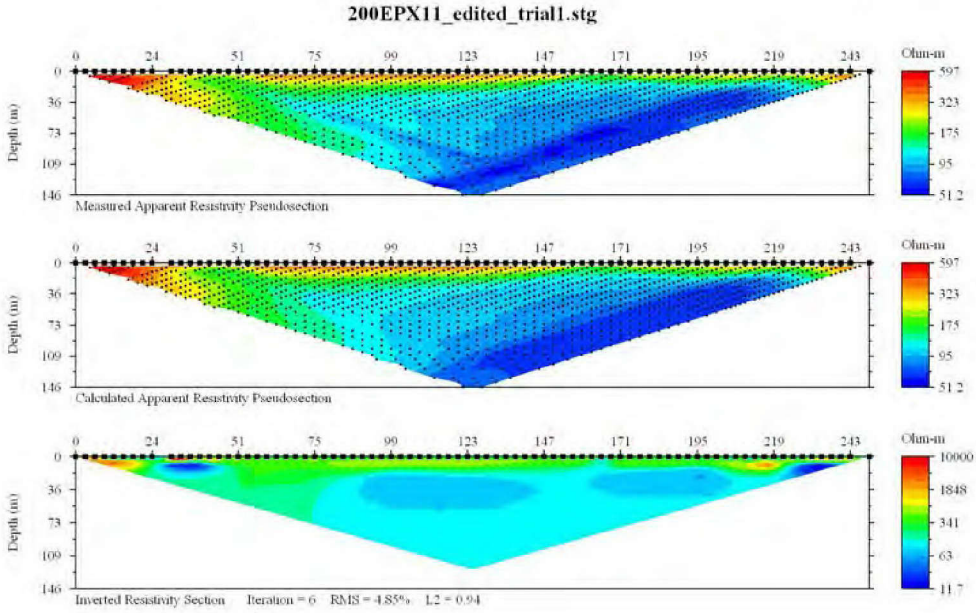

Figure A-30. Inversion Results for Line 200EPX11.

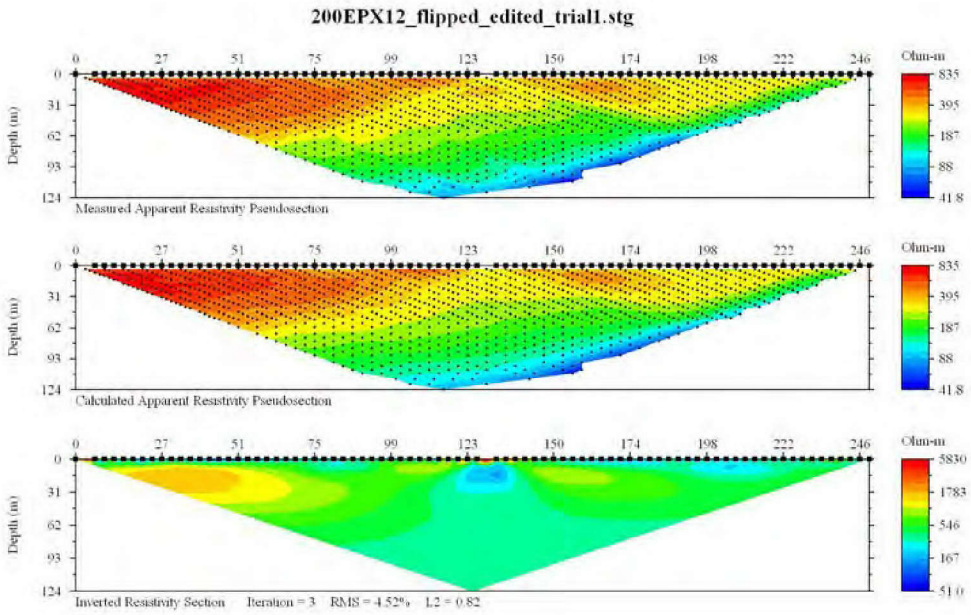

Figure A-31. Inversion Results for Line 200EPX12.

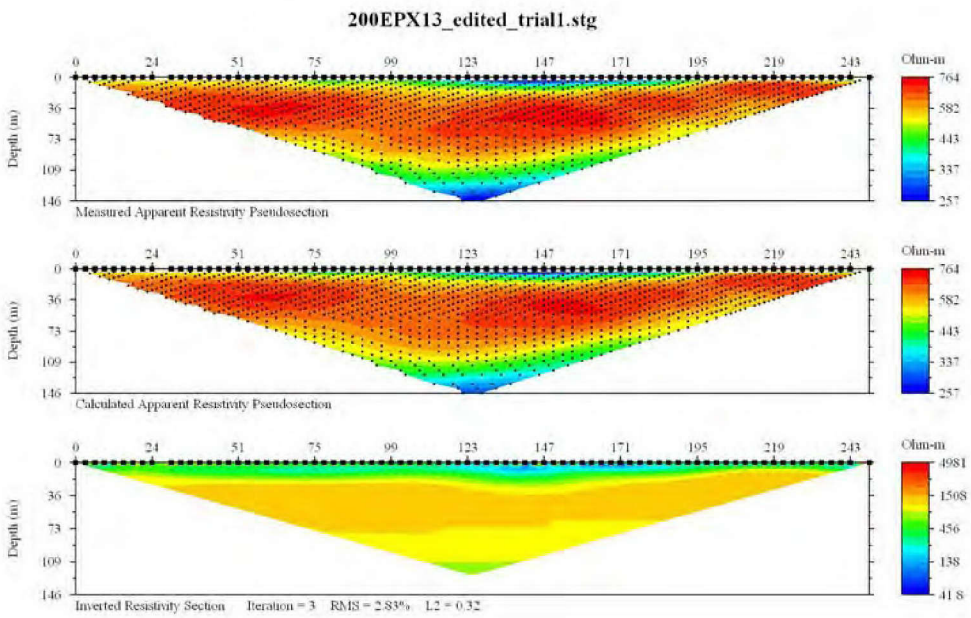

Figure A-32. Inversion Results for Line 200EPX13.

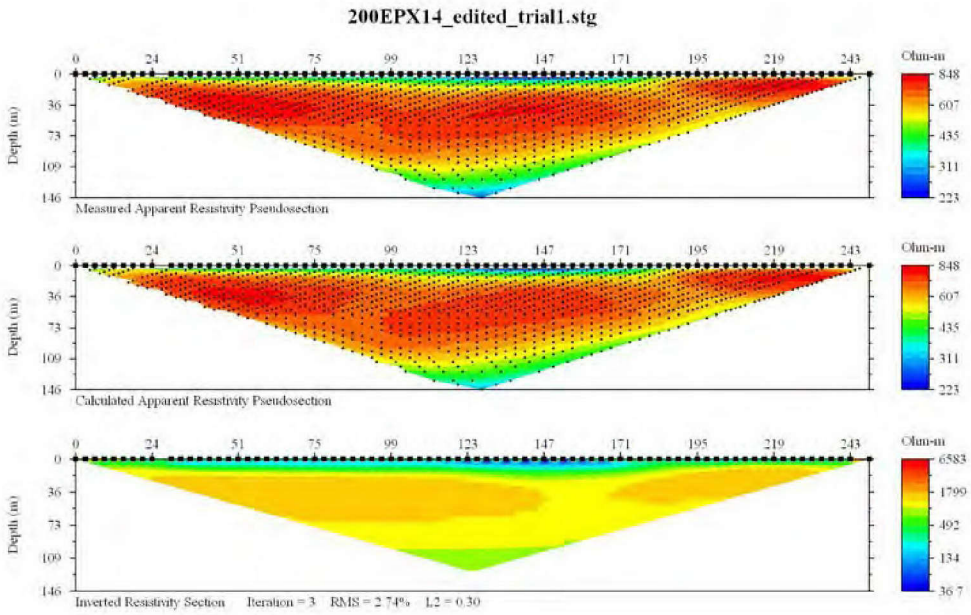

Figure A-33. Inversion Results for Line 200EPX14.

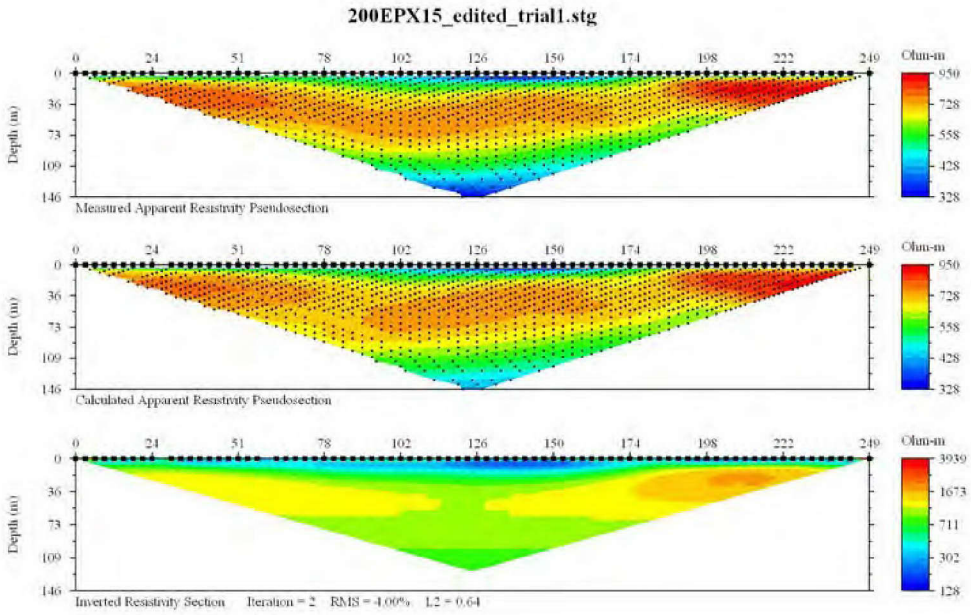

Figure A-34. Inversion Results for Line 200EPX15.

200 WEST: S-COMPLEX

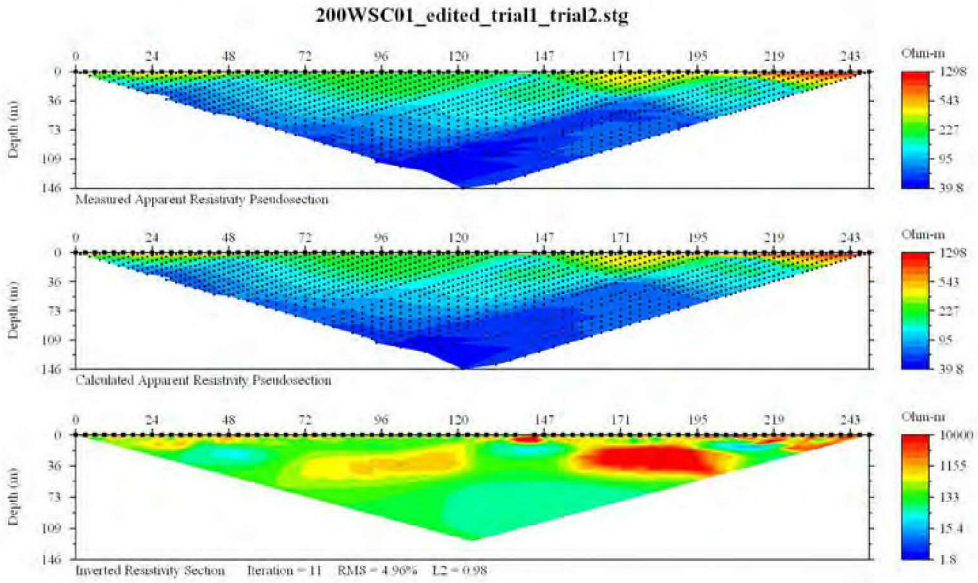

Figure A-35. Inversion Results for Line 200WSC01.

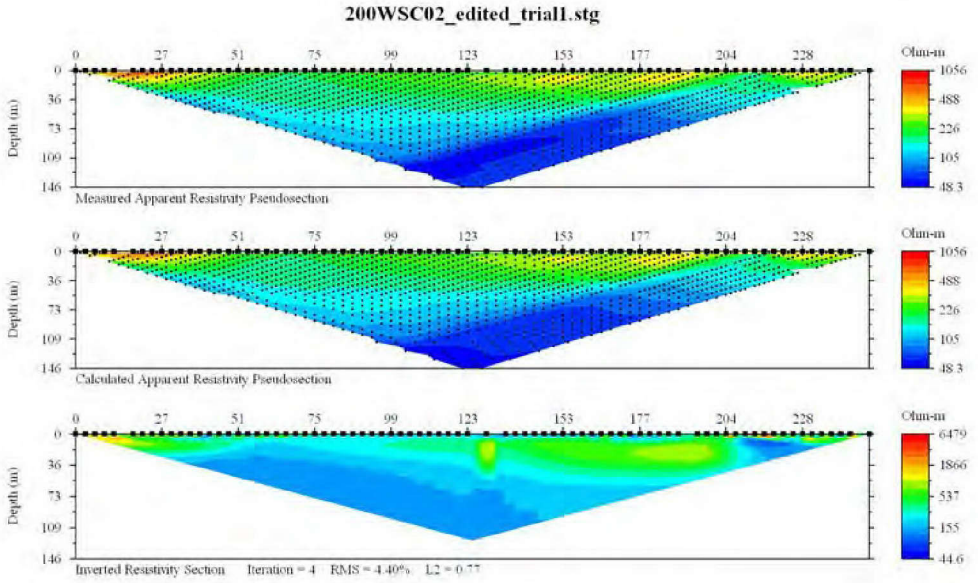

Figure A-36. Inversion Results for Line 200WSC02.

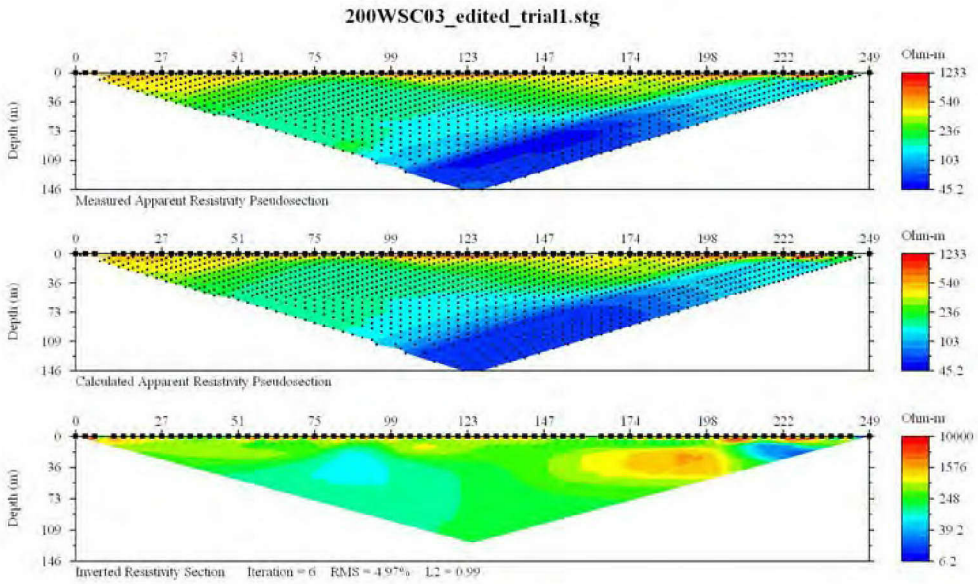

Figure A-37. Inversion Results for Line 200WSC03.

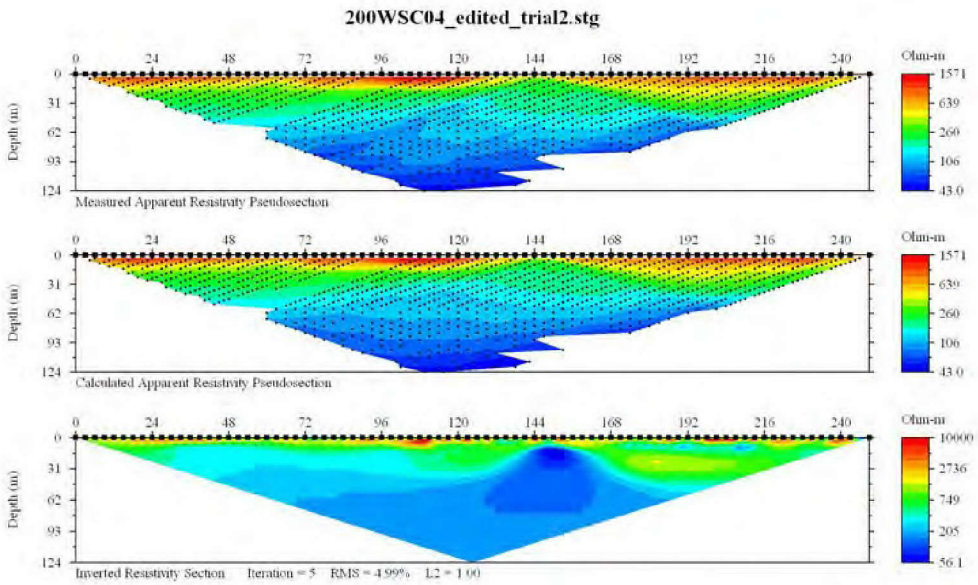

Figure A-38. Inversion Results for Line 200WSC04.

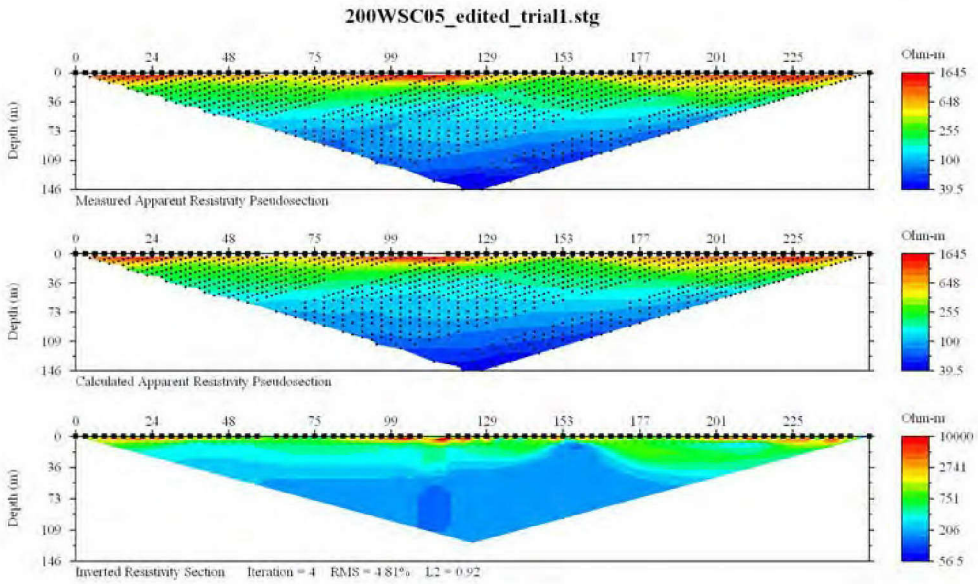

Figure A-39. Inversion Results for Line 200WSC05.

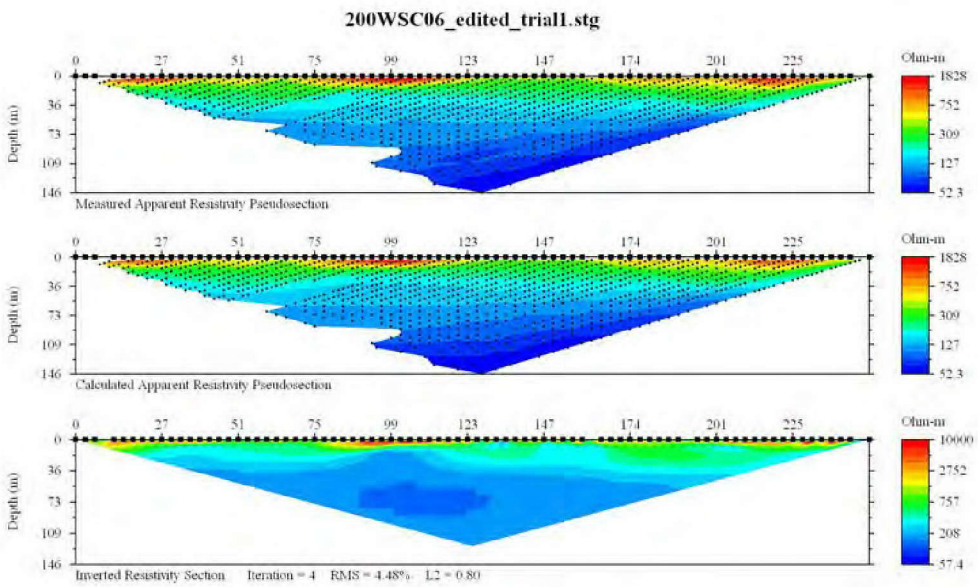

Figure A-40. Inversion Results for Line 200WSC06.

200 WEST: T-PLANT

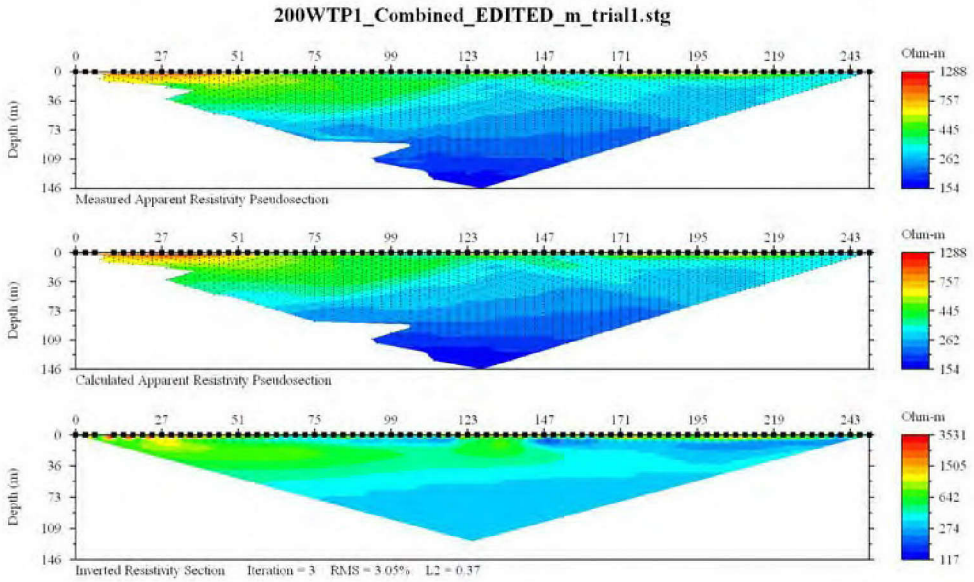

Figure A-41. Inversion Results for Line 200WTP01.

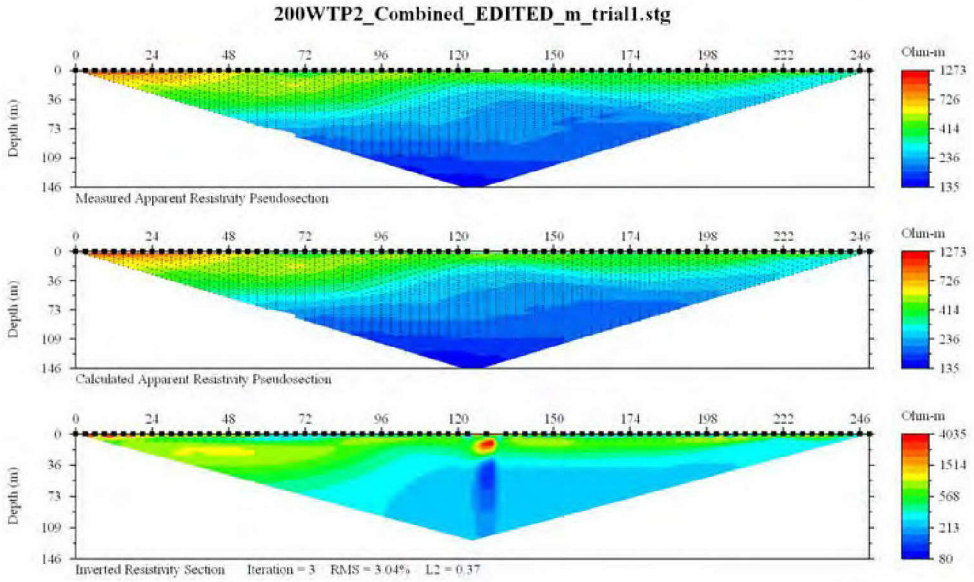

Figure A-42. Inversion Results for Line 200WTP02.

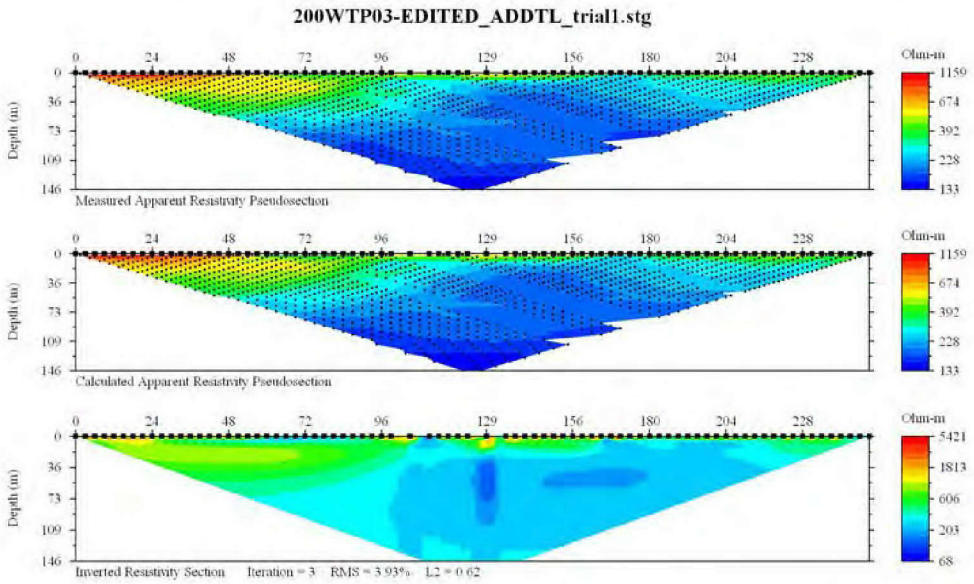

Figure A-43. Inversion Results for Line 200WTP03.

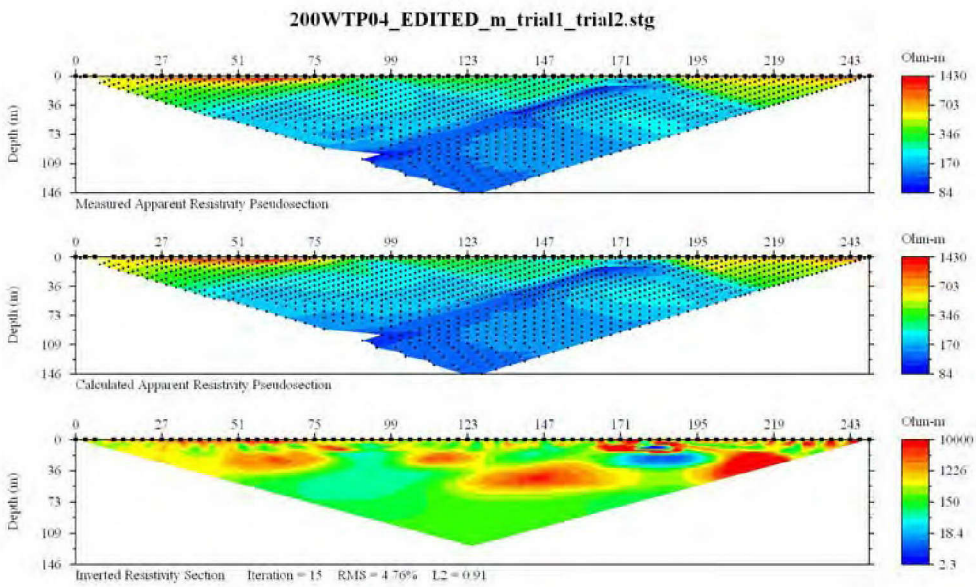

Figure A-44. Inversion Results for Line 200WTP04.

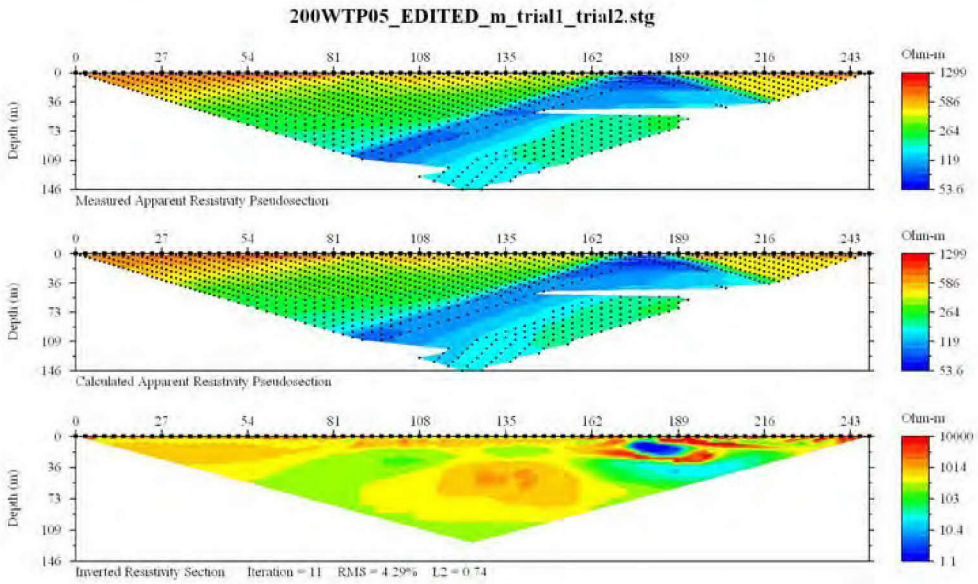

Figure A-45. Inversion Results for Line 200WTP05.

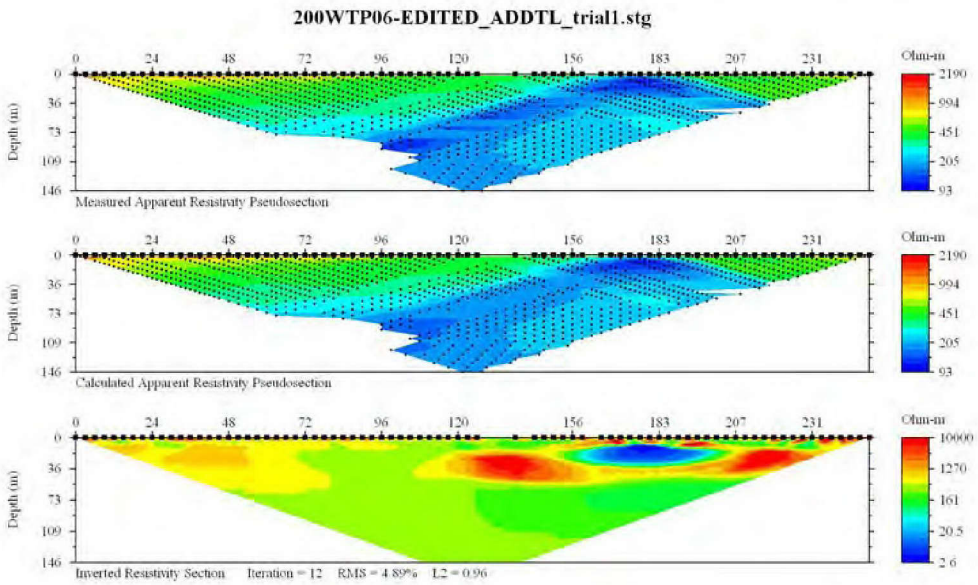

Figure A-46. Inversion Results for Line 200WTP06.

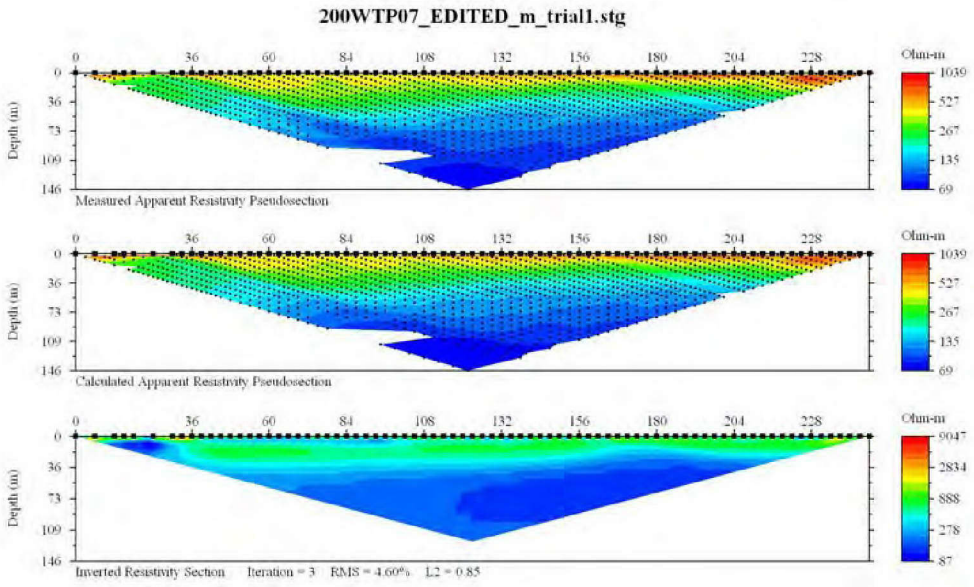

Figure A-47. Inversion Results for Line 200WTP07.

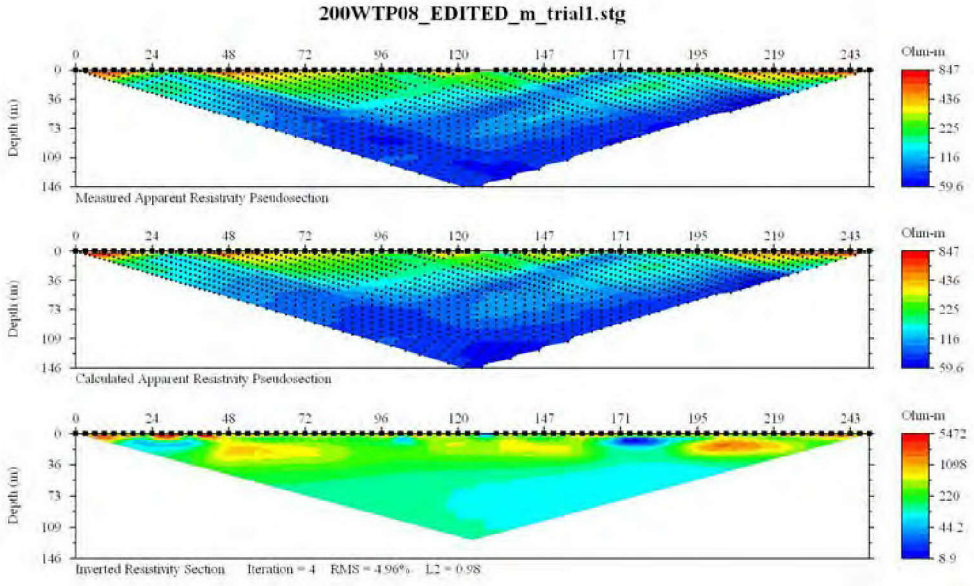

Figure A-48. Inversion Results for Line 200WTP08.

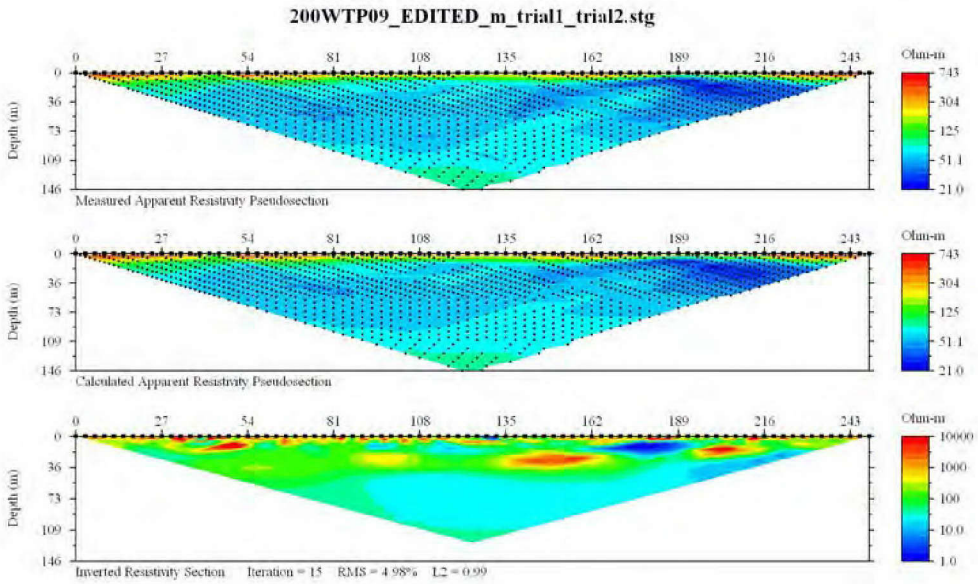

Figure A-49. Inversion Results for Line 200WTP09.

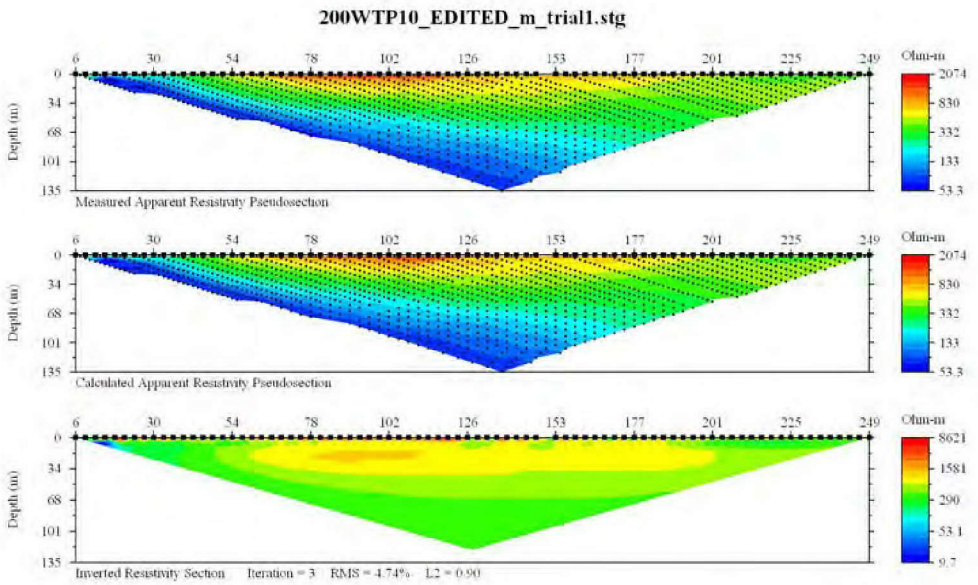

Figure A-50. Inversion Results for Line 200WTP10.

200 WEST: 216-Z-16 TRENCH

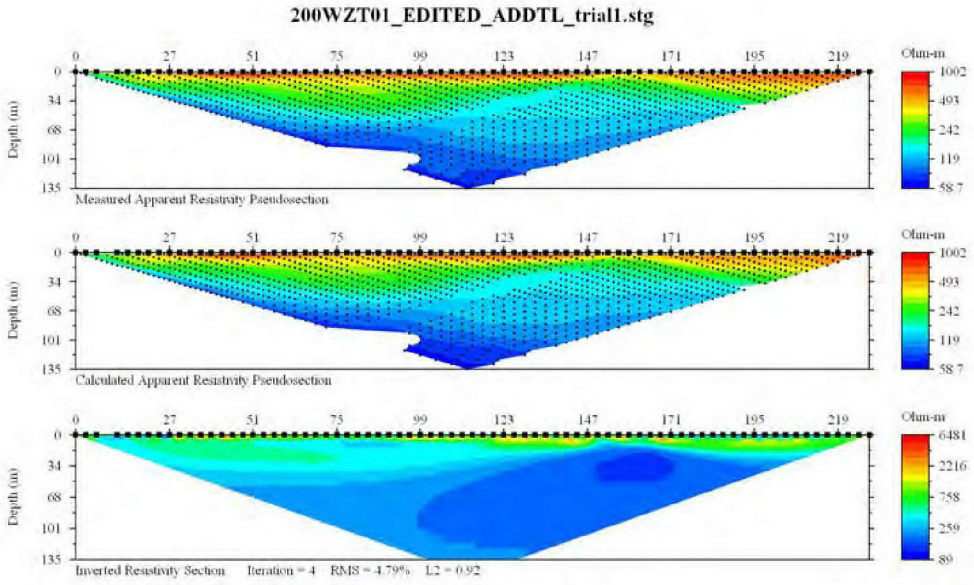

Figure A-51. Inversion Results for Line 200WZT01.

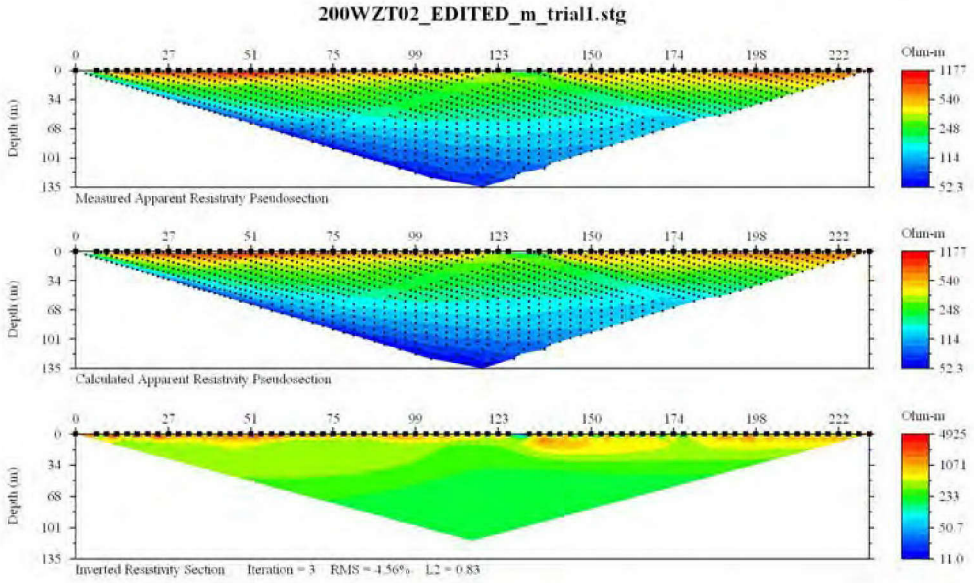

Figure A-52. Inversion Results for Line 200WZT02.

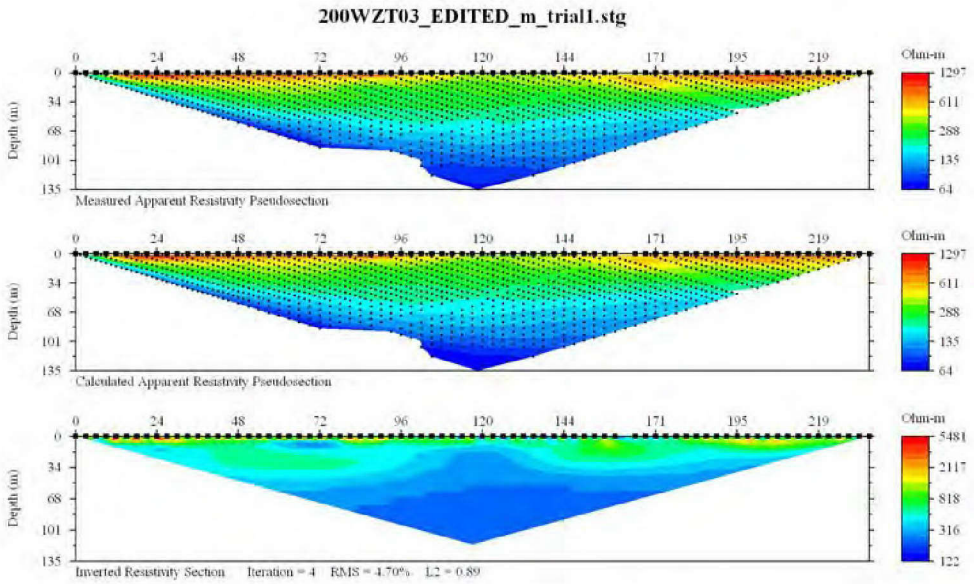

Figure A-53. Inversion Results for Line 200WZT03.

DISTRIBUTION

Onsite

1	U.S. Department of Energy Richland Operations Office	
	DOE Public Reading Room	H2-53
1	Pacific Northwest National Laboratory	
	Hanford Technical Library	P8-55
1	Lockheed Martin Enterprise Solutions & Services	
	Document Clearance	H6-08

This page intentionally left blank.